

Cover Page



Universiteit Leiden

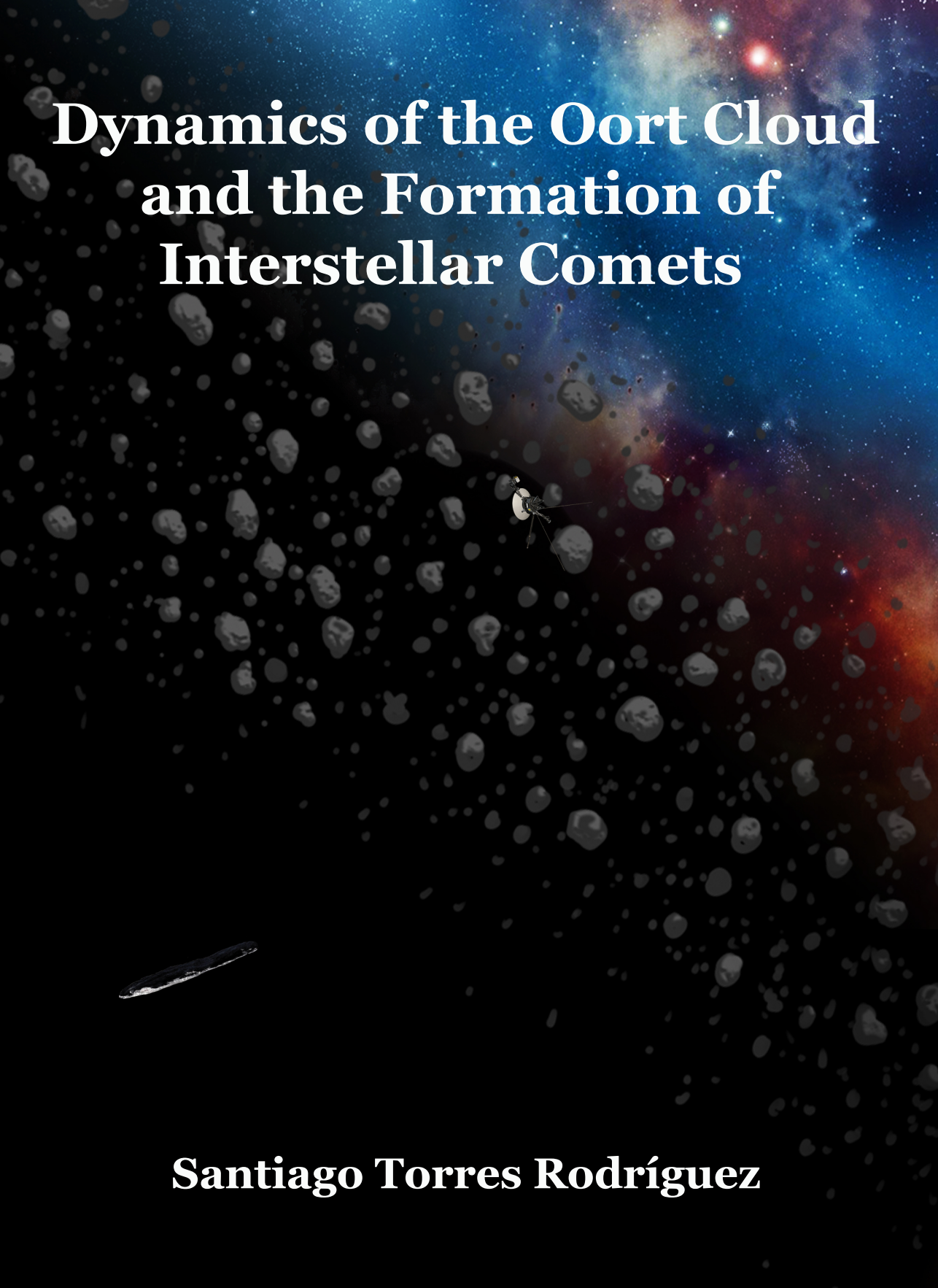


The handle <http://hdl.handle.net/1887/87515> holds various files of this Leiden University dissertation.

Author: Torres Rodriguez, S.

Title: Dynamics of the Oort cloud and formation of interstellar comets

Issue Date: 2020-04-30



Dynamics of the Oort Cloud and the Formation of Interstellar Comets

Santiago Torres Rodríguez

Cover:

-Design: Santiago Torres Rodríguez

-Advisor: Christian Chávez López

-Image credit: NASA, ESO, ESA, Science Photo Library

ISBN: 978-94-028-2033-1

Dynamics of the Oort Cloud and Formation of Interstellar Comets

Proefschrift

ter verkrijging van
de graad van Doctor aan de Universiteit Leiden,
op gezag van Rector Magnificus prof.mr.C.J.J.M. Stolker,
volgens besluit van het College voor Promoties
te verdedigen op donderdag 30 april 2020
klokke 13:45 uur

door

Santiago Torres Rodríguez
geboren te Mexico City
in 1987

Promotor: Prof. dr. Simon Portegies Zwart (Sterrewacht Leiden)
Co-promotor: Dr. Anthony Brown (Sterrewacht Leiden)

Promotiecommissie: Prof. dr. H.J.A. Rottgering (Sterrewacht Leiden)
Prof. dr. I.A.G. Snellen (Sterrewacht Leiden)
Prof. dr. M.R. Hogerheijde (Sterrewacht Leiden/UvA)
Dr. R.A. Capuzzo Dolcetta (Sapienza University of Rome)
Dr. J. Zuluaga (University of Antioquia)

To Bárbara

L'ordre est le plaisir de la raison, mais le désordre est le délice de l'imagination.
—Paul Claudel, 1929.

Contents

1	Introduction	1
1.1	Comets	5
1.1.1	Short period comets	5
1.1.2	Long period comets	6
1.1.3	Interstellar comets	10
1.2	Methods and data	12
1.2.1	Gaia	12
1.2.2	AMUSE	13
1.3	Thesis	17
2	The origin of interstellar asteroidal objects like 1I/2017 U1 'Oumuamua	23
2.1	Introduction	25
2.2	'Oumuamua as a rare object	26
2.2.1	Observational constraints	26
2.2.2	Dynamical ejection from the Sun's Oort cloud	27
2.2.3	Origin from the Oort cloud of another star	28
2.2.4	Origin from the debris disc of another star	29
2.3	Where did 'Oumuamua come from	30
2.3.1	An origin from the solar neighbourhood	30
2.3.2	An origin from beyond the solar neighbourhood	31
2.4	Discussion and conclusions	36
3	Galactic tide and local stellar perturbations on the Oort cloud: creation of interstellar comets	39
3.1	Introduction	41
3.2	Model for stellar encounters	44
3.2.1	Analytic model	44
3.2.2	Perturbations on the Oort cloud	46
3.3	Close encounters with the solar system	48
3.3.1	Observational model	49
3.3.2	Stellar encounters with the Solar System	53
3.3.3	The case of GJ 710/HIP 89825	58

Contents

3.4 Dynamical evolution of the Oort cloud 61
3.4.1 Numerical model 61
3.4.2 Galactic tide and Gaia star perturbation 63
3.5 Summary and Conclusions 70

4 Dynamical evolution of the solar system debris disk in its birth cluster 75
4.1 Introduction 77
4.2 Numerical implementation 79
4.3 Effect of stellar encounters on the early solar system 82
4.3.1 Extended models 82
4.3.2 Compact models 97
4.3.3 Extended vs compact models and the Oort cloud . . . 110
4.4 Interstellar objects 111
4.5 Summary and Conclusions 114

5 Dynamical evolution of exo-Oort clouds around the Sun’s closest neighbour stars due to local stellar perturbations and the Galactic tidal field 117
5.1 Introduction 119
5.2 Close stellar encounters experienced by the Sun’s nearest neighbours 121
5.3 Dynamical evolution of exo-Oort clouds of the Sun’s neighbour stars 132
5.3.1 TICs/ISOs in the solar neighbourhood 141
5.4 Summary and Conclusions 142

Bibliography 147

Summary 157

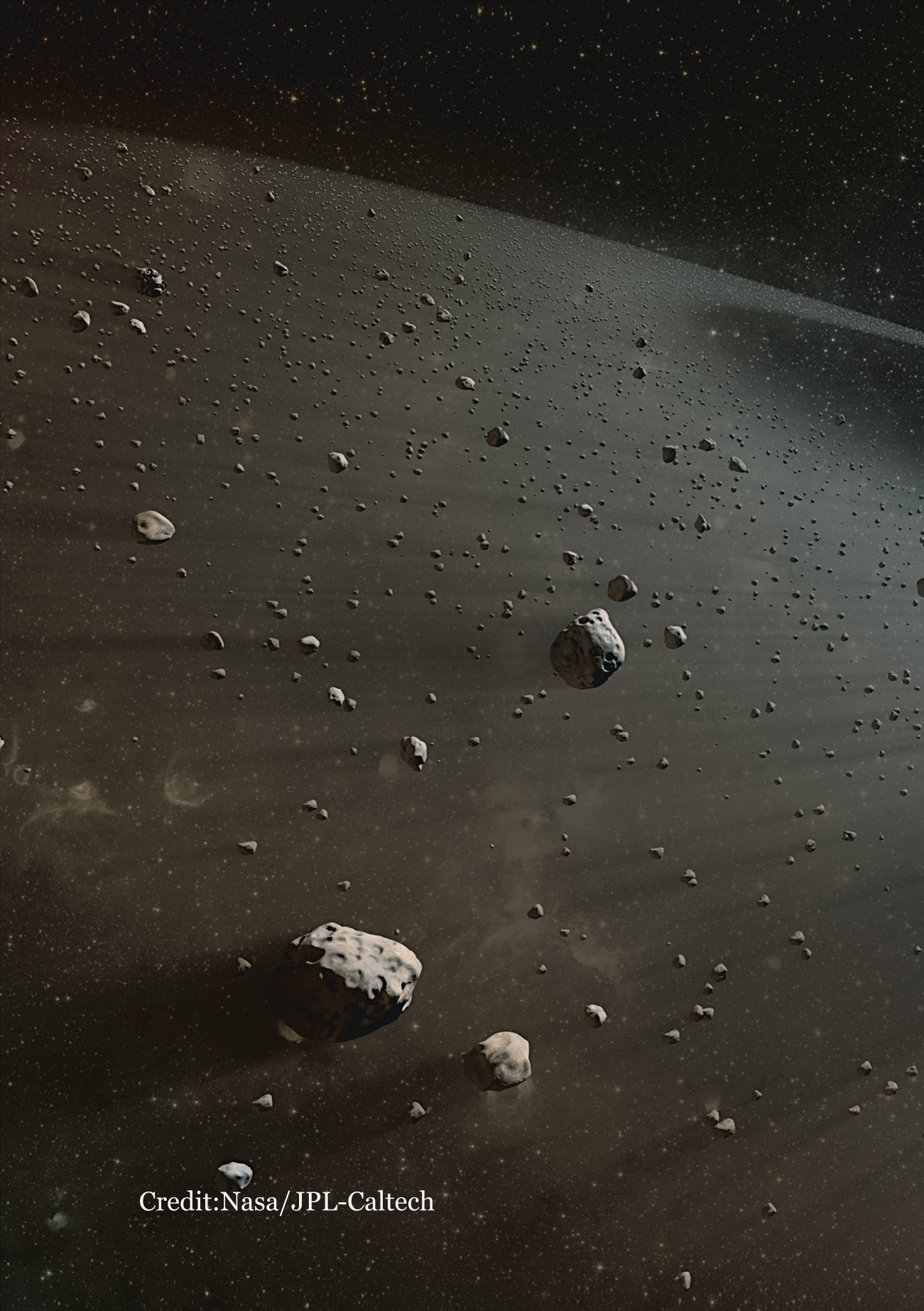
Resumen 163

Samenvatting 169

List of publications 175

Curriculum Vitae 179

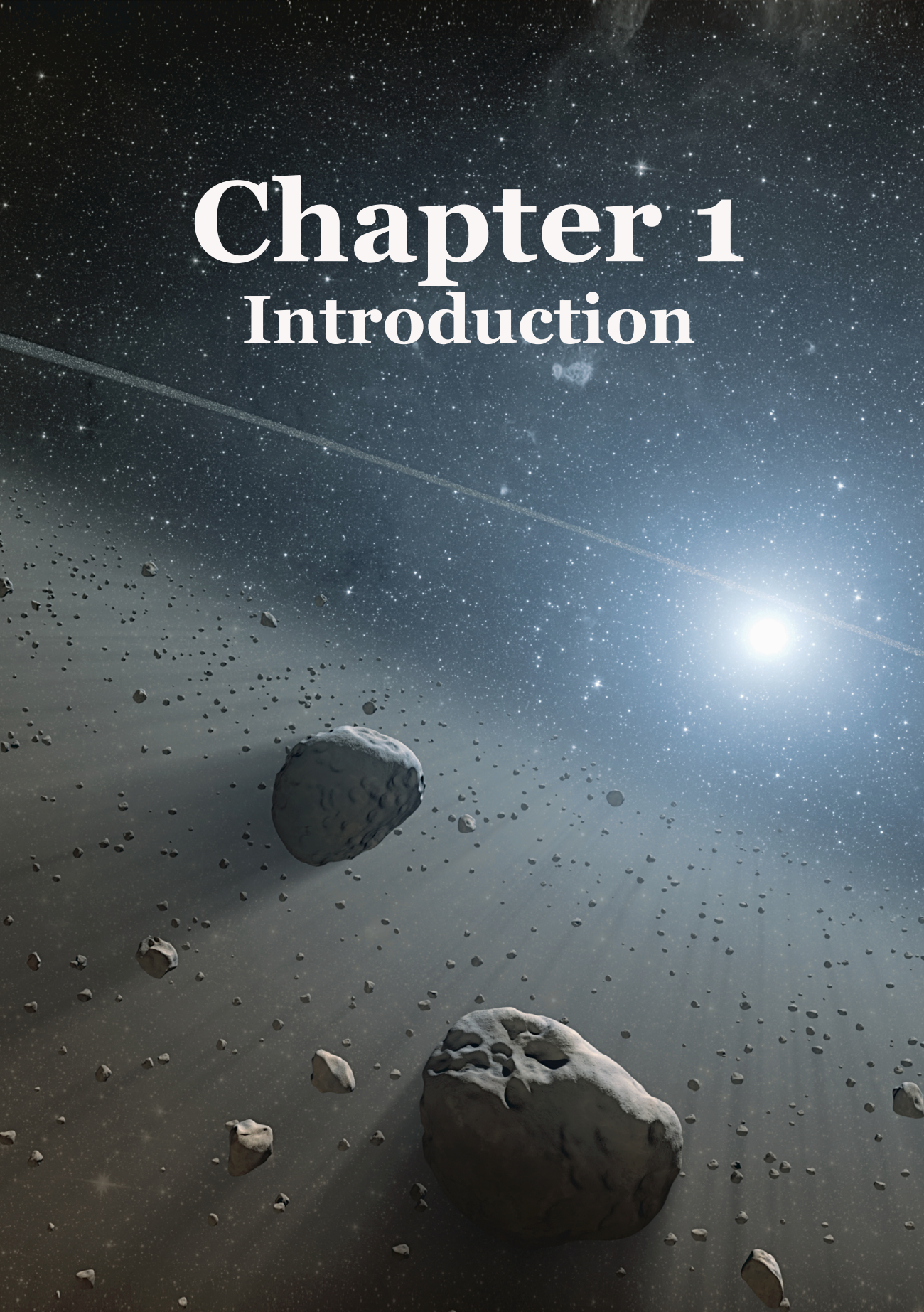
Acknowledgements 183



Credit:Nasa/JPL-Caltech

Chapter 1

Introduction



1 Introduction

The solar system was formed approximately 4.56 billion years ago. Despite the numerous theories that have been developed over the years, the formation and evolution of the solar system still remains unclear (Pfalzner et al. 2015, and references therein). However, several advances have been made in our knowledge about the solar system. The most accepted theory about its formation and early evolution describes a gravitational collapse of a dense cloud of interstellar gas and dust. The conservation of angular momentum induced a rapid rotation of the collapsing cloud, flattening it until it became a protoplanetary disk. In the central, most dense region of the disk, a star was created — our Sun. In a similar manner, clumpy structures developed in the disk. These eventually grew to form the planets, dwarf planets and moons. The leftovers of this process led to the formation of small bodies, such as asteroids and comets. This is how the five main types of objects in the solar system were formed; the Sun, planets, dwarf planets, moons, and minor bodies (asteroids and comets). A schematic representation of the solar system is shown in Fig. 1.1.

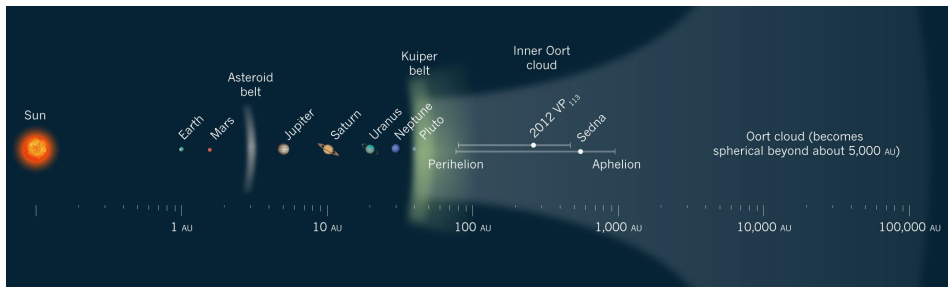


Figure 1.1: The solar system. Taken from Schwamb (2014).

The Sun is the main object in the solar system. It is a yellow dwarf star with a mass of $\sim 2 \times 10^{30}$ kg or $1 M_{\odot}$ and temperature at the centre of $\sim 1.5 \times 10^7$ K. It is mainly made up of hydrogen ($\sim 73\%$) and helium ($\sim 25\%$), and it is located at the centre of the solar system where its gravity holds the entire system together. Planets are celestial bodies that orbit around the Sun. They are sufficiently massive for the gravitational forces that hold them together to be strong. These strong forces cause the interior of planets to be hot and melt, which in turn leads to their characteristic round shape. Additionally, planets cleared their orbit from smaller bodies. There are eight planets in the solar system: Mercury, Venus, Earth, Mars, Jupiter, Saturn, Uranus and Neptune. Planets are located in the inner part of the solar system, which is commonly called the planetary region. The

planetary region extends from the innermost planet (Mercury) located at 0.38 au from the Sun to the outermost one (Neptune) at 30 au.

Moons are celestial bodies that orbit around a planet or dwarf planet. To date, 182 moons have been discovered in the solar system. In contrast to planets, dwarf planets (e.g., Pluto, Ceres, Makemake) do not have a sufficiently strong gravitational field to empty their surroundings of small objects. They are therefore found in regions full of smaller rocks, such as in the asteroid belt and in the transneptunian region. The asteroid belt is situated between the orbits of Mars and Jupiter. The transneptunian region extends from the orbit of Neptune (~ 30 au) out to the outer edge of the scattered disk, around 100 au from the Sun.

Finally, the minor bodies are divided in two categories: asteroids and comets. They are located in three main regions: the asteroid belt, Kuiper belt/scattered disk and the Oort cloud. Asteroids are small and often irregularly shaped celestial bodies mainly found in the asteroid belt. Comets, on the other hand, are icy objects that belong to the Kuiper belt/scattered disk and the Oort cloud. The Kuiper belt/scattered disk, is the source of short-period comets (comets with orbits lasting less than 200 years). The Kuiper belt extends from 30 au to ~ 50 au, while the scattered disk extends from ~ 50 au to ~ 100 au. The Oort cloud, the source of long-period comets (comets with orbits lasting more than 200 years), starts right after the scattered disk and extends half the way to the nearest star to the Sun, Proxima Centauri (Oort 1950).

To better understand the formation and evolution of the solar system, dynamical models are needed. In particular, the study of comets can reveal critical pieces of information about this process. The orbits of the comets in the inner part of the Oort cloud form a frozen record of the evolution of the solar system. At present, comets in this region are located at such large distances from the center of the solar system that perturbations from planets are negligible. They are rather at risk to be ripped away by passing stars or even the gravitational field of the Milky Way itself. Especially comets in the outermost regions are sensitive to such external influence, already during the early phases of the formation of the solar system (e.g., Torres et al. 2019a,b). These external influences have been shaping the Oort cloud over its history, producing comet showers reaching into the planetary region and stripping comets out into the interstellar space, forming interstellar comets.

Studying the dynamical evolution of comets can help us to constrain and to understand the formation and evolution of the solar system. Both

1 Introduction

the history of encounters between the solar system and nearby stars and the effect of the tides from the Galaxy are key components. The current distribution of nearby stars and the Galactic potential are reasonably well known. The Gaia mission (Gaia Collaboration et al. 2018, 2016) delivered a magnitude-limited complete sample of nearby stars. These stars dominate the local Galactic potential, and they give rise to occasional close encounters. Therefore, data from Gaia can be used as templates for the initial conditions in detailed simulations at different moments in time. Combining analytical, observational and numerical techniques are the key components to constrain and better understand the formation and dynamical evolution of the solar system.

In this thesis, I explored the formation and dynamical evolution of comets in the Kuiper belt/scattered disk and the Oort cloud, accounting for external perturbations such as passing stars and the galactic tidal field. As a consequence of these perturbations, the formation and evolution of interstellar comets were investigated. This thesis is divided into four main chapters. Chapter 2 treats the origin of the interstellar object 1I/2017 U1 ‘Oumuamua by comparing estimates based on observations with simulations (Sect. 2). Chapter 3 focuses on the dynamical evolution of the Oort cloud after the interaction with passing stars and the Galactic tidal field (Sect. 3). In Chapter 4, I studied the formation and evolution of the solar system’s Kuiper belt/scattered disk and Oort cloud in the early stages of their formation, when the Sun was still in its birth cluster (Sect. 4). Finally, Chapter 5 explores the formation of interstellar comets from the neighbouring stars of the Sun (Sect. 5). A summary of the main results of each chapter can be found in Sect. 1.3. The key research questions addressed in this thesis are:

1. What is the effect of multiple stellar encounters and the Galactic tidal field on comets in Oort cloud-like structures? (Chapters 3 and 5).
2. Was the formation of the Oort cloud triggered by planet-disk interaction and stellar encounters in the early solar system? (Chapter 4).
3. Where do interstellar comets come from and how do they form? (Chapters 2 and 4).

Comets

Comets are icy objects that travel from the outer parts of the solar system (beyond the orbit of Neptune) into the planetary region. Once they approach the Sun, they are heated by solar radiation and become active. The sublimation of water ice produces a tail composed of dust and gas, commonly known as a coma (Nesvorný 2017). The study of comets started thousands of years ago when the first civilizations painted on the walls of caves what now can be interpreted as a comet. There are three main categories of comets: short period (Sect. 1.1.1), long period (Sect. 1.1.2), and interstellar (Sect. 1.1.3). The study of comets can reveal key processes during the formation and early evolution of the solar system. Chemical studies indicated that comets carry organic molecules and share the same origin (Eistrup et al. 2019). They have, therefore, been considered as building blocks of life. This view is now also supported by the Rosetta mission (Glassmeier et al. 2007; Alves et al. 2015), which recently successfully visited a comet (67/P Churyumov-Gerasimenko). Rosetta discovered amino acids, glycine and phosphorus (all key components of DNA and cell membranes) in the coma of 67/P Churyumov-Gerasimenko (Altwegg et al. 2016) along with other organic compounds (Alves et al. 2015; Capaccioni et al. 2015). These results suggested a strong possibility that comets play an important role in the emergence of life on Earth (e.g., Rettberg et al. 2002; Horneck et al. 2010; Wickramasinghe 2011). With the recent discovery of the first interstellar comet (1I/Oumuamua, Williams 2017) and the indications of water on the second (2I/Borisov, McKay et al. 2019), a new era in the study of comets has begun.

1.1.1 Short period comets

Comets with orbital period (P) shorter than 200 yr are classified as a short-period comet (SPCs). Short-period comets are subdivided into two types: Halley-type comets (HTCs) and Jupiter family comets (JFCs) (Morbidelli 2005; Nesvorný et al. 2017). These classifications are mainly based on the period of the comets, $P_{JFC} < 20$ yr and $P_{HTC} > 20$ yr). In the solar system, there are 393 short-period comets confirmed (Minor Planet Center 2020). The primary source of SPCs is the Kuiper belt and scattered disk, also known as the transneptunian region (Fig. 1.2).

1 Introduction

Figure 1.2: Artistic representation of the Kuiper belt. Taken from ESA.

The formation and dynamical evolution of comets in the transneptunian region was mainly due to giant planets (Jupiter, Saturn, Uranus, and Neptune). The giant planets of the solar system did not occupy their current orbits after the gas was removed from the protoplanetary disk of the solar system. Several theories have been proposed to explain the migration of the giant planets. Fernández & Ip (1984) and later Malhotra (1993) showed that a disk of planetesimals around the giant planets would have driven the migration. However, a smooth planetesimal-driven migration could not explain several aspects of the orbital distribution of the Kuiper belt and scattered disk. Later, Thommes et al. (1999) showed that a dynamical instability produced among the giant planets would lead to an excitation of the Kuiper belt, which, in turn, forced the planets to their current orbits. A culmination of all these theories led to the development of the classic *Nice Model* (named after the city Nice in France, Gomes et al. 2005; Tsiganis et al. 2005; Morbidelli et al. 2005).

According to the Nice Model, the giant planets formed in a compact configuration with Jupiter around 5.5 au. Saturn was placed in such a way that it was slightly interior to the 2:1 mean motion resonance between itself and Jupiter. Neptune and Uranus were placed in orbits around 11–15 au. Simulations showed (Morbidelli et al. 2007) that a disk with a mass of $\sim 35 M_{\oplus}$ led to a slight migration of the orbits of Jupiter and Saturn until they crossed the 2:1 mean motion resonance, which made the system unstable. As a result of this instability and the interaction between the giant planets and the planetesimal disk, the short-period comets were formed

1.1.2 Long period comets

The outer regions of the solar system are populated by a large number of comets with period $P > 200$ yr, known as long period comets (LPCs). Beyond the Kuiper belt/scatter disk and almost extending to the nearest stars (out to 100,000 au), resides the Oort cloud, the origin of LPCs (Fig. 1.3). The Oort cloud was proposed in the late 1950s, by the Dutch astronomer Jan Hendrik Oort at the Sterrewacht Leiden. Oort (1950) realized that long period comets, with semi-major axes (a) larger than 40 au bound to the Sun must come from an area well beyond Neptune. Oort (1950) pointed out that there is a spike in the distribution of $1/a$ of the long period comets with an

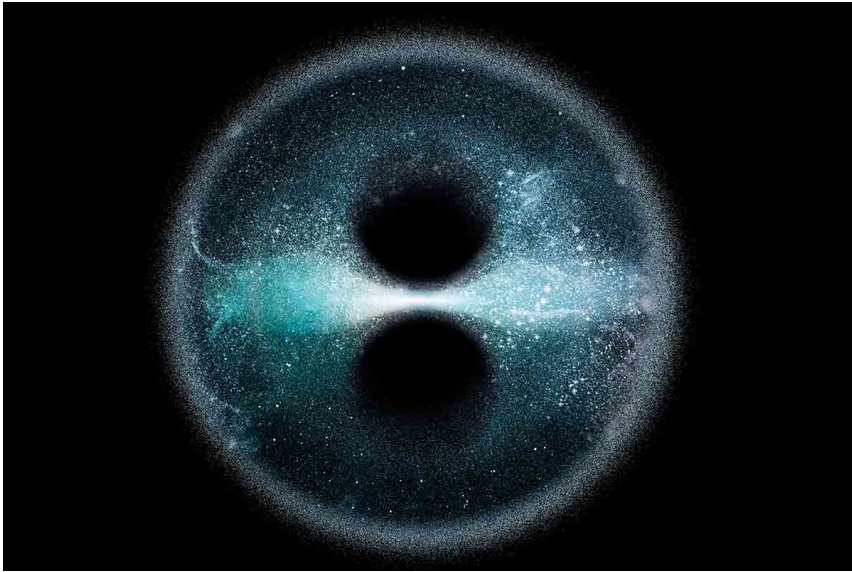


Figure 1.3: Artistic representation of the Oort cloud. Taken from Science Photo Library / Claus Luna.

$a < 10^4$ au (see Fig. 1.4 taken from Wiegert & Tremaine 1999). The LPCs also showed an isotropic distribution of their orbital inclinations. These findings argue for the existence of a reservoir of objects in quasi-spherical symmetry surrounding the solar system.

The estimated number of LPCs is around 1×10^{12} with a total mass of $\sim 4 \times 10^{25}$ kg (Morbidelli 2005), however, only about 1,065 have been observed (Królikowska & Dybczyński 2019). The Oort cloud is divided into two main regions: the *inner* one is usually reserved for comets that reside in the cloud with semi-major axes $a < 20,000$ au, which are invisible unless there is a comet shower; and the *outer* that refers to comets with semi-major axes $a > 20,000$ au. The shape of Oort cloud has remained unobserved to date, but its existence is derived from observations of LPCs.

Shortly after the solar system was formed, small bodies called planetesimals remained among the giant planets region ($5 < a < 30$ au). The giant planets scattered the planetesimals throughout the solar system until they reached eccentric orbits with large semi-major axis, but with a perihelion distance still in the planetary region. Those that reached a semi-major axis of $\sim 10,000$ au started to feel a Galactic tide strong enough to modify their orbit on a timescale of an orbital period. Scattering by planets

1 Introduction

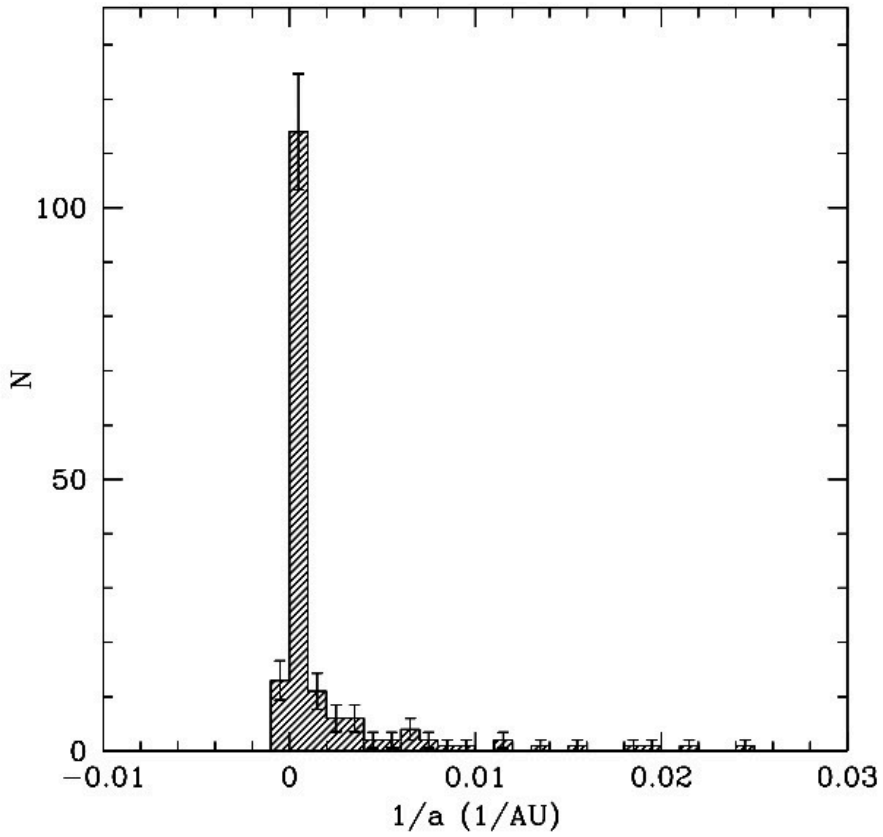


Figure 1.4: The differential distribution of LPCs as a function of the inverse semi-major axis. The big spike at $1/a < 10^{-4}$ is due to the "new comets", and is usually called the Oort spike (taken from Wiegert & Tremaine 1999).

alone should distribute planetesimals in a disk-like structure, close to the ecliptic plane (path of the Sun’s motion as seen from the Earth). However, since the long-period comets are only loosely bound to the solar system, their orbits are significantly influenced by the Galactic tide, pushing them to large eccentricity e and inclinations i . Their perihelion distances were lifted beyond the planets’ reach, thus they could not be scattered anymore and they became Oort cloud objects (Brasser & Morbidelli 2013, and references therein).

The evolution of the comets in the Oort cloud is strongly affected by the overall gravitational field due to mass distribution in the galaxy (galactic tide), sporadic passing stars, and giant molecular clouds, pulling up the comet perihelion out of the planetary region (e.g., Heisler & Tremaine 1986; Rickman 2014; Torres et al. 2019b). Passing stars change the perihelion distances of LPCs much more than they change the overall size of their orbit, deflecting the cometary trajectories and injecting the comets into the inner solar system ((Morbidelli & Nesvorny 2019)). In practical terms, the role of passing stars is to reshuffle the comet distribution in the Oort cloud, and to refill the high inclination region where comets are pushed into the planetary region by the Galactic disk’s tide.

On the other hand, comets with a high inclination relative to the galactic plane under the effect of the tides from the galaxy increase their orbital eccentricity and decrease their perihelion distance q , so that they become planet-crossers. If this evolution is fast enough that q decreases from beyond 10 au to less than $\sim 3\text{ au}$ within half an orbital period, the comet becomes active during its first dive into the inner solar system without having interacted with Jupiter or Saturn during its previous orbits, namely it appears as a “new comet” (Dones et al. 2004). The rate at which comets are fed into the planetary region from the Oort cloud due to the galactic tide is probably slightly larger than the influx due to stellar passages (Heisler & Tremaine 1986). Assuming that the galaxy has a disk-like structure, the galactic tide would have a *disk* and *radial* force components. The z component of the *disk* causes the oscillation in and out of the planetary region in q , with a period of the order of 1 Gyr for comets with $a \sim 10,000\text{ au}$ and initial $q \sim 25\text{ au}$. The *radial* component breaks conservation of the component of a comet’s angular momentum perpendicular to the galactic plane, modulating the cometary perihelion distances (Heisler & Tremaine 1986; Duncan 2008). In general terms, the external perturbation of the Oort cloud delivers a rate of comets to the planetary system due mainly to

1 Introduction

galactic tides and during rare comet showers caused by an unusually close stellar passage.

1.1.3 Interstellar comets

Interstellar objects (ISOs) are asteroids or comets located in the interstellar space and are not bound to any stellar system. Before becoming ISOs, they most probably belonged to the reservoir of asteroids or comets in other planetary systems like the main asteroid belt, Kuiper belt and Oort cloud in our solar system. The origin of ISOs can be explained by several scenarios, like giant planet ejection, the mass loss associated with the creation of white dwarfs and binary systems or stripped from another star (e.g., Portegies Zwart et al. 2018; Bannister et al. 2019). In our solar system, there is two detected ISOs up to date, 1I/'Oumuamua (Williams 2017; Meech et al. 2017, Fig. 1.5 top panel) and 2I/Borisov (Borisov 2019, Fig. 1.5 bottom panel). However, the number density of ISOs in the interstellar space is expected to be large, about 0.1 per cubic au (Portegies Zwart et al. 2018; Do et al. 2018).

1I/'Oumuamua was discovered on 2017 October 19 by the PanSTARRS Near-Earth Object survey (Meech et al. 2017). Its closest approach to the Earth was at 0.16 au. The surface composition of 'Oumuamua showed red features at optical wavelengths of $\sim 10\text{-}20\%/100\text{ nm}$ (Bannister et al. 2019), similar to minor bodies in the solar system and consistent with organic-rich surfaces. The extreme brightness variations (a factor of ten, >2.5 magnitudes) implied that the core of 'Oumuamua was rotating in an excited state and its shape was highly elongated (Meech et al. 2017). Even though 'Oumuamua looked like a minor body from the solar system (due to its red colour), its highly eccentric orbit ($e \simeq 1.2$) and high velocity at infinity $V \simeq 26\text{ km s}^{-1}$ (Williams 2017) reveal its interstellar origin. On the other hand, 2I/Borisov was discovered on 2019 August 30. The surface composition showed a similar colour to that of 'Oumuamua, however, 2I/Borisov was found to be actively outgassing (Jewitt & Luu 2019). 2I/Borisov's trajectory is extremely hyperbolic ($e \simeq 3.36$) with a high velocity at infinity $V \simeq 32.2\text{ km s}^{-1}$ (Borisov 2019; Jewitt & Luu 2019). 'Oumuamua and Borisov's origin is still unknown, however, their high velocity implies that it was ejected during its host star's protoplanetary phase, and therefore is part of the left-over debris of star and planet formations processes in the galaxy (e.g., Portegies Zwart et al. 2018; Bannister et al. 2019; Higuchi & Kokubo 2019).



Figure 1.5: Top: artistic representation of 1I/'Oumuamua (taken from ESO/M. Kornmesser). Bottom: image of 2I/Borisov (taken from NASA, ESA, and D. Jewitt (UCLA)).

Methods and data

1.2.1 Gaia

The European Space Agency's Gaia Spacecraft¹ launched in December 2013 (Perryman 2003; Gaia Collaboration et al. 2016, 2018): aims to make the most extensive and precise three-dimensional map of our Galaxy. This is done by surveying an unprecedented more than 1 billion stars, with about 70 observations of each star. Gaia provides us with the astrometric properties (positions and motion on the plane of the sky) of approximately 1 billion stars, radial velocities of about 150 million stars, and physical parameters like temperature and chemical composition of observed stars, extra-solar planets, near-Earth objects, among several other objects in the Galaxy. The scientific goals of the mission mainly focus on the study of the structure and dynamics of the Galaxy, star formation history, stellar astrophysics, photometric variability, planetary systems, solar system, and fundamental physics (Perryman 2003).

In the particular case of the solar system, Gaia is detecting nearly all of the local stellar systems within 50 pc from the Sun (compared to the 20% identified with Gaia's predecessor Hipparcos (Perryman et al. 1997; Anderson & Francis 2012)). This allows the trajectories of a large number of stars in the solar neighbourhood to be traced back far in time. The accurate data from Gaia is cornerstone for the work presented in this thesis. With this information, I have synthesized an accurate census of the distribution and motions of stars in the solar neighbourhood. With this, in turn, I could determine the frequency and encounter history of nearby stars and the solar system and their impact on the comets of the Oort cloud.

The first Gaia data release (Gaia DR1, Gaia Collaboration, Brown et al. 2016) provided astrometry and photometry for over 1 billion sources with magnitude brighter than 20 and, positions, parallaxes, and proper motions for about 2.5 million Tycho-2 stars (TGAS, Michalik et al. 2015).

To estimate the current 3-dimensional positions and velocities of stars, I combined their positions, parallaxes and proper motions from the TGAS catalogue with their radial velocities presented in catalogues from RAVE-DR5 (Kunder et al. 2017), Geneva-Copenhagen (Nordström et al. 2004), Pulkovo (Gontcharov 2006), and XHIP (Anderson & Francis 2012) catalogues. To identify the past and future stellar encounters with the solar

¹<http://sci.esa.int/gaia/>

system, I then used these 3D positions and velocities for the stars in the immediate solar neighbourhood (< 30 pc) to compute their trajectories backwards and forwards in time (± 10 Myr). The orbital integration of the stars was performed using an axisymmetric Galactic potential included in the module *Galaxia* in the AMUSE framework (Portegies Zwart & McMillan 2018).

The outcome of these simulations resulted in a catalogue of nearby stars to the Sun in the last 10 Myr and the coming 10 Myr (Torres et al. 2018). This catalogue served as a base to determine with more accuracy the closest encounters with the solar system. Particularly, the star Gliese 710 was found to have its closest approach to the Sun in $1.35 Myr$ at a distance of 0.06 pc (Torres et al. 2018) instead of 0.33 pc as it was predicted using Hipparcos data (e.g., Jimenez-Torres et al. 2011). Additionally, the catalogue of nearby stars provided the initial conditions necessary for calculating the close encounters that 1I/'Oumuamua had in the past 10 Myr before encountering the solar system (Portegies Zwart et al. 2018).

With the second release of Gaia (Gaia DR2, Gaia Collaboration et al. 2018), the accuracy of the data and the number of sources increased significantly with respect to the first data release. About 1.7 billion sources and approximately 7.2 million radial velocities were presented in the DR2 of Gaia. I updated the catalogue of stellar encounter (Torres et al. 2018, 2019a) with the more precise data from Gaia DR2 and now also including radial velocities from the catalogues of RAVE-DR5 (Kunder et al. 2017), GALAH DR2 (Buder et al. 2018), LAMOST DR3 (Zhao et al. 2012), APOGEE DR14 (Abolfathi et al. 2018), and XHIP (Anderson & Francis 2012). I used this catalogue, to study the dynamical evolution of the comets in the Oort cloud (Sect. 3) and the exo-Oort clouds around Sun's neighbour stars (Sect. 5) accounting for the cumulative effect of passing stars and the Galactic tidal field.

1.2.2 AMUSE

The Astrophysical Multi-purpose Software Environment or AMUSE² (Portegies Zwart & McMillan 2018) is an open source component library and a community effort with the main development by a team at Leiden Observatory. In AMUSE, existing numerical codes are combined into one single system employing a framework written in Python. AMUSE is made for performing astrophysical simulations and it is primarily created for the

²<https://amusecode.github.io>

1 Introduction

fields of gravitational dynamics, stellar evolution, hydrodynamics and radiative transfer with Python framework. The AMUSE architecture is based on three main components: the user script, AMUSE library and the community codes. The user script is written by the user and acts as the interface to the AMUSE framework. The AMUSE library provides an object-oriented interface on top of the legacy codes, created for unit handling and data conversion. It contains the state engine and the associated data repository. A few examples of community codes that are included in AMUSE are Hermite0, Bonsai, Kepler, Mercury, Gadget-2, Huayno, Twobody, among several others. The user script and the AMUSE library that communicates with the code to perform the calculations. Overall, AMUSE is developed so that several different codes can be used to model and give a more complete picture of one astrophysical problem.

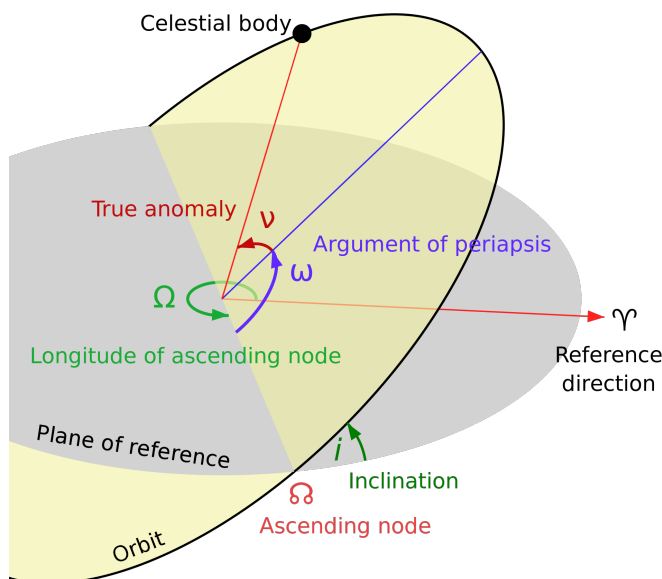


Figure 1.6: Orbital elements for a celestial body. Taken from Science Photo Library.

Taking advantage of the flexibility of AMUSE to use different codes to solve multiple physical problems, all the numerical tools of this thesis were built within the AMUSE framework. The community codes used in this work are: Kepler, ABIE, LonelyPlanets, Rebound, Gala, NBODY6++GPU, and Galaxia. Below I summarise the numerical tools developed and the codes used for the chapters in this thesis.

Chapter 2 – To find the possible home for 1I/'Oumuamua, I used the code *Galaxia* (Martínez-Barbosa et al. 2016) to perform the orbital integration of the stars within 50 pc from the Sun and 'Oumuamua. *Galaxia* is a galaxy model which contains axisymmetric and non-axisymmetric structures of the Milky Way. To perform our calculations, I adopted an analytic axisymmetric model of the Galaxy accounting for a spherical nucleus and bulge (Hernquist 1990), an axisymmetric disk (Miyamoto & Nagai 1975; Bovy 2015), and a spherical dark matter halo (NFW, Navarro et al. 1996). The galactocentric position of the Sun and the local circular velocity parameters were taken from Reid et al. (2014): $Z_{\odot} = 27$ pc, $R_{\odot} = 8.34$ kpc, and $V_{c,\odot} = 240$ km/s. The peculiar velocity of the Sun was adopted from Schönrich et al. (2010): $(U_{\odot}, V_{\odot}, W_{\odot}) = (11.1, 12.24, 7.25)$ km/s.

Chapters 3 and 5 – I explored the dynamical evolution of the comets in the Oort cloud under the effect of passing stars and the Galactic tidal field. To do this, I first constructed an artificial Oort cloud. I used the package *Kepler* to calculate the orbital elements and perform the orbit integration of the particles in an isotropic and spherical distribution emulating the Oort cloud. The main function in the user script was built in such a way that it returns relative positions and velocity vectors in cartesian coordinates for the particles with orbital elements –semi-major axes, eccentricities, and mean anomalies. I considered that the 3D orientation of orbits were random (inclination, the longitude of ascending node and argument of periapsis). The distribution of the particles in the Oort cloud are set spherically symmetric and isotropic following a uniform distribution in the orbital elements $\cos i, \varpi, \Omega$, and M (Fig. 1.6). The initial eccentricities, e , are selected with a probability density distribution $p(e) \propto e$ and the perihelia, q , are chosen outside of the planetary region ($q > 32$ au). The semi-major axes, a , are distributed proportional to $a^{-1.5}$ over the range 3×10^3 - 10^5 au.

Then using the GPU-accelerated direct N-body code *ABIE* (Cai et al. in prep) and the Astropy-affiliated python package for galactic dynamics *Gala* (Price-Whelan 2017), I integrated the orbits of the particles in the Oort cloud for a period of 20 Myr. *ABIE* and *Gala* were coupled in such a way that *ABIE* advances the positions of the Oort cloud particles and *Gala* calculates the accelerations on each particle due to the Galactic tidal field, based on the positions provided by *ABIE*. The calculated accelerations are subsequently inserted into the Gauss-Radau integrator in *ABIE* as additional forces. Additionally, the trajectories of nearby stars and their effect on the Oort cloud was calculated in *ABIE* by providing their positions and velocities as input.

1 Introduction

Chapter 4 – To study the dynamical evolution of the solar system debris disk in a dense environment we used the codes `LonelyPlanets` which combines `NBODY6++GPU` (Wang et al. 2015) and `Rebound` (Rein & Liu 2012). I first used `NBODY6++GPU` with a Plummer sphere model (Plummer 1911) to simulate the open cluster, with an initial mass function ranging from 0.08 to $100 M_{\odot}$ (Kroupa 2001), 2000 stars, and a virial radius of 1 pc. Using `LonelyPlanets` the solar system is constructed by placing the host star (a Sun-like star with $1 M_{\odot}$), the giant planets (Jupiter, Saturn, Uranus, and Neptune), and a debris disk of 2000 test particles. Then the solar system and the cluster are evolved for 100 Myr. During this calculation, the code uses a data structure in a space with k dimensions (K-D tree algorithm) to find the five closest stars to the Sun at any given time. These five stars and the solar system are then evolved together using the `IAS15` (Rein & Spiegel 2014) integrator, thus simulating the effect of encounters between the solar system and stars in the cluster.

Thesis

The major results of this thesis can be summarized in three main parts. The formation and density distribution of interstellar comets (Chapter 2 and Chapter 4). The prediction of a new type of comets: the transitional interstellar comets (Chapter 3 and Chapter 5). And, a new mechanism for the formation and evolution of short and long-period comets (Chapter 4). Below, I summarize each chapter.

Chapter 2 *The origin of interstellar asteroidal objects like 1I/2017 U1 'Oumuamua* (Portegies Zwart, Torres et al. 2018). I studied the origin of the interstellar object 1I/ 'Oumuamua by comparing estimates based on observations with simulations. Using the astrometric data from Gaia-TGAS (Gaia Collaboration, Brown et al. 2016), I integrated the orbit of 'Oumuamua and all the stars within 50 pc from the Sun. I find that about 1.3 Myr ago 'Oumuamua passed nearby the star HIP 17288 (label a in Fig. 1.7), and had three other close encounters during its journey towards the Sun (Fig. 1.7). I explored the different scenarios of formation for 'Oumuamua and concluded that objects like 'Oumuamua are formed in the debris disc as a leftover from the star and planet formation process, and subsequently liberated. I find that the mean galactic density of interstellar comets in the solar neighbourhood is $\sim 10^{14}$ per cubic parsec, which means that we expect about 2–12 such visitors per year within 1 au from the Sun.

Chapter 3 *Galactic tide and local stellar perturbations on the Oort cloud: creation of interstellar comets* (Torres et al. 2019a). Using the positions, parallaxes and proper motions from the Gaia survey and combining them with radial velocities from RAVE-DR5 (Kunder et al. 2017), GALAH DR2 (Buder et al. 2018), LAMOST DR3 (Zhao et al. 2012), APOGEE DR14 (Abolfathi et al. 2018), and XHIP (Anderson & Francis 2012). I constructed a catalogue of the Sun's neighbour stars. Then, I calculated the closest encounters that the Sun has had with other stars in the recent past and will have in the near future (Torres et al. 2018, 2019a). I find that the star GJ710 will approach the Sun in 1.3 Myr at the distance of 0.06pc instead of 0.3pc as predicted by previous studies (e.g., Dybczyński & Berski 2015, and references therein). Then, using the catalogue of nearby stars, I studied the

1 Introduction

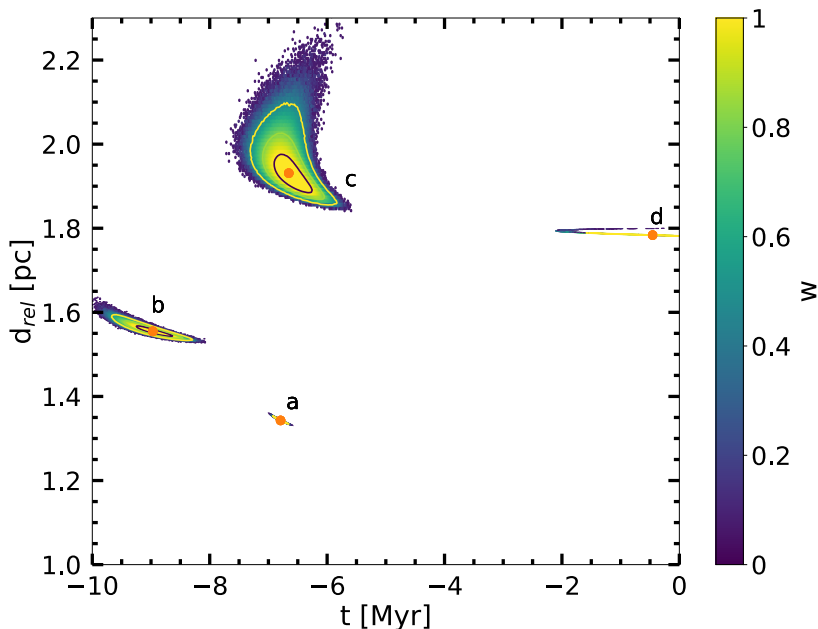


Figure 1.7: Probability density distribution in time of closest approach (t) and relative distance (d_{rel}) between 'Oumuamua and the four closest stars. Labels a (GDR1 5108377030337405952), b (GDR1 4863923915804133376), c (GDR1 5140501942602437632), and d (GDR1 1362592668307182592) corresponds to the closest star to 'Oumuamua. Adapted from Portegies Zwart, Torres et al. (2018).

dynamical evolution of comets in the Oort cloud, accounting for the perturbation of the galactic tidal field and the cumulative effect of nearby passing stars. I find that the comets at the edge of the Oort cloud (80,000-100,000 au) get heavily perturbed and, as a result, the semi-major axis of $\sim 1.1\%$ of the comets have increased to extend into interstellar regions (Fig. 1.8). Since the comets are still bound to the solar system, we consider them *transitional interstellar comets* (TICs). The first TIC candidate is the comet C/2018 V1 proposed by de la Fuente Marcos & de la Fuente Marcos (2019).

Chapter 4 *Dynamical evolution of the solar system debris disk in its birth cluster* (Torres et al. 2019b). I studied the creation and evolution of the solar system's Oort cloud in the early stages of its formation when the

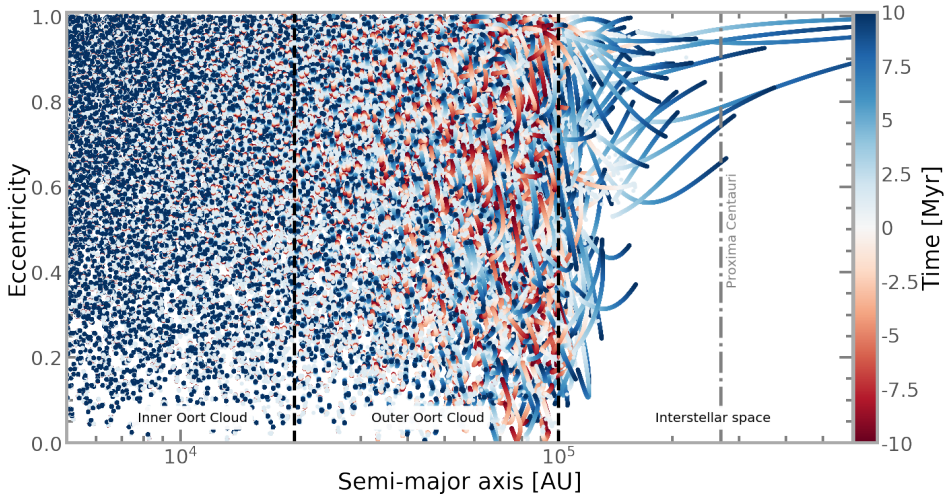


Figure 1.8: Orbital evolution of the particles in the simulated Oort cloud. The figure shows the evolution of the eccentricity as a function of the semi-major axis over the period of 20 Myr (± 10 Myrs.). The colour bar represents the integration time. Adapted from Torres et al. (2019a).

Sun was still in its birth cluster (Torres et al. 2019b). I constructed two models for the solar system. In the first model, I assumed a compact debris disk (16-35 au), while the second we assumed an extended debris disk (40-1000 au). For both models, I account for the perturbations of the giant planets and nearby stars in the cluster. I find that the most efficient way to perturb a disk is when the angle of interaction between the solar system and the perturber is between 0-30 degrees independently of the size of the disk. Additionally, I find that the creation of the Oort cloud was triggered by secular encounters, which produce the scattered disk, Sedna, and Oort Cloud like objects (Fig. 1.9), while the giant planets creates Kuiper belt objects. Additionally, approximately 36% of the planetesimals are ejected becoming interstellar comets.

Chapter 5 *Dynamical evolution of exo-Oort clouds around the Sun's closest neighbours stars due to local stellar perturbations and the Galactic tidal field* (Torres et al. 2020). Using the catalogue of the closest stars constructed in Torres et al. (2018, 2019a), and the methods developed in Torres et al. (2019a,b), I calculated the closest encounter for each of the Sun's neighbour stars within 3 pc and with accurate astrometric data from Gaia DR2, i.e., Proxima Centauri, Barnard star, Gliese 65, Ross 154, and Ross

1 Introduction

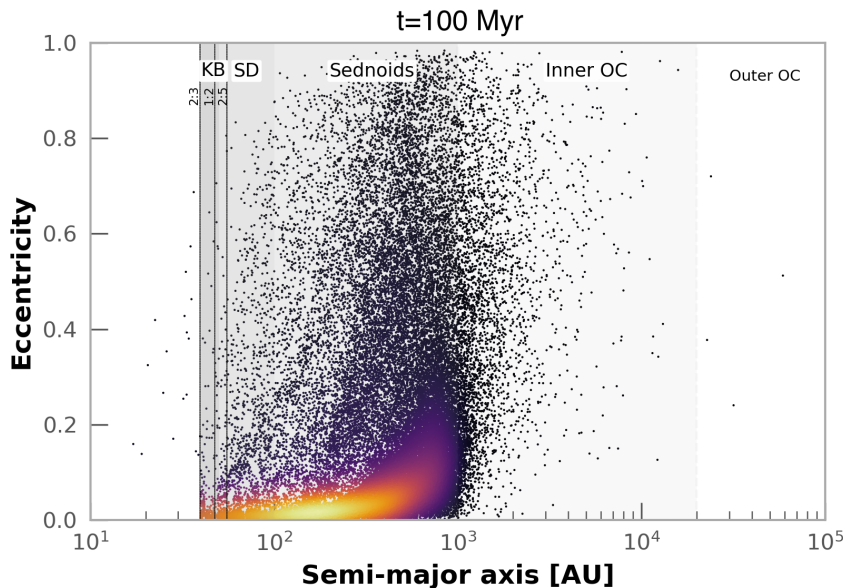


Figure 1.9: Semi-major axis as a function of eccentricity (top panel) and orbital inclination (bottom panel). The gray areas represent the different regions of the solar system (Kuiper belt (KB), scattered disk (SD), Sednoids, inner and outer Oort cloud (OC)), while the dashed lines show the 2:3, 1:2, and 2:5 resonances with Neptune. The integration time is set to 100 Myr. Adapted from Torres et al. (2019b).

248. I find that on average the stars in the solar neighbourhood experience around 40-55 close encounters during 20 Myr (Fig. 1.10), primarily with M-dwarf stars. I then calculated the effect of passing stars and the Galactic tidal field on the comets in exo-Oort clouds around the Sun's neighbour stars. The most perturbed system over a time interval of 20 Myr is Gliese 65 followed by Ross 154, Barnard's star and Ross 248 and finally Proxima Centauri. For Gliese 65 the production rate of transitional interstellar comets and interstellar objects is about 40×10^8 TIC Myr^{-1} and 1.4×10^{10} ISO Myr^{-1} . For the rest of the systems the rate of TIC production is about 2.1 to 3.8×10^8 TIC Myr^{-1} . This implies that a considerable number of interstellar comets reside in the local neighbourhood. Therefore the Sun and its neighbours are visited by interstellar comets originating from other stars. In this way, it is plausible that an interstellar comet cloud exists.

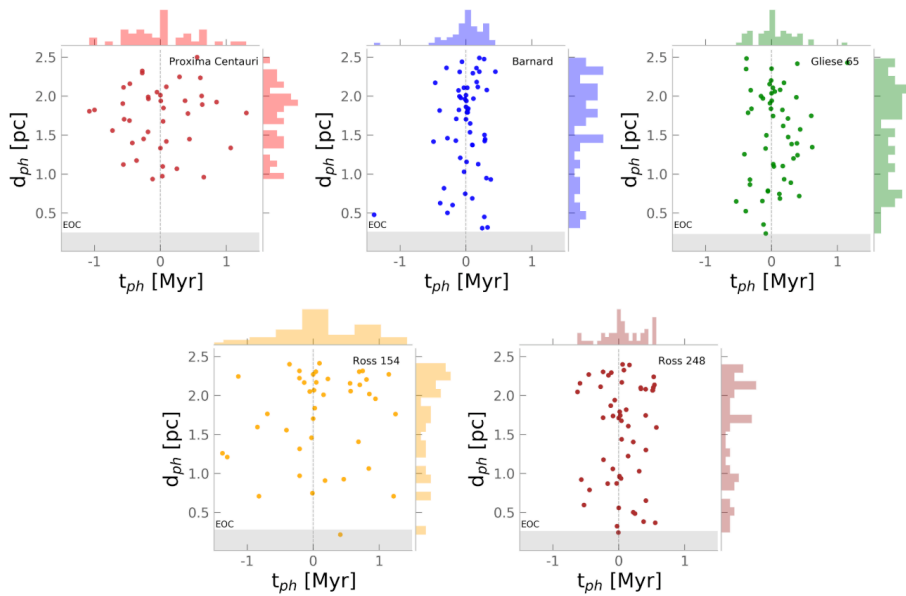


Figure 1.10: Closest approach distance vs time. The first panel corresponds for the closest encounters for Proxima Centauri (red), followed by the systems Barnard (blue), Gliese 65 (green), Ross 154 (yellow), and Ross 248 (brown). The histogram in each panel represents the distribution of the particles. The shaded areas represent the boundaries of the outer Oort cloud for each star, respectively. Adapted from Torres et al. (2020).



Credit: ESO/M. Kornmesser

Chapter 2

The origin of interstellar
asteroidal objects like 1I/2017 U1
'Oumuamua



S. Portegies Zwart, **S. Torres**^{*},
I. Pelupessy, J. Bédorf, and M. X. Cai.
Monthly Notices of the Royal Astronomical
Society 479, L17-L22, 2018

^{*}Equal contribution as the first author.

Abstract

We study the origin of the interstellar object 1I/2017 U1 'Oumuamua by juxtaposing estimates based on the observations with simulations. We speculate that objects like 'Oumuamua are formed in the debris disc as left over from the star and planet formation process, and subsequently liberated. The liberation process is mediated either by interaction with other stars in the parental star-cluster, by resonant interactions within the planetesimal disc or by the relatively sudden mass loss when the host star becomes a compact object. Integrating 'Oumuamua backward in time in the Galactic potential together with stars from the Gaia-TGAS catalogue we find that about 1.3 Myr ago 'Oumuamua passed the nearby star HIP 17288 within a mean distance of 1.3 pc. By comparing nearby observed L-dwarfs with simulations of the Galaxy we conclude that the kinematics of 'Oumuamua is consistent with relatively young objects of 1.1–1.7 Gyr. We just met 'Oumuamua by chance, and with a derived mean Galactic density of $\sim 3 \times 10^5$ similarly sized objects within 100 au from the Sun or $\sim 10^{14}$ per cubic parsec we expect about 2 to 12 such visitors per year within 1 au from the Sun.

Introduction

1I/2017 U1 'Oumuamua (hereafter 'Oumuamua), a genuine interstellar object that was discovered on 19 October 2017 in the Pan-STARRS survey (Bacci et al. 2017; Meech et al. 2017a,b), was initially identified as a comet but quickly reclassified as an *unusual minor planet*. Most notable orbital parameters are the distance at pericentre, $q = 0.25534 \pm 0.00007$ au, the eccentricity, $e = 1.1995 \pm 0.0002$ and the relative velocity at infinity $v \simeq 26.32 \pm 0.01$ km/s with respect to the Sun (Bacci et al. 2017; Meech et al. 2017a; Mamajek 2017). This makes the object unambiguously unbound on an en-passant orbit through the Solar system (de la Fuente Marcos & de la Fuente Marcos 2017; Bannister et al. 2017), not unlike the prediction by Moro-Martín, Turner, & Loeb (2009). The absence of a tail indicates that the object is probably rock-like (Meech 2018), which, together with its unusual elongated shape (~ 35 by 230 m reported by Meech et al. 2017, and explained by Fitzsimmons et al. (2018) and Domokos et al. (2017)) and rapid spin (with an 8.10 ± 0.02 hour period, see Jewitt et al. 2017; Bolin et al. 2018), has been hosted by a star for an extensive period of time (Katz 2018; Hoang et al. 2018). In this period it may have lost most of its volatiles and ice by sputtering (Meech 2018; Fitzsimmons et al. 2018). By the lack of other terminology for this class of objects and for convenience, we refer in this work to *sōlus lapis*, which is Latin for “lonely stone”.

Spectra taken by several instruments indicate that its colour ($g - r = 0.2 \pm 0.4$ and $r - i = 0.3 \pm 0.3$ (Masiero 2017), $g - r = 0.41 \pm 0.24$ and $r - i = 0.23 \pm 0.25$ (Bolin et al. 2018), and $g' - r' = 0.60 \pm 0.23$ (Ye et al. 2017)) matches that of objects in the Kuiper belt (Kuiper 1951) but that it is somewhat red compared to the main belt asteroids and trojans (see also Bannister et al. 2017; Jewitt 2018). However, it cannot be excluded that 'Oumuamua is the left over nucleus of a comet from another star (Ferrin & Zuluaga 2017; Meech 2018; Raymond et al. 2018b).

Based on its velocity, 'Oumuamua is unlikely to have originated from a nearby star (Mamajek 2017; de la Fuente Marcos & de la Fuente Marcos 2017), although Gaidos, Williams, & Kraus (2017) argue that it could have been ejected with a low velocity (of $1-2$ km/s) from the nearby young stellar associations Carina or Columba or from the Pleiades moving group (Feng & Jones 2018). Tracing back the trajectory of 'Oumuamua through the local neighbourhood is hindered by the magnification of small uncertainties in

2 Rendezvous with ‘Oumuamua

its orbit and in the positions and velocities of nearby stars (Zhang 2018). Even with the high accuracy achieved by Gaia and TGAS, backtracing its orbit can only be done reliably for some 10 Myr or over a distance of about 30 pc (Mamajek 2017).

Since we doubt that ‘Oumuamua formed as an isolated object, it seems most plausible that it formed around another star, from which it was liberated. This could be the result of copious mass loss resulting from the end phase of the nuclear burning of a star (Veras et al. 2011; Hansen & Zuckerman 2017; Rafikov 2018), by a close encounter in a young star cluster (Jílková et al. 2016), or by internal scattering of planetary systems (Brasser & Morbidelli 2013; Raymond, Armitage, & Veras 2018a) or in a binary star (Jackson et al. 2018; Čuk 2018). It is even possible that one of the Sun’s own Oort cloud objects was scattered by a yet unknown planet (Wright 2017; de la Fuente Marcos, de la Fuente Marcos, & Aarseth 2018).

Here we discuss the possible origin of ‘Oumuamua (see § 2.2). We analyse its orbital properties and compare those with our expectations for a random population of free-floating debris in the solar neighbourhood (see § 2.3). Our estimates of the occurrence of objects similar to ‘Oumuamua is juxtaposed with several alternative scenarios. In the near future when the Large Synoptic Telescope comes online many more *sōli lapidēs* are expected to be found at a rate of 2 to 12 per year.

Section 2.2

‘Oumuamua as a rare object

2.2.1 Observational constraints

A simple estimate of the number density of *sōli lapidēs* implied by the detection of ‘Oumuamua can be derived by calculating the effective volume surveyed by the Pan-STARRS telescope (A much more elaborate analysis was recently presented in Do et al. 2018). This telescope has a limiting magnitude of $m \sim 22$ (Bacci et al. 2017; Meech et al. 2017a). ‘Oumuamua was observed with a magnitude $H = 20.19$ and was within a distance of about 0.16 au from Earth before being detected.[†]

[†]The quoted value for H is the absolute magnitude which is defined as the magnitude at 1 au from both the Earth and the Sun.

2.2 'Oumuamua as a rare object

The volume surveyed by the Pan-STARRS telescope is approximately:

$$V \simeq Av\Delta t_{\text{PAN}}. \quad (2.1)$$

Here A is the effective cross section for the object passing the Solar system:

$$A = \pi r_{\text{detect}}^2 \left(1 + \left(\frac{v_{\text{esc}}}{v} \right)^2 \right). \quad (2.2)$$

In which πr_{detect}^2 is the geometric cross section and the second term corrects for the gravitational focusing. Here v is the relative velocity of 'Oumuamua at infinity with respect to the Solar system's barycentre and $v_{\text{esc}} \simeq 42$ km/s is the escape velocity of the Sun at a distance of 1 au. The period over which Pan-STARRS has observed $\Delta t_{\text{PAN}} \simeq 5$ yr (the first data release in 2014 covers 3 years, see Engelhardt et al. 2017). When we naively assume that the telescope has a 100 % detection efficiency over these 5 years we arrive at a density of ~ 0.08 au $^{-3}$ or $\sim 7.0 \times 10^{14}$ pc $^{-3}$. The statistical uncertainty implied by a single detection means that a wide range of values (0.004–0.24 au $^{-3}$ or 3.5×10^{13} – 2.1×10^{15} pc $^{-3}$) is consistent with the observations at the 95% level.

This simple estimate ignores the modeling of the detection efficiency. In spite of this, we obtain a value higher than the upper limits for finding *sōlī lapidēs* derived from the absence of detections using the Pan-STARSS1 survey up to that time by Engelhardt et al. (2017). Their estimates lead to a lower density because they considered larger objects with a cometary tail that could have been detected to a much larger distance from the Earth. We will now discuss the possible origin of *sōlī lapidēs* and their relation to 'Oumuamua.

2.2.2 Dynamical ejection from the Sun's Oort cloud

Considering the orbital parameters of 'Oumuamua, it seems unlikely to have been launched from the Kuiper belt or Oort cloud (Oort 1950). Asteroids and comets are frequently launched from the Kuiper belt and the Oort cloud but they rarely penetrate the inner Solar system (de la Fuente Marcos et al. 2018). Objects in the Oort cloud, however, could possibly launch into the inner Solar system after a strong interaction with a passing star (Rickman et al. 2008) or a planet (Fouchard et al. 2014).

The highest velocity, in this case, is obtained when the object would have been the member of a close binary with another, more massive, rocky

2 Rendezvous with ‘Oumuamua

object; much in the same way in which hypervelocity stars are ejected from the supermassive black hole in the Galactic centre (Hills 1988). Binaries are known to be common in the outer regions in the Solar system, and possibly the majority of planetesimals in the Kuiper belt formed as pairs (Fraser et al. 2017). The mean orbital separation of 13 trans-Neptunian objects is 13900 ± 14000 km (Noll et al. 2008) with a minimum of 1830 km for the pair Ceto/Phorcys (object #65489), but there is no particular reason why Oort cloud or Kuiper-belt binaries could not have tighter orbits (Fraser et al. 2017), such as is suspected of 2001 QG298 (Sheppard & Jewitt 2004). An interaction of an object much like the binary (136108) 2003 EL61 (Brown 2005) with a planet with ten times the mass of Jupiter could result in a runaway velocity of the least massive member of ~ 1 km/s, but with the parameters for Ceto/Phorcys the mean kick velocity of ~ 0.13 km/s. This would be sufficient to change a circular orbit at a distance of $1000\text{--}10^4$ au around the Sun into an unbound orbit with the eccentricity observed for ‘Oumuamua.

We perform Monte Carlo experiments in which we distribute Oort cloud objects around the Sun using the parameters adopted in Hanse et al. (2016). We introduce a velocity kick v_{kick} , taken randomly from a Gaussian distribution with dispersion of 0.13 km/s in each of the Cartesian directions, which results in a wide distribution in semi-major axis and eccentricity. More than 85% of the objects remain bound and the remaining 15% unbound objects tend to have high eccentricities with a median of ~ 1.2 , but only a very small fraction of $\lesssim 10^{-3}$ objects pass the Sun within 100 au on their unbound orbit (see also de la Fuente Marcos et al. 2017). We subsequently performed several direct N -body simulations to verify this result. For these we adopted the connected-component symplectic integrator Huayno (Jänes, Pelupessy, & Portegies Zwart 2014) within the AMUSE (Portegies Zwart & McMillan 2018) framework. The mild kicks expected due to an interaction with an Oort cloud binary and a massive planet, either passing through or bound to the Oort cloud, are insufficient to explain the observed velocity of ‘Oumuamua. We, therefore, conclude that ‘Oumuamua is unlikely to have originated from either the Kuiper belt or the Oort cloud (see also de la Fuente Marcos et al. 2018).

2.2.3 Origin from the Oort cloud of another star

Naive estimates of the density of interstellar comets can be derived from the stellar density and assuming that each star has a rich Oort cloud with

2.2 'Oumuamua as a rare object

$N_{\text{comets}} \sim 10^{11}$ comets per star (Kaib & Quinn 2009)

$$n_{\text{comets}} = \eta n_{\text{stars}} N_{\text{comets}}. \quad (2.3)$$

With a mean mass density in the solar neighbourhood of $\rho_0 = 0.119^{+0.015}_{-0.012} M_{\odot}/\text{pc}^3$ (Widmark & Monari 2019) (or $0.09 \pm 0.02 M_{\odot}/\text{pc}^3$ according to Kipper, Tempel, & Tenjes 2018) and a mean stellar mass $\sim 0.37 M_{\odot}$ (Chabrier 2003), we arrive at a local stellar number density in the Galactic disc of $n_{\text{stars}} \simeq 0.32 \text{ pc}^{-3}$. The efficiency at which comets are ejected from a star when it orbits the Galaxy was recently estimated to be $\eta \sim 0.1/\text{Gyr}$ (Hanse et al. 2016). With a mean stellar age of 6 Gyr, we arrive at a local comet density of $n_{\text{comets}} \sim 2.5 \times 10^{-6} \text{ au}^{-3}$ (or $2.2 \times 10^{10} \text{ pc}^{-3}$), which is consistent with the upper limit on the density of interstellar comets of $\lesssim 0.0007 \text{ au}^{-3}$ by Stern (1990) and $< 0.001 \text{ au}^{-3}$ by McGlynn & Chapman (1989) and Francis (2005). Here we did not correct for the intrinsic size and mass distribution of Oort cloud objects. The density of *sōli lapidēs* that originate from ejected Oort-cloud objects are considerably lower than our expected density based on the observations derived in § 2.2.1, and we conclude that 'Oumuamua cannot have originated from the hypothetical exo-Oort cloud of other stars.

Copious loss of circumstellar material, however, can be initiated when a star turns into a compact remnant either on the post-asymptotic giant branch (Veras et al. 2011) or in a supernova (Boersma 1961). If each of the 2.0×10^9 white dwarfs in the Galactic disc (Napiwotzki 2009) has produced $\mathcal{O}(10^{11})$ free-floating objects, the number of *sōli lapidēs* would be over-produced by ~ 5 orders of magnitude.

2.2.4 Origin from the debris disc of another star

A young planetary system with a circumstellar disc may be rather rich in relatively large $\gtrsim 100$ m objects, because it is the expected equilibrium size for collisional cascade of material-strength dominated bodies (Schlichting, Fuentes, & Trilling 2013). Disruption of such a disc may inject a large number of these objects into interstellar space. This would happen in the early evolution of the star when it still was a member of its parental cluster. A similar estimate as in § 2.2.3 then reveals a total mass of ejected disc-material to be

$$m_{\text{debris}} \sim f_{\text{debris}} Z \rho_0 \quad (2.4)$$

When we adopt a disc mass $M_{\text{disc}} = 0.01 M_{\odot}$, and a metallicity of the disc, $Z = 0.02$, the fraction of expelled material is harder to estimate but it may

2 Rendezvous with 'Oumuamua

be in the range of $f_{\text{debris}} \sim 0.1$. This fraction could even be higher if we argue that the Solar system may have lost a fraction $\gtrsim 10\%$ of its disc in a resonance interaction between the outer most planets (Gomes et al. 2005). The total mass of ejected metals is then of the order $\sim 2.4 \times 10^{-6} M_{\odot}/\text{pc}^{-3}$. The density of 'Oumuamua is estimated to be $\sim 2.0 \text{ g/cm}^3$ (see e.g. Trilling et al. 2017), which is in the range of densities observed for the relatively ordinary Kuiper-belt object Orcus ($\rho_{\text{KBO}} = 1.65_{-0.24}^{+0.34} \text{ g/cm}^3$, see e.g. Brown & Butler 2017) and the dense metal-rich 16 Psyche ($4.5 \pm 1.4 \text{ g/cm}^3$, see e.g. Shepard et al. 2017). With the observed dimensions of a cylinder of $25 \times 230 \text{ m}$ (Knight et al. 2017), we arrive at a mass of $m \simeq 1.2 \times 10^9 \text{ kg}$. A hypothetical young Solar system could then have ejected 3.3×10^{16} objects during its early evolution, leading to a mean density of $\sim 3.9 \times 10^{15} \text{ pc}^{-3}$, exceeding our observational estimate by a factor of ~ 6 . These objects may be cometary or non-cometary in nature depending on whether these are ejected from inside or outside the snow line. The large uncertainties in this estimate, and those in § 2.2.3 make it plausible that an enormous population of expelled objects exists in the Galaxy with a density consistent with, or even exceeding our number-density estimate in § 2.2.1.

Section 2.3

Where did 'Oumuamua come from

Having compared the number of interstellar objects produced by asteroidal or cometary ejection in § 2.2 it seems plausible that 'Oumuamua was formed around another star, and was liberated upon either close planetary encounters within the young planetary system, or due to the copious mass loss when the star became a compact remnant. We now discuss the possible origin of 'Oumuamua .

2.3.1 An origin from the solar neighbourhood

Results by the Gaia Collaboration, Brown et al. (2016) provide the most complete and accurate census of the distribution of stars in the solar neighbourhood (for which we adopt a volume centred around the Sun with a radius of 50 pc). The radial velocity components are not (yet) part of this database, but they can be completed using other catalogues. By matching the TGAS catalogue with the radial velocities from Kunder et al. (2017), Pulkovo (Gontcharov 2006), and Geneva-Copenhagen (Holmberg, Nordström, & Andersen 2009), we constructed a catalogue of 270,664 stars with

2.3 Where did 'Oumuamua come from

position and velocity information (Torres, Portegies Zwart, & Brown 2018), we selected those stars with relative proper motions and parallax errors $< 1\%$, with radial velocity < 100 km/s, with errors < 10 km/s (see also Feng & Jones 2018).

The orbits of the selected stars as well as 'Oumuamua are integrated backwards in time for 10 Myr in the Galactic potential. The uncertainty in the Gaia database and in the orbital parameters of 'Oumuamua are too large to integrate reliably backwards in time any further (see also Mama-jek 2017, who adopted similar criteria). The integration was performed using Galaxia (Antoja, Helmi, Dehnen, Bienaymé, Bland-Hawthorn, Famaey, Freeman, Gibson, Gilmore, Grebel, Kordopatis, Kunder, Minchev, Munari, Navarro, Parker, Reid, Seabroke, Siebert, Steinmetz, Watson, Wyse, & Zwitter 2014). This semi-analytic Milky Way Galaxy model is incorporated in the AMUSE software framework (Portegies Zwart, McMillan, van Elteren, Pelupessy, & de Vries 2013a; Portegies Zwart & McMillan 2018) using the parameters derived by Martínez-Barbosa, Brown, & Portegies Zwart (2015). As position for the Sun, we adopted $x = 8300$ pc, with a z component of 27 pc, and a velocity vector of (11.1, 232.24, 7.25) km/s.

We now generate one million objects within the error ellipsoid (in astrometric and radial velocity) of each of the selected stars. This results, for each star, in a probability density-distribution in time, relative distance and relative velocity of the closest approach between that particular star and 'Oumuamua. In Fig. 2.1 and Fig. 2.2 we show the various probability distributions for time of closest approach, relative distance, and relative velocity for the 4 stars within 2 pc that have a closest approach. We identify these stars in Table 2.1. About 6.8 Myr ago, 'Oumuamua passed the star HIP 17288 within a distance of ~ 1.3 pc and with a relative velocity of ~ 15 km/s which is consistent with the result of Feng & Jones (2018) and Dybczyński & Królikowska (2018). We find several other relatively close encounters which, despite their close proximity with 'Oumuamua, we have not included here because of the large uncertainty in the radial velocity. Based on this data, we do not expect that 'Oumuamua was launched from any of the nearby stars in the Gaia catalogue. We speculate that 'Oumuamua originates from well beyond the solar neighbourhood.

2.3.2 An origin from beyond the solar neighbourhood

If 'Oumuamua is part of the Galactic background distribution of *sōlī lapidēs*, its velocity is expected to be consistent with the distribution of low-

2 Rendezvous with ‘Oumuamua

Table 2.1: Closest star encounters with ‘Oumuamua within 2 pc. Columns 1 to 3 give the identity of the star, the following columns give the time of the encounter, the closest relative distance with ‘Oumuamua, relative velocity, and the variation intervals of the samples in time, distance and velocity. Note that time is negative, indicating that the encounter happened in the past.

ID	Gaia identity	HIP	t [Myr]	t_{sample}	d_{rel} [pc]	d_{sample}	v_{rel} [km/s]	v_{sample}
^a	5108377030337405952	17288	-6.793	[-7.011, -6.574]	1.342	[1.330, 1.363]	14.854	[12.917, 17.184]
^b	4863923915804133376		-8.970	[-10.135, -8.037]	1.554	[1.526, 1.644]	22.106	[17.281, 27.255]
^c	5140501942602437632		-6.653	[-7.755, -5.481]	1.931	[1.840, 2.447]	40.228	[32.951, 85.899]
^d	1362592668307182592	86916	-0.455	[-2.083, 2.223]	1.783	[1.781, 1.799]	43.430	[28.745, 62.525]

2.3 Where did 'Oumuamua come from

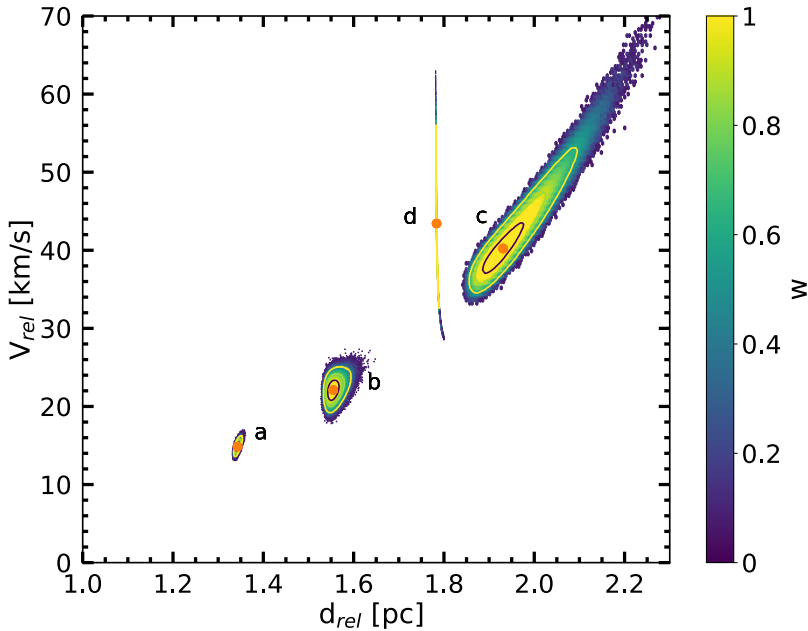


Figure 2.1: Probability density-distribution in relative distance (d_{rel}) and relative velocity (v_{rel}) between 'Oumuamua and the four closest stars *a*, *b*, *c* and *d* (see Table 2.1). The colour bar to the right gives a weighing (w) with respect to the A and v from Eq. 2.1 and Eq. 2.2 with respect to the same values of 'Oumuamua.

mass objects in the Galaxy. To analyse quantitatively this hypothesis, we compare the velocity of 'Oumuamua with the distribution of the stars in Gaia-TGAS. This distribution is presented in Fig. 2.3.

Ideally, we would like to compare 'Oumuamua to a population of objects with similar characteristics. We decide to take the population of L-dwarfs, which in mass are sufficiently small that they could be considered mass-less in the Galactic potential. In addition, there is a reasonable consistent census of the population of L-dwarfs within 20 pc of the solar neighbourhood (Kirkpatrick et al. 2012). For these dwarfs, the velocity has been measured as a function of age (Burgasser et al. 2015), and this distribution follows:

$$v \simeq \frac{t}{[\text{Gyr}]} \times 6 \text{ km/s} + 20 \text{ km/s}. \quad (2.5)$$

2 Rendezvous with ‘Oumuamua

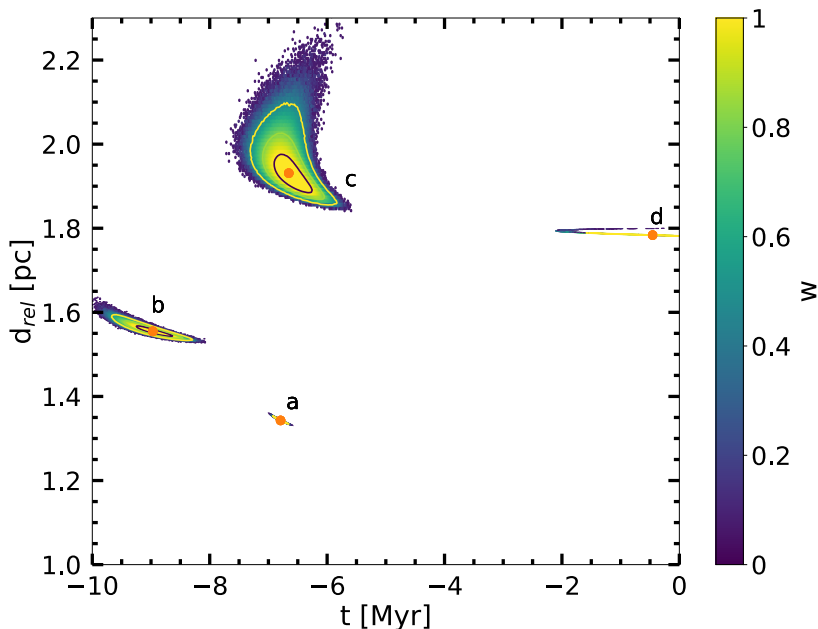


Figure 2.2: Probability density-distribution in time of closest approach (t) and relative distance (d_{rel}) between ‘Oumuamua and the four closest stars (see Table 2.1).

Inverting this relation leads to an age estimate for ‘Oumuamua of ~ 1 Gyr, which is consistent with the sample of youngest (1.1–1.7 Gyr) L-dwarfs (Burgasser et al. 2015). Considering the velocity distribution of the entire population of brown dwarfs results in an average age of about 5 Gyr (see Fig. 2.3), which is consistent with the estimate of 5.2 ± 0.2 Gyr by Burgasser et al. (2015), whereas for the Gaia-TGAS data, we find 3 ± 0.5 Gyr. The difference between the brown-dwarf age-estimates and those in the Gaia-TGAS catalogue is possibly due to a selection effect caused by the magnitude-limited sample in the latter (see also Bailer-Jones 2018).

To further validate the use of the brown-dwarf velocity-distribution to constrain the age of ‘Oumuamua, we compare it to the velocity distribution of objects in recent simulations of the Milky Way Galaxy by Fujii et al. (2018). This calculation, performed with the Bonsai (Bédorf et al. 2012, 2014) gravitational tree-code using a shared time-step of ~ 0.6 Myr, a gravitational softening length of 10 pc and with opening angle $\theta = 0.4$ are car-

2.3 Where did 'Oumuamua come from

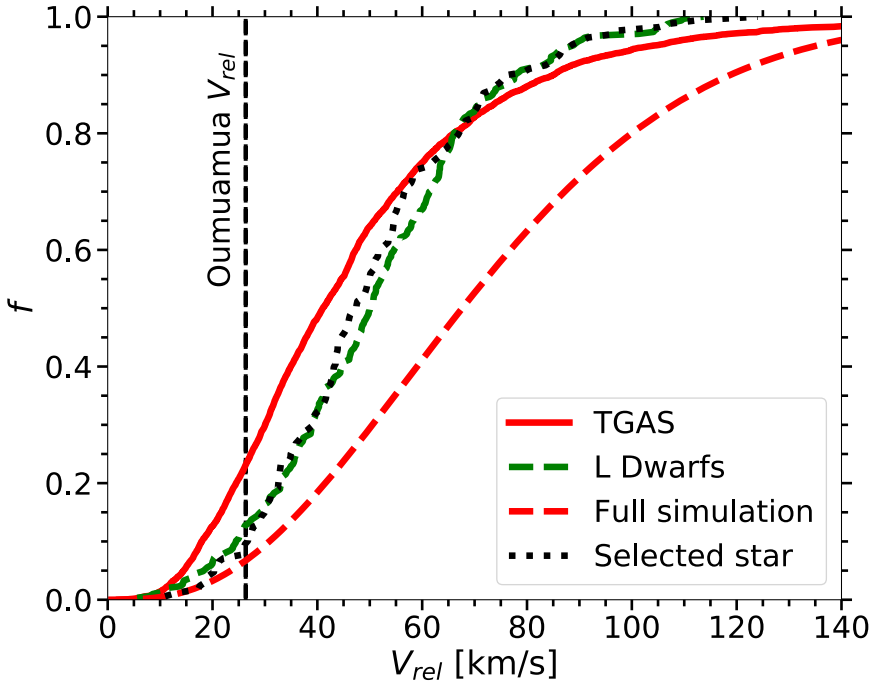


Figure 2.3: Cumulative relative velocity distributions of single objects in the solar neighbourhood. 'Oumuamua is presented as the vertical line near 26 km/s. The solid red curve gives the velocity distribution of stars within 30 pc of the Sun from the Gaia-TGAS catalogues. The green dashed curve gives the distribution of 100 L-dwarfs within ~ 20 pc of the Sun (Schmidt et al. 2010). The red dashed curve gives the mean relative velocity-distribution of all stars within 7.5-8.5 kpc from the Galactic centre, whereas the black dotted curve gives the distribution between one Sun-like star (at a distance of ~ 7.2 kpc from the centre with a velocity of ~ 223.1 km/s and at an angle of $\sim 20^\circ$ from the tip of the bar, Holmberg et al. 2009) and its neighbours. The latter distribution is statistically consistent with that of the brown dwarfs with KS-probability of ~ 0.3 .

ried out with 8×10^9 particles in a stellar disc and include a live halo, bulge, and bar. In this snapshot at an age of 10 Gyr, we selected objects within 30 pc around a hypothetical star that matches the current relative location of the Sun in the Milky Way. At this distance, the structure of the disc is no longer visible and the inclination distribution is flat. The resulting relative velocity distribution of the full sample is presented as the red-dashed curve

2 Rendezvous with ‘Oumuamua

and a sample star that matches closest to the L-dwarfs is represented by the black-dotted curve in Fig. 2.3.

The age distribution of all the objects in the simulations is consistent with an age of ~ 8.3 Gyr, but for the star representing the Sun it is comparable to the age-velocity distribution of 100 L-dwarfs in the age-range of 1.1–1.7 Gyr of Yu & Liu (2018). Instead of comparing the relative velocity-distributions directly, they should be weighted by the encounter rate and corrected for gravitational focusing (see Eq. 2.2). For the relevant velocity range ($v_{\text{rel}} \lesssim 100$ km/s) however, this correction is small ($< 25\%$).

Section 2.4

Discussion and conclusions

Based on the existence of ‘Oumuamua, we derive a local density of $3.5 \times 10^{13} - 2.1 \times 10^{15} \text{ pc}^{-3}$ ($0.0040 - 0.24 \text{ au}^{-3}$). This is a high density, but in line with other estimates (Do et al. 2018). It is consistent with the amount of debris ejected during the star and planet formation process, but inconsistent with expulsion of exo Oort-cloud or asteroidal objects (see § 2.2).

If each star contributes to the formation of *sōlī lapidēs* then the entire Galaxy may be swarming with such objects, with $O(10^{23})$ *sōlī lapidēs* in the Milky Way. Once liberated from their parent stars, it is quite possible that such an object grazes any other star, much in the same way ‘Oumuamua passed close to the Sun. The velocity of ‘Oumuamua is low compared to the stars in the Gaia-TGAS catalogue, and low compared to the mean velocity distribution of L-dwarfs. Young L-dwarfs have a considerably lower velocity than their older siblings, and the velocity of ‘Oumuamua is consistent with the youngest population of brown dwarfs (1.1–1.7 Gyr). Based on its velocity, we argue that ‘Oumuamua has a similar age (see also Feng & Jones 2018).

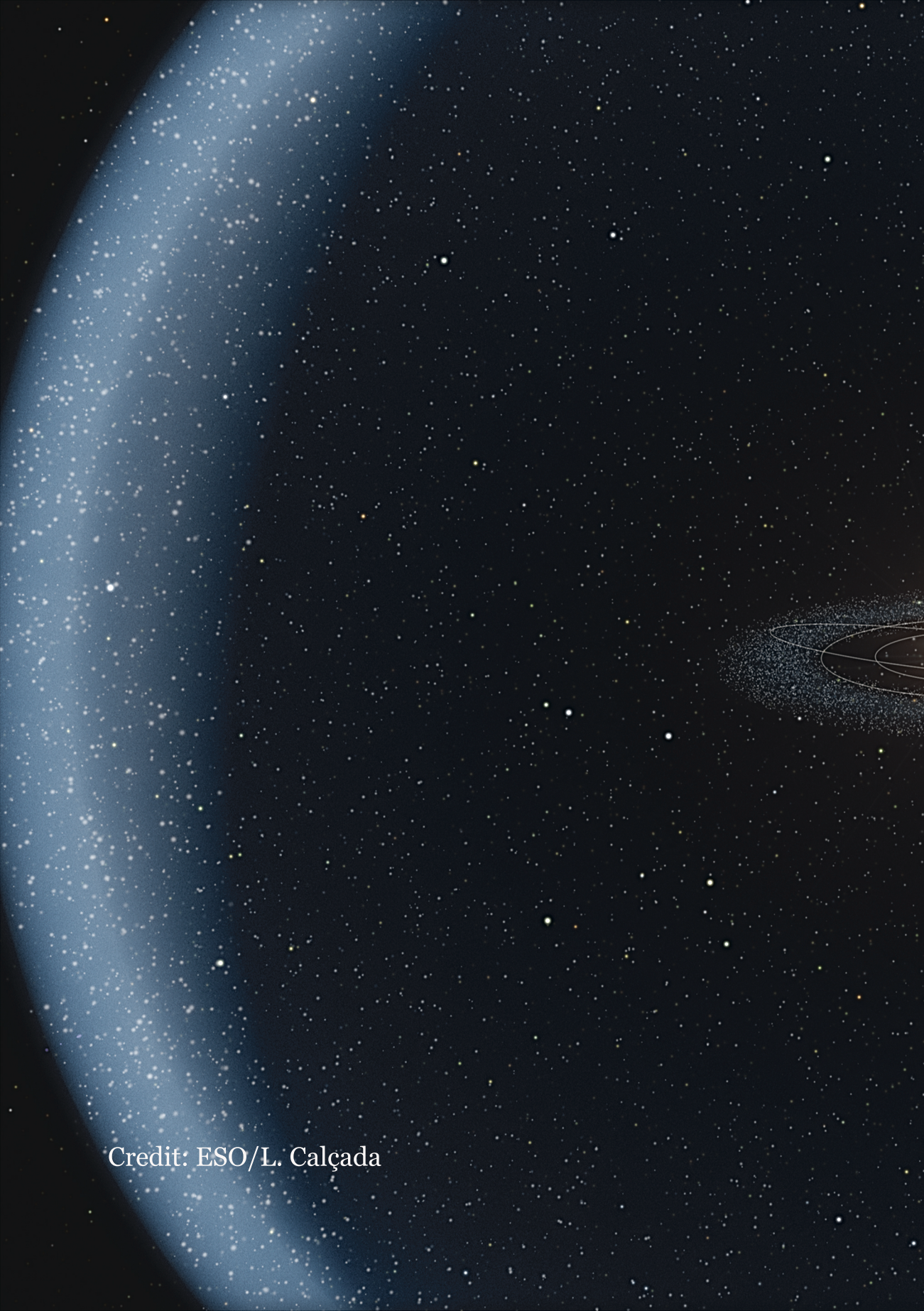
Earlier estimates of the interstellar asteroid density were carried out to explain the daily X-ray flares on the super-massive black-hole in the Galactic centre Sgr A* (Hamers & Portegies Zwart 2015). They argue that the daily X-ray flares in the direction of Sgr A* can be explained with a local density of $\sim 10^{14}$ asteroids pc^{-3} , which is consistent with the density of *sōlī lapidēs* derived here.

We conclude that ‘Oumuamua is part of the left-over debris of the star and planet formation process in the Galaxy. We expect that the Galaxy is

2.4 Discussion and conclusions

rich in such objects, with a density of $\sim 10^{14}$ or 10^{15} objects per cubic parsec. We estimate the probability that a *sōlus lapis* passes the Sun within 1 au, taking the gravitational focusing corrected cross-section into account, at an event rate of about 2–12 per year.

Acknowledgements We thank Fabo Feng for discussions on a possible origin of 'Oumuamua in the Oort cloud. ST expresses his gratitude to the Mexican National Council for Science and Technology (CONACYT) for the grant #291004-410780. We thank Ben Pole, Yohai Meiron and Maura Portegies Zwart for the translation of the term “lonely rock” into Latin. We thank the referees for their thorough checking of facts, the corrections to our interpretation of the MNRAS style documents, and lessons in the subtle differences between British and American English. This work was supported by the Netherlands Research School for Astronomy (NOVA) and NWO (grant #621.016.701 [LGM-II]). This work was supported by a grant from the Swiss National Supercomputing Centre (CSCS) under project ID s716. This work used the public git version of the AMUSE software environment which can be found at <https://github.com/amusecode>. This work has made use of data from the European Space Agency (ESA) mission Gaia (<https://www.cosmos.esa.int/gaia>), processed by the Gaia Data Processing and Analysis Consortium (DPAC, <https://www.cosmos.esa.int/web/gaia/dpac/consortium>). Funding for the DPAC has been provided by national institutions, in particular the institutions participating in the Gaia Multilateral Agreement.



Credit: ESO/L. Calçada

Chapter 3

Galactic tide and local stellar perturbations on the Oort cloud: creation of interstellar comets



S. Torres, M. X. Cai,
S. Portegies Zwart, and A. G. A. Brown
Astronomy & Astrophysics
629, A139 2019a

Abstract

Comets in the Oort cloud evolve under the influence of internal and external perturbations, such as giant planets, stellar passages, and the Galactic gravitational tidal field. We aim to study the dynamical evolution of the comets in the Oort cloud, accounting for the perturbation of the Galactic tidal field and passing stars. We base our study on three main approaches; analytic, observational, and numerical. We first construct an analytical model of stellar encounters. We find that individual perturbations do not modify the dynamics of the comets in the cloud unless very close (< 0.5 pc) encounters occur. Using proper motions, parallaxes, and radial velocities from *Gaia* DR2 and combining them with the radial velocities from other surveys, we then construct an astrometric catalogue of the 14 659 stars that are within 50 pc of the Sun. For all these stars we calculate the time and distance of closest approach to the Sun. We find that the cumulative effect of relatively distant (≤ 1 pc) passing stars can perturb the comets in the Oort cloud. Finally, we study the dynamical evolution of the comets in the Oort cloud under the influence of multiple stellar encounters from stars that pass within 2.5 pc of the Sun and the Galactic tidal field over ± 10 Myr. We use the Astrophysical Multipurpose Software Environment (AMUSE), and the GPU-accelerated direct N-body code ABIE. We considered two models for the Oort cloud, compact ($a \leq 0.25$ pc) and extended ($a \leq 0.5$ pc). We find that the cumulative effect of stellar encounters is the major perturber of the Oort cloud for a compact configuration while for the extended configuration the Galactic tidal field is the major perturber. In both cases the cumulative effect of distant stellar encounters together with the Galactic tidal field raises the semi-major axis of $\sim 1.1\%$ of the comets at the edge of the Oort cloud up to interstellar regions ($a > 0.5$ pc) over the 20 Myr period considered. This leads to the creation of transitional interstellar comets (TICs), which might become interstellar objects due to external perturbations. This raises the question of the formation, evolution, and current status of the Oort cloud as well as the existence of a “cloud” of objects in the interstellar space that might overlap with our Oort cloud, when considering that other planetary systems should undergo similar processes leading to the ejection of comets.

Introduction

The outer region of the solar system is populated by a large number of planetesimals. Further away, more than 1 000 au from the Sun, and almost extending to the nearest stars, is the Oort cloud. Its existence was proposed in the late 1950s by the Dutch astronomer Jan Hendrik Oort, who realised that long-term comets (with orbital semi-major axes $a > 40$ au) bound to the Sun must come from an area well beyond Neptune. Oort (1950) pointed out that a spike in the distribution of $1/a$ of the long-period comets with $a > 10^4$ au, and isotropic inclinations in $\cos i$, ω , and Ω , would argue for the existence of a reservoir of objects in quasi-spherical symmetry surrounding the solar system. The Oort cloud has remained unobserved to date.

There have been numerous studies aimed at trying to explain the formation, evolution, and structure of the Oort cloud, mostly through numerical simulation (e.g. Hills 1981; Heisler & Tremaine 1986; Duncan et al. 1987; Weissman 1996; Wiegert & Tremaine 1999; García-Sánchez et al. 1999; Dybczyński 2002; Levison et al. 2004; Dones et al. 2004; Morbidelli 2005; Duncan 2008; Brassier et al. 2006; Fouchard et al. 2006; Kaib & Quinn 2008; Brassier & Morbidelli 2013; Shannon et al. 2014; Dones et al. 2015). There is general agreement on some properties of the Oort cloud, in particular that it is composed of the residual planetesimals after the planet formation epoch. The Oort cloud is divided into two regions: the *inner* Oort cloud is usually reserved for comets with semi-major axes $a < 20\,000$ au and is invisible unless there is a comet shower. The *outer* Oort cloud refers to comets with semi-major axes $a > 20\,000$ au (e.g. Dones et al. 2015). Its shape is thought to be nearly spherical and limited at 0.5 pc mainly by the influence of the Galactic tidal field and stellar flybys (e.g. Heisler & Tremaine 1986). The Oort cloud is thought to contain around 10^{12} objects with a total mass of $\sim 3 \times 10^{25}$ kg (e.g. Morbidelli 2005). However, these estimations are highly uncertain. The above-mentioned studies also concluded that in order for long-period comets to still exist today they need to be replenished. Otherwise they would have been depleted on a timescale much shorter than the lifetime of the solar system.

The orbits of the comets in the Oort cloud form a frozen record of the evolution of the solar system and preserve the memory of its birth environment (Portegies Zwart & Jílková 2015; Martínez-Barbosa et al. 2016; Fouchard et al. 2011, 2018). External perturbations such as Galactic tides,

3 Dynamics of the Oort cloud

stellar flybys, and molecular clouds play an important role in the understanding of the formation and evolution of the Oort cloud and Oort cloud-like structures in other planetary systems (see e.g. Veras et al. 2013, 2014). Passing stars can perturb the comets, changing their perihelion distances much more than they change the overall size of the orbit, changing the cometary trajectories and injecting the comets into the inner solar system (Morbidelli 2005 and Duncan 2008). The outer Oort cloud has been affected quite substantially by external influences. Not only by passing stars in the parental cluster of the Sun but also by occasional relatively close encounters that have occurred after the Sun has left its birth cluster (Jílková et al. 2016). Jílková et al. (2015) pointed out that the planetesimals *Sedna* and *2008PV113* belong to the inner Oort cloud and that they may have been captured during an encounter with another star in the birth cluster of the Sun. This star is conjectured to have passed the solar system within about 340 au and would have deposited approximately 1 400 other planetesimals together with the two currently known objects in this family. The orbital characteristics of these objects share similar properties which can be used to reconstruct the encounter.

Close encounters with the solar system have been studied by a number of authors (e.g. Rickman 1976; Robert A. J. Matthews 1994; Weissman 1996; Dehnen & Binney 1998; García-Sánchez et al. 1999; Levison et al. 2004; Jimenez-Torres et al. 2011; Bailer-Jones 2015; Dybczyński & Berski 2015; Higuchi & Kokubo 2015; Feng & Bailer-Jones 2015; Berski & Dybczyński 2016). Most of them calculated the closest encounters with the solar system within ± 10 Myr using the astrometric data of the stars in the solar neighbourhood (< 50 pc) provided by Hipparcos mission (Perryman et al. 1997). They find that the closest approach (~ 0.3 pc) in the future (~ 1.3 Myr from the present) will be with the star HIP 8982 (GJ 710), which will cause minor changes in the perihelion distance of the comets. The most recent close stellar encounter was with the so-called Scholz's star ($M_{\star} \simeq 0.15 M_{\odot}$ at a distance of $0.25_{-0.07}^{+0.11}$ pc, Scholz 2014, Mamajek et al. 2015). All of the studies cited above were limited by the observational data due to the incompleteness of the Hipparcos survey.

The first data release (*Gaia* DR1) of the European Space Agency's *Gaia* mission (Gaia Collaboration, Brown et al. 2016; Gaia Collaboration et al. 2016) opened a new window for understanding the Milky Way. In the particular case of the solar system, *Gaia* detected nearly all of the local star systems within 50 pc of the Sun (compared to the 20% detected by Hipparcos). Using *Gaia* DR1, several authors (Berski & Dybczyński 2016; Bobylev

& Bajkova 2017; Torres et al. 2018; Bailer-Jones 2018) re-computed the orbit of the closest stars to the Sun. They found new stars and new parameters for some of the very well known encounters, such as GJ 710, which gets closer (0.064 pc) based on the *Gaia* DR1 data. The recent second *Gaia* data release – *Gaia* DR2 (Gaia Collaboration et al. 2018) –, provided 7.2 million radial velocities. This provided an opportunity to find new and more accurately characterised stellar encounters. Using *Gaia* DR2, Bailer-Jones et al. (2018) found 693 new stars with closest-encounter distances within 5 pc and 15 Myrs from now; accounting for the incompleteness they also re-calculate the present rate of encounters, which within ~ 1 pc of the Sun is estimated to be $20 \pm 2 \text{ Myr}^{-1}$. From Hipparcos data García-Sánchez et al. (1999) derived $11.7 \pm 1.3 \text{ Myr}^{-1}$ within ~ 1 pc and Martínez-Barbosa et al. (2017) employed simulations to derive rates of 21, 39, and 63 Myr^{-1} within ~ 2 pc for three different scenarios (orbital migration from the Milky Way inner disk, migration from the outer disk, and no migration, respectively).

We aim to obtain a conservative estimate of the combined effects of stellar encounters and the Galactic tidal field on the Oort cloud, by only considering the encounters from stars listed in *Gaia* DR2 within ± 10 Myr from the present. The latter sample is incomplete and thus provides a lower limit on the effects of passing stars. In Sect. 5.2 we present a simple analytical model for stellar encounters and discuss the cumulative effect of passing stars on the Oort cloud, using the impulse approximation. In Sect. 5.3 we present a catalogue of nearby stars and we calculate the effect of individuals encounters with stars within 2.5 pc of the Sun. In Sect. 5.4 we present a numerical model for multiple stellar encounters and study the dynamical evolution of a simulated Oort cloud after the interaction with the nearby stars and the Galactic tidal field. Finally, in Sect. 3.5 we present our summary and conclusions.

3 Dynamics of the Oort cloud

Section 3.2

Model for stellar encounters

The estimated extent of the Oort cloud is $\sim 0.5\text{pc}$ (Oort 1950; Dones et al. 2015), which means that the orbital velocity of bodies in the Oort cloud is limited to 0.13 km s^{-1} . This implies that comets at the edge of the Oort cloud are barely bound to the Sun and thus the condition for a comet ejection due to an external perturbation, $\Delta v_{\perp} > v_{\text{esc}}$ (where v_{esc} is the escape velocity) is easily met. The Galactic tidal field is the most important perturbation to the outer Oort cloud at large distances (Heisler & Tremaine 1986). However close encounters with stars also play an important role in the evolution of the Oort cloud.

3.2.1 Analytic model

A simple analytical model of stellar encounters can help us to better understand the effect of passing stars on the Oort cloud. To construct such a model, we followed the works of Rickman (1976); García-Sánchez et al. (2001); Rickman et al. (2004, 2008); Martínez-Barbosa et al. (2017). We first compiled data for the mass, velocity dispersion, and the space density of the stars in the solar neighbourhood for 13 spectral types, as in Table 8 in García-Sánchez et al. (2001). The mass of the stars corresponding to the spectral types B0V to M5V was taken from the data compiled by Mamajek (2018)* (see also Pecaut & Mamajek 2013). While the mean value for white dwarfs (WD) was taken from Jiménez-Esteban et al. (2018). The peculiar velocity of the Sun (v_{\odot}) and the velocity dispersion of the stars (v_{*}) were taken from Rickman et al. (2008). The space density of spectral types A to K and Giants was obtained from Bovy (2017). For B and M type stars the values were obtained from Rickman et al. (2008), and for the WD from Jiménez-Esteban et al. (2018). The compiled data are shown in Table 3.1.

We consider the effect of the stars with different masses (M_{*}) and spectral types in the solar neighbourhood on the comets in the Oort cloud. We assume that the stars move on a straight line trajectory, and with a constant velocity relative to the Sun (v_{*}). For high stellar velocities, we can assume that the comet is at rest during the stellar passage. Using the impulse approximation (Oort 1950; Rickman 1976), we then calculate the change of the velocity (ΔV_{\perp}) imparted to a comet in the Oort cloud due to a random

*http://www.pas.rochester.edu/~emamajek/EEM_dwarf_UBVIJHK_colors_Teff.txt

3.2 Model for stellar encounters

Table 3.1: Stellar parameters. Columns represent the spectral type of the stars followed by their mass, velocity dispersion, and the peculiar velocity of the Sun with respect to each spectral type. The relative velocity of the encounter within the Sun–comet system and the star is shown in column 5. The number density of stars in the solar neighbourhood is shown in column 6.

$S.T$	$M_*[M_\odot]$	$v_*[\text{km s}^{-1}]$	$v_\odot[\text{km s}^{-1}]$	$v_{enc}[\text{km s}^{-1}]$	$\rho_*[10^{-3}pc^{-3}]$
BoV	15	14.7	18.6	24.6	0.06
AoV	2.3	19.7	17.1	27.5	0.26
A5V	1.85	23.7	13.7	29.3	0.34
FoV	1.59	29.1	17.1	36.5	0.61
F5V	1.33	36.2	17.1	43.6	1.51
GoV	1.08	37.4	26.4	49.8	1.61
G5V	0.98	39.2	23.9	49.6	1.73
KoV	0.87	34.1	19.8	42.6	4.21
K5V	0.68	43.4	25.0	54.3	5.26
MoV	0.55	42.7	17.3	50.0	8.72
M5V	0.16	41.8	23.3	51.8	41.55
WD	0.6	63.4	38.3	80.2	4.9
Giants	2.2	41.0	21.0	49.7	3.9

stellar encounter by integrating the perpendicular force generated by each passing star:

$$\Delta V_\perp \approx \frac{2GM_*}{v_*} \left[\frac{\mathbf{r}_c}{r_c^2} - \frac{\mathbf{r}_\odot}{r_\odot^2} \right], \quad (3.1)$$

where r_c and r_\odot correspond to the vectors from the comet and the Sun to the point of closest approach of the star (assuming that the comet has not been deflected by the gravity of the star). If we consider r the heliocentric distance of the comet and we assume that the distance of the encounter is large enough compared to the distance Sun–comet, we can approximate Equation (3.1) with:

$$\Delta V_\perp \propto \frac{M_* r}{v_* r_\odot^2}. \quad (3.2)$$

For the case of a very close encounter with the comet, Equation (5.3) can be approximated as

$$\Delta V_\perp \propto \frac{M_*}{v_* r_c}. \quad (3.3)$$

3 Dynamics of the Oort cloud

It is important to stress that the impulse approximation is based on a number of simplifying assumptions, and therefore it should be used for statistical analysis only. For our propose, it gives us a general idea of the effect of the different stars in the solar neighbourhood on the comets in the Oort cloud.

Following Rickman (1976) we can calculate the frequency of the stellar encounters using

$$f = \pi r_*^2 v_{\text{enc}} \rho_* , \quad (3.4)$$

where r_* is the distance of the encounter, $v_{\text{enc}} = \sqrt{v_{\odot}^2 + v_*^2}$ is the relative velocity of the Sun and a random passing star (v_{\odot} represents the peculiar velocity of the Sun, and v_* the velocity dispersion of the parent population of the passing star), and ρ_* is the number density of stars of a given spectral type in the solar neighbourhood. Equation (3.4) can be used to determine the number of stars passing by within a sphere of radius r_s centred on the Sun or a random comet (assuming that stars of the solar neighbourhood are uniformly distributed at any time and the stellar velocities relative to the Sun are constant, Rickman 1976):

$$N_* = r_s^2 f t . \quad (3.5)$$

3.2.2 Perturbations on the Oort cloud

Using Eq. (5.3) and the values in Table 3.1, we calculated the frequency of the stars passing within a distance r_* from the Oort cloud. We find that the total frequency of stars passing within 1 pc is around 12.5 Myr^{-1} (see Table 3.2). Following the same method, García-Sánchez et al. (1999) found a lower value (11.7 Myr^{-1}). The main difference with our result is due to the updated values for the mass and density of the stars used in this work. The most probable perturber of the Oort cloud is the low mass, high-relative-velocity stars.

Using Eq. (5.3), in Fig. 3.1 we show the change of the velocity of a comet due to an encounter with a star for different spectral types and as a function of the distance of the encounter for an interval of 0.1–2.5 pc. The lower distance corresponds to the inner Oort cloud, while the larger distance corresponds to the limit where a passing star can start perturbing a comet at

3.2 Model for stellar encounters

Table 3.2: Analytical model for stellar encounters for an encounter distance of 1 pc. The spectral type is shown in column 1, the frequency of the stellar encounters is shown in column 2, the change in the velocity of a comet due to an interaction with a star is shown in column 3, and the total number of stars entering a sphere of radius 1 pc around the Sun-comet system over a time interval of 1 *Gyr* is shown in column 4.

S.T	$f_*^{1\text{pc}}$ [Myr ⁻¹]	$\Delta V_{\perp,*}^{1\text{pc}}$ [km s ⁻¹]	$N_*^{1\text{pc}}$
BoV	0.005	8.77e-03	4.742
AoV	0.023	1.005e-03	22.973
A5V	0.032	6.716e-04	32.007
FoV	0.072	4.701e-04	71.536
F5V	0.212	3.161e-04	211.527
GoV	0.258	2.485e-04	257.608
G5V	0.276	2.151e-04	275.696
KoV	0.576	2.195e-04	576.229
K5V	0.918	1.348e-04	917.675
MoV	1.401	1.108e-04	1400.844
M5V	6.915	3.293e-05	6915.189
WD	1.263	8.143e-05	1262.623
Giants	0.623	4.617e-04	622.765

the edge of the cloud. In the rest of this work we refer to the latter distance as the *critical radius*.

As shown in Fig. 3.1 the change induced by a single encounter is relatively small. Massive stars are effective in exciting the object in the Oort cloud, but they are rare. Low-mass stars are very common, but their effect on the orbits of a comet is small. However the number of stars encountering the solar system increases over time.

The model presented in this section is based on a number of simplifying assumptions. Specifically, the impulse approximation provides a quick but inaccurate estimate of the effect of a random passing star on a comet in the Oort cloud. As we show in Table 3.2 the effect of individual stars is relative small. However, considering the frequency and the number of stars approaching the Sun to within 1 pc over 1 Gyr, their cumulative effect might change the structure and dynamics of the Oort cloud. In order to have a better understanding of the evolution of the Oort cloud it is necessary to employ a detailed numerical model which accounts for the effects of the Galactic tidal field and stellar distribution of stars around the

3 Dynamics of the Oort cloud

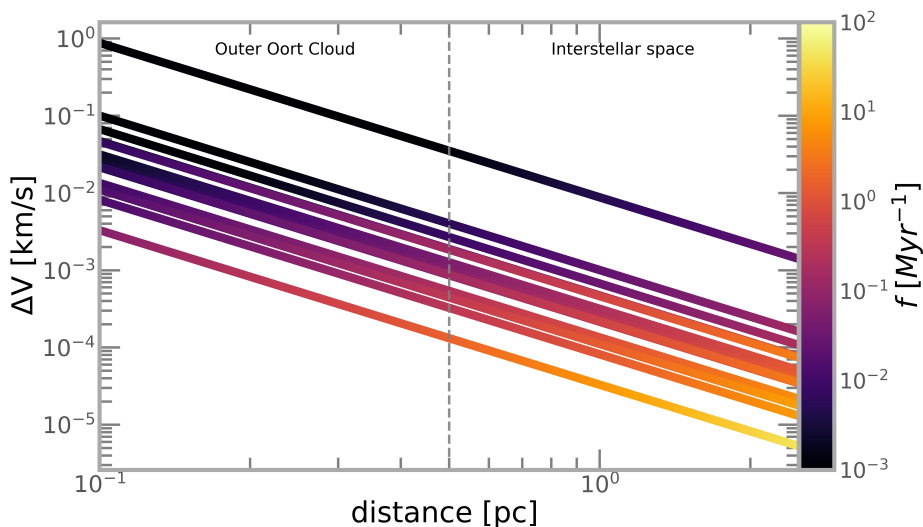


Figure 3.1: Change of the velocity of a comet due to random stellar encounters for the 13 stellar spectral types listed in Table 3.1 as a function of the encounter distance. The colour coding of the lines represents the frequency of stellar encounters as a function of the distance of the encounter for the corresponding types of stars. The lines represent the different spectral types in the order listed in Table 3.1. The mass of the stars decreases from the top to the bottom lines.

Sun. In Sect. 5.3 we present a list of nearby stars within 50 pc of the Sun for which *Gaia* DR2 astrometry and radial velocities (including from other surveys) are available. This provides us with accurate kinematic information on nearby stars that could influence the Oort cloud in the recent past or near future. In Sect. 5.4 we use numerical simulations to analyse their effect on the comets in the Oort cloud and estimate their cumulative effect over ± 10 Myr, including the effect of the Galactic tidal field.

Section 3.3

Close encounters with the solar system

Our knowledge of close stellar encounters in the recent past or near future has been limited by the availability of precise and accurate astrometry and radial velocities for the nearby stars. The *Gaia* mission has considerably increased the availability of astrometric and radial velocity data for the

3.3 Close encounters with the solar system

closest stars, even if about 20% of the stars with high proper motions are not listed in *Gaia* DR2 and those tend to be close to the Sun (Bailer-Jones et al. 2018).

Table 3.3: Overview of the catalogue of stars within 50 pc of the Sun for which encounter parameters were calculated. The full catalogue can be download from: <https://home.strw.leidenuniv.nl/~storres/#Research>

Input catalogue(s)	No. Stars ≤ 50 pc
<i>Gaia</i> DR2	10,744
<i>Gaia</i> DR2 + RAVE DR5	2356
<i>Gaia</i> DR2 + GALAH DR2	11
<i>Gaia</i> DR2 + LAMOST DR3	307
<i>Gaia</i> DR2 + APOGEE DR14	1092
<i>Gaia</i> DR2 + XHIP	149
Total	14 659

3.3.1 Observational model

To construct the list of stars within 50 pc of the Sun for which the encounter parameters (closest approach distance, velocity, and time) can be calculated we used the data from the *Gaia* DR2 catalogue. To increase the number of stars for which radial velocity information is available we cross-matched *Gaia* DR2 with the following catalogues: RAVE-DR5 (Kunder et al. 2017), GALAH DR2 (Buder et al. 2018), LAMOST DR3 (Zhao et al. 2012), APOGEE DR14 (Abolfathi et al. 2018), and XHIP (Anderson & Francis 2012). We selected only stars with relative uncertainty on the parallax (ϖ) smaller than 20%, such that $1/\varpi$ is a good estimator of the distance to the stars. Following Lindegren et al. (2018) we further filtered the list of stars according to

$$u^2 < 1.44 \times \max[1, \exp(-0.4(G - 19.5))], \quad (3.6)$$

and

$$1.0 + 0.015(G_{\text{BP}} - G_{\text{RP}})^2 < E < 1.3 + 0.06(G_{\text{BP}} - G_{\text{RP}})^2, \quad (3.7)$$

where G , G_{BP} , and G_{RP} correspond to the photometric measurements, covering a wavelength from the near-ultraviolet to the near-infrared for the

3 Dynamics of the Oort cloud

G passband, 330 to 680nm, and 630 to 1050 nm for G_{BP} , and G_{RP} , respectively. The $u = (\chi^2/\nu)^{1/2}$ corresponds to the unit weight error, and E is the flux excess factor. This filter selects sources with high-quality astrometry and weeds out stars which appear to be nearby because of spuriously high values of the parallax (see appendix C in Lindegren et al. 2018). The resulting catalogue contains 14 659 stars within 50 pc of the Sun (Table 3.3).

For the selected stars we estimated the distance, time, and velocity of closest approach using the linear approximation method of Robert A. J. Matthews (1994) in the formulation presented in Bailer-Jones (2015):

$$v_{\text{tot}} = \sqrt{v_{\text{T}}^2 + v_{\text{rad}}^2} \quad (3.8)$$

$$t_{\text{ph}} = -\frac{cv_{\text{rad}}}{\varpi v_{\text{tot}}^2} \quad (3.9)$$

$$d_{\text{ph}} = \frac{10^3}{\varpi} \frac{v_{\text{T}}}{v_{\text{tot}}}, \quad (3.10)$$

where $v_{\text{T}} = 4.74 [(\mu_{\alpha^*}^2 + \mu_{\delta}^2)^{0.5}/\varpi]$ is the transverse velocity, v_{rad} is the radial velocity of the star, ϖ is the parallax, $c = 10^3 \text{ pc km}^{-1} \text{ yr}^{-1}$, and the subscript ‘ph’ stands for perihelion. We estimated the mass of the stars using the effective temperature provided in *Gaia* DR2 (Andrae et al. 2018) and linearly interpolating in the Tables in Mamajek (2018) and Pecaut & Mamajek (2013).

Of the 14 659 stars within 50 pc there are 31 that pass within 2.5 pc of the Sun (Fig. 3.2, big dots) over a period of 20 Myr centred on the present (i.e. 10 Myr in the past and 10 Myr in the future). Figure 3.2 shows the observational Hertzsprung-Russell diagram of our sample. In Fig. 3.3 we show the closest approach distance and time of the stars in our sample with respect to the Sun. The limited distance range of the stars under study only allows us to find very close encounters within ± 3 Myr.

In Fig. 3.3 the large dots show the distribution of the stars passing within 2.5 pc and those tend to be the major perturber of the Oort cloud (referred to as ‘*Gaia* stars’ below). The closest encounter with the solar system is GJ 710 which will penetrate deep inside the inner Oort cloud. As shown in Fig. 3.2 most of the closest encounters involve M dwarfs, with a considerable fraction of solar type stars. This implies that the effect of a single encounter with the Oort cloud will be minimal, mainly due to the low mass of the perturber and its high velocity with respect to the Sun.

3.3 Close encounters with the solar system

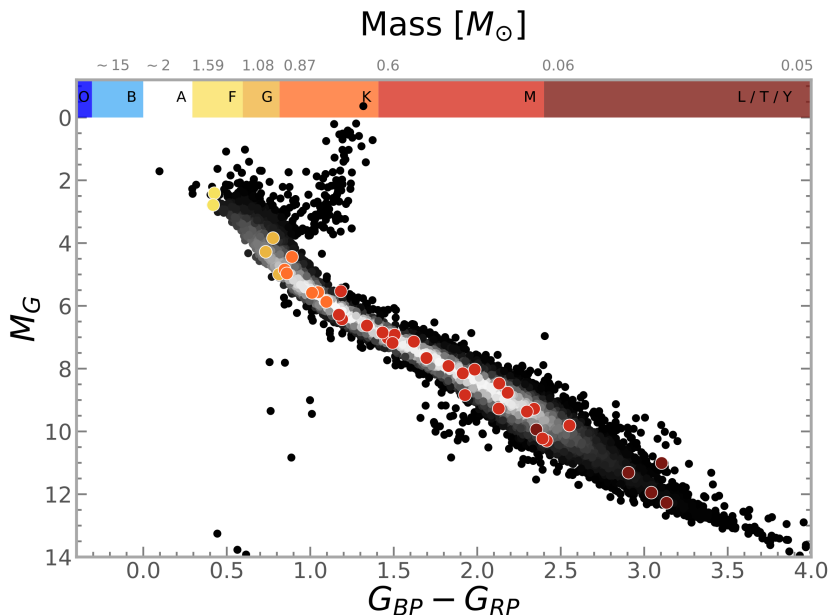


Figure 3.2: Observational HR diagram of the nearby stars contained in the catalogue summarised in Table 3.3. The big dots represent the stars within 2.5 pc of the Sun colour coded according to their spectral type. The density map shows all the stars in our sample.

Bailer-Jones et al. (2018) find 62 new stellar encounters, which partially overlap with our list. Their list of encounters is larger than ours mostly because they did not apply the strict filtering on the astrometric quality of the *Gaia* DR2 data employed in this work. For stars appearing in both studies we find similar results.

We stress that the sample of the closest stars presented here is incomplete. The observational incompleteness is evident in the decrease in encounter frequency as one moves away from the present epoch in time. A complete census of stellar encounters requires all the stars within a certain distance to be identified. The main limitations in using the *Gaia* survey for finding the closest encounters are the survey magnitude limit, which prevents the identification of encounters with faint low-mass stars, and the lack of radial velocities. The *Gaia* DR2 radial velocity survey is limited to effective temperatures in the range ~ 3550 – 6900 K and to stars brighter than $G = 14$ mag (see e.g. Bailer-Jones et al. 2018). An additional lim-

3 Dynamics of the Oort cloud

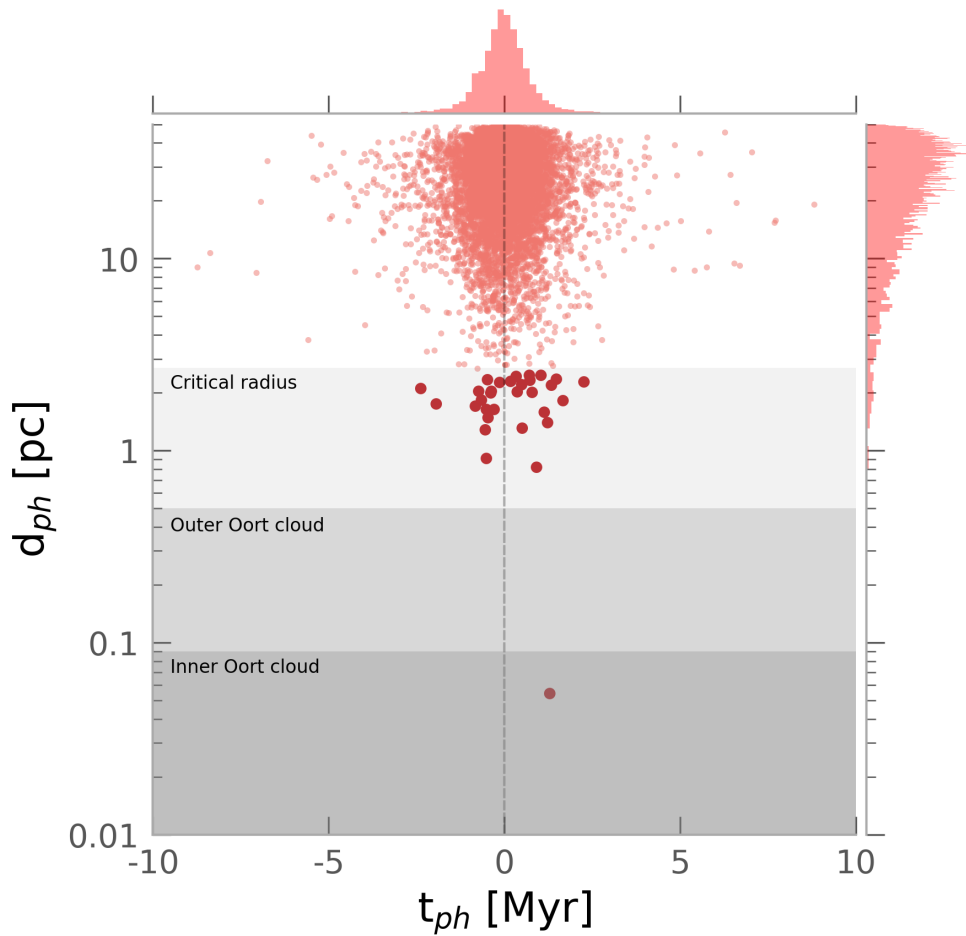


Figure 3.3: Closest approach distance vs. closest approach time. The shaded areas represent the critical radius within which stars can affect an object in the Oort cloud, and the boundaries of the outer and inner Oort cloud, respectively. The big dots correspond to those stars that pass within 2.5 pc of the Sun.

3.3 Close encounters with the solar system

itation is that some of the brightest stars in the sky are missing from the *Gaia* DR2 catalogue (Gaia Collaboration et al. 2018).

A detailed study correcting for incompleteness in *Gaia* DR2 was carried out by Bailer-Jones et al. (2018). These latter authors constructed a completeness map (Fig. 12, Bailer-Jones et al. 2018), interpreted as the probability of detecting a given close encounter in the *Gaia* DR2 sample. They found that only 15% of the encounters within 5 pc in a period of 5 Myr have been identified. Using this result, the authors used a simulated Milky Way galaxy to infer the encounter rate averaged over 5 Myr, in the past and future. They found that the encounter rate of stellar encounters within 1 pc is $20 \pm 2 \text{ Myr}^{-1}$.

3.3.2 Stellar encounters with the Solar System

In Section 3.3.1 we employed a simple method to estimate the perihelion distances and times for stars approaching the Sun by assuming the stars follow a uniform motion along straight lines with respect to the Sun (see also Bailer-Jones 2015). We now seek a better estimation of the perihelion distance through the joint integration of the orbits of the Sun and the stars that are predicted to approach to within 2.5 pc (Table 3.4) backwards and forwards in time for 10 Myr. We first transformed the astrometric and radial velocity data into galactocentric Cartesian frame using *Astropy* (The Astropy Collaboration et al. 2018). We adopted the position of the Sun and the local circular velocity parameters from Reid et al. (2014): $Z_{\odot} = 27 \text{ pc}$, $R_{\odot} = 8.34 \text{ kpc}$, and $V_{c,\odot} = 240 \text{ km s}^{-1}$; while the peculiar velocity of the Sun was adopted from Schönrich et al. (2010): $(U_{\odot}, V_{\odot}, W_{\odot}) = (11.1, 12.24, 7.25) \text{ km s}^{-1}$. We used the *Gala* (Price-Whelan 2017) package to perform the orbital integration. The Milky Way potential used is described by an analytic axisymmetric model which contains a spherical nucleus and bulge (Hernquist 1990), a Miyamoto-Nagai disk (Miyamoto & Nagai 1975; Bovy 2015), and a spherical Navarro-Frenk-White (NFW) dark matter halo (Navarro et al. 1996).

To account for the observational uncertainties we sample the astrometric and radial velocity observables for each star, taking the full covariance matrix into account. For each star, 10^6 samples of the astrometry and radial velocity are drawn and for each of these the above described orbit integration is carried out. The end result is a sampling of the distribution of possible perihelion distances and times. This distribution obtained through Monte Carlo sampling is then treated as the probability density function

3 Dynamics of the Oort cloud

(PDF) of the encounter parameters. The shape of the confidence regions is mainly affected by the relative errors on parallax and radial velocity. The relative error in the proper motion likewise affects the shape of the confidence regions around the mean. Figures 3.4, 3.5, and 3.6 show the resulting PDFs.

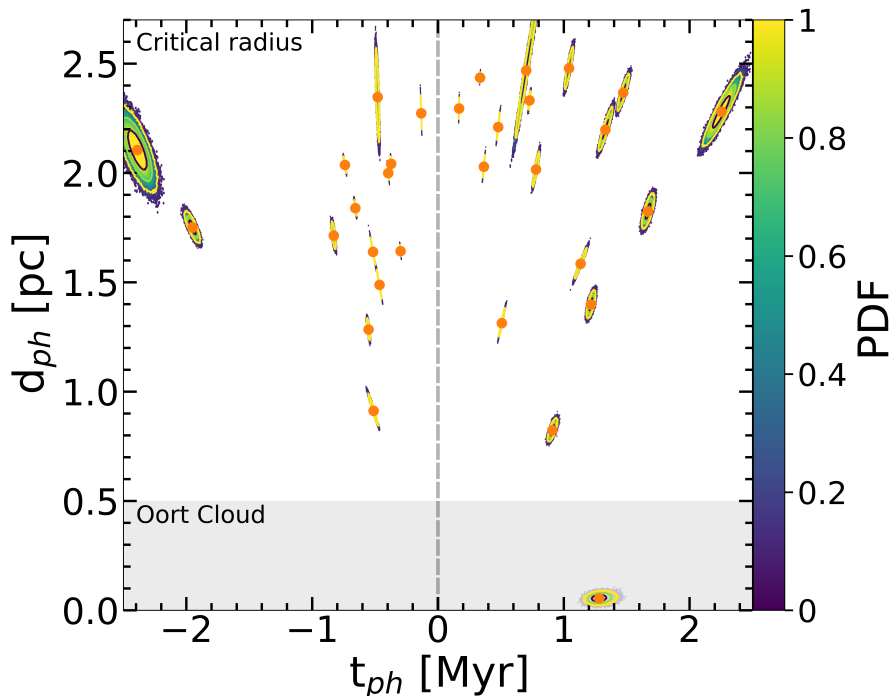


Figure 3.4: Joint probability density of the time and distance of closest approach for those stars that are predicted to pass within 2.5 pc of the Sun (listed in Table 3.3). The contour levels indicate regions enclosing 0.6, 0.9, and 0.99 % cumulative probability (colour bar). The shape of each PDF is affected by the relative errors in the observational data of each star, particularly the errors on parallax and radial velocity.

In Fig. 3.4 we show the distribution of time and distance of closest approach for the time interval ± 3 Myr from the present. The closest encounter found is, as expected, the very well known case of GJ 710. In Fig. 3.5 we show the distribution of the total relative velocity and distance of closest approach. Most stars in our sample have high velocities (20 to 80 km s^{-1}) meaning that their effect on the Oort cloud is small. Figure 3.6 shows the

3.3 Close encounters with the solar system

Table 3.4: Stars predicted to approach the Sun within 2.5 pc over the ± 10 Myr from today. The columns represent the Gaia DR2 ID, the time, distance and velocity at the perihelion with its respective confidence interval. These are followed by the effective temperature listed in Gaia DR2, the estimated mass of the star, and the change in the velocity due to the encounter with the Sun for each star.

Gaia DR2 ID	t_{ph} [Myr]	t_{sample}	d_{ph} [pc]	d_{sample}	v_{tot} [km s $^{-1}$]	v_{sample}	T_{eff} [K]	Mass [M_{\odot}]	Δv_{\perp} [km s $^{-1}$]
4270814637616488064	1.282	[1.123, 1.488]	0.054	[0.006, 0.107]	14.525	[12.515, 16.564]	4116	0.654	1.305e-01
553219967007245312	1.670	[1.595, 1.742]	1.824	[1.714, 1.952]	24.163	[23.187, 25.284]	5175	0.851	9.106e-05
258179971749627776	0.365	[0.352, 0.378]	2.028	[1.955, 2.107]	78.377	[75.746, 81.470]	4507	0.717	1.915e-05
4575928186606190336	0.479	[0.462, 0.500]	2.210	[2.126, 2.307]	51.102	[48.983, 52.973]	3795	0.559	1.925e-05
3240424426786618624	-0.552	[-0.572, -0.534]	1.284	[1.214, 1.368]	83.029	[80.325, 85.666]	3836	0.580	3.647e-05
4795598309045006208	-0.739	[-0.737, -0.723]	2.037	[1.985, 2.091]	32.470	[31.698, 33.194]	5343	0.901	5.755e-05
3274130814728561792	-2.390	[-2.645, -2.158]	2.105	[1.834, 2.447]	19.171	[17.362, 21.165]	4471	0.715	7.240e-05
98137526780564608	0.508	[0.476, 0.548]	1.314	[1.229, 1.422]	53.595	[49.613, 57.211]	3875	0.601	5.589e-05
6684504722300935680	-0.465	[-0.495, -0.436]	1.488	[1.400, 1.587]	43.104	[40.449, 45.973]	3619	0.494	4.451e-05
443023805199001216	0.167	[0.165, 0.171]	2.295	[2.225, 2.379]	67.699	[66.901, 68.396]	6017	1.128	2.724e-05
2417069815934357248	2.253	[2.049, 2.486]	2.280	[2.068, 2.531]	14.047	[12.746, 15.408]	4613	0.741	8.735e-05
3089711447388931584	-0.133	[-0.139, -0.127]	2.273	[2.164, 2.389]	63.544	[60.457, 66.818]	3820	0.571	1.497e-05
3339921875389105152	-0.516	[-0.544, -0.485]	1.639	[1.541, 1.732]	21.455	[20.317, 22.843]	4105	0.653	9.746e-05
1134618591670426112	0.728	[0.713, 0.742]	2.331	[2.273, 2.394]	63.885	[62.639, 65.223]	4887	0.787	1.950e-05
5861048509766415616	-0.297	[-0.304, -0.290]	1.643	[1.601, 1.682]	59.275	[57.962, 60.702]	3795	0.559	3.005e-05
681999884156922368	1.134	[1.066, 1.209]	1.585	[1.483, 1.697]	15.785	[14.795, 16.794]	3956	0.615	1.336e-04
32600792279255564160	0.910	[0.851, 0.968]	0.823	[0.754, 0.905]	33.395	[31.465, 35.704]	3998	0.629	2.395e-04
2648914040357320576	1.473	[1.412, 1.544]	2.367	[2.257, 2.502]	13.235	[12.616, 13.823]	5630	0.976	1.133e-04
397213027669560288	-0.511	[-0.572, -0.458]	0.912	[0.818, 1.025]	31.845	[28.459, 35.551]	3980	0.623	2.025e-04
2118161219075485824	0.779	[0.743, 0.816]	2.016	[1.908, 2.126]	56.180	[53.650, 58.906]	4122	0.654	2.466e-04
1392610405193517952	0.702	[0.586, 0.882]	2.468	[2.067, 2.095]	64.956	[51.343, 77.613]	5057	0.823	1.790e-05
20898896827311035336	1.041	[0.997, 1.090]	2.478	[2.346, 2.633]	46.407	[44.351, 48.454]	3965	0.618	1.866e-05
2272191085754928768	0.335	[0.331, 0.338]	2.436	[2.401, 2.469]	76.760	[75.892, 77.614]	5859	1.060	2.003e-05
475887919121831104	-0.395	[-0.405, -0.385]	2.000	[1.952, 2.050]	31.680	[30.850, 32.497]	4893	0.788	5.352e-05
4839132097557586560	-0.828	[-0.856, -0.803]	1.713	[1.624, 1.815]	46.116	[44.687, 47.522]	3865	0.597	3.798e-05
5076260164798852864	-0.479	[-0.503, -0.456]	2.347	[2.063, 2.673]	50.434	[49.277, 51.577]	4837	0.781	2.418e-05
4546557031272743680	1.216	[1.163, 1.272]	1.398	[1.311, 1.490]	35.688	[34.137, 37.245]	4395	0.695	8.573e-05
875071278432954240	1.331	[1.250, 1.413]	2.198	[2.057, 2.351]	16.389	[15.429, 17.435]	5714	0.998	1.083e-04
2924339469735490560	-1.951	[-2.039, -1.862]	1.751	[1.646, 1.864]	14.766	[14.128, 15.488]	5743	1.009	1.918e-04
3371908043029299840	-0.372	[-0.379, -0.366]	2.041	[1.994, 2.085]	82.969	[81.685, 84.203]	4330	0.700	1.742e-05
3369080353797965056	-0.656	[-0.670, -0.643]	1.839	[1.788, 1.894]	40.659	[39.870, 41.541]	6020	1.130	7.066e-05

3 Dynamics of the Oort cloud

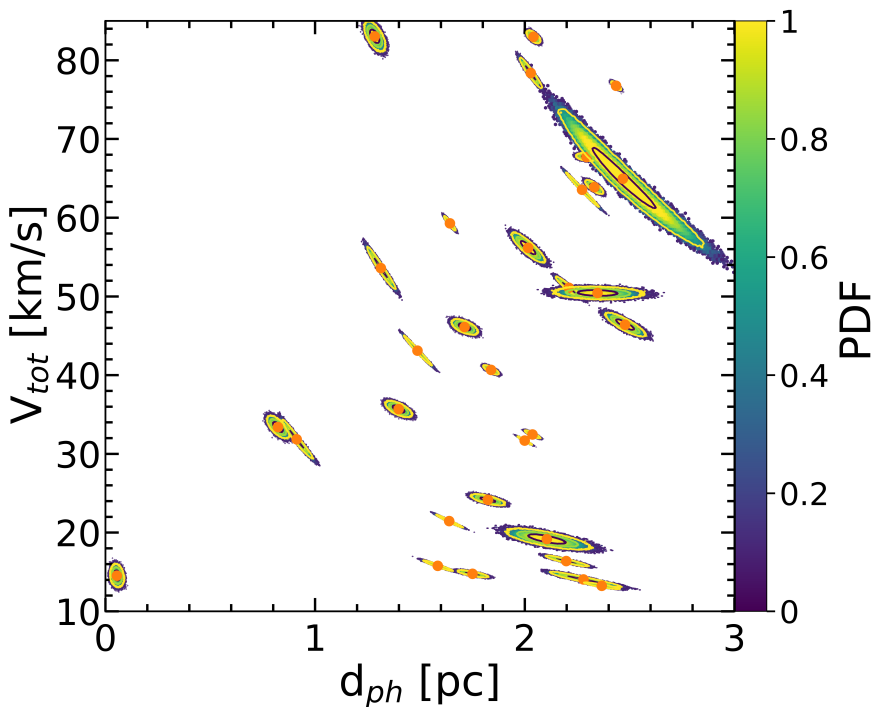


Figure 3.5: Joint probability density of the time and relative velocity of closest approach for the stars in Table 3.3.

distribution of the time and relative velocity of closest approach, showing a triangular shape with a peak toward high velocities and the present time. This is a selection effect caused by our limitation of the total studied sample to stars that are currently within 50 pc of the Sun (this means that very fast-moving stars that would approach the Sun far in the past or the future are currently not in the 50 pc volume).

We calculate the effect on a comet of a passing star that approaches to within 2.5 pc (Table 3.4), using the impulse approximation (Eq. (5.3)). We find that the change in the velocity of a comet is relatively small (in the order of 10^{-3} – 10^{-4} km s $^{-1}$, Table 3.4). The exception is for the passage of GJ 710, which causes a velocity change of ~ 0.13 km s $^{-1}$, creating an important perturbation in the inner Oort cloud. Overall if only individual encounters are considered the Oort cloud comets barely feel the effect of

3.3 Close encounters with the solar system

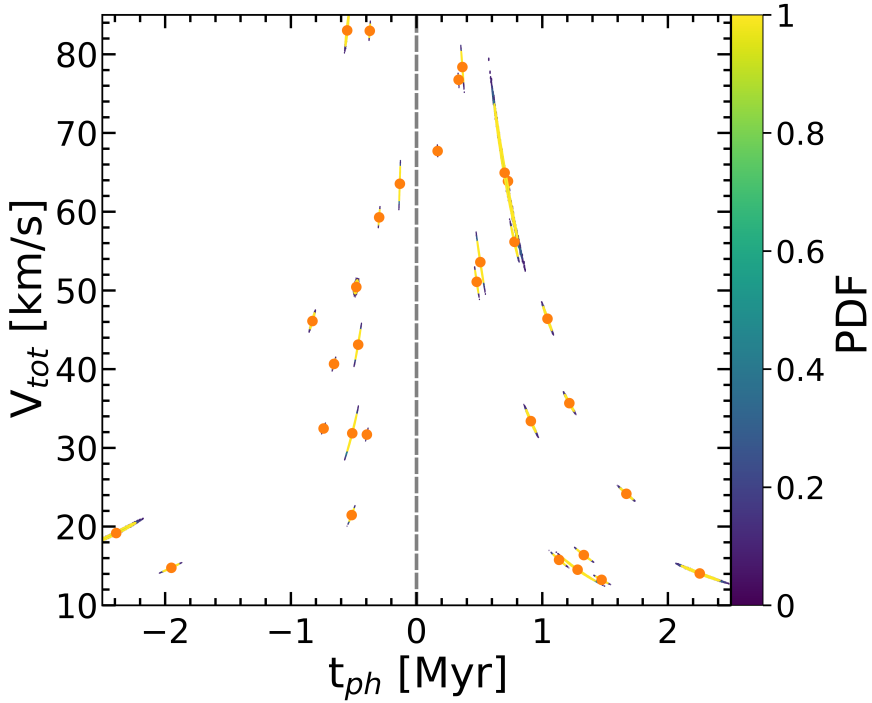


Figure 3.6: Joint probability density of the distance and relative velocity of closest approach for the stars in Table 3.3.

passing stars. The impulse approximation is based on a number of simplifying assumptions, but this approach gives us a general panorama of the individual effect of the nearby stars on a comet in the Oort cloud. In order to quantify the global effect of passing stars, it is necessary to integrate their orbits backwards and forward in time (see Sect. 3.3.1). Such a scenario is shown in the third row of Figure 3.9. The cumulative effect of nearby stars is strong enough to lift the perihelion of $\sim 0.38\%$ of the objects in the Oort cloud (Fig. 3.9, third row). Particularly the effect of GJ 710 is strong (Fig. 3.8), but encounters within ~ 1 pc also have an important contribution.

3 Dynamics of the Oort cloud

3.3.3 The case of GJ 710/HIP 89825

For decades GJ 710 has been pointed out as the major future perturber of the Oort cloud. The first calculations using Hipparcos catalogue led to an encounter distance of 0.33 pc, 1.38 Myr from the present time (see e.g. García-Sánchez et al. 2001; Torres et al. 2018). Using *Gaia* DR1, Torres et al. (2018) pointed out that the encounter distance is even smaller, at 0.062 pc, 1.35 Myr from today (see also Berski & Dybczyński 2016; Bobylev & Bajkova 2017; Bailer-Jones 2018). With the data from *Gaia* DR2 in hand, the distance and time of closest approach have again slightly decreased to 0.054 pc and 1.28 Myr (Table 3.3, Table 3.5). de la Fuente Marcos & de la Fuente Marcos (2018) and Bailer-Jones et al. (2018) found similar but slightly discrepant results. The small discrepancy in the various results is mainly due to the orbit integration method and the Galactic potential used in their calculations, considering that the input data are the same.

A comparison of the results obtained for GJ 710 from Hipparcos, *Gaia* DR1, and *Gaia* DR2 data is shown in Fig. 3.7. Calculations were performed following the method described in Sect. 3.3.1, using the astrometric data described in Table 3.5. The discrepancy between Hipparcos and *Gaia* is due to the difference in the value of the astrometric parameters and radial velocity. This results in a shift in the perihelion distance of GJ 710. Using different parameters for the Galactic potential will also lead to slightly different values (see e.g. Bailer-Jones et al. 2018). We note that the time of perihelion is more uncertain for the *Gaia* DR2 data, which is caused by the larger uncertainty in the radial velocity. Following the method described in Sect. 3.3.2 and Sect. 5.4, we investigated the effect of GJ 710 on a simulated Oort cloud (Fig. 3.9, first row). The perturbation because of GJ 710 lifts the semi-major axis of the comets within the region between $\sim 10\,000$ and $100\,000$ au (Fig. 3.8), creating $\sim 0.01\%$ hyperbolic objects, while $\sim 0.30\%$ of the comets gain a semi-major axis beyond the edge of the Oort cloud ($a > 100\,000$ au).

3.3 Close encounters with the solar system

Table 3.5: Comparison of the different astrometric parameters and radial velocities obtained for GJ 710 from Hipparcos, Gaia DR1, and Gaia DR2 data. The last two rows represents the time and the closest approach distance to the Sun of GJ 710 with its respective confidence interval.

Parameters	Hipparcos	Gaia DR1	Gaia DR2
ϖ [mas]	51.12 ± 1.63	52.35 ± 0.27	52.51 ± 0.04
μ_{α^*} [mas/yr]	1.15 ± 1.66	-0.47 ± 0.13	-0.45 ± 0.08
μ_{δ} [mas/yr]	1.99 ± 1.22	-0.18 ± 0.09	-0.02 ± 0.07
μ_{tot} [mas/yr]	2.30 ± 2.06	0.50 ± 0.16	0.46 ± 0.11
v_{rad} [km/s]	$-13.80 \pm 0.30^*$	$-13.80 \pm 0.30^*$	$-14.52 \pm 0.43^{**}$
t_{ph} [Myr]	$1.385 [1.109, 1.500]$	$1.353 [1.219, 1.541]$	$1.281 [1.109, 1.500]$
d_{ph} [pc]	$0.302 [0.302, 0.324]$	$0.062 [0.014, 0.116]$	$0.054 [0.003, 0.106]$

*Pulkovo catalogue (Gontcharov 2006), ** Gaia DR2 radial velocity catalogue (Soubiran et al. 2018).

3 Dynamics of the Oort cloud

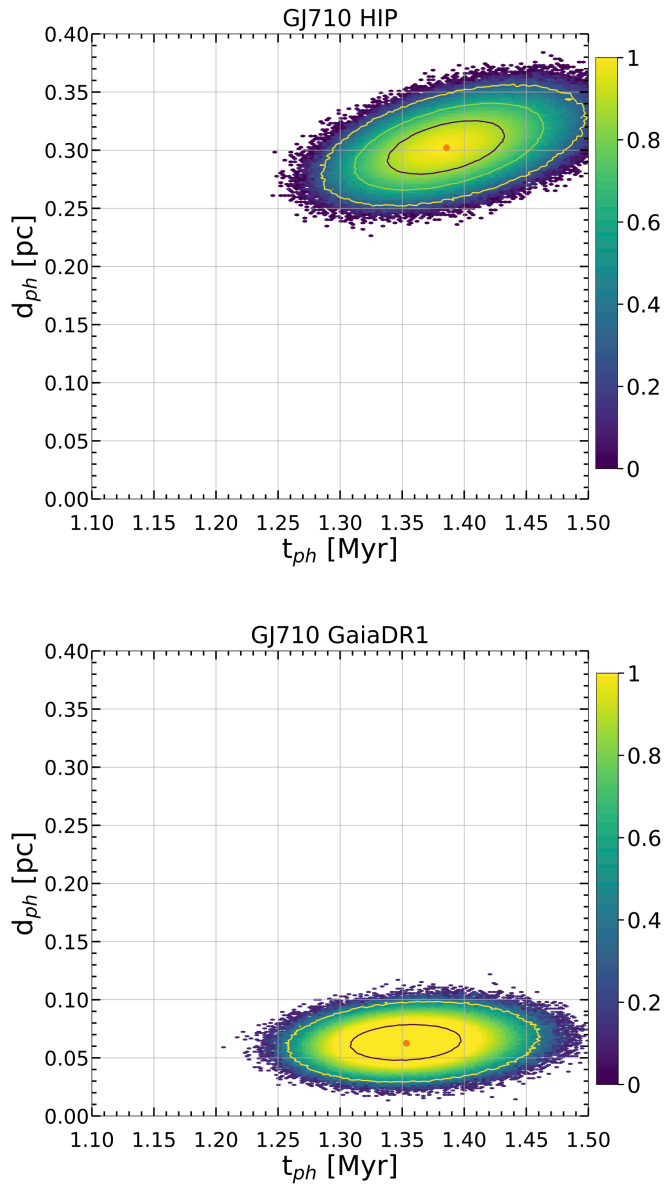


Figure 3.7: Continue...

3.4 Dynamical evolution of the Oort cloud

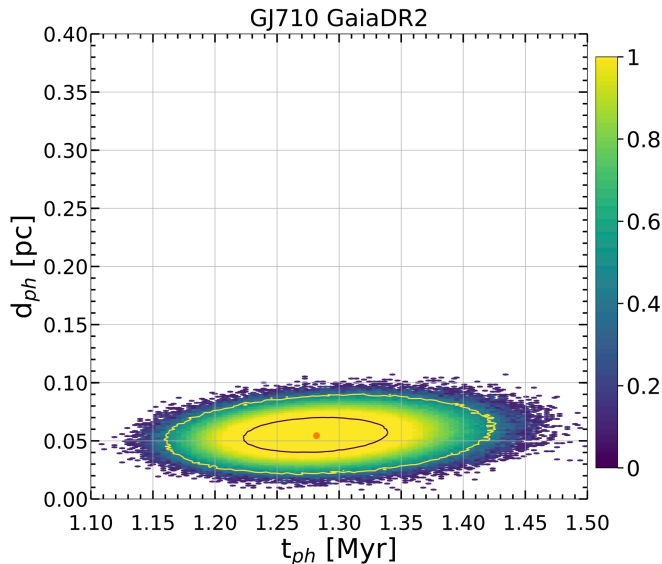


Figure 3.7: Joint distribution of the time and distance of closest approach for GJ 710. The first panel shows results obtained with Hipparcos data, while the middle and bottom panels show the results for Gaia DR1 and Gaia DR2, respectively (see Table 3.5). The contour levels indicate regions enclosing 0.60, 0.90, and 0.99% cumulative probability (color bar).

Section 3.4

Dynamical evolution of the Oort cloud

As pointed out by Heisler & Tremaine (1986) the Galactic tidal field is a major contributor to Oort cloud perturbations at large distances, while as we showed in Sect. 3.3.2 the cumulative effect of passing stars can also lead to substantial perturbations of the Oort cloud comets. In this section we study the cumulative effects of the known stellar encounters (Table 3.4) and the Galactic tidal field over the interval of 20 Myr centred on the present time. This provides a lower limit to the combined effect of stellar encounters and the Galactic tidal field on the dynamical evolution of the Oort cloud.

3.4.1 Numerical model

We use the Astrophysical Multi-purpose Software Environment – AMUSE (Portegies Zwart et al. 2009; Pelupessy et al. 2013; Portegies Zwart et al.

3 Dynamics of the Oort cloud

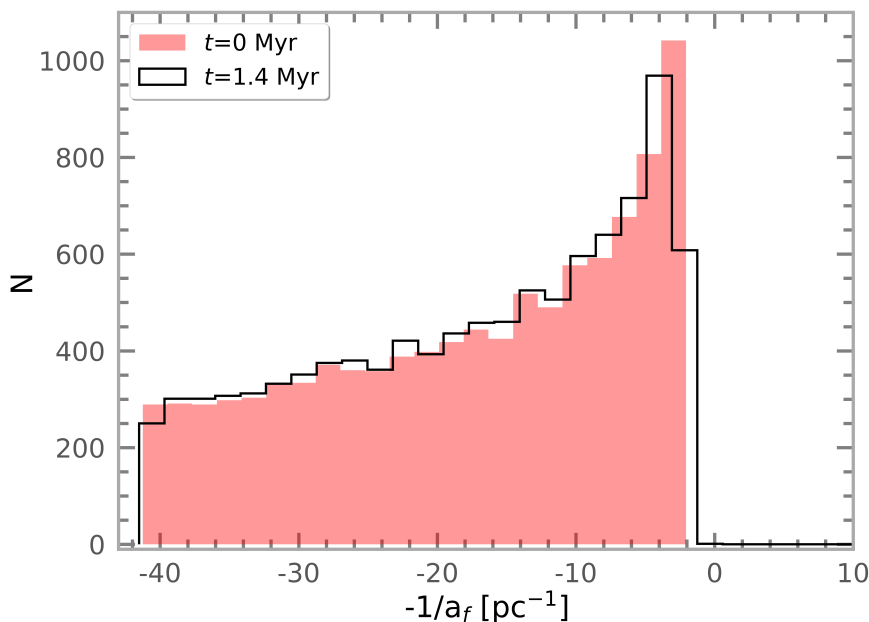


Figure 3.8: Histogram of the orbital energy distribution of the particles in the Oort cloud, before and after the encounter with the star GJ710. The red histogram corresponds to the initial semi-major axis distribution, and the black curve to the final one.

2013b; Portegies Zwart & McMillan 2018) – for our calculations. Following the works of Rickman et al. (2008) and Hanse et al. (2016) we first construct an isotropic Oort cloud of 10,000 test particles (Fig. 3.9, first row). The distribution of Oort cloud particles is spherically symmetric and isotropic, and they follow a uniform distribution in the orbital elements $\cos i$, ω , Ω , and M . The initial eccentricities, e , are selected with a probability density distribution $p(e) \propto e$ and the perihelia, q , are chosen outside of the planetary region ($q > 32$ au). The semi-major axes, a , are distributed proportional to $a^{-1.5}$ over the range $3 \times 10^3 - 10^5$ au. In order to ensure a thermalised Oort cloud (e.g. Duncan et al. (1987); Dybczyński (2002); Rickman et al. (2008)) we used a radial density profile of $r^{-3.5}$ (where r is the distance between the comets and the Sun).

Subsequently we used the GPU-accelerated direct N-body code ABIE (Cai et al. in preparation) with a fifteenth-order Gauss-Radau integrator

3.4 Dynamical evolution of the Oort cloud

(Everhart 1985) optimised for close encounters. We couple ABIE and the Gala package in such a way that ABIE advances the positions of the Oort cloud particles and Gala calculates the accelerations on each particle due to the Galactic tidal field, based on the positions provided by ABIE. The calculated accelerations are subsequently inserted into the Gauss-Radau integrator in ABIE as additional forces. Using the catalogue of nearby stars (Table 3.3), we selected all the stars (31) that are predicted to pass within 2.5 pc of the Sun (Table 3.4) ± 10 Myr from today. These stars are included in the integrator with their present-day positions and velocities with respect to the Sun. Hence we evolve a system for a period of 20 Myr which consists of one host star (the Sun) surrounded by 10,000 test particles (Oort cloud) under the influence of external perturbations due to passing stars and the Galactic tidal field.

3.4.2 Galactic tide and Gaia star perturbation

In order to disentangle the effects of the Galactic tidal field and the encounters with stars identified in *Gaia* DR2 we considered three main cases for external perturbations, *Galactic tidal field*, *Gaia stars*, *Galactic tidal field + Gaia stars*. We focus now on the effect of the external perturbations considering an extended Oort cloud ($a \leq 100\,000$ au). The first row of Fig. 3.9 shows the initial conditions followed by the final perihelion distance as a function of the final semi-major axis for the three scenarios previously discussed. Considering a short integration of 20 Myr (10 Myr in the past, and 10 Myr in the future). The green area represents the original location of the ejected particles (yellow dots).

The effect of the Galactic tidal field on the Oort cloud decreases from the outskirts to the inner regions of the cloud (second row Fig. 3.9). The particles at the edge of the cloud suffer a considerable change in their orbital elements. Specifically, for $\sim 0.91\%$ (yellow dots, Fig. 3.9) of the objects, their semi-major axes increase up to interstellar distance ($a > 100\,000$ au). The particles in the inner Oort cloud remain unaffected. A small fraction of the particles ($\sim 0.02\%$) acquire hyperbolic orbits. When *Gaia* stars are the only perturber (Fig. 3.9, third row) their effect is much less pronounced than that of the Galactic tidal field in particular in the outskirts on the Oort cloud. The effect of *Gaia* stars is dominated by the star GJ 710 (Fig. 3.8). However, the cumulative effect of relatively distant encounters (~ 1 pc) helps to change the semi-major axis of $\sim 0.38\%$ of the comets in the

3 Dynamics of the Oort cloud

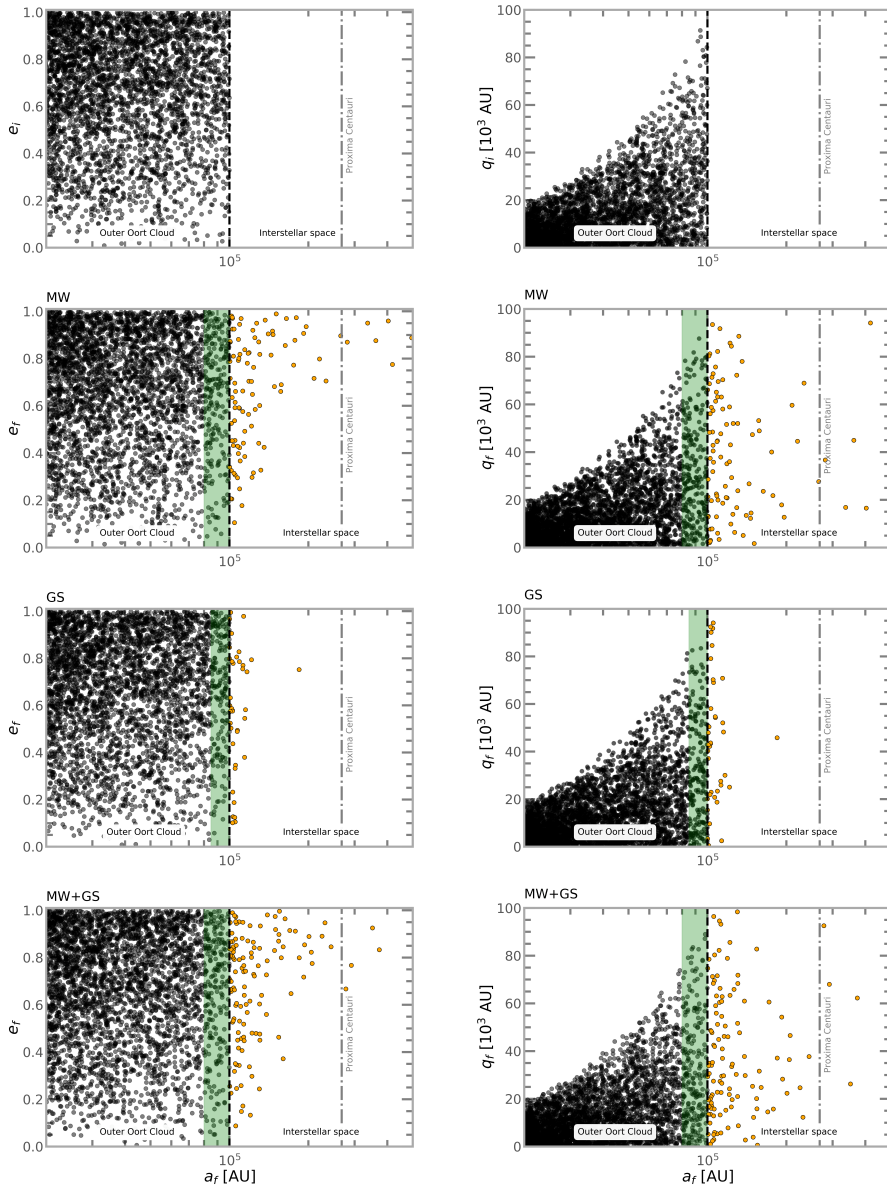


Figure 3.9: Final eccentricity and perihelion as a function of final semi-major-axis, for a total integration of 20 Myr. The first row corresponds to the initial conditions. The second and third rows show the effect of the Galactic tidal field and Gaia stars, respectively. The last row corresponds to the combined effects of the Galactic tides and Gaia stars. The green area corresponds to the initial position of the ejected particles, coloured yellow.

3.4 Dynamical evolution of the Oort cloud

outer Oort cloud, whereas 0.01% of the outer Oort cloud objects acquire hyperbolic orbits.

The combination of the Galactic tidal field and *Gaia* stars (Fig. 3.9, last row) enhances the perturbations on the Oort cloud, causing 0.03% of the initial objects to become unbound from the solar system, while $\sim 1.12\%$ acquire orbits with semi-major axis in the interstellar regions, i.e., $a \geq 100\,000$ au. In all three scenarios for external perturbations, a considerable population of objects with $a \geq 100\,000$ au is created. Their orbits remain elliptic, but the effect of external perturbations lifts their semi-major axis beyond the Oort cloud (yellow dots, Fig. 3.9). This effect is only relevant for the outermost regions of the Oort cloud ($\sim 80\,000$ – $100\,000$ au). The orbital elements of the particles in the inner parts of the cloud will not be affected as strongly.

We now consider a compact Oort cloud with semi-major axes up to $50\,000$ au. The effect of the Galactic tidal field has a negligible effect (first panel, Fig. 3.10) over the particles in the cloud. The second panel in Fig. 3.10 shows the effect of the *Gaia* stars. The effect of GJ 710 is prominent, and causes a major perturbation. The last panel in Fig. 3.10 shows that the effect of the *Gaia* stars dominates over the Galactic tidal field, however it is the combined effect which efficiently increases the number of particles (by $\sim 1.20\%$) with semi-major axis beyond the limits of the cloud ($a > 50\,000$ au).

We conclude that the cumulative effect of passing stars and the Galactic tidal field are efficient mechanisms in the creation of comets for which the semi-major axis is larger than the extent of the Oort cloud ($a > 100\,000$ au), but with bound and eccentric orbits. Hereafter we refer to such objects as transitional interstellar comets (TICs). If we consider an Oort cloud with $a \leq 100\,000$ au, the Galactic tidal field is the major perturber, while for an Oort cloud with $a \leq 50\,000$ au passing stars provide the major effect, mainly due to the close encounter with GJ 710 (Fig. 3.8).

For long timescales (on the order of gigayears), the synergy between Galactic tides and stellar encounters to bring comets into the observable zone is now well understood (Rickman et al. 2008; Fouchard et al. 2011). Both perturbations strongly depend on the semi-major axis of the comets. In general the Galactic tidal field rapidly changes the perihelia of the outer regions, while passing stars are a good mechanism to eject or inject particles when a close encounter happened (see e.g. Portegies Zwart & Jílková 2015). For short timescales (~ 20 Myr), the Galactic tide and stellar en-

3 Dynamics of the Oort cloud

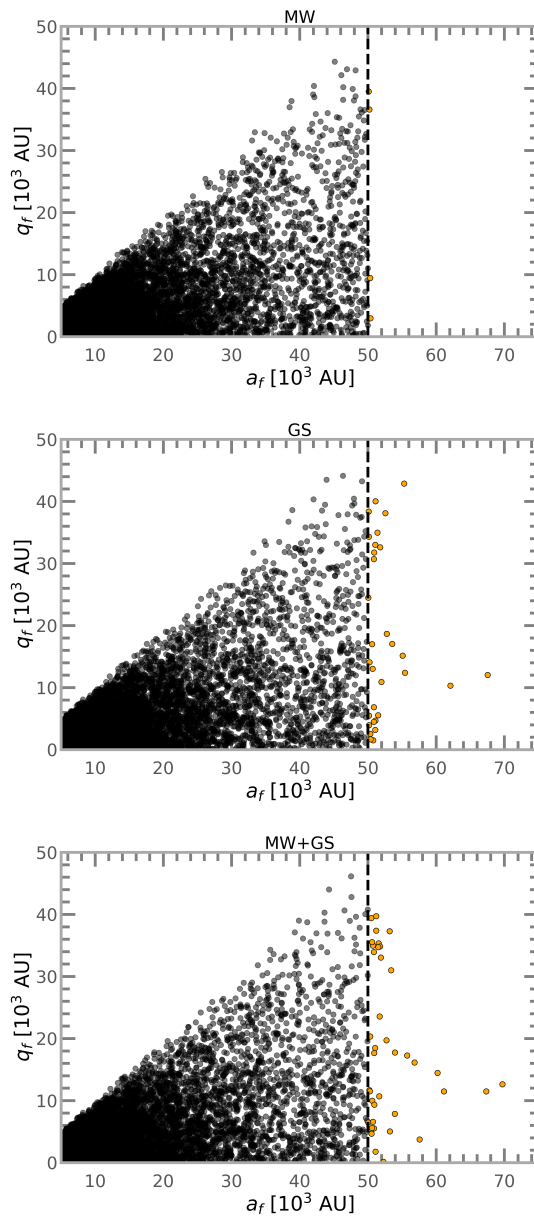


Figure 3.10: Final perihelion as a function of final semi-major axis for an Oort cloud size of 50,000 au. The first panel shows the effect of the Galactic tidal field (marked as a MW). The second and third panels show the effect of Gaia stars (GS) and the combination of both the Galactic tide and Gaia stars (MW+GS), respectively. Black dots represent the particles in the Oort cloud, while the yellow dots represent the ejected ones.

3.4 Dynamical evolution of the Oort cloud

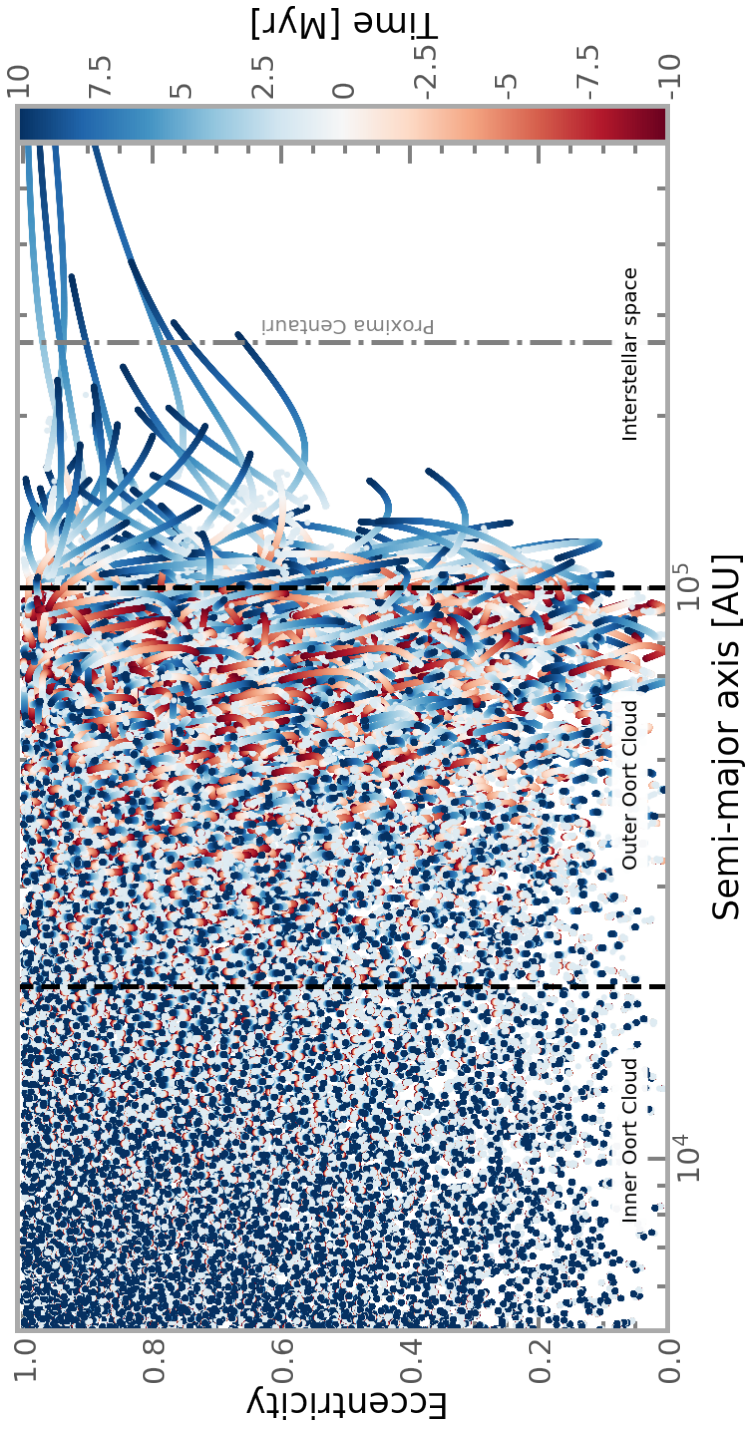


Figure 3.11: Orbital evolution of the particles in the simulated Oort cloud. The figure shows the evolution of the eccentricity as a function of the semi-major axis over the period of 20 Myr (± 10 Myrs.). The colour bar represents the integration time. An animation can be found at: <https://home.strw.leidenuniv.nl/~storres/#Research>

3 Dynamics of the Oort cloud

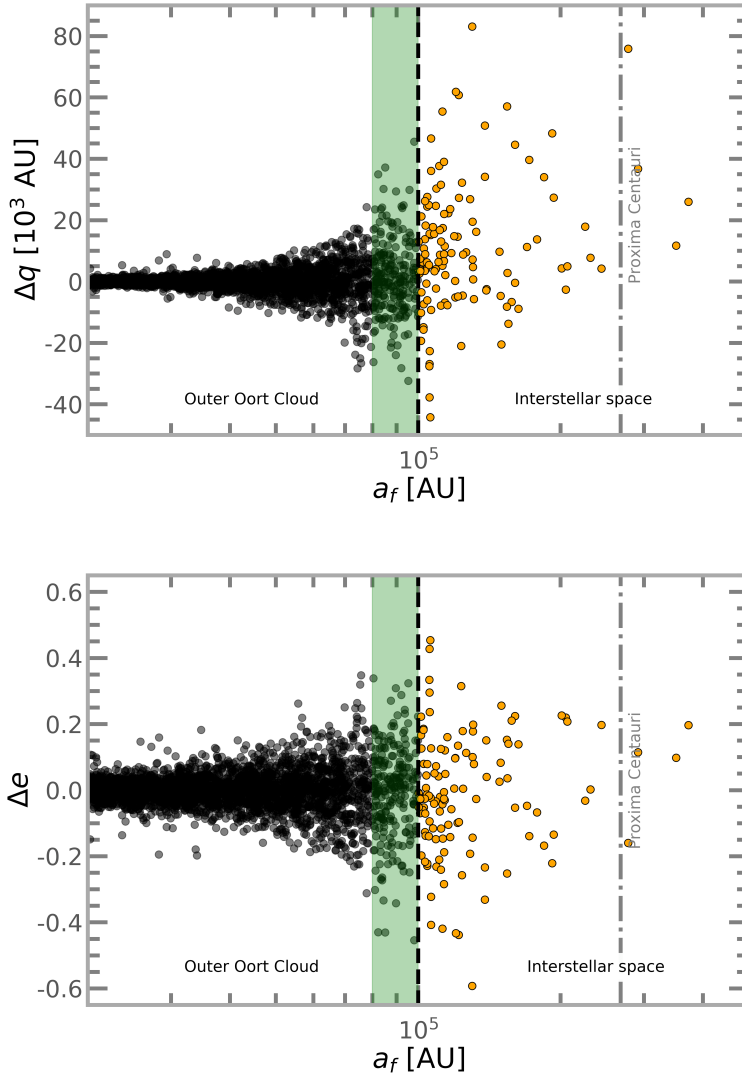


Figure 3.12: Mean perihelion and eccentricity changes as a function of the semi-major axis of the comets. The green area corresponds to the region of the initial position of the particles ejected, represented as a yellow dots.

3.4 Dynamical evolution of the Oort cloud

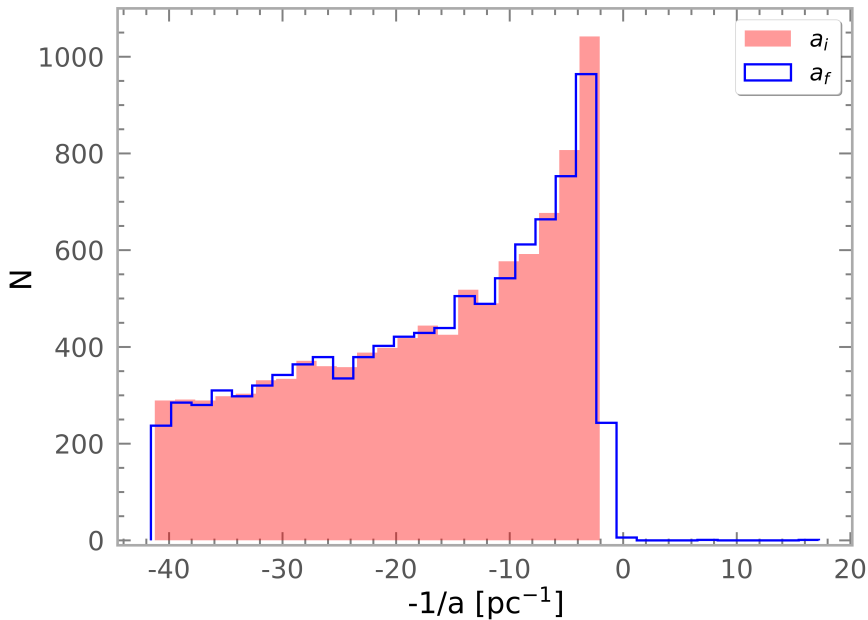


Figure 3.13: Histogram of the orbital energy distribution of the particles in the Oort cloud. The blue curve corresponds to the final semi-major axis, while the red curve shows the initial distribution.

counters prove to be an efficient mechanism for the creation of TICs. The outermost part of the cloud ($\sim 80\,000\text{--}100\,000$ au, Fig. 3.11) is heavily perturbed, whereas the innermost part remains unchanged ($3000\text{--}50\,000$ au, Fig. 3.11). This implies that the edge of the Oort cloud is sensitive to external perturbations and is relatively easy to strip. The particles in the outermost part of the Oort cloud have a considerable change in their orbital elements. The change of the perihelion and eccentricity increases as a function of the semi-major axes (Fig. 3.12), whereas the semi-major axes reach interstellar distances. These objects previously referred to as transitional interstellar comets remain bound to the Sun with eccentric orbits (Fig. 3.13). The detailed effects of subsequent perturbations due to passing stars and the Galactic tidal field will determine if these objects will return to the solar system or become unbound.

3 Dynamics of the Oort cloud

Considering the efficiency of external perturbations on circumstellar comet clouds in the creation of interstellar objects, and noting that Valtonen & Innanen (1982) pointed out that objects with a relative velocity above 0.5 km/s can probably enter and leave the solar system, we speculate that a ‘cloud’ of objects exists in interstellar space which overlaps with our Oort cloud and constantly exchanges material with it. An indication that this may be the case was provided by the first interstellar comet detected, ‘Oumuamua (Williams 2017), which opened a new era in the study of interstellar objects. Estimates of the local density of interstellar objects range from 10^{14} pc^{-3} (Portegies Zwart et al. 2018), to $8 \times 10^{14} \text{ pc}^{-3}$ (Jewitt et al. 2017), to $2 \times 10^{15} \text{ pc}^{-3}$ (Do et al. 2018). The existence of an interstellar comet cloud could partly explain the slightly hyperbolic comets and potential interstellar objects that might have been detected in the solar system but not yet classified as such (see e.g. de la Fuente Marcos & de la Fuente Marcos 2019). A future detailed study of the evolution of the TICs created by the tides and stellar encounters is needed to draw more solid conclusions.

The results presented here are based on the assumption of a hypothetical present day spheroidal cloud of comets extending up to 100,000 au from the Sun. If we consider a smaller structure (Fig. 3.10), passing stars are the main perturbers, while the Galactic tidal field barely influences the orbit of the comets. In addition we stress that our sample of stars considered as perturbers of the Oort cloud is incomplete due to the *Gaia* survey limits combined with our data quality filtering and the upper limit we imposed on the distance to the stars in our sample. A more complete inventory of Oort cloud perturbers would increase the effects of the stellar encounters.

Section 3.5

Summary and Conclusions

In this work we present a study of the combined effect of the Galactic tidal field and close stellar encounters predicted to occur over a time interval of 20 Myr around the present on the Oort cloud of the solar system. Our focus is on the loss of comets to interstellar space. Following Rickman et al. (2008), we first presented a simple model of stellar encounters based on data compiled for 13 spectral types of the stars in the solar neighbourhood. We confirm that individual perturbations of randomly passing stars cannot alter the orbits of the comets in the Oort cloud unless a very close encounter

3.5 Summary and Conclusions

occurs. However, from a consideration of the stellar encounter statistics we show that the comets in the cloud may be lost to interstellar space over a short period of time due to the cumulative effect of stellar encounters.

Motivated by this result we used *Gaia* DR2 data to identify 14,659 stars passing within 50 pc of the Sun over the time period of ± 10 Myr centred on the present. Out of this sample 31 stars are predicted to be major perturbers of the Oort cloud, approaching the Sun to within 2.5 pc. This catalogue of perturbing stars (presented in Table 3.3) constitutes an astrometrically clean sample, which is nevertheless incomplete due to the *Gaia* survey limitations, the upper limit imposed on the distance to the stars in the sample (50 pc), and the strict data-quality filtering. Our estimates of the effect of known stellar encounters is therefore conservative (we note that Bailer-Jones et al. 2018, find a larger number of stellar encounters from *Gaia* DR2 due to their less stringent data-quality filtering). Using the impulse approximation (Eq. (3.1)) we then calculated the impulse that each star passing within 2.5 pc of the Sun imparts to a comet in the Oort cloud. We found that (as expected) the effect of individual encounters is relatively small (on the order of 10^{-3} to 10^{-4} km s $^{-1}$). The cumulative effect of *Gaia* stars was then investigated. We found that the collective effect of stars passing within ~ 1 pc can lift the perihelion of members of the Oort cloud in a relatively short period of time.

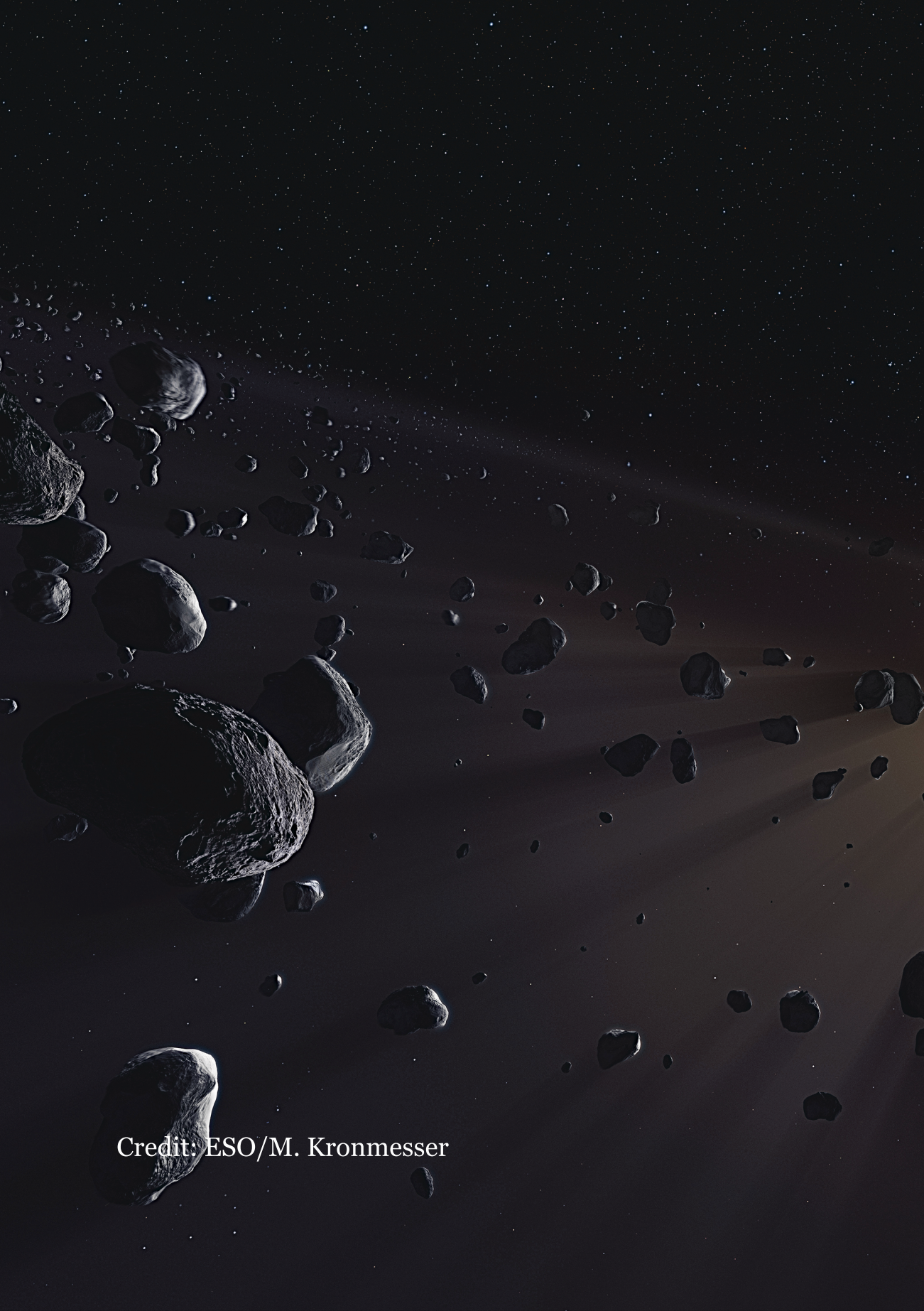
Finally, we focused our study on the combined effect of multiple stellar encounters and the Galactic tidal field on a simulated Oort cloud. To achieve this we used a detailed N -body simulations, evolving a system of one host star (the Sun) surrounded by 10,000 test particles (the Oort cloud) and affected by three different sets of external perturbations (*Gaia* stars only, Galactic tidal field only, and the combination of both), over a period of 20 Myr (± 10 Myr centred on today). When we consider an extended Oort cloud ($a \leq 100\,000$ au), we find that the effect of the Galactic tidal field alone leads to the creation of TICs of around 0.91% of the initial comets, while the collective effect of the passing stars only leads to a smaller fraction of 0.38%. For the compact model of the Oort cloud ($a \leq 50\,000$ au), passing stars dominate the perturbations, mainly due to the star GJ 710, while the effect of the Galactic tidal field is almost negligible. Overall for an extended cloud, the Galactic tide dominates over the passing stars, for the case of a compact cloud the opposite is true. However, it is the combined effect of passing stars and the Galactic tidal field which significantly increases the perturbation on the Oort cloud. These combined effects raise the semi-major axis of around 1.12% of the initial particles for the compact

3 Dynamics of the Oort cloud

model, and $\sim 1.20\%$ for the extended one, up to the interstellar regions (i.e. $a > 100\,000$ au). The estimates presented in this work are conservative and based on a small sample of known stars that pass near to the Sun during ± 10 Myr. The effects of a more complete sample will increase the number of TICs. Overall the external perturbations are an efficient mechanisms in the formation of interstellar comets over a short period of time (in the order of tens of megayears).

The further evolution of the transitional interstellar comets depends on the perturbations introduced by passing stars and the Galactic tidal field. These perturbations determine whether the transitional interstellar comets will remain bound to the solar system or eventually become interstellar comets. Under the hypothesis that other planetary systems also possess Oort cloud-like structures, they most probably experience the same mechanism of erosion due to external perturbations. This leads us to speculate that there is a large population of cometary bodies that occupy interstellar space. Therefore, visits to the solar system by interstellar comets such as 'Oumuamua may well be a frequent occurrence.

Acknowledgements We thank the referee for the constructive reports and helpful suggestions to improve the present work. ST expresses his gratitude to the Mexican National Council for Science and Technology (CONACYT) for the grant #291004-410780; to Leiden Observatory for the unconditional support; and to Daniel Hestroffer, Eric Mamajek, Konstantin Batygin, and Ylva Götberg, for the discussions and comments on the manuscript. This project was shaped in part at the 2018 New York Gaia Sprint. This work was supported by the Netherlands Research School for Astronomy (NOVA) and by NWO (grant #621.016.701 [LGM-II]). This work has made use of data from the European Space Agency (ESA) mission *Gaia* (<https://www.cosmos.esa.int/gaia>), processed by the *Gaia* Data Processing and Analysis Consortium (DPAC, <https://www.cosmos.esa.int/web/gaia/dpac/consortium>). Funding for the DPAC has been provided by national institutions, in particular the institutions participating in the *Gaia* Multilateral Agreement. This work was carried out on the Dutch national e-infrastructure with the use of *Cartesius* the Dutch national supercomputer and the support of SURF Cooperative.



Credit: ESO/M. Kronmesser

Chapter 4

Dynamical evolution of the solar system debris disk in its birth cluster

S. Torres, M. X. Cai, D. Mukherjee,
S. Portegies Zwart, and A. G. A. Brown
Submitted to *Astronomy & Astrophysics*,
recommended for publication, 2019b

Abstract

The Sun, like many other stars in the Milky Way galaxy, probably formed in a star cluster. Due to the relatively high stellar density in such a cluster, encounters are expected to affect the early stage of the dynamical evolution of the solar system. In particular, the outer parts of the solar system are vulnerable to such perturbations. Here, we investigate the role of stellar flybys on the formation of the Oort cloud. This is done using the LonelyPlanets module in the AMUSE framework. In LonelyPlanet the effect of a star cluster on individual planetary systems is resolved in two steps: first, we simulate the star cluster without planets to subsequently evolve each planetary system while taking the perturbations of nearby stars into account. In our calculations, each star receives a debris disk and a population of planets. Calculations are performed with small disks (of 16-35 au) and large disks (of 40-1000 au). The calculations are carried out with two arrangements of planets. One configuration that mimics the current solar system and one case in which we adopt a compact configuration with planets closer together than they are today. Objects in the outer edge of the debris disk are scattered by passing stars and in the inner edge by the interaction with the planets. The planets cause asteroids to be ejected and park them in resonant orbits. Stellar encounters play an important role in heating the debris disks, resulting in eccentric and inclined orbits with respect to the initial conditions. Up to $\sim 36\%$ of the original disk material is ejected from the planetary systems to become *sōlī lapidēs* such as 'Oumuamua. These objects are ejected with a typical velocity of 1-3 km/s.

Introduction

Oort (1950) proposed the existence of a cloud of comets that surrounds the solar system which was subsequently named after him. The Oort cloud is thought to contain about 10^{11} – 10^{12} comets (Brasser & Morbidelli 2013), with a total mass of around 2–3 (e.g., Francis 2005; Morbidelli 2005). Its shape is conjectured to be nearly spherical, with the cloud extending up to 0.5 pc from the Sun, limited by the Hill sphere of the solar system (Oort 1950; Chebotarev 1965). Because these estimates of the Oort cloud properties are highly uncertain (mainly because of the lack of observations of the long-period comets), the creation, evolution and even the existence of the Oort cloud remain a puzzle today. One of the main questions related to the origin of the Oort cloud is related to the moment of its formation. Sev-

eral works have explored the origin and evolution of the Oort cloud, mainly by performing numerical simulations. These studies follow two main ideas of formation: a *primordial* or a *late* formation of the Oort cloud. The *primordial* model occurs in the early stages of the solar system when the Sun was still in its birth cluster (see e.g., Oort 1950; Hills 1981; Heisler & Tremaine 1986; Duncan et al. 1987; Weissman 1996; Wiegert & Tremaine 1999; Dones et al. 2004; Levison et al. 2010). In this scenario the planetesimals were scattered due to the interaction with the growing giant planets and started populating the Oort cloud. The *late* model assumes that the Sun already left its birth cluster. In this alternative scenario the Oort cloud was created in the later stages of the solar system formation possibly due to gravitational instabilities when the giant planets experienced an orbital resonance, which caused the minor bodies to be ejected onto almost unbound orbits (see e.g., Levison et al. 2004; Brasser et al. 2006; Fouchard et al. 2006; Kaib & Quinn 2008; Morbidelli 2005; Duncan 2008; Brasser & Morbidelli 2013; Shannon et al. 2014; Dones et al. 2015; Nesvorný 2018; Shannon et al. 2019; Vokrouhlický et al. 2019).

Nowadays the model is adopted that the solar system was born in a star cluster (Portegies Zwart 2009; Adams 2010) and that it was still a cluster member when the planets formed (Pichardo et al. 2012; Portegies Zwart & Jílková 2015; Martínez-Barbosa et al. 2016). Considering that the lifetime of an open cluster is around 100 Myr and stellar clusters are dense environments, the probability of close encounters is higher than in the case the

4 Formation and Evolution of the Oort cloud

Sun would be isolated (Portegies Zwart & Jílková 2015). Therefore the Oort cloud most probably faced interactions with the siblings of the Sun.

Nordlander et al. (2017) discussed the evolution of a primordial Oort cloud for different models of the birth cluster of the Sun (low, intermediate, and high mass). They considered the evolution of the cloud in a long-lived cluster starting at 100 Myr and finishing with the late heavy bombardment (~ 500 Myr). They found that a primordial Oort cloud will likely not survive for any of the cluster models, with the low-mass cluster having the best chance for the solar system to survive. This result thus favours a delayed formation of the Oort cloud (e.g., Brassier & Morbidelli 2013). Other authors suggested (see e.g., Levison et al. 2010; Jílková et al. 2016; Pfalzner et al. 2018; Hands et al. 2019) that part of the Oort cloud was captured through the interactions with passing stars while the Sun was in its birth cluster, and that also objects like Sedna are the consequence of a dynamical interaction with closely passing stars. Overall, the formation of the Oort cloud while the Sun was still in its birth cluster is constrained by two scenarios. One which is in favour of a dynamical instability of a protoplanetary disk due to the migration of the giant planets and random passing stars (see e.g. Fernández & Brunini 2000; Brassier et al. 2012); and the other propose that a fraction of the Oort cloud was capture due to the interaction with the stars in the cluster (see e.g, Levison et al. 2010; Hands et al. 2019).

Motivated by the idea that the formation of the Oort cloud occurred while the Sun was in its birth cluster, we aim to study the formation and evolution of the Oort cloud in such an environment. Direct N-body simulations were used, where specifically we performed a set of simulations modelling the evolution of the solar system debris disk while the Sun is still in its birth cluster. We studied the dynamical evolution of the debris disk under the influence of a single and multiple random stellar encounters and the giant planets. We explore two models of the solar system, *extended* and *compact*. The *extended* model is based on the present-day orbits of the giant planets (i.e, Jupiter at 5.2 au, Saturn at 9.5 au, Uranus at 19.2 au and Neptune at 30.1 au) and an extended debris disk ($40 < a < 1000$ au). The *compact* model is a Nice-based model (Gomes et al. 2005; Tsiganis et al. 2005; Morbidelli et al. 2005) with giant planets in compact orbits (Jupiter at 5.5 au, Saturn at 8.1 au, Neptune at 11.5 au, and Uranus at 14.2 au) and a compact disk ($16 < a < 35$ au). In Section 5.2 we describe our numerical implementation. In Section 5.3 we present the results for our N-body simulations for the evolution of the solar system in a birth cluster environment for the two models mentioned before. In Section 5.4 we discuss the effect

of a dense environment on the creation of *transitional interstellar comets* (Torres et al. 2019a) and hyperbolic objects like 'Oumuamua (Meech et al. 2017; Williams 2017). Finally in Section 4.5 we present our summary and conclusions.

Section 4.2

Numerical implementation

To study the dynamical evolution of the solar system in a dense environment, we considered two alternative models, which we refer to as *extended* and *compact*. For each model we performed two sets of simulations, one in which only one close encounter between the solar system and another star (*Extended 1* and *Compact 1* models) is considered and the other in which multiple random encounters are considered (*Extended N* and *Compact N* models). The initial conditions of the four models are listed in Table 4.1 and a schematic representation is provided in Fig. 4.1.

For the simulations and the generation of the initial conditions for the *Extended 1* and *Compact 1* models we used REBOUND (Rein & Liu 2012) with the WH-Fast integrator (Rein & Liu 2012). We ran 32 simulations in which we assumed a Sun-like star approaching the solar system at distance ranging from 225 au to 400 au, at inclinations i of 0, 30, 60, and 90 degrees, and with a velocity relative to the Sun of $\sim 1 \text{ km s}^{-1}$, typical for an open cluster environment (Binney & Tremaine 2008). The planetesimals in the disk are approximated as massless test particles (1000 per simulation), and the evolution time is set to 20 000 yr, with the encounter happening 10 000 yr after the start of the simulation.

For the models *Extended N* and *Compact N* we simulated the solar system in an open cluster-like environment. We first used the code *LonelyPlanets* (Cai et al. 2015, 2017, 2018). *LonelyPlanets* combines NBODY6++GPU (Wang et al. 2015) and REBOUND (Rein & Liu 2012) through the framework of the Astrophysical Multi-purpose Software Environment – AMUSE (Portegies Zwart et al. 2009; Pelupessy et al. 2013; Portegies Zwart et al. 2013b; Portegies Zwart & McMillan 2018). We used NBODY6++GPU and a Plummer sphere model (Plummer 1911) to simulate the open cluster, with an initial mass function ranging from 0.08 to 100 (Kroupa 2001), 2000 stars, and a virial radius of 1 pc. A Sun-like star is then chosen randomly by the *LonelyPlanets* module and the solar system is placed around it and is evolved for 100 Myr. The code then uses a KD

4 Formation and Evolution of the Oort cloud

Table 4.1: Initial conditions for the extended and compact models. The first column indicates the type of model. The second column shows the size of the disk. The third column represents the positions of the giant planets (Jupiter (J), Saturn (S), Uranus (U), and Neptune (N)), followed by the integration time, the number of encounters and the perturber distance.

Model	disk [au]	Position of the Planets [au]	Time [Myr]	Encounters	Perturber distance [au]
<i>Compact 1</i>	16–35	J:5.5, S:8.1, N:11.5, U:14.2	0.02	one	225 – 400
<i>Extended 1</i>	40-200	J:5.2, S:9.5, U:19.2, N:30.1	0.02	one	225 – 400
<i>Compact N</i>	16–35	J:5.5, S:8.1, N:11.5, U:14.2	100	multiple	$10^2 - 10^4$
<i>Extended N</i>	40-1000	J:5.2, S:9.5, U:19.2, N:30.1	100	multiple	$10^2 - 10^4$

4.2 Numerical implementation

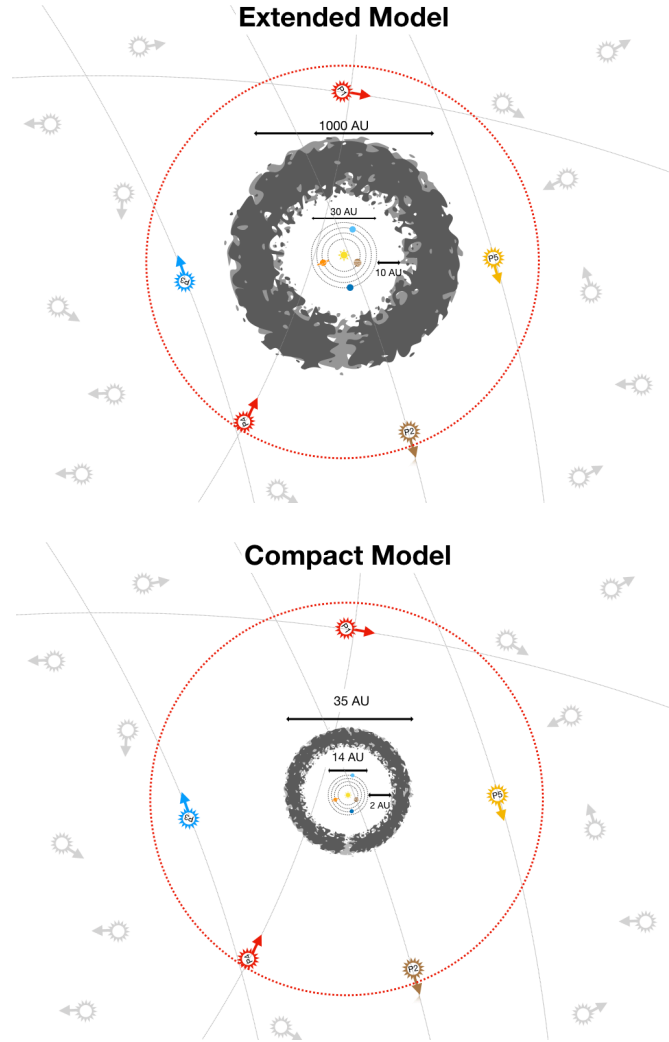


Figure 4.1: Illustration of the solar system for the extended (top panel) and compact (bottom panel) models. The planetary region for the extended model uses the present day positions of the planets. In the compact model the giant planets are in compact orbits (Jupiter at 5.5 au, Saturn at 8.1 au, Neptune at 11.5 au, and Uranus at 14.2 au). The grey disk represents the debris disk of which the size is set to 1000 au for the extended model (top panel) and 30 au for the compact model (bottom panel). The dotted red circle indicates the boundary of the neighbour sphere, beyond which we ignore the influence of any perturbations by passing stars (distance not to scale). Grey stars represent the stars in the cluster that are ignored. The coloured star symbols (P1, P2, P3, P4, and P5) represent the five nearest stars that perturb the solar system at a given time. The arrows indicate the direction of motion of the perturbors.

4 Formation and Evolution of the Oort cloud

tree to find the five closest stars to the Sun at any given time. These stars and the solar system are then evolved together using the IAS15 (Rein & Spiegel 2014) integrator, thus simulating the effect of encounters between the solar system and stars in the cluster. IAS15 was chosen as it is a high order, adaptive time step integrator which attains relative energy errors of $\sim 10^{-14}$ for timescales of the order of 100 Myr. Even though this integrator is non-symplectic, it preserves energy better than symplectic integrators. Its adaptive time step scheme helps resolve collisions with more precision. We first made a rough study with a grid of low-resolution simulations (200 simulations with 200 test particles in the debris disk). We then selected 24 systems and used these to initialize high-resolution simulations including 2000 test particles in the disk. In each of those simulations the Sun is born in a different position in the cluster.

Section 4.3

Effect of stellar encounters on the early solar system

Debris disks are the remnants of planet formation. Several observations suggest that the disk sizes range from the inner part of the planetary systems (~ 10 au) to ~ 1000 au (Stark et al. 2009; Hughes et al. 2018). The architecture, structure and dynamics of these disks depend on several factors, but primarily on the type of star and the cluster environment, considering that most of the stars are born in the stellar clusters (Lada & Lada 2003). Several studies suggested that the Sun was born in a stellar cluster (e.g., Portegies Zwart 2009; Adams 2010; Pichardo et al. 2012). However, it is still unclear if the current configuration of the solar system was reached when the Sun was still in the cluster, or after the Sun left the cluster. In this section we present the results of the simulations described above and focus on the evolution of the particles in the solar system debris disk.

4.3.1 Extended models

We first explore the dynamical evolution of a medium sized (40–200 au) debris disk suffering only one encounter with another stars (Sect. 4.3.1) and of a large debris disk (40–1000 au) which experiences multiple encounters with other stars (Sect. 4.3.1).

4.3 Effect of stellar encounters on the early solar system

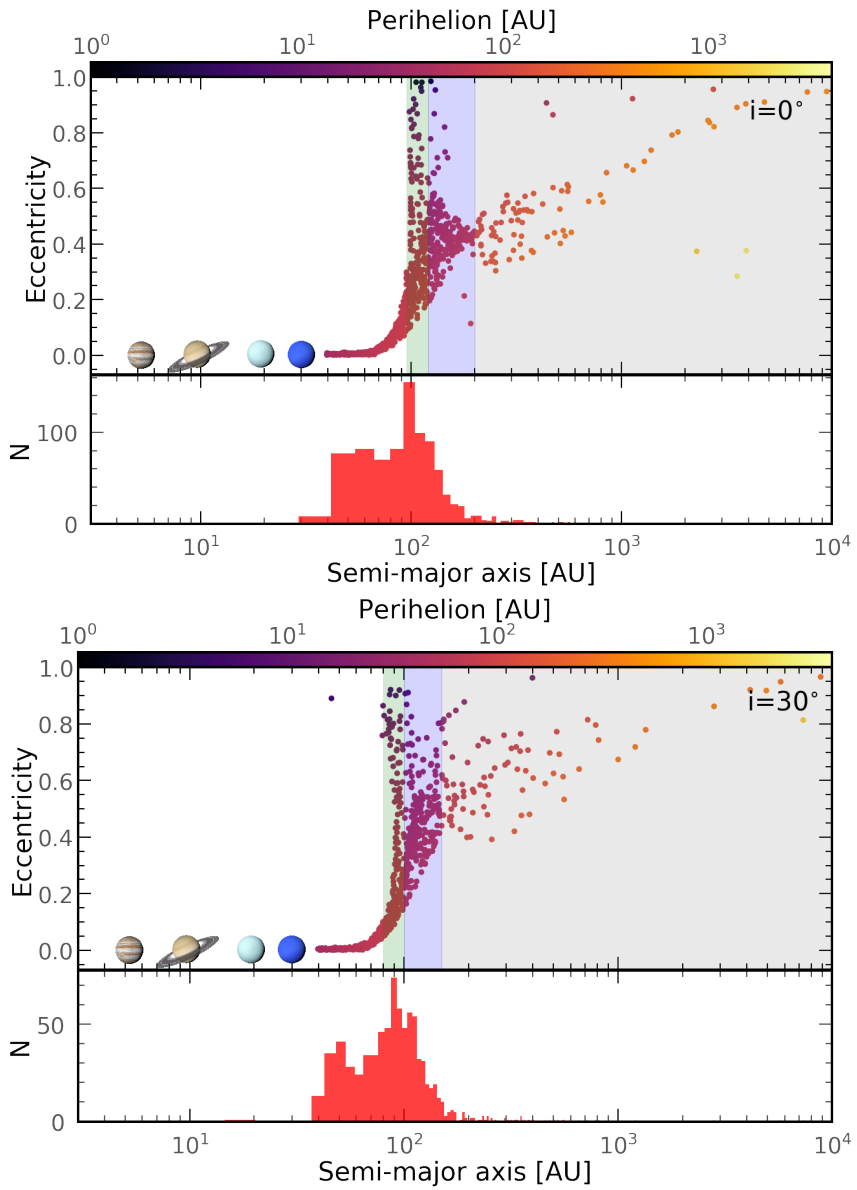


Figure 4.2: Continue...

4 Formation and Evolution of the Oort cloud

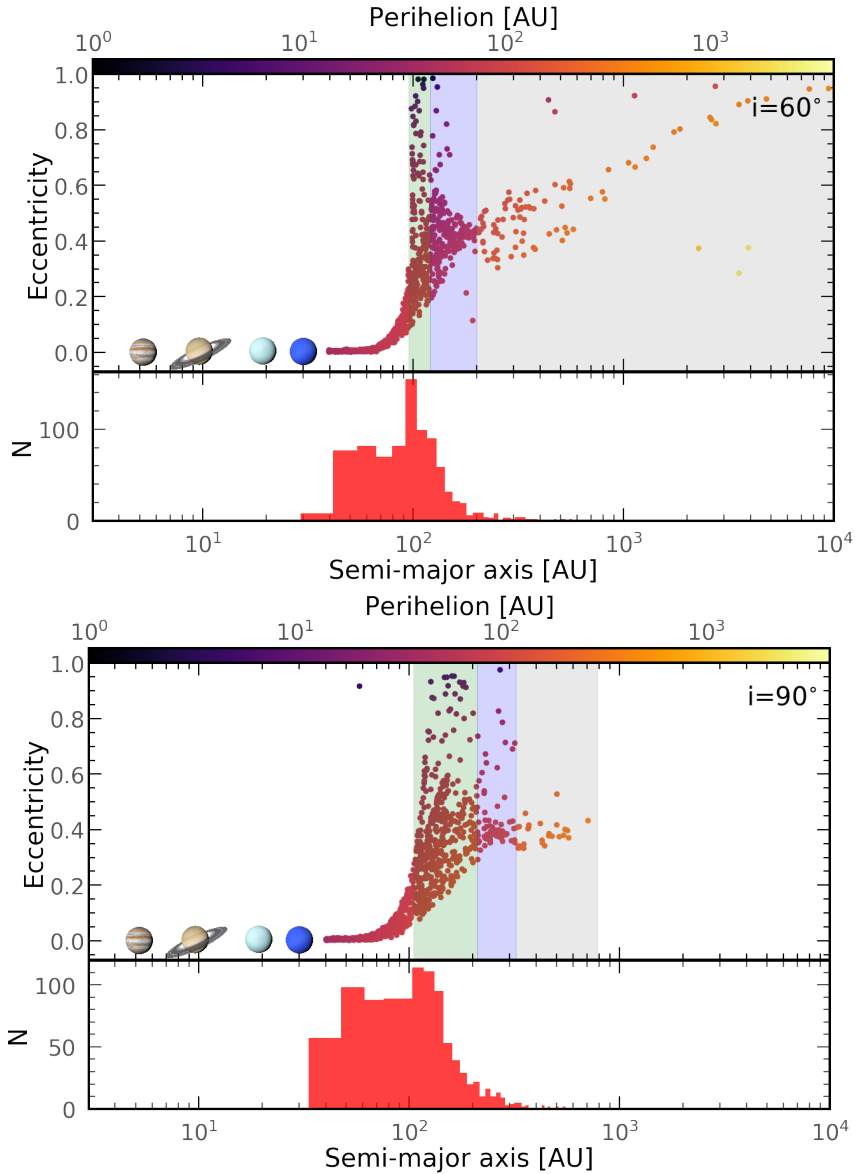


Figure 4.2: Extended 1 model. The top panel in each plot shows the semi-major axis a as a function of eccentricity, while the distribution of the particles over a is shown in the bottom panel. The different rows represent the inclination angle i of the encounter (0, 30, 60, and 90 degrees). The impact parameter is set to 300 au and the mass of the perturber is 1 . The positions of the four giant planets are shown with symbols in the bottom left of the top panel in each plot.

4.3 Effect of stellar encounters on the early solar system

Table 4.2: Extended 1 model. Semi-major axis distribution of the particles in the disk after a close encounter with a Solar-like star. The impact parameter is set to 300 au, for an encounter angle of 0, 30, 60 and 90 degrees. The first column represents the different regions of the solar system, divided into four. The first row represents the original disk over which the particles were initially distributed ($40 < a < 200$ au), in which the transneptunian region ranges from 40 - 50 au. Followed by the planetary region ($0 < a < 30$ au), the inner Oort cloud ($200 < a < 10\,000$ au), and finally the unbound particles (hyperbolic comets).

Inclination angle	0°	30°	60°	90°
Original disk	73%	76.4%	81.2%	88%
Planetary region	0.4%	0%	0%	0%
Inner Oort cloud	6.4%	5.2%	9.4%	12%
Unbound	20.2%	18.4%	9.4%	0%

Extended 1

Following the method described in Sect. 5.2 and using the initial conditions listed in Table 4.1 second row, we performed 32 simulations for the *Extended 1* model. In Fig. 4.2 and Fig. 4.3 we show the most interesting case, when the perturber passes to within 300 au from the Sun (Table 4.2). When the inclination angle of the encounter is set to 0°, most particles ($\sim 73\%$) remain in the original disk despite the close encounter. The particles with semi-major axes between 40 and 60 au retain eccentricities near zero. The eccentricities for the rest of the particles range from 0.1 to 0.9 (the same holds for the 30° inclination angle). The transneptunian region ($30 < a < 100$ au) gains $\sim 8.5\%$ more particles as compared to the original distribution, and the inner Oort cloud region ($200 < a < 10\,000$ au) acquires $\sim 6.4\%$ of the initial particles. Additionally 20.2% of the particles become unbound (Fig. 4.3). When the inclination angle is set to 30°, the perturbation is very similar to the previous case (see Table 4.2) but less strong. The transneptunian region gains 1.7% more particles than the case for 0° and the inner Oort cloud region is less populated (5.2% of the initial particles gets semi-major axis between 200 and 10 000 au). The effect of a close encounter decreases further for the 60 and 90 degree inclination angle cases (see also, Punzo et al. 2014; Pfalzner et al. 2018). For a 60 degree inclination angle, the population in the inner Oort cloud increases 3% and 4.2% with respect to the 0 and 30 degrees cases, respectively. When the angle is set to 90 degrees around 12% of the original particles acquire a semi-major

4 Formation and Evolution of the Oort cloud

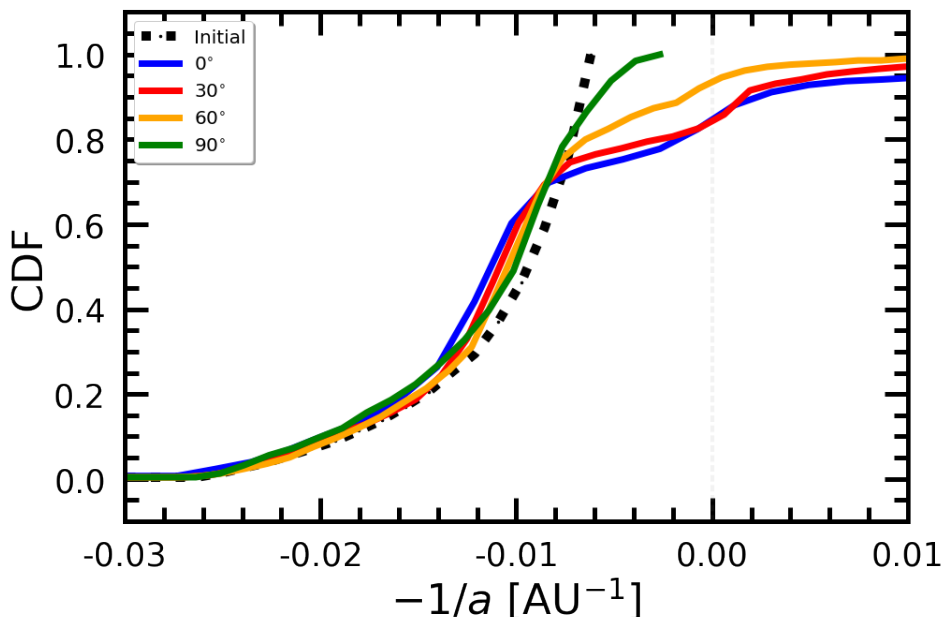


Figure 4.3: Extended 1 model. Cumulative distribution of the final energy of particles in the disk. Coloured lines represents the different inclination angles of the encounter (0, 30, 60, 90 degrees). While the black dotted line shows the initial distribution. The impact parameter is set to 300 au and the mass of the perturber is 1 . Negative values represent the bound particles, while the positive ones the unbound. The distributions have KS-probability of $\sim 0.90\%$ for 0° , $\sim 0.19\%$ for 30° , $\sim 0.07\%$ for 60° , and $\sim 0.05\%$ for 90° , respect to the initial one

axis in the Oort cloud region. The transneptunian region increases its population similarly for 60 (6.8%) and 90 (5.2%) degrees inclination angles.

The geometry of an encounter will define the fate of the debris disk. Even if the impact parameter is rather small (300 au for the cases presented here) the inclination angle of the encounter strongly affects the resulting structure and dynamics of the particles in the system. The differences are reflected in the properties of the particles in the different regions of the solar system after the encounter. For $i = 0^\circ$ about 0.4% of the initial particles end up with their semi-major axes in the planetary region ($0 < a < 30$ au), while for $i = 30^\circ$, 60° or 90° no particles end up in this region. In the transneptunian region, an increase of planetesimals occurs for $i = 30^\circ$, while the most efficient inclination angle to populate the inner Oort cloud region is 90 degrees, with the encounter lifting the semi-major axis of 12% particles to the regions between 200 and 10 000 au. The structure of the

4.3 Effect of stellar encounters on the early solar system

initial disk however is similar for all the inclination angles. Particles with semi-major axes between 40 and 65 au remain unperturbed, while particles at 65–200 au reach eccentricities up to 1 (Fig. 4.2). Additionally, as shown by the shaded areas in Fig. 4.2, after the encounter the disk is divided into three main populations for all the interaction angles (Fig. 4.2):

Green shading: Eccentricities are ranging from ~ 0.1 to 1, and perihelion distance from 0 to 50 au.

Blue shading: Eccentricities are ranging from ~ 0.2 to 0.6, and perihelion distance from 50 to 100 au.

Grey shading: Eccentricities are ranging from ~ 0.4 to 1, and perihelion distance from 100 to 1000 au.

Even though the encounters at different inclination angles produce a different structure in the disk, the three populations are discernible in all cases.

Finally, it is well known that a very close encounter between a star and a planetary system, can lead to the capture (see e.g., Jílková et al. 2015; Pfalzner et al. 2018) and ejection of a considerable fraction of its debris disk, creating a large population of unbound objects (see e.g., Cai et al. 2017; Pfalzner et al. 2018; Torres et al. 2018, 2019a, and references therein). However, it is worth mentioning that even for a very close encounter like the one described in this section (300 au), the angle of the interaction will determine the rate of ejection. When the angle of the interaction is around 90 degrees all the particles remain in the system. On the other hand if the angle is between 0 and 30 degrees around 20.2% of the initial disk gets unbound from the system (positive values in Fig. 4.3), creating a considerable fraction of interstellar comets such as 'Oumuamua.

Extended N

Following the method described in Sect. 5.2 and the initial conditions listed in Table 4.1 (fourth row), we performed a set of 200 simulations. For each simulation, we focused on the effect of the five closest stars in the cluster to the Sun at any given time. In Fig. 4.4 we show the final distribution of the orbital elements of all the particles in the 200 systems. The particles in mean-motion resonance with Neptune (2:3, 3:5, 4:7, 1:2, 2:5) between 50 and 100 au, resembles the Kuiper belt objects in the solar system.

4 Formation and Evolution of the Oort cloud

Most of the particles have eccentricities between 0 and 0.4 ($\sim 82\%$), and orbital inclinations between 0 and 20 degrees ($\sim 88\%$). The inner part of the disk in all our experiments is perturbed enough to create sub-structure within the disk (see Fig. 4.7). In the outer part of the disk approximately 7.5% of the planetesimals are ejected and start populating the inner Oort cloud ($1000 < a < 20\,000$ au). Just a tiny fraction ($\sim 0.02\%$) reaches the outer part of the current outer Oort cloud ($a > 20\,000$ au). Overall, in these simulations, the effectiveness of close encounters with other stars injecting energy into the orbits of the planetesimals is high. A notable number of planetesimals have already started populating the Oort cloud, and a considerable number of planetesimals acquired eccentric orbits ($\sim 18\%$). Some of the objects in eccentric orbits have planet-crossing perihelia which can lead to further scattering them to even wider orbits with a higher eccentricity. The combined effects of planet scattering (internal) and stellar encounters (external) appears to be very effective in populating the bound Oort cloud. It should also be noted that a considerable fraction of planetesimals ($\sim 36\%$) were ejected from the systems after the encounter with the stars (to panel Fig. 4.14). These would be essential in creating the unbound comets and can explain the existence of objects like 'Oumuamua in other planetary systems (see e.g., Portegies Zwart et al. 2018; Torres et al. 2019a).

Fig. 4.4 shows the final distribution of the orbital elements of the particles over all 200 simulated systems. We now take a closer look at the selected individual systems. Figures 4.5, 4.6, and 4.7 show the results for the selected cases. We selected two systems that undergo a series of weak to moderate encounters, but no strong encounters (systems 128 and 14), the majority of asteroids in this system remain bound to the body star. A further system was selected that experienced some stronger encounters as well as a series of weak encounters (system 100). Two systems that undergo a series of moderate to strong encounters (system 86 and 157) complete the selected set. In Fig. 4.5 we show the orbital evolution of the particles in the disk after 100 Myr. Additionally the distance of the encounter is shown in the top panel of each plot. After 100 Myr in all of our five selected experiments, the giant planets remained in stable orbits. This result implies that in a dense environment such as stellar clusters, the planets in our solar systems could have survived a series of encounters without changing their orbits. If the planetesimal disk was more compact and closer to Neptune, the planet-disk interaction could have triggered the migration of the planets and the ejection of the particles as we show in Sect. 4.3.2.

4.3 Effect of stellar encounters on the early solar system

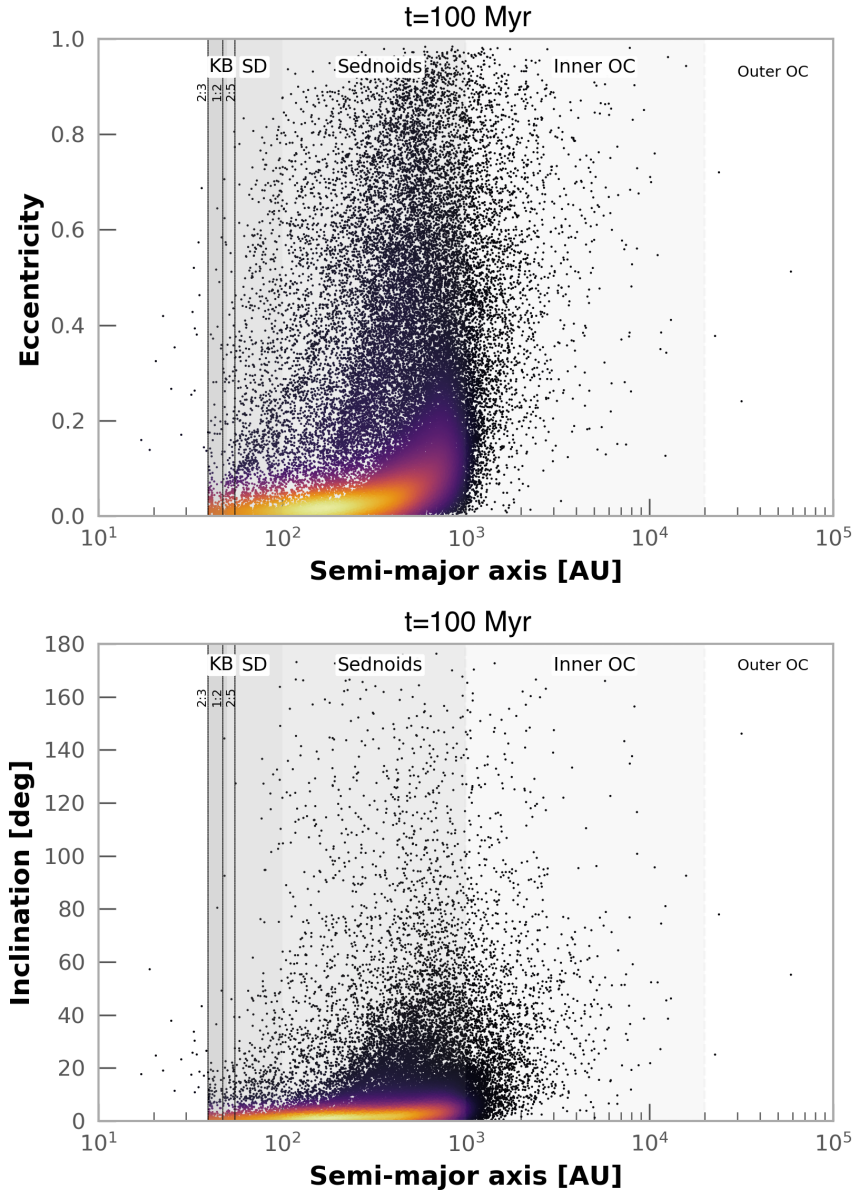


Figure 4.4: Extended N model. Semi-major axis as a function of eccentricity (top panel) and orbital inclination (bottom panel) for all the particles in the 200 simulated systems. The grey areas represent the different regions of the solar system (Kuiper belt (KB), scatter disk (SD), Sednoids, inner and outer Oort cloud (OC)), while the dash lines show the 2:3, 1:2, and 2:5 resonances with Neptune. The integration time is set to 100 Myr. An animation can be found online.

4 Formation and Evolution of the Oort cloud

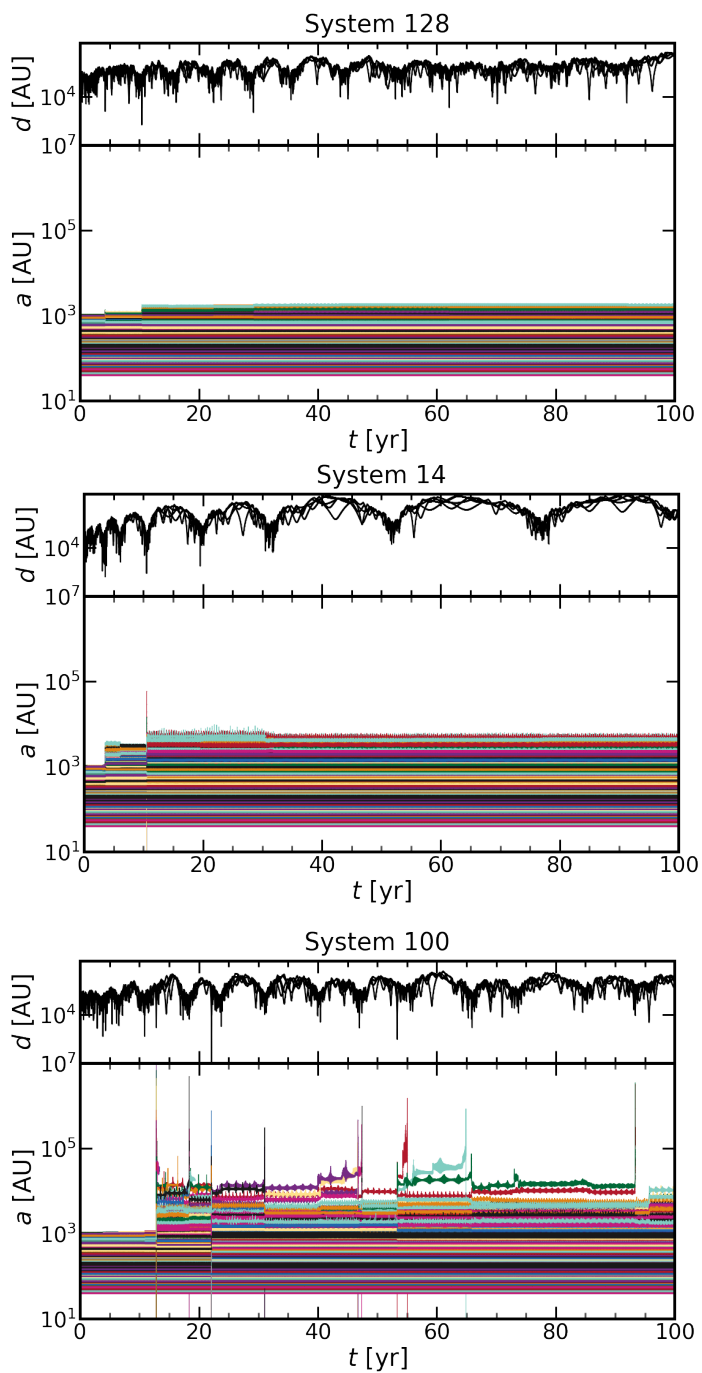


Figure 4.5: Continue...

4.3 Effect of stellar encounters on the early solar system

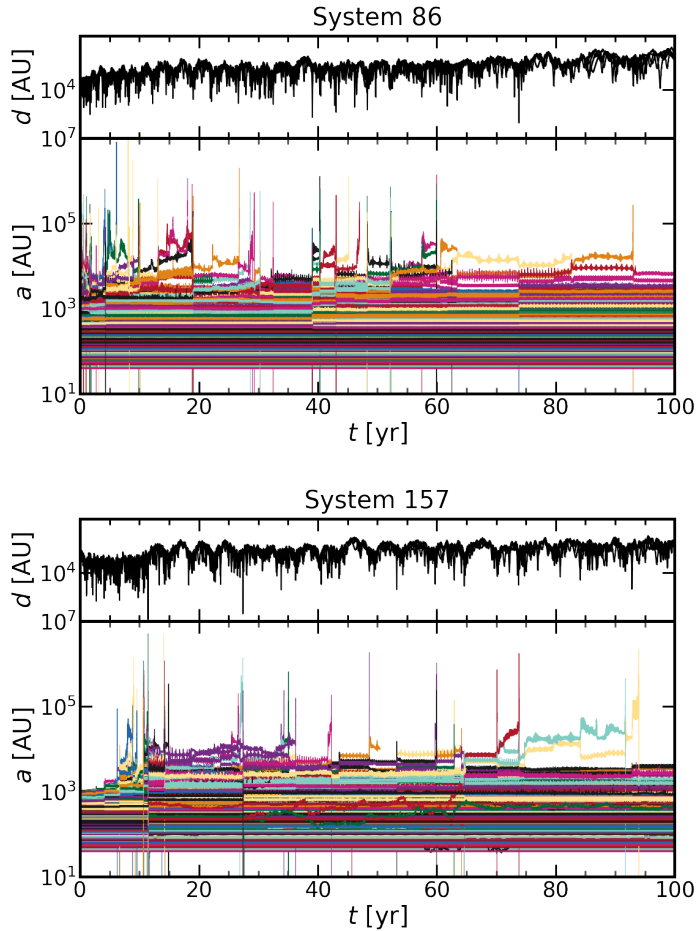


Figure 4.5: Extended N model. Orbital evolution of the particles in the disk after 100 Myr. The bottom panels in each plot shows the semi-major axis as a function of time, while the top panels show the distance of the perturber as a function of time. The different panels represents the systems numbered 128, 14, 100, 86, 157. Coloured lines correspond to each particle in the system.

The most stable system is no. 128 (first row in Fig. 4.6). All the particles remain in the disk after multiple encounters. The five closest encounters over 100 Myr range from 1000 to 5000 au (first panel, Fig. 4.5) are not close enough to inflict a considerable perturbation. However, the disk is heated somewhat in its outer parts, with a small fraction of particles reaching semi-major axes up to 2000 au. System 14 (second row in Fig. 4.6) retains 99.5% of the initial particles, but an early close encounter (second panel, Fig. 4.5)

4 Formation and Evolution of the Oort cloud

leads to 2.1% of the particles reaching eccentricities between 0.4 and 1 and 7.1% reaching semi-major axes larger than 1000 au. In system 100 17% of the particles are ejected from the disk due to the closest encounters (with impact parameter ~ 300 au) with a very low mass star (~ 0.2). Approximately 71% of the particles remain with semi-major axes between 40 and 1000 au, while 9.6% attain semi-major axes between 1000 and 5000 au with eccentricities ranging from 0.1 to 1. Most of the particles have orbital inclinations between 0 and 50 degrees (78.4%), and the rest of the inclinations are distributed between 50 and 150 degrees (third row in Fig. 4.6). The most perturbed systems are no. 86 (fourth row in Fig. 4.6) and no. 157 (fifth row in Fig. 4.6). System 86 experienced two close encounters, the first one with a red dwarf star with a mass of 0.5 at 488 au and later on with a brown dwarf (0.08) at 899 au. This causes the ejection of 13.4% of the initial particles and the creation of three main populations of objects. The first one, planetesimals in the disk, acquired semi-major axes around 200 au, and eccentricities from 0.2 to 1 (green shaded region, fourth-row Fig. 4.6). The second population has semi-major axes ranging from 100 to 1000 au (blue shaded region, fourth-row Fig. 4.6), and orbital inclinations between 0 and 20 degrees. About 23% of the particles gained eccentricities between 0.4 and 1, while the rest has eccentricities ranging from 0.2 to 1. The third and final population contains about 2.1% of the initial planetesimals with semi-major axes from ~ 500 to 6000 au (grey shaded region, fourth-row Fig. 4.6) and eccentricities from 0.2 to 1 and orbital inclinations up to 80 degrees.

The most strongly perturbed system is no. 157 which loses 57.5% of the initial planetesimals. As in the previous cases, this is due to two very close encounters at impact parameters of 336 au and 507 au (Fig. 4.5) with stars with masses of 0.5 and 0.1, respectively. As a consequence of the close encounters a tail is created. The tail contains three main populations and several branches produced by subsequent (weak) stellar encounters, as is shown in the fifth panel of Fig. 4.6). The first population has semi-major axes between 40 and 100 au (green shaded region, fifth-row Fig. 4.6), with eccentricities within 0 and 1 and orbital inclinations from 5 to 50 degrees. The second population (blue shaded region, fifth-row Fig. 4.6) has semi-major axes from 100 to 300 au, with eccentricities from 0.3 to 1 and inclinations up to 20 degrees. The final population (grey shaded region, fifth-row Fig. 4.6) has orbital inclinations distributed between 20 and 180 degrees, while eccentricities range from 0 to 1. About 2.2% of the particles reaches semi-major axes between 1000 and 4000 au (Oort Cloud region). Despite the close encounters experienced by this system, only a small fraction of

4.3 Effect of stellar encounters on the early solar system

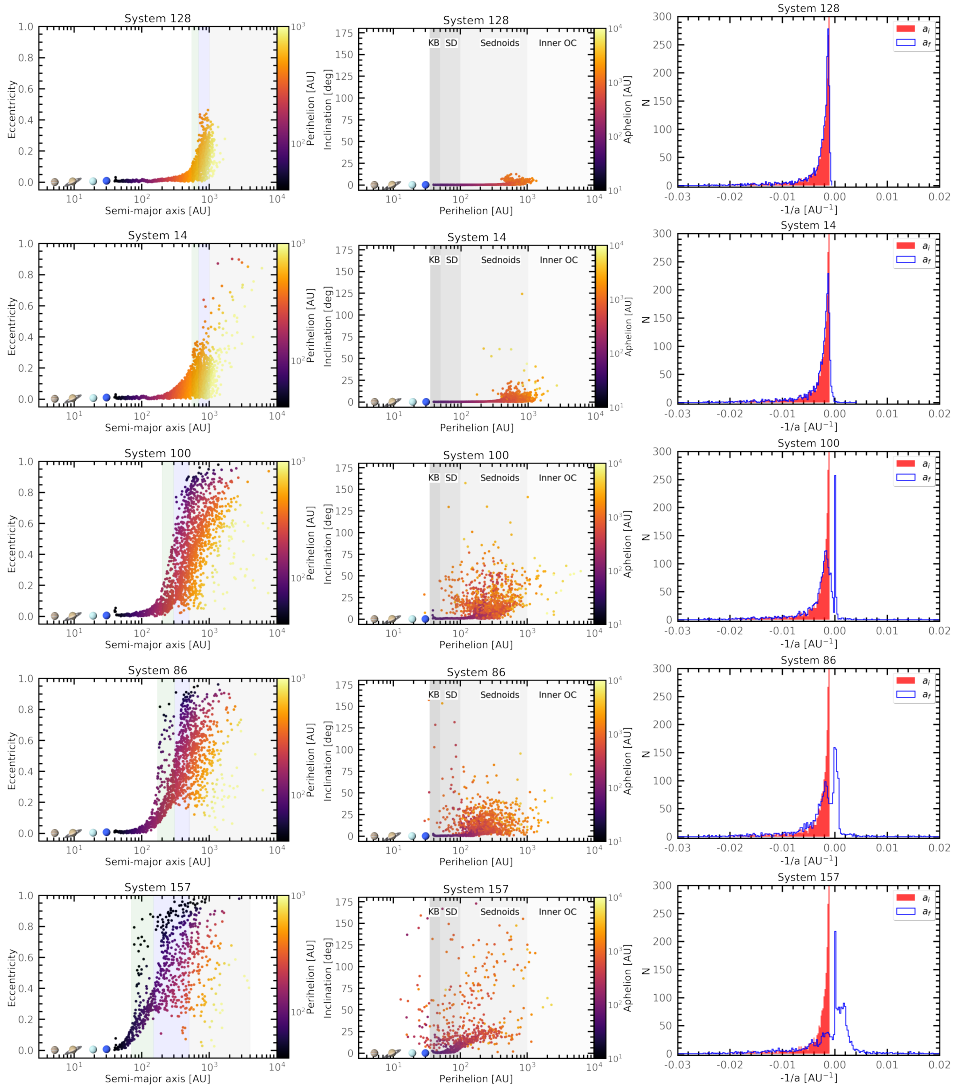


Figure 4.6: Extended N model. Orbital elements of the particles in the disk after 100 Myr and multiple stellar encounters. The leftmost column shows the semi-major axis as a function of the eccentricity, with the dots colour coded by perihelion. The green, blue and grey shaded regions show the different populations created after the encounters in each system. The middle column shows the perihelion as a function of orbital inclination, with the dots colour coded by aphelion. The grey shaded areas show the different regions of the solar system (Kuiper belt (KB), scatter disk (SD), Sednoids, and inner Oort cloud (OC)). The rightmost column shows the distribution of the orbital energy of the particles in the disk, the red histograms corresponding to the initial energy and the blue curve to the final energy. Each row corresponds to the systems numbered 128, 14, 100, 86, and 157, respectively.

4 Formation and Evolution of the Oort cloud

particles populates the outer Oort cloud. This is mainly because the encounter happened in the inner part of the disk, creating a considerable fraction of hyperbolic objects (57.5%). On the other hand, the planets remain in a stable orbit, the objects within $\sim 40 - 50$ au entered in mean motion resonance with Neptune.

In all of the systems presented here a tail in $a-e$ space is created due to strong encounters. In some cases (system 100, 86, and 157) multiple branches are visible which are produced by weak stellar encounters. Additionally three populations of objects are created (green, blue, grey shaded regions in the first column of Sect. 4.6). The multiple stellar encounters trigger the ejection of the particles up to the edge of the current inner Oort cloud (20 000 au). Subsequent perturbations due to the Galactic tidal field will circularise the orbits of particles with large semi-major axes (see Brasser et al. 2012), thus turning them into Oort cloud particles. The particles with small semi-major axes where the Galactic tidal field is not efficient remain in (highly) eccentric orbits which will become unstable on a secular timescale. As such the tail in $a-e$ will disappear in due time. The overall structure of the systems strongly depends on the geometry of the encounter, as we discussed in Sect. 4.3.1 and as illustrated in Fig. 4.7.

Overall, the experiments presented here illustrate different scenarios of how the solar system could have been perturbed in its early stages. A condition for a stable system is that the disk of planetesimals is far enough from the planets, otherwise the planet instability due to the interaction with the disk will heat the disk and most of the particles will be ejected to large distances. In the scenarios explored here, the formation of the Oort cloud could have been Initiated by a close encounter between one or more stars and the solar system without considering orbital instabilities for the planets (Morbidelli 2005), assuming that the planets reached their current positions while the solar system still was in its birth cluster and the gas in the protoplanetary disk disappeared from the disk (see also Brasser et al. 2012). Further dynamical evolution of the planetesimals in the inner Oort cloud induced by the Galactic tidal field, and occasional close encounters will start populating the outer Oort cloud. During interactions with passing stars the Sun can also capture material from the other stars. Sedna was argued to present an example thereof (Jílková et al. 2016).

4.3 Effect of stellar encounters on the early solar system

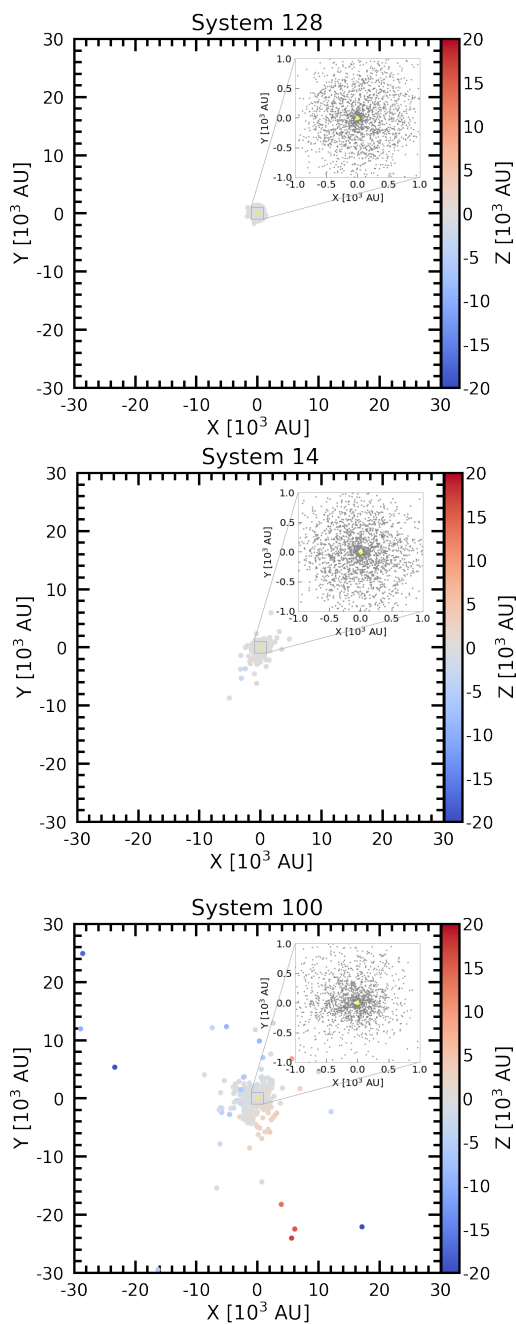


Figure 4.7: Continue...

4 Formation and Evolution of the Oort cloud

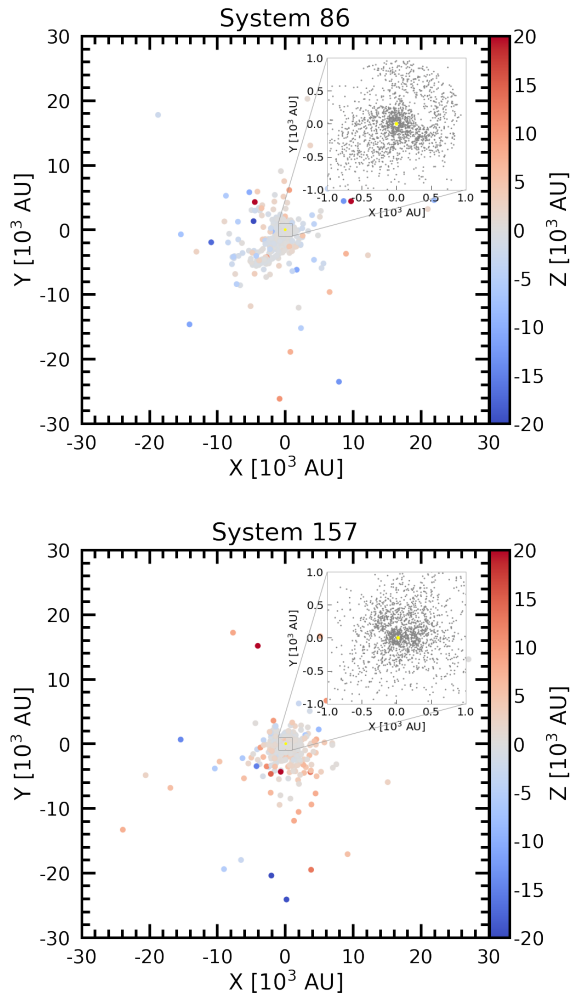


Figure 4.7: Extended N model. Final positions of the particles in the disk, represented with Cartesian coordinates Y vs. X , with the dots colour coded by Z . The panels correspond to the systems numbered 128, 14, 100, 86, and 157.

4.3 Effect of stellar encounters on the early solar system

4.3.2 Compact models

For the construction of the compact models we followed the classical Nice model (Gomes et al. 2005; Tsiganis et al. 2005; Morbidelli et al. 2005) for the early solar system. Although new versions of the model were presented (Morbidelli et al. 2007; Nesvorný & Morbidelli 2012; Morbidelli & Nesvorný 2019), Morbidelli et al. (2007) point out that the orbit evolution of planets was similar to the original version. The classical Nice model thus fulfills our propose and provides us with the tools to understand the dynamical instability of the giant planets and the scattering of planetesimals which attain Oort cloud orbits. In Sect. 4.3.2 we present our results for one encounter between the solar system and another star, while in Sect. 4.3.2 the results for multiples encounters are presented.

Compact 1

For the *Compact 1* model we performed 32 simulations considering the parameters describe in the Sect. 5.2 and Table 4.1. We find that the velocity of the Sun after the encounter with the perturber ranged from $\sim 0.06 \text{ km s}^{-1}$ to 0.08 km s^{-1} when the inclination of the perturber was 0 degrees. However, when the inclination of the perturber was increased to 30 degrees, the velocity of the Sun (after impact) ranged from $\sim 0.07 \text{ km s}^{-1}$ to 0.5 km s^{-1} . This velocity is lower than the mean velocity of stars in a cluster ($\sim 2 \text{ km s}^{-1}$). This indicates that an impact with a GO star even at a very close distances between 225 and 400 au would not be strong enough to eject the Sun from the cluster, but it will strip a considerable fraction of the particles in the disk. The particle ejection efficiency for a close encounter is maximum when the perturber is inclined at an angle of 30 degrees. The perturber does not produce any noticeable effects on the disk when it is inclined at an angle of 90 degrees. Although the perturber with an impact parameter of 275 au does not produce a lot of unbound particles, it produces the highest number of bound particles with a semi-major axis greater than 150 au. Encounters at close distances, especially at 250, 275, and 300 au resulted in the migration of planets.

For an impact parameter of 300 au and an angle of 60 degrees, Uranus and Neptune swap positions and their final semi-major axis resembles the present day positions of the giant planets in the solar system (third row Fig. 4.8). At 10 000 yr after the impact Jupiter is at 5.12 au, Saturn at 10.69 au, Uranus at 18.42 au and Neptune at 29.83 au. For all the simulations performed, we also investigate the effect of a retrograde approach by

4 Formation and Evolution of the Oort cloud

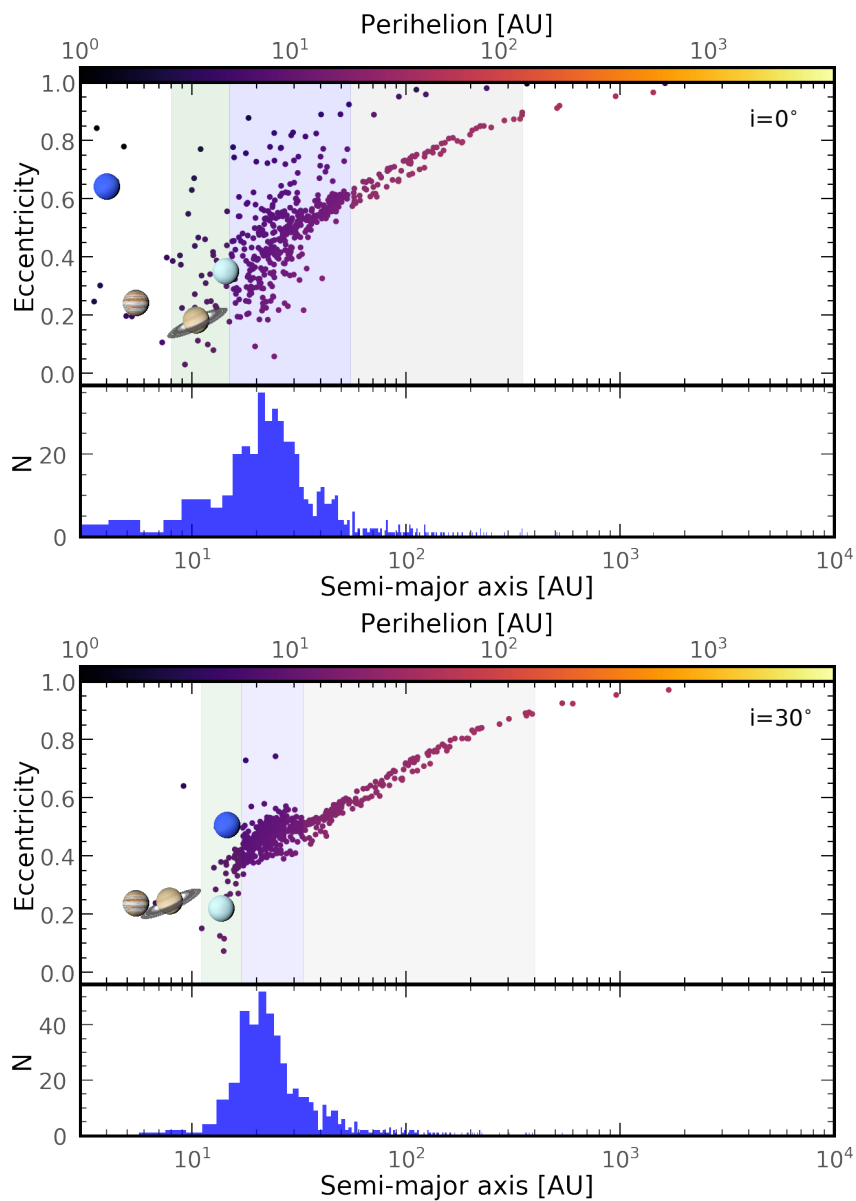


Figure 4.8: Continue...

4.3 Effect of stellar encounters on the early solar system

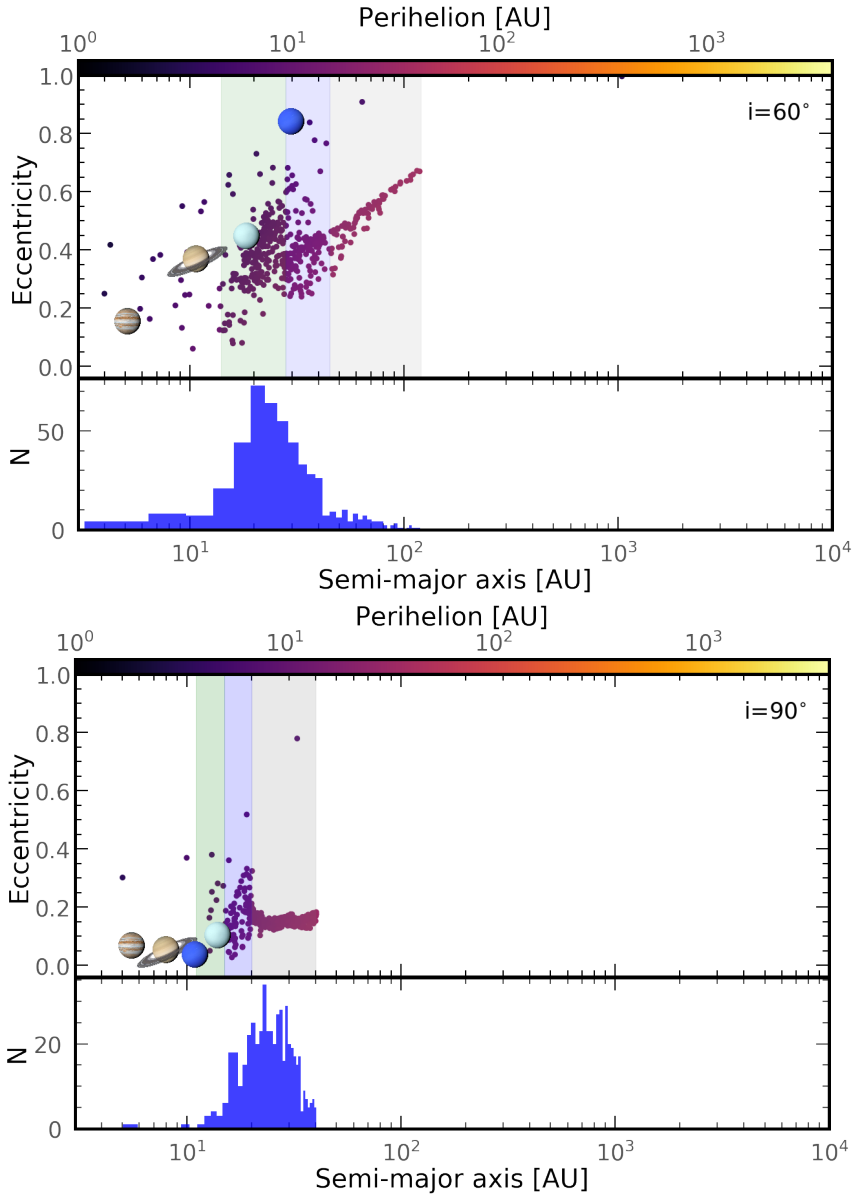


Figure 4.8: Compact 1 model. The top panel in each plot shows the semi-major axis of the debris disk particles as a function of eccentricity, while the distribution of the particles over semi-major axis is shown in the bottom panel. The different rows represent the different inclination angles of the encounter (0, 30, 60, 90 degrees). The impact parameter is set to 300 au and the mass of the perturber is 1 . The positions of the four giant planets are shown with symbols in the bottom left of the top panel in each plot.

4 Formation and Evolution of the Oort cloud

Table 4.3: Compact 1 model. Semi-major axis distribution of the particles in the disk after a close encounter with a Solar-like star. The impact parameter is set to 300 au, for an encounter inclination angle of 0, 30, 60 and 90 degrees. The first column represents the different regions of the solar system, divided into five. The first represent the original disk over which the particles were distribute ($16 < a < 35$ au), followed by the planetary region ($0 < a < 16$ au), the transneptunian region ($35 < a < 100$ au), the inner Oort cloud ($200 < a < 10\,000$ au), and finally the unbound particles (hyperbolic comets).

Inclination angle	0°	30°	60°	90°
Original disk	52.4%	63%	62.4%	87.6%
Planetary region	11.8%	6%	8.2%	6%
TNOs region	25.2%	22%	27.8%	6.4%
Inner Oort cloud	9.4%	9%	1.3%	0%
Unbound	1.2%	0%	0.3%	0%

the perturber (with respect to the debris disk). We found that a retrograde approach is more efficient at disrupting material from the protoplanetary disk. In general, the migration of the planets and therefore the evolution of a protoplanetary disk is dictated by the geometry of the encounter. Inclinations within 0–60 degrees can lead to migration of the giant planets and the ejection of transneptunian objects to very wide and highly eccentric orbits (Fig. 4.9).

In Fig. 4.9 the energy distribution of the particles in the disk is shown for an impact parameter of 300 au. As previously discussed the strongest disruption occurs for angles between 0 and 60 degrees. For an angle of zero degrees about 11.8% of the particles enter into the inner planetary region ($a < 5$ au) and 25.2% reach the present day transneptunian region (35 to 100 au). Only a small fraction (9.4%) reach the inner Oort cloud regions ($100 < a < 3000$ au) and 1.2% become hyperbolic objects (Table 4.3). The weakest perturbation occurs when the angle is set at 90 degrees. Considering that 300 au is a very close encounter the perturbation is ruled by the planet-disk interaction, but the stellar encounter triggers the ejection of the particles, with a considerable fraction ($\sim 25\%$) penetrating the transneptunian region Table 4.3.

4.3 Effect of stellar encounters on the early solar system

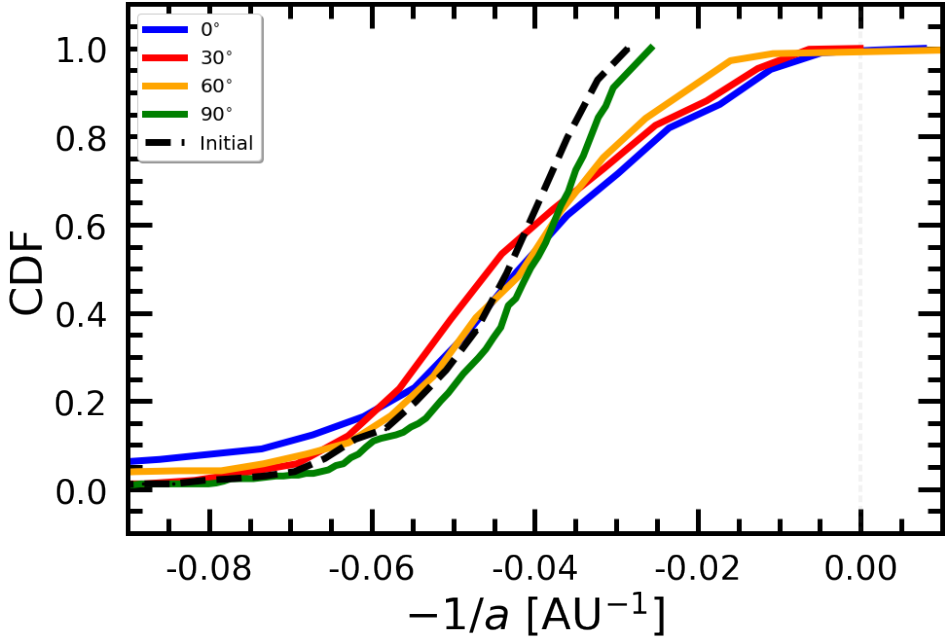


Figure 4.9: Compact 1 model. Cumulative distribution of the final energy of the particles in the disk. Coloured lines represent the different inclination angles at which the perturber approaches the solar system (0, 30, 60, and 90 degrees). The black dotted line shows the initial distribution. The impact parameter is set to 300 au and the mass of the perturber 1 . Negative values represent the bound particles, while the positive ones the unbound. The distributions have KS-probability of $\sim 0.08\%$ for 0° , $\sim 0.12\%$ for 30° , $\sim 0.08\%$ for 60° , and $\sim 0.03\%$ for 90° , respect to the initial one.

4 Formation and Evolution of the Oort cloud

Compact N

As described in Sect. 5.2 we performed a set of 200 simulations for the *Compact N* model which were set up similar to the *Extended N* models. We evolved the systems for 100 Myr, accounting for multiple stellar encounters during the evolution. In Fig. 4.10 we show the final distribution of all the particles. The particles with semi-major axes between 15 and 20 au are in mean-motion resonance with Uranus (resembling the objects in Kuiper belt in our solar systems). The external part of the disk is only slightly perturbed by the stellar encounters. Approximately 0.8% of the planetesimals are ejected into Kuiper belt region, 0.45% to the scattered disk range and 0.40% into the Sednoids range. None of the particles reaches the Oort cloud region. Overall, the strongest perturbation that the planetesimals experience is due to the interaction with the giant planets, particularly Uranus. The orbital evolution of the giant planets after 100 Myr is stable. The planets did not migrate in any of our simulations, mainly because the encounters are distant and the disk massless. Around 12.5% of the particles acquired eccentricities between 0.1 and 0.7 and $\sim 7\%$ are ejected from the system, creating interstellar comets.

In Sect. 4.3.1 we studied the five most interesting cases in our *Extended N* simulations. In this section for comparison we analyze the same systems, i.e. numbers 128, 14, 100, 86, and 157. In Figs. 4.11, 4.12 and 4.13 we show the evolution of the orbital elements of the disk particles, the final orbital elements and the energy distribution, and the position of the particles after 100 Myr, respectively. System 128 (first row in Fig. 4.12) has an early close encounter (1000 au), which in combination with the interaction between the giant planets and the disk and the following encounters leads to the ejection of 6.5% of the initial planetesimals. The remaining planetesimals concentrate in the original disk (95%) with eccentricities near zero, while the rest reaches the scattered disk region with eccentricities between 0.2 and 0.6. System 14 (second-row in Fig. 4.12) does not suffer an important change in the orbital parameters and remains mostly stable during 100 Myr. A small fraction (1.5%) of particles reach high eccentricities ($0.1 < e < 0.6$) and approximately 6% are ejected mainly because of the interaction with Uranus. The particles between 16 and 20 au enter in mean-motion resonance with Uranus. Systems 100 (third-row in Fig. 4.12) and 86 (fourth row in Fig. 4.12) retain 94.5% of the initial particles.

4.3 Effect of stellar encounters on the early solar system

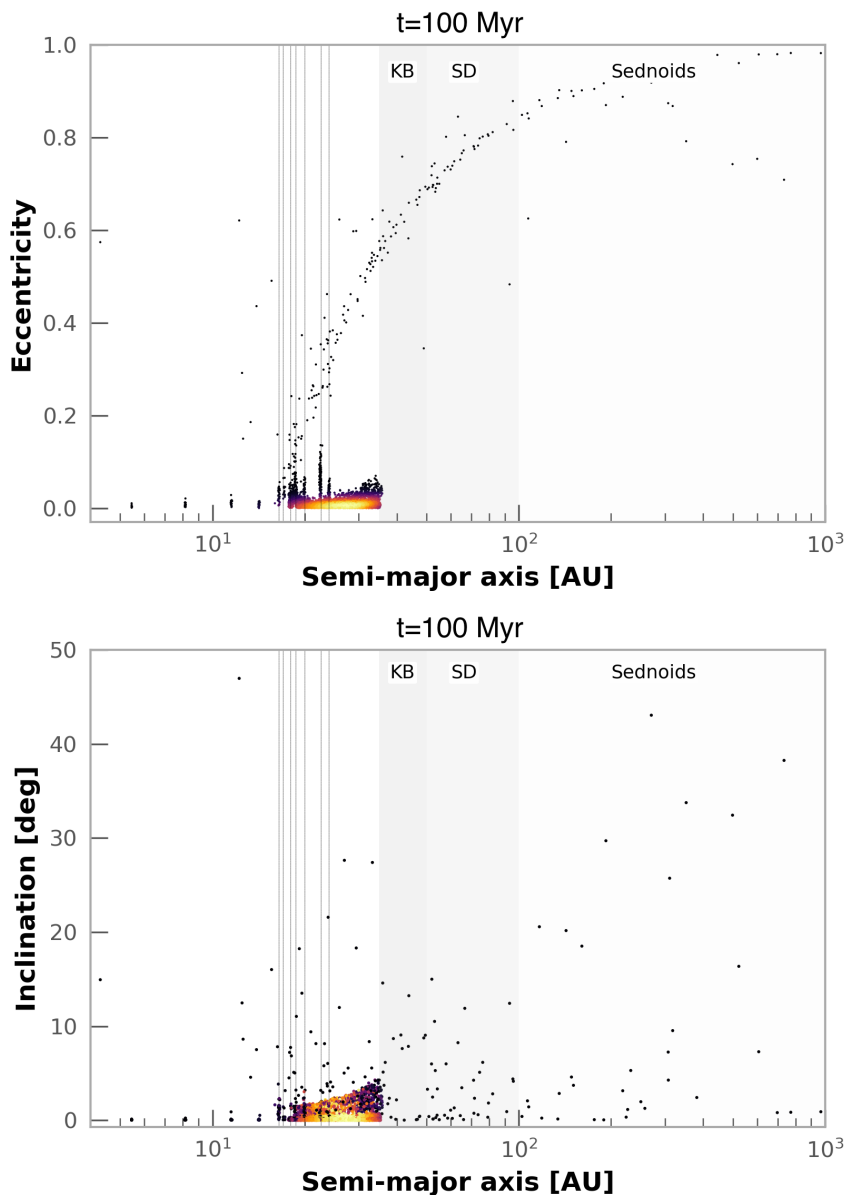


Figure 4.10: Compact N model. The semi-major axis as a function of eccentricity (top panel) and inclination (bottom panel) for all the disk particles in the 200 simulated systems. The grey shaded areas represent the different regions of the solar system (Kuiper belt (KB), scatter disk (SD), Sednoids), while the dashed lines indicate the mean motion resonance of the particles with Neptune. The integration time is set to 100 Myr. An animation can be found online.

4 Formation and Evolution of the Oort cloud

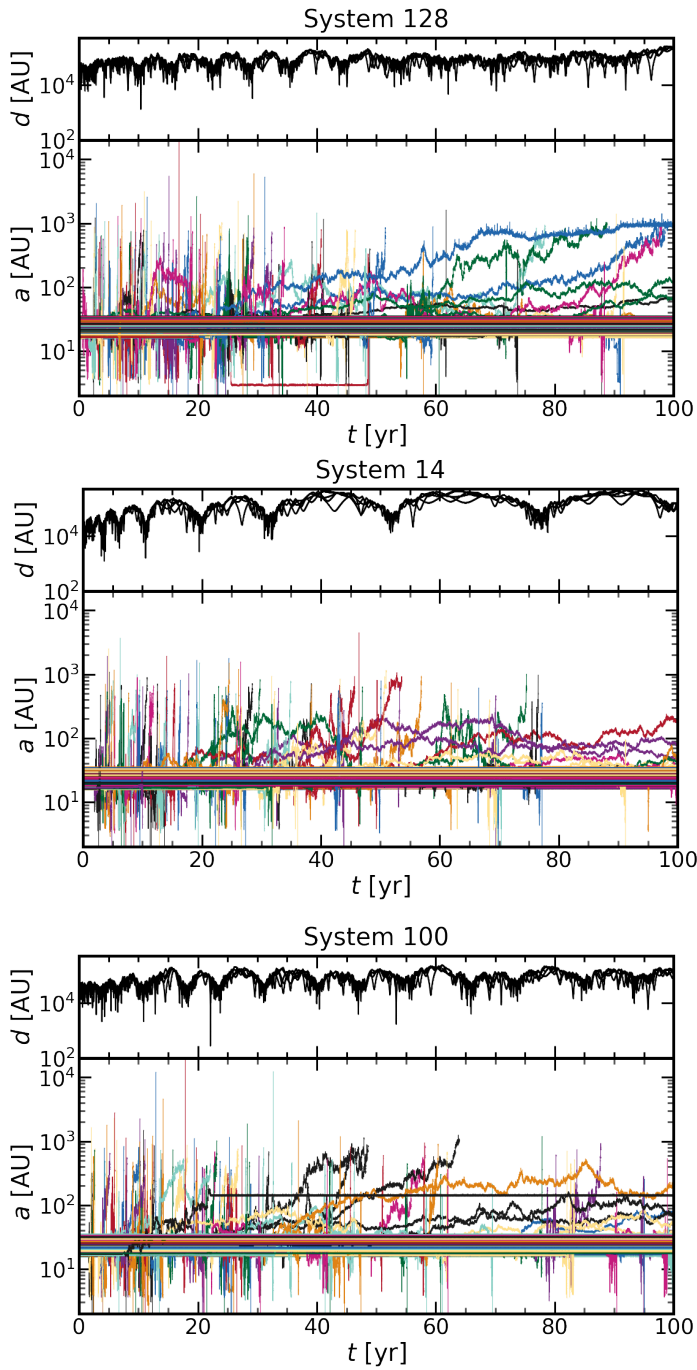


Figure 4.11: Continue...

4.3 Effect of stellar encounters on the early solar system

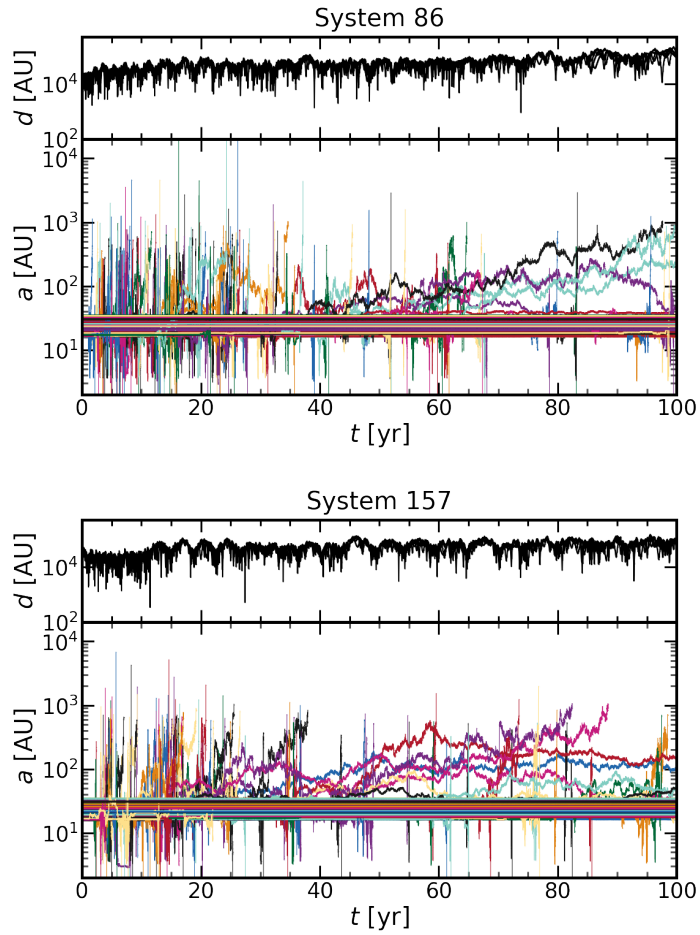


Figure 4.11: Compact N model. Orbital evolution of the particles in the disk over the 100 Myr simulation. The bottom panels in each plot show the semi-major axis as a function of time, while the top panels show the distance of the perturber. The different panels represents the systems 128, 14, 100, 86, and 157. Coloured lines corresponds to each particle in the system.

4 Formation and Evolution of the Oort cloud

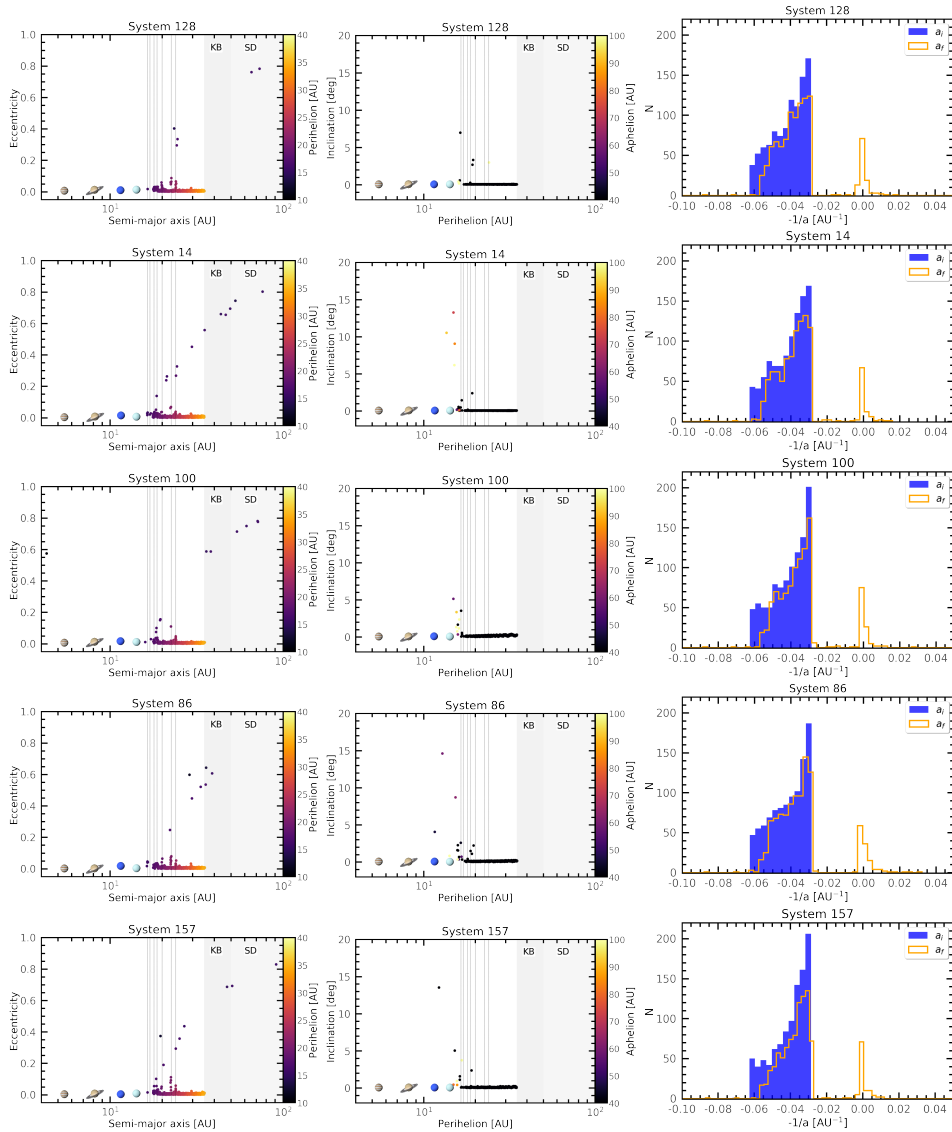


Figure 4.12: Compact N model. Orbital elements of the particles in the disk after 100 Myr and multiple stellar encounters. The leftmost column shows the semi-major axis as a function of the eccentricity, with the dots colour coded by perihelion. The middle column shows the perihelion as a function of inclination, with the dots colour coded by aphelion. Dashed line represent the regions where the particles are in mean motion resonance. The grey shaded areas represent the different regions of the solar system (Kuiper belt (KB), and scatter disk (SD)). The rightmost column represents the orbital energy of the particles in the disk after 100 Myr. The red histogram corresponds to the initial energy, and the blue curve to the final energy. The rows correspond to the systems 128, 14, 100, 86, and 157, respectively.

4.3 *Effect of stellar encounters on the early solar system*

The most important perturbation is due to Uranus which perturbs all the particles between 16 and 20 au (as in systems 14 and 128). Such particles become attached to Uranus in a mean-motion resonance. In both systems 100 and 86 5.5% of the particles end up on hyperbolic orbits, while the two systems have a similar disk structure after 100 Myr (Fig. 4.13). However, system 100 suffered only one close encounter with a very low mass star (0.3) at 273 au at an early stage (~ 20 Myr), while system 86 faced two close encounters, the first one with a red dwarf star with a mass of 0.5 at 488 au and later on with a brown dwarf (0.08) at 899 au. The most perturbed system is no. 157. Approximately 7% of the particles are ejected from the system, attaining hyperbolic orbits. This system faced two very close encounters at 336 au and 507 au, with masses of 0.5 and 0.1 , respectively. Both encounters took place at an early stage (10 and 27 Myr). Even though system 157 faced two close encounters, the particles with semi-major axes between 20 and 36 au do not suffer an important change. As in the previous systems, Uranus produces the strongest perturbation and about 12.5% of the particles between 16 and 20 au enter in resonance with the giant planet.

The dynamical evolution of the particles in a compact disk depends primarily on the evolution of the giant planets. However, close encounters define their further evolution depending on the mass of the perturber. In the five systems presented here we examined different scenarios. For stellar encounters we find that in all the cases a small fraction of the particles was ejected from the systems ($\sim 5\text{--}7\%$) in hyperbolic objects. The number of objects ejected not only depends on the perturbation due to the planet closest to the disk but also depends on the proximity of the encounter. This suggests that the solar system faced at least one encounter in its early evolution, which partly determined in the evolution of the inner regions. It is essential to highlight that in all our experiments, the inner solar system and particularly the planets do not get perturbed even when a close encounter occurs. The scenario presented here is a simplification of the classic Nice model, which however gives us an idea of the relative importance of the giant planets in forming and shaping the Kuiper belt.

4 Formation and Evolution of the Oort cloud

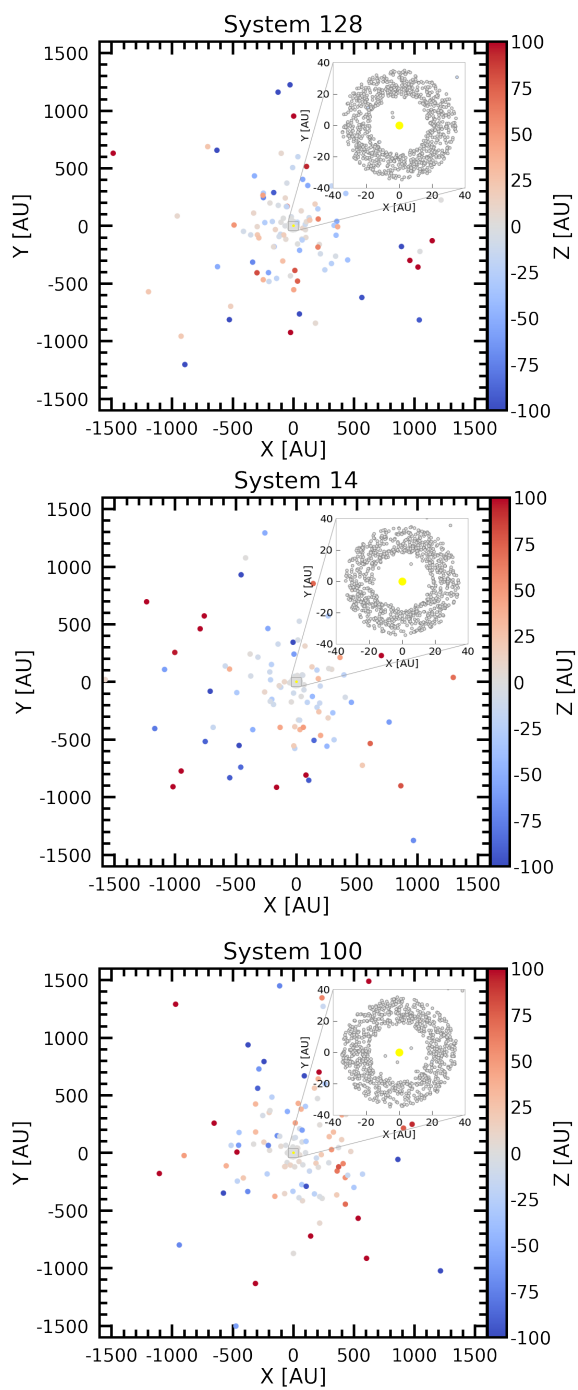


Figure 4.13: Continue...

4.3 Effect of stellar encounters on the early solar system

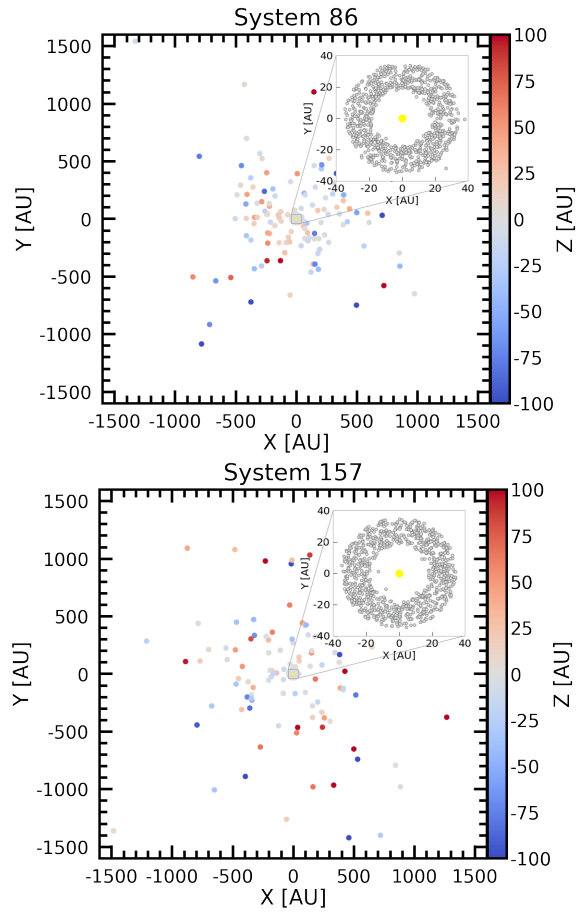


Figure 4.13: Compact N model. Final positions of the particles in the disk show in Cartesian coordinates Y vs X . The dots are colour coded by the value of Z . The units are au. The panels correspond to the systems 128, 14, 100, 86, and 157.

4 Formation and Evolution of the Oort cloud

4.3.3 Extended vs compact models and the Oort cloud

In Sect. 4.3.1 and Sect. 4.3.2 we presented our results for the numerical simulations for the *extended* and *compact* models. First we focused on the effects of a single but close encounter (Sect. 4.3.1 and Sect. 4.3.2) and then studied the effect of multiple encounters (Sect. 4.3.1 and Sect. 4.3.2) in a star cluster environment, over a time span of 100 Myr. For the *Extended 1* model we found that a close encounter with the present day planet configuration of the solar system and a disk extending up to 200 au can produce different structure and populations in the disk but the planets remain in stable orbits. On the other hand for the *Compact 1* model a close encounter triggers the migration and excitation of the planets and the debris disk. The original disk gets perturbed but most of the particles remain in the system. If we compare Fig. 4.3 and Fig. 4.9 we see that the production of unbound particles is higher for the extended case (5.6% of the original disk) than for the compact model (1.4%). It is important to highlight that even when a perturbing star comes close (~ 300 au) to a planetary system the evolution of the planetesimal disk will be determined by its size. If the disk is compact the perturbations due to the planets will dominate over the effect of the stellar encounter. If the disk is large the planets will not suffer any orbital variation, while the planetesimals in the disk can be heavily perturbed.

When considering multiple encounters (Fig. 4.4 and Fig. 4.10) the effect on the disk for the case of the *Extended N* model is similar to the case of one encounter. However, the multiple effects of the passing stars create branches (several populations of objects) in the orbital element diagrams. These structures can be associated with different families in the solar system, particularly the Sednoids region (Jílková et al. 2016; Pfalzner et al. 2018). This region ($100 < a < 1000$ au, Fig. 4.4) is populated with large numbers of objects with eccentricities ranging from 0.2 to 1 with orbital inclinations from 25 to ~ 150 degrees. When we compare this to the *Compact N* model, we can see that the disk is barely perturbed due to the passing stars. The major perturbations are because of the interaction with the giant planets, which produces at least six resonances with the planetesimals with semi-major axes between 16 and 20 au (Fig. 4.10).

Overall the most efficient mechanism to create inner Oort cloud objects in our simulations is through stellar encounters (one or multiple, relatively distant or close). The effect of these perturbations result in an outward of particles from the disk in a short period of time (on the order of a few Myr).

On the other hand giant planets are responsible for shaping the inner solar system on a time scale of the order of tens of Myr. Our simulations suggest that the Kuiper belt objects are the result of dynamical instabilities and interactions with the giant planets, which is consistent with the various instances of the Nice model. Taking this farther, the dynamical evolution of any planetary system will be defined by its birth environment, the size of its disk and the orbital configuration of its planets. If we consider that planet formation is common among stars, Oort cloud and Kuiper belt-like structures should be universal (see also Hands et al. 2019), and shaped by the birth environment of the host star, which also will determine the survivability of these structures. This implies that the creation of interstellar comets should also be common among planetary systems and that interstellar space is populated by a large number of bodies ejected from their systems.

Section 4.4

Interstellar objects

The discovery of the first interstellar comet 'Oumuamua (Williams 2017; Meech et al. 2017), and the recently detected interstellar comet C/2019 Q4 Borisov (Borisov 2019; Guzik et al. 2019) opened up a new era in the study and exploration of the solar system and other planetary systems in our galaxy. The origin of *sōlī lapidēs* (lonely rock) or interstellar objects (asteroid/comet) is still unclear but many scenarios have been proposed to explain their creation and evolution (see e.g., Portegies Zwart et al. 2018; Torres et al. 2019a; Bannister et al. 2019). One scenario for the formation of interstellar objects is due to gravitational instabilities induced by a massive body. This body can be either a nearby planet, a star passing close by, or a combination of both. In the previous sections we studied such scenarios but focused primarily on the particles that remain in the solar system. Hands et al. (2019) points out that a planetesimal can escape a stellar cluster with v_∞ of few km s^{-1} , and there should be several objects ejected from the same cluster making their way through the interstellar space like 'Oumuamua. Torres et al. (2019a) suggested that interstellar space is full of objects which might interact with nearby planetary systems, and therefore it may be common that planetary systems, including the solar system, are polluted with objects originating from interstellar space. In this section we analyse all the particles ejected from the *Extended N* (top panel Fig. 4.14) and *Compact N* (bottom panel Fig. 4.14) models.

4 Formation and Evolution of the Oort cloud

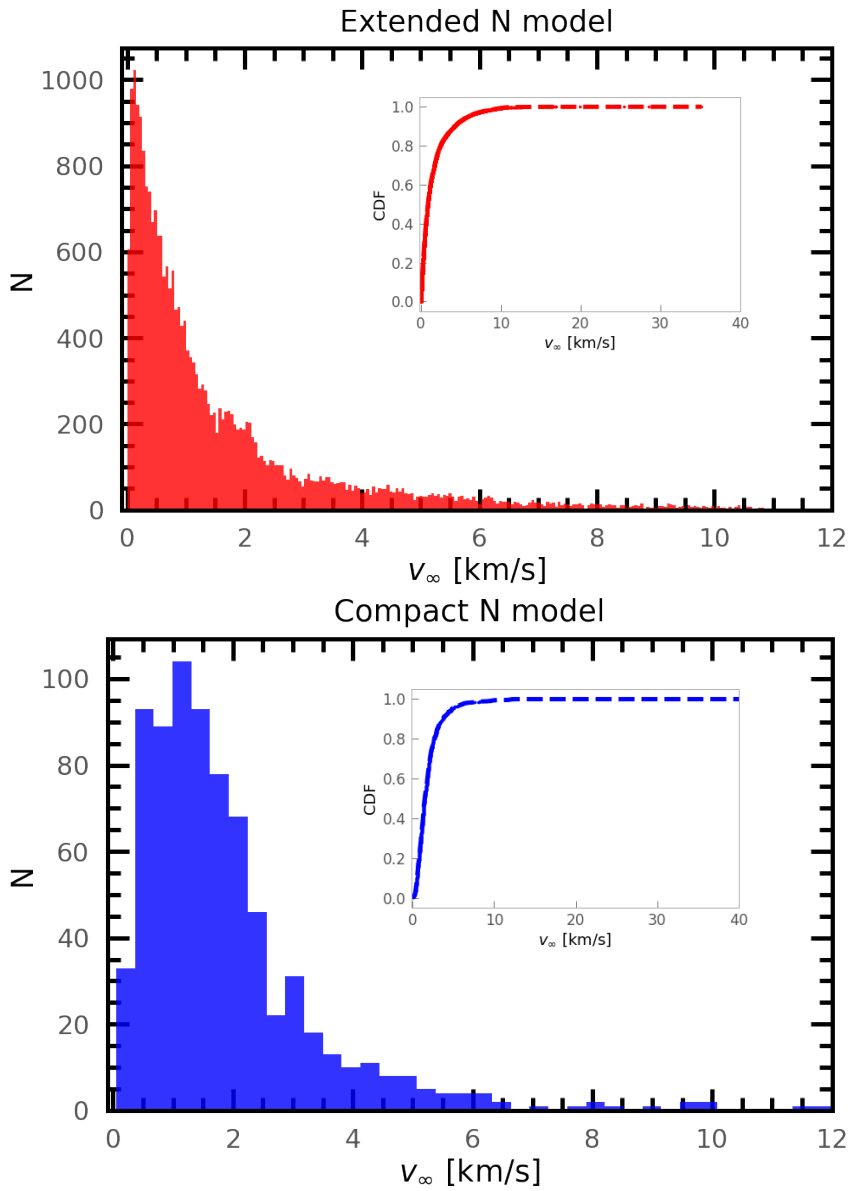


Figure 4.14: Hyperbolic excess velocity for the unbound objects of all the simulated systems, for the extended (top, red) and compact (bottom, blue) models. The histogram show the distribution of the particles, while the inset shows the cumulative distribution.

4.4 Interstellar objects

Our simulations show that the hyperbolic speed v_∞ of the particles ejected from the solar system for the *Extended N* and *Compact N* models is of order $1\text{--}3\text{ km s}^{-1}$ (Fig. 4.14). The planetesimals in the *Extended N* model acquire more energy due to the strong interaction with passing stars and reach velocities from ~ 0.5 up to 40 km s^{-1} (inset top panel Fig. 4.14). Approximately 36% of the total number of particles in the 200 systems become interstellar comets (Fig. 4.14). On the other hand for the *Compact N* model the effect of to the planet-disk interactions is weaker than the effect of a passing star. Around 7% of the particles are ejected from the system with velocities between 0.5 and 40 km s^{-1} (inset bottom panel Fig. 4.14). Overall, the ejection of the asteroids and comets to interstellar space from a cluster environment is dominated by the interaction of stars passing close by. The efficiency increases when the angle of interaction is between 0 and 30 degrees, independent of the distance of the encounter (Fig. 4.3). If the planets near the disk become unstable and the interaction with the disk induces migration, the efficiency of the planets at creating interstellar objects dominates over the stellar encounters (Raymond et al. 2010). However, if the planets orbits are stable only a small fraction ($\sim 7\%$) of particles is ejected.

The further evolution of the interstellar comets will be dominated by the dynamical interaction with other stars in the cluster, and those that manage to escape will also be perturbed by the gravitational tides from the Milky Way. These future perturbations will increase their velocity at infinity passing from few km s^{-1} to tens of km s^{-1} as in the case of 'Oumuamua. The estimations of the number of the local density of interstellar objects range from 10^{14} pc^{-3} (Portegies Zwart et al. 2018), to $8 \times 10^{14}\text{ pc}^{-3}$ (Jewitt et al. 2017), to $2 \times 10^{15}\text{ pc}^{-3}$ (Do et al. 2018). Recently Bannister et al. (2019) estimated the underlying mass density of interstellar objects by considering planet instability models. They found that the total mass of interstellar objects ejected due to a planet-disk interaction is on the order of 0.004 to $3 M_\oplus\text{ pc}^{-3}$. However, due to the lack of observations of interstellar objects these numbers are still highly uncertain. What is clear from the mentioned works and the results presented in this work is that a large fraction of objects may be ejected from a planetary system and that therefore interstellar space may be full of asteroids and comets.

Summary and Conclusions

We explored the dynamical evolution of the solar system debris disk while the Sun was still in its birth cluster, accounting for planetary perturbations and multiple stellar encounters. The goal is to investigate the role of external perturbations in the formation of the Oort cloud. We also explored the creation of interstellar comets. We aimed to find which stellar flybys can initialise the creation of short and long-period comets, without the perturbations due to the encounter being strong enough to completely destroy the debris disk. We explored two models of the solar system, the *extended* and the *compact* models. For each model, we perturb the system with one close encounter or with multiple encounters. The results can be summarized as follows:

- The dynamical properties of the outer solar system can indeed be produced with the *Extended-N* model, where stellar flybys act as a progenitor to stir up the disk, making the disk more fluffy, and secular planet-asteroid interaction gradually lift up the perihelia of the disk objects and make the distribution more homogenous.
- The solar system is likely to undergo multiple stellar encounters during its time in the birth cluster. One of the consequences of multiple stellar encounters is that they drive particles in the extended disk to migrate outwards and become increasingly eccentric. The semi-major axis of these orbits are large enough for the Galactic tide to be efficient in circularising their orbits (Heisler & Tremaine 1986). This process can be seen in the $a - e$ space as tail-shaped feature. At smaller semi-major axes where the Galactic tide is not efficient, particles remain in (highly) eccentric orbits but will become unstable on secular timescales.
- The gravitational perturbation of a stellar flyby tends to be maximum when the interaction angle is between $0^\circ - 30^\circ$, independent of the size of the disk.
- Planet-disk interaction produces a non-uniform density distribution of Kuiper Belt Objects. Higher density of Kuiper Belt Objects coincide with the low-order mean-motion resonance with the giant planet.

4.5 Summary and Conclusions

- Kuiper belt objects are shepherded by giant planets. The orbital instabilities of giant planets can be triggered by close stellar encounters, which in turn lead to the restructuring of the Kuiper belt, and potentially the production of interstellar objects.
- The formation of the interstellar objects is dominated by relatively close stellar encounters rather than planet-disk interactions.
- The Kuiper belt, scattered disk, the Sednoids region, the Oort cloud, and the formation of interstellar objects in planetary systems may be common if the assumption that stars form in clusters is valid.

Even though our initial conditions for the simulations are based on several assumptions and simplifications that might not fully correspond to the early solar systems, our results provide a possible picture of the ingredients that shaped the solar system in its early stages and suggests that the solar system must have faced at least one encounter in its early stages of formation. Additionally our results imply that the structure and evolution of the solar system may be a consequence of multiple external interactions.

Acknowledgements ST expresses his gratitude to the Mexican National Council for Science and Technology (CONACYT) for the grant #291004-410780; and to the LEAPS program and Leiden Observatory for the unconditional support. This work was carried out on the Dutch national e-infrastructure with the use of *Cartesius* the Dutch national supercomputer and the support of SURF Cooperative. Simulations in this paper made use of *LonelyPlanets* (Cai et al. 2018), NBODY6++GPU (Wang et al. 2015), REBOUND (Rein & Liu 2012), and Astrophysical Multi-purpose Software Environment – AMUSE (Portegies Zwart & McMillan 2018).



Credit: Science Photo Library

Chapter 5

**Dynamical evolution of exo-Oort clouds
around the Sun's closest neighbour
stars due to local stellar perturbations
and the Galactic tidal field**

S. Torres, Portegies Zwart,
and A. G. A. Brown. Submitted to
Astronomy & Astrophysics, 2020

Abstract

The dynamical evolution of the outer Oort cloud in the solar system is affected by passing stars and the Galactic tidal field. These perturbations can strip comets from the cloud, forming *sōlī lapidēs* (interstellar objects). If we assume that the Sun's neighbour stars also have Oort cloud-like structures, and therefore undergo similar perturbations, interstellar comets are expected to be common in the local solar neighbourhood. In this work we investigate the dynamical evolution of comets in an exo-Oort cloud around the Sun's neighbour stars, accounting for the effect of passing stars and the Galactic tidal field. Using proper motions, parallaxes, and radial velocities from Gaia DR2, we studied a subset of the stars within 3 pc from the Sun, i.e., the systems: Proxima Centauri, Barnard's star, Gliese 65, Ross 154, and Ross 248. For each system, we then calculate the closest encounter with other stars they had in the last 10 Myr and will have in the next 10 Myr. We find that on average the stars in the local solar neighbourhood experiences around 40-55 encounters within 2.5pc from each star during 20 Myr, primarily with M-dwarfs stars. Using the Astrophysical Multipurpose Software Environment (AMUSE), and the GPU-accelerated direct N-body code ABIE, we then calculate the effect of passing stars and the Galactic tidal field on the comets in exo-Oort clouds around the Sun's neighbour stars. The most perturbed system is the binary system Gliese 65. Approximately 40×10^8 TIC Myr^{-1} becomes transitional interstellar comets (TICs), while 1.4×10^{10} ISO Myr^{-1} interstellar objects (ISOs) over a time interval of 20 Myr. The semi-major axes of these comets are comparable with the distance between Gliese 65 and the Sun. Comets from the system Gliese 65 might reach the solar system in the case that an Oort Cloud-like structure around this star exists. For the remaining systems studied in this work, the rate of TIC production over a time interval of 20 Myr is about 2.1 to 3.8×10^8 TIC Myr^{-1} . This implies that a considerable fraction of interstellar comets reside in the local neighbourhood. Therefore the Sun and its neighbours are visited by interstellar comets originating from other stars. In this way, it is plausible that an interstellar comet cloud exists.

Introduction

Internal and external perturbations drive the dynamical history and evolution of the population of minor bodies in the solar system. The internal perturbations are due to the instabilities induced by the giant planets on a planetesimal disk at the early stages of the solar system. The external perturbations are due to stars passing near the sun and the Galactic tidal field. These effects play a crucial role in the formation and evolution of the Kuiper belt (e.g., Morbidelli 2005; Brassier & Morbidelli 2013), Oort cloud (e.g., Fouchard et al. 2006; Vokrouhlický et al. 2019) and interstellar comets (e.g., Portegies Zwart et al. 2018; Torres et al. 2019a,b). Close encounters with other stars can disrupt the comets in the Kuiper belt (e.g., Punzo et al. 2014), strip the Oort cloud (e.g. Nordlander et al. 2017; Jílková et al. 2016; Hanse et al. 2016; Bailey & Fabrycky 2019), and create interstellar objects (asteroids/comets). In the early history of the solar system the Sun may have been expelled from its birth cluster due to interaction with the other cluster stars (Portegies Zwart & Jílková 2015; Martínez-Barbosa et al. 2016; Cai et al. 2017). Even though close encounters between the sun and other stars might be rare today, they might have been quite common in the early stages of the solar system, and they will happen in the near future (Torres et al. 2018, 2019a). Studying the effect of multiple interactions with stars and the galactic tidal field can help us to better understand the dynamics of the outer regions of planetary systems with architectures similar to the solar system.

If we assume that other planetary systems undergo similar processes of formation as the solar system, structures like the Kuiper belt and Oort cloud must be common (see, e.g., Potemine 2010; Veras et al. 2014; Caiazzom & Heyl 2017; Baxter et al. 2018; Schwarz et al. 2018; Moro-Martín 2019). Several studies have detected these structures in a variety of primarily low mass stars (see e.g., Vicente & Alves 2005; Kiefer et al. 2014; Pawellek et al. 2014; Welsh & Montgomery 2015; Boyajian et al. 2016; Schwarz et al. 2018). These indicate that reservoirs of comets around stars might be common. Such comet reservoirs will be affected by perturbations due to planets, passing stars, and the Galactic tidal field, which may lead to the production of interstellar comets (Torres et al. 2019a), leading to the extrapolation that interstellar space might be full of such objects.

5 Dynamics of exo-Oort clouds in the solar neighbourhood

The discovery of the first interstellar comet, 1I/'Oumuamua (Williams 2017; Meech et al. 2017), and the interstellar comet, 2I/Borisov (Borisov 2019; Guzik et al. 2019), opened up a new era in the study and exploration of the solar system and other planetary systems in our galaxy. The ejection of minor objects from a planetary system, subsequently becoming *sōli lapidēs* (Portegies Zwart et al. 2018; Torres et al. 2019a,b) or commonly known as interstellar objects or ISOs, is mainly due to the post AGB stellar mass loss and gravitational instability induced by a massive body. This body can be either a nearby planet, a star passing close by or a combination of both (see e.g., Portegies Zwart et al. 2018; Torres et al. 2019a,b; Banister et al. 2019). Using a catalogue of nearby stars, Torres et al. (2019a) studied the dynamical evolution of comets in the Oort cloud, accounting for perturbations from passing stars and the Galactic tidal field. They found that the cumulative effect of distant stellar encounters and the Galactic tidal field raises the semi-major axis of $\sim 1.2\%$ of the total number of comets in the cloud out to interstellar regions. Such comets become transitional interstellar comets (hereinafter TICs) satisfying the condition $e_c \leq 1$ and $a_c > a_{EOC}$. Where e_c and a_c are the eccentricity and the semi-major axis of the comet in the cloud and a_{EOC} is the semi-major axis of the exo-Oort cloud (Eq. (5.1)).

Following up on the results of Torres et al. (2019a) in this work we aim to study the formation of TICs around nearby stars (assuming that they have an exo-Oort cloud) to investigate if ISOs from the nearby stars could interact with the solar system. We explore the history of stellar encounters for stars within 3 pc from the Sun, using astrometric data from Gaia DR2 (Gaia Collaboration et al. 2018, 2016). The stars studied are Proxima Centauri, Barnard's star, Gliese 65, Ross 154, and Ross 248. We consider the scenario in which these stars have an exo-Oort cloud and focus on the dynamical evolution of the comets in those clouds due to the stellar encounters and the Galactic tidal field, leading to the production of TICs and ISOs. In Sect. 5.2 we present the closest encounters that each of the nearby stars to the Sun has had in the past 10 Myr and will have in the next 10 Myr. In addition we quantify the change of the velocity produced for the closest stars using the impulse approximation. In Sect. 5.3 we study the dynamical evolution of exo-Oort clouds around the Sun's nearest neighbours under the influence of passing stars and the Galactic tidal field. We analyse the production of TICs and ISOs. Finally, in Sect. 5.4, we present our summary and conclusions.

Close stellar encounters experienced by the Sun's nearest neighbours

Using the catalogue of nearby stars presented in Torres et al. (2019a) we selected the stars for which we model the exo-Oort clouds from within a 3 pc radius around the Sun at the present time; Proxima Centauri, Barnard's star, Sirius B, GJ 65B, GJ 65A, Ross 154, and Ross 248. The binary system GJ 65 A/B is in a sufficiently tight orbit to be modelled (for simplicity) as one system with a shared exo-Oort cloud. We have chosen to exclude Sirius A and B from the exo-Oort cloud modelling as it is uncertain whether a binary hosting an evolved star which has experienced significant mass loss will have retained any exo-Oort clouds (circumstellar or circumbinary) that may have existed in the past. However, the effect of Sirius B on the Oort clouds of the 5 systems above is taken into account in our calculations. The stars for which we model the exo-Oort clouds are shown in Fig. 5.1 and Table 5.1. The estimates presented in this work are conservative and based on a small sample of known stars. Therefore this corresponds to a lower limit of the total number of Sun's neighbour stars. The catalogue of nearby stars was built using only Gaia DR2 astrometric data, this excludes the well known nearby stars within ~ 3 pc from the Sun, α Cen A, α Cen B, WISEA J085510.74-071442.5, GJ 406, GJ 411, and Sirius.

The Torres et al. (2019a) catalogue was constructed using the positions, parallaxes, proper motions, and radial velocities from Gaia DR2, and includes additional radial velocities from RAVE-DR5 (Kunder et al. 2017), GALAH DR2 (Buder et al. 2018), LAMOST DR3 (Zhao et al. 2012), APOGEE DR14 (Abolfathi et al. 2018), and XHIP (Anderson & Francis 2012). It contains 14 659 stars and it constitutes an astrometrically clean sample which is incomplete due to the Gaia survey limitations, the upper limit imposed on the distance to the stars in the sample (50 pc), and the strict data-quality filtering from Lindegren et al. (2018). Using Galactocentric Cartesian coordinates we integrated the orbit of the stars in the Torres et al. (2019a) catalogue 10 Myr forwards and backwards in time for a total time of 20 Myr. The orbit integrations were done with the Gala package (Price-Whelan 2017), using an analytic axisymmetric model for the galactic potential, which consists of a spherical nucleus and bulge (Hernquist 1990), a Miyamoto-Nagai disk (Miyamoto & Nagai 1975; Bovy 2015), and a spherical Navarro-Frenk-White (NFW) dark matter halo (Navarro et al.

5 Dynamics of *exo-Oort clouds* in the solar neighbourhood

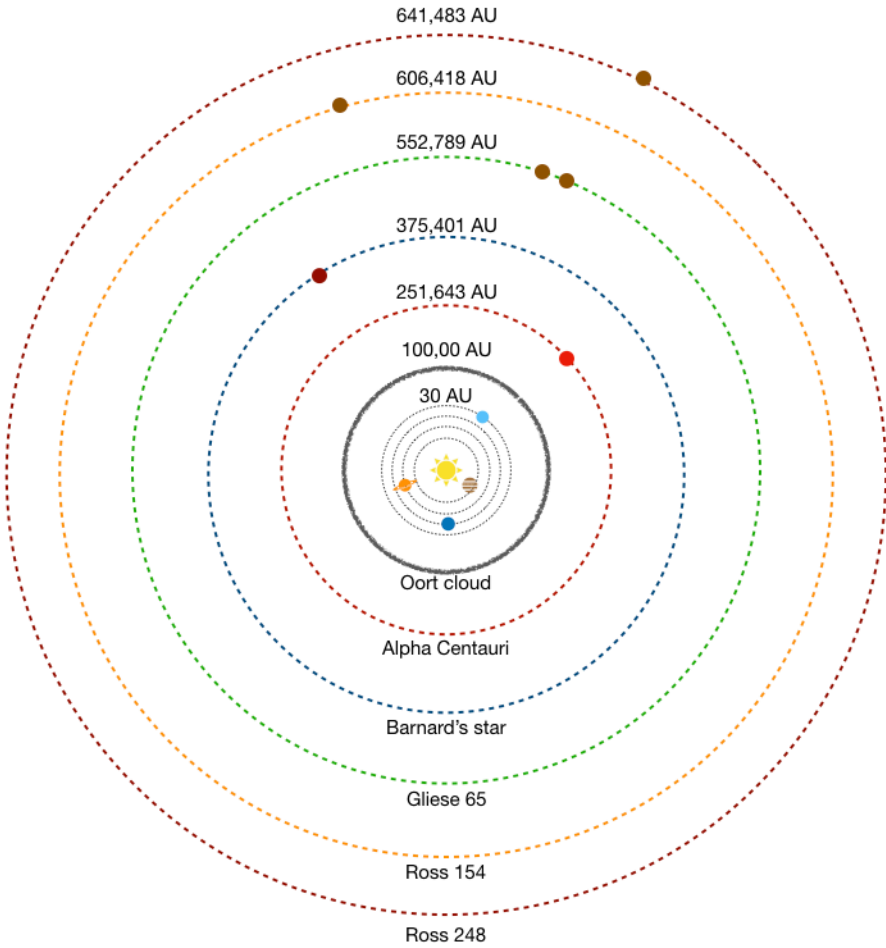


Figure 5.1: Schematic representation of the stars within 650 000 au (~ 3 pc) from the Sun (not to scale). The inner part of the figure shows the solar system and the Oort cloud. The surrounding rings represent the closest stars to the Sun: Proxima Centauri (red), Barnard's star (blue), Gliese 65 (green), Ross 154 (yellow), and Ross 248 (brown). The distances to the stars are listed at the top of the rings. Coloured dots represents the spectral type of the stars; brown stands for brown dwarfs, red for red dwarfs, and yellow for G stars.

5.2 Close stellar encounters experienced by the Sun's nearest neighbours

1996). Using a KD-Tree we identified stars from the Torres et al. (2019a) catalogue that approach the stars under study here to within 2.5 pc. The results are listed in Table 5.2. In Fig. 5.2 we show the time and the distance of the closest approach for each close stellar encounter experienced by the stars listed in Table 5.2. On average the nearby systems experience ~ 50 encounters during 20 Myr (third column, Table 5.2).

For the stars within 3 pc from the Sun we calculate the size of the exo-Oort clouds that potentially surround them (Table 5.2). Following the works of Hanse et al. (2016) we scale the outer edge of the exo-Oort cloud to the Hill radius of the parent star in the Galactic potential:

$$\approx a_{\text{OC}} \frac{R_*}{R} \left(\frac{M_*}{M} \frac{M_G(R)}{M_G(R_*)} \right)^{1/3} \quad (5.1)$$

where a_{OC} is the semi-major axis of the Oort cloud of the Sun, while R and R_* are the Galactocentric radii of the Sun and the star, respectively. The terms $M_G(R)$ and $M_G(R_*)$ are the cumulative mass of the Galaxy enclosed within the radius R , and are calculated from our Galactic potential. Considering that the stars listed in Table 5.2 have $R_* \approx R$, Eq. (5.1) can be written as follows:

$$\approx a_{\text{OC}} \left(\frac{M_*}{M} \right)^{\frac{1}{3}}. \quad (5.2)$$

To calculate the effect of a nearby star on the comets in an exo-Oort cloud two ingredients are needed; the escape velocity (v_{esc}) from the comet's host star, and the change in velocity of the comets (Δv) after the interaction. If the final velocity of the comets after the interaction with the passing star is larger than the escape velocity, these will be dislodged from the cloud. The escape velocity (Fig. 5.3) is calculated considering the values for the outer edge of the exo-Oort cloud of each star, calculated using Eq. (5.2) and listed in Table 5.1. Subsequently, using the impulse approximation (Oort 1950; Rickman 1976) we calculate the change of the velocity due to a passing star as:

$$\propto \frac{M_* r_c}{v_* r_h^2}, \quad (5.3)$$

5 Dynamics of exo-Oort clouds in the solar neighbourhood

Table 5.1: Stars within 3 pc from the Sun. The first column shows the name of the star, followed by the Gaia DR2 identification, the distance to the Sun, the spectral type (ST), and the mass.

Star	Gaia DR2 ID	*Distance (pc)	ST	Mass (M)
Proxima Centauri	5853498713160606720	1.30	M5	0.122 ^a
Barnard's star	4472832130942575872	1.82	M4	0.144 ^b
Gliese 65	5140693571158739712	2.69	M5	0.202 ^c
Ross 154	4075141768785646848	2.98	M3	0.170 ^d
Ross 248	1926461164913660160	3.16	M6	0.136 ^e

* Distance calculated from Gaia DR2 parallaxes. ^(a)Mann et al. (2015), ^(b)Ribas et al. (2018),

^(c) Considering the mass of Gliese 65 a and b Delfosse et al. (2000), ^(d)Davison et al. (2015),

^(e)Jenkins et al. (2009).

5.2 Close stellar encounters experienced by the Sun's nearest neighbours

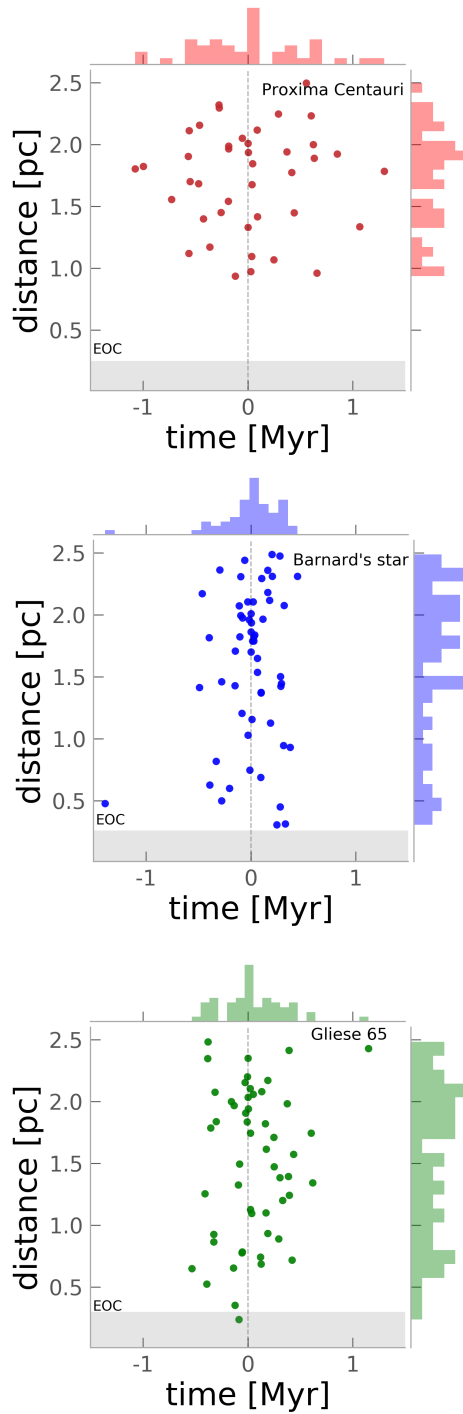


Figure 5.2: Continue...

5 Dynamics of exo-Oort clouds in the solar neighbourhood

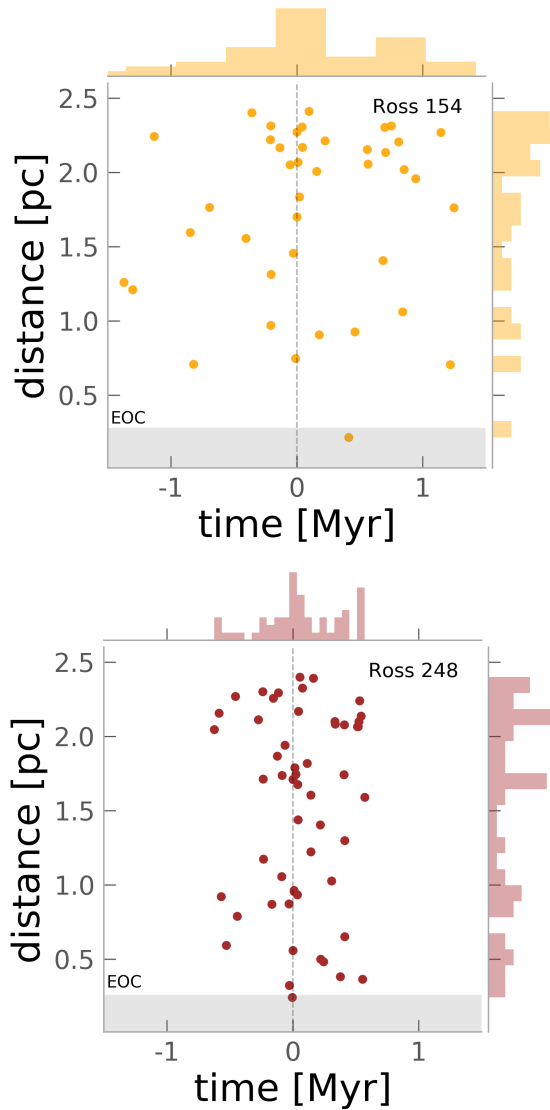


Figure 5.2: Closest approach distance versus the time of closest approach. The top panel (red colours) shows the closest encounters between Proxima Centauri and the stars in the Torres et al. (2019a) catalogue over a time interval of 20 Myr centred on the present. Following by Barnard's star (blue), Gliese 65 (green), Ross 154 (yellow), and Ross 248 (brown). The histograms in each panel represents the marginal distributions in distance and time. The shaded areas represent the boundaries of the outer Oort cloud for each star.

5.2 Close stellar encounters experienced by the Sun's nearest neighbours

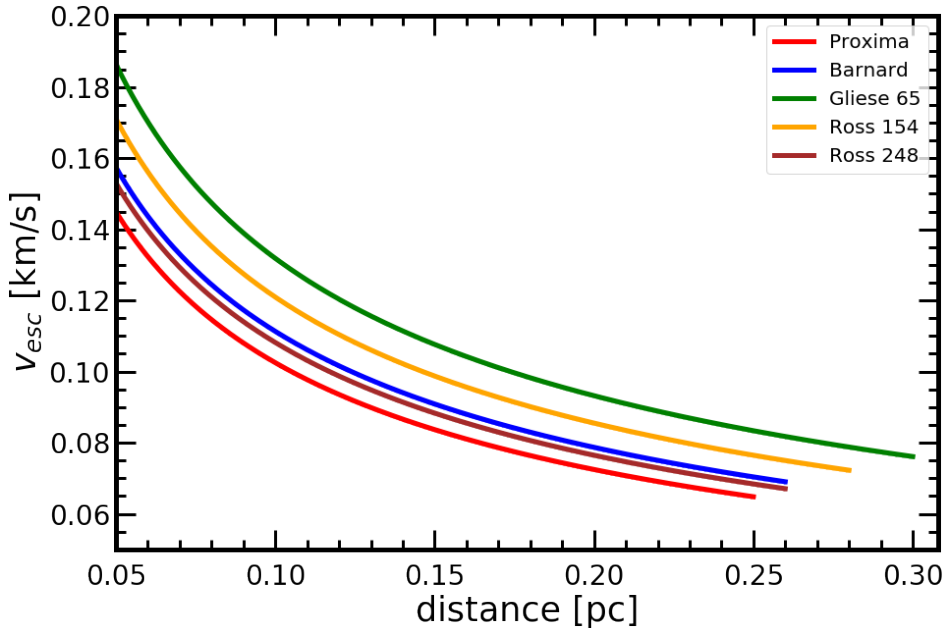


Figure 5.3: Escape velocity as a function of the distance from the star for Proxima Centauri (red), Barnard's star (blue), Gliese 65 (green), Ross 154 (yellow), and Ross 248 (brown).

where M_* and v_* are the mass and velocity of the passing star in M_\odot and km s^{-1} , respectively. The distance of the exo-comet to its host star is r_c , while r_h is the distance of the host star to the passing star at the point of closest approach. The total change of the velocity induced by the stars passing closest to the solar neighbours studied in this work is listed in the last column of Table 5.2.

In Fig. 5.2 and Table 5.2 we show the closest approach distance and time for each of the Sun's closest neighbours. The limited distance range of the stars in the Torres et al. (2019a) sample only allows us to find close encounters (< 2.5 pc) that occur within ± 1.5 Myr from the present for the total period of integration (± 10 Myr). Here we discuss the effect exclusively due to the impulse imparted to the comets during the close encounters between the stars in Table 5.1 and the stars in the Torres et al. (2019a) catalogue. The full cumulative effect of the encounters and Galactic tidal field are studied in the next section. For the systems discussed below Table 5.2 lists both the circular and the escape velocity at the edge of the exo-Oort

5 Dynamics of exo-Oort clouds in the solar neighbourhood

Table 5.2: Stellar encounter statistics for the Sun and its closest neighbours. The first column shows the name of the star followed by the distance and time of the closest approach by another star from the Torres et al. (2019a) catalogue. The fourth column indicates the number of encounters closer than 2.5 pc that each system experiences during 20 Myr, followed by the circular and escape velocity in the (exo-)Oort cloud. Columns seven and eight show the average and the total change of the velocity (Eq. (5.3)) induced by the closest encounters for each star. The last column shows the size of the outer edge of the (exo-)Oort cloud (λ). The Full list of the stellar encounters for each star in this table can be found online. The encounter statistics for the Sun are taken from Torres et al. (2019a).

Star	d_{ph} (pc)	t_{ph} (Myr)	N_{enc} < 2.5 pc	v_{cir} (km s ⁻¹)	v_{esc} (km s ⁻¹)	$\langle \Delta V_{\perp} \rangle$ (km s ⁻¹)	$\Sigma \Delta V_{\perp}$ (km s ⁻¹)	EOC (pc)
Sun	0.05	1.28	31	0.092	0.131	4.275e-03	1.325e-01	0.50
Proxima Centauri	0.93	-0.11	40	0.045	0.064	5.929e-05	2.371e-03	0.25
Barnard's star	0.30	0.24	55	0.048	0.069	1.765e-04	1.006e-02	0.26
Gliese 65	0.23	-0.08	51	0.043	0.061	1.846e-04	9.786e-03	0.30
Ross 154	0.21	0.41	45	0.051	0.072	2.244e-04	1.032e-02	0.28
Ross 248	0.24	-0.005	53	0.047	0.067	2.060e-04	1.133e-02	0.26

5.2 Close stellar encounters experienced by the Sun's nearest neighbours

clouds. Comets in those clouds can be stripped away if their velocity change due to the stellar encounters is at least large enough to bridge the gap between the circular speed and the escape speed.

Proxima Centauri encounters 40 stars that approach to within 2.5 pc over the 20 Myr integration interval (first panel, red dots Fig. 5.2). These close approaches all take place over a ~ 3 Myr time interval which is an artifact of the limited volume from which we draw the stellar encounter candidates. The closest approach to Proxima Centauri is a low mass star at 0.93 pc at -0.11 Myr from the present. The total velocity change for the comets in the exo-Oort cloud of Proxima Centauri due to the close encounters is approximately $2.3 \times 10^{-3} \text{ km s}^{-1}$, on average $5.9 \times 10^{-5} \text{ km s}^{-1}$ per encounter. This means that the effect of the close encounters is small and exo-comets around Proxima Centauri will not suffer an important change in their orbital elements, considering that the escape velocity at the edge of its exo-Oort cloud is $\sim 0.064 \text{ km s}^{-1}$.

Barnard's star experiences 55 close encounters (second panel, blue dots Fig. 5.2), where the closest encounter will happen in 0.24 Myr from today at the distance of 0.30 pc. The total impulse induced by the stars approaching to within 2.5 pc from Barnard's star generates a total change of the velocity of $\sim 1 \times 10^{-2} \text{ km s}^{-1}$, on average $1.7 \times 10^{-4} \text{ km s}^{-1}$ per encounter. Although on average the effect of the passing stars is relatively small compared to the escape velocity at the edge of the cloud (0.069 km s^{-1}), the final velocity of the comets in this region after the encounters, will be close to their escape velocity. This implies an important change in their orbital elements.

Gliese 65 has the largest exo-Oort cloud (0.3 pc) among the stars in Table 5.2. Gliese 65 experiences 51 close encounters (Fig. 5.2, third panel, green dots) and two very close encounters. The first one with a red dwarf (~ 0.6) at the edge of its exo-Oort cloud (0.23 pc) which produces a change in the comet velocity of $2.2 \times 10^{-3} \text{ km s}^{-1}$. While the second with a solar type star (~ 1) at a distance of 0.35pc, leading to a change in the comet velocity of $1.8 \times 10^{-3} \text{ km s}^{-1}$. If we considered that the escape velocity is limited by 0.076 km s^{-1} at the edge of the cloud the individual effect of these stars, will not perturb enough the comet to strip them from the cloud. However the orbital elements of the comets will be modify by these encounters.

5 Dynamics of exo-Oort clouds in the solar neighbourhood

The total change in the comet velocity induced by the closest encounters is $\sim 9.7 \times 10^{-3} \text{ km s}^{-1}$, on average the change of the velocity is around $1.8 \times 10^{-4} \text{ km s}^{-1}$ per encounter.

Ross 154 has the second largest exo-Oort cloud (0.28 pc) among the stars in Table 5.2. Ross 154 will face a close encounter with a solar-type star ($\sim 1.1 \text{ } \text{M}_{\odot}$) passing at a distance of 0.21 pc (through the exo-Oort cloud) in 0.41 Myr from today. The change of the velocity produced by this star is approximately $5.5 \times 10^{-3} \text{ km s}^{-1}$. This means a comet at the edge of the cloud where the escape velocity is around 0.07 km s^{-1} will not be stripped from the exo-Oort cloud due to this encounter, but its orbital elements will change. The total change induced by the 45 stellar encounters (see Fig. 5.2, fourth panel, yellow dots) is of the order of $1.03 \times 10^{-2} \text{ km s}^{-1}$, on average of $2.2 \times 10^{-4} \text{ km s}^{-1}$ per encounter.

Ross 248 experiences 53 encounters (Fig. 5.2, fifth panel, brown dots), including a close encounter with an M-dwarf with a mass of $0.5 \text{ } \text{M}_{\odot}$ passing at 0.24 pc (just outside its exo-Oort cloud of which the edge is at 0.26 pc). This close encounter produces a change in the velocity of approximately $1.3 \times 10^{-3} \text{ km s}^{-1}$ in comet at the edge of the Ross 248 exo-Oort cloud. This change is not enough to strip the comet from the cloud but it is enough to perturb their orbits. The rest of the encounters do not provide a considerable effect on the cloud. On average the close encounters with Ross 248 produce a change of the velocity of $\sim 2.06 \times 10^{-4} \text{ km s}^{-1}$ per encounter for a total change of $\sim 1.13 \times 10^{-2} \text{ km s}^{-1}$.

The effect of the close stellar encounters on the systems studied here is small, the total change of the comet velocities due to the passing stars ranges from $\sim 2.3 \times 10^{-3}$ to $\sim 1.1 \times 10^{-2} \text{ km s}^{-1}$. The escape velocity for these systems ranges from 0.061 to 0.076 km s^{-1} , while the circular velocities at the edge of the exo-Oort clouds range from 0.045 to 0.051 km s^{-1} (Fig. 5.2, Table 5.2). This means that the final velocity of the comets after the encounters are not sufficiently large for them to escape the systems. The systems Gliese 65, Barnard's star, Ross 154, and Ross 248 are the most perturbed systems with final velocities just below their escape velocity at the edge of the cloud. For the system Proxima Centauri comets will not suffer an important change and their orbits and they will remain relatively stable after the encounters.

5.2 Close stellar encounters experienced by the Sun's nearest neighbours

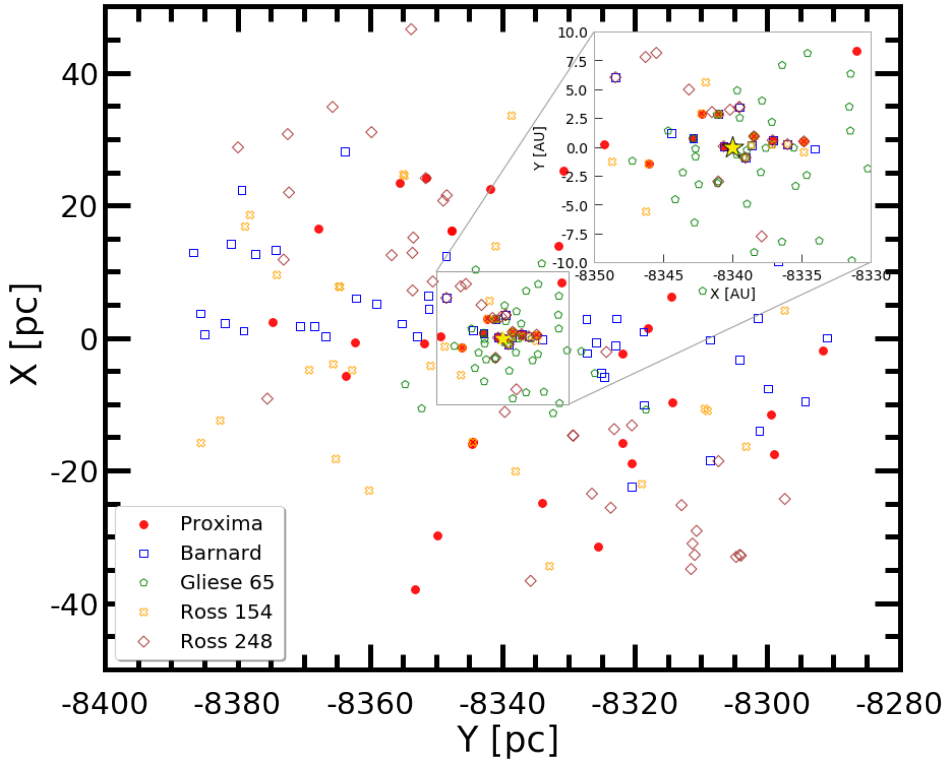


Figure 5.4: Galactocentric coordinates of the present day positions of the stars that have made or will make close approaches to the systems Proxima Centauri (red dots), Barnard's star (blue squares), Gliese 65 (green pentagons), Ross 154 (yellow cruces), and Ross 248 (brown diamonds). The inner plot represents a zoom-in of the central area, where the big yellow star represents the Sun and the mentioned systems.

The low mass of perturbers ($0.1-1$) as well as the relatively large distance of closest approach (as compared to the exo-Oort cloud sizes) explains the small effect produced by the flybys. It is interesting to point out that even though the closest systems to the Sun are not heavily perturbed by their nearest neighbour stars, the local solar neighbourhood is crowded as shown in Fig. 5.4 where the current positions of all the stars interacting with the systems in Table 5.2 are shown. This indicates that the journey through interstellar space of the comets dislodged from their host system will be determined by the stars in the solar neighbourhood.

The results presented in this section gave us a general picture of the encounter history of the Sun's nearest neighbours and the effects thereof on

5 Dynamics of exo-Oort clouds in the solar neighbourhood

the comets in an Oort cloud like structure. However, to have more accurate information about the dynamics of the comets in the exo-Oort clouds it is necessary to integrate their orbits in a Galactic potential, accounting not only for the effect of single stellar encounters but studying the cumulative effect of the encounters and the Galactic tidal field. This is the topic of the next section.

Section 5.3

Dynamical evolution of exo-Oort clouds of the Sun's neighbour stars

Torres et al. (2019a) studied the cumulative effects on the Sun's Oort cloud due to the flybys of nearby stars and the Galactic tidal field over a period of 20 Myr (centred on the present time). They found that relatively close encounters (< 2.5 pc) and the tides from the Galaxy considerably perturbed the outer regions of the Oort cloud, turning about 1.2% of the comets into transitional interstellar comets (TICs). Motivated by these results we investigate the dynamics of the Oort Cloud-like structures around some of the Sun's nearest neighbours (Table 5.1). We first assume that these stars possess an Oort cloud-like structure. Following the method of Torres et al. (2019a) we add an artificial isotropic cloud of comets to each star with 10 000 test particles each. We limited the size of the Oort cloud according to Eq. (5.2) for each star in Table 5.2. The exo-Oort clouds are constructed in such a way that the distribution of the particles is symmetric and isotropic, and they follow a uniform distribution in the orbital elements $\cos i$ (inclination), ω (argument of periapsis), Ω (longitude of the ascending node), and M (mean anomaly). The initial eccentricities, e , are selected with a probability density distribution $p(e) \propto e$. The semi-major axes, a , are distributed proportional to $a^{-1.5}$ over the range 3×10^3 au and the outer edge of each cloud. To ensure a thermalised Oort cloud (e.g. Duncan et al. (1987); Dybczyński (2002); Rickman et al. (2008)) we used a radial density profile of $r^{-3.5}$ (where r is the distance between the comets and the star).

Our numerical simulations rely on the Astrophysical Multi-purpose Software Environment, AMUSE (Portegies Zwart et al. 2009; Pelupessy et al. 2013; Portegies Zwart et al. 2013b; Portegies Zwart & McMillan 2018) and the GPU-accelerated direct N-body code ABIE (Roa et al. in press, Cai et al. in preparation) with a fifteenth-order Gauss-Radau integrator (Everhart 1985) optimised for close encounters. We investigate the effect of

5.3 Dynamical evolution of exo-Oort clouds of the Sun's neighbour stars

stellar encounters and the galactic tidal field on the exo-Oort cloud of each system in Table 5.1. To achieve that we couple ABIE and the Gala (Price-Whelan 2017) package in such a way that ABIE advances the positions of the exo-Oort cloud particles and Gala calculates the accelerations on each particle due to the Galactic tidal field, based on the positions provided by ABIE. The calculated accelerations are subsequently inserted into the Gauss-Radau integrator in ABIE as additional forces.

The stars listed in Table 5.1 are primarily brown dwarfs, with masses around $0.1 M_{\odot}$. This means that the outer edge of their exo-Oort clouds extends to about 0.2 pc from the host star. For this size of exo-Oort cloud the contribution of the Galactic tidal field is rather small and therefore the effect on the comets at the edge will be minimal (Torres et al. (2019a)). Therefore, the predominant perturbation is due to the relatively close passing stars. In Fig. 5.5 and Fig. 5.6, we show the change of the perihelion as a function of the final semi-major axis and eccentricity for the particles in the exo-Oort cloud for each system in Table 5.1. For each individual system we find the following results.

Note that below we present the number of TICs or ISO produced in two ways; as the percentage of the 10 000 simulated particles and as a rate of TIC/ISO production per Myr which is found by scaling the simulated exo-Oort clouds to the number of comets estimated to exist in the solar system Oort cloud ($\sim 10^{12}$ comets, Morbidelli et al. 2005).

Proxima Centauri The effect of the Galactic tidal field and stellar encounters on the exo-Oort cloud of Proxima Centauri is relatively small, with the closest approach of another star happening at a distance of 0.93 pc. Nevertheless a small fraction, $\sim 0.42\%$ of the initial comets in the cloud are turned into TICs after 20 Myr (Fig. 5.5 and Fig. 5.6). The production rate of TICs of Proxima Centauri during those 20 Myr is $\sim 2.1 \times 10^8$ TIC Myr $^{-1}$. The change of perihelion for the particles in the cloud is up to 10 000 au for the particles with initial semi-major axes between 47 000 and 51 500 au, which is the most disturbed region of the cloud. The inner parts of the cloud are nearly unperturbed. In Fig. 5.5 yellow particles represent the change of the perihelion as a function of the final semi-major axis for the TICs originating from the solar system (compare to Fig. 12 in Torres et al. 2019a). As can be seen in Fig. 5.5, due to its proximity to the Sun the Hill sphere of Proxima Centauri overlaps with the simulated TICs originating from the solar system and we may thus speculate about comets originating from the

5 Dynamics of exo-Oort clouds in the solar neighbourhood

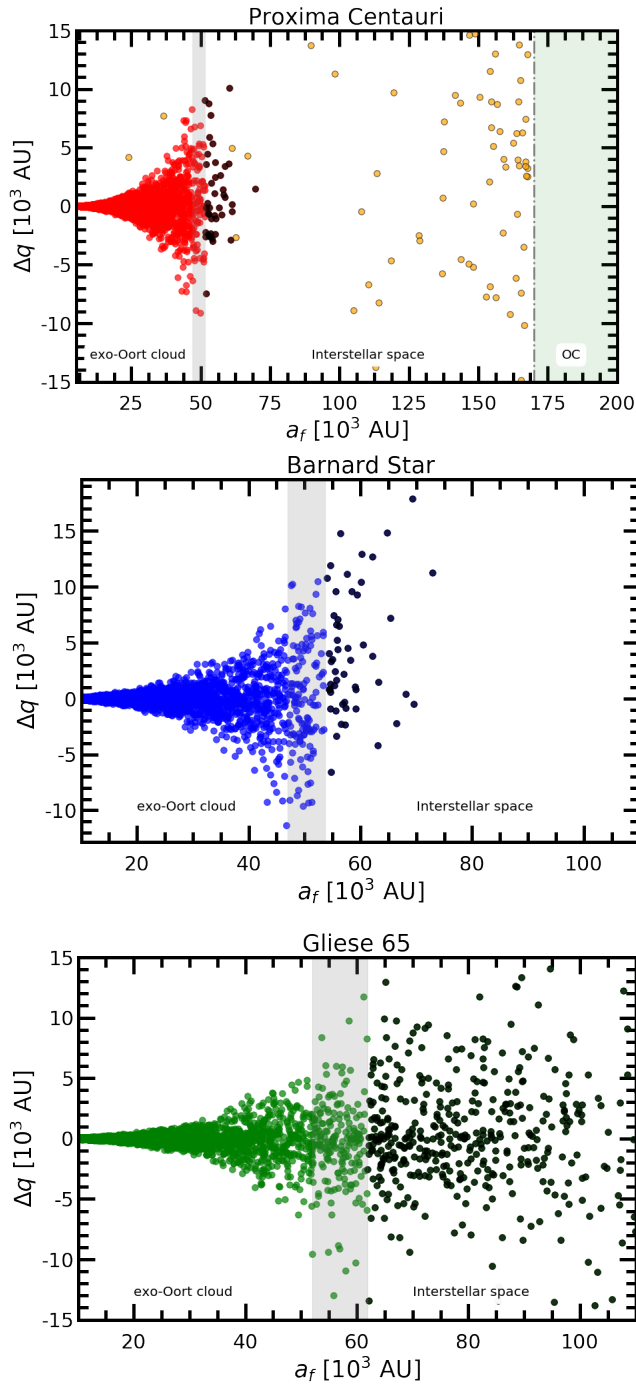


Figure 5.5: Continue...

5.3 Dynamical evolution of exo-Oort clouds of the Sun's neighbour stars

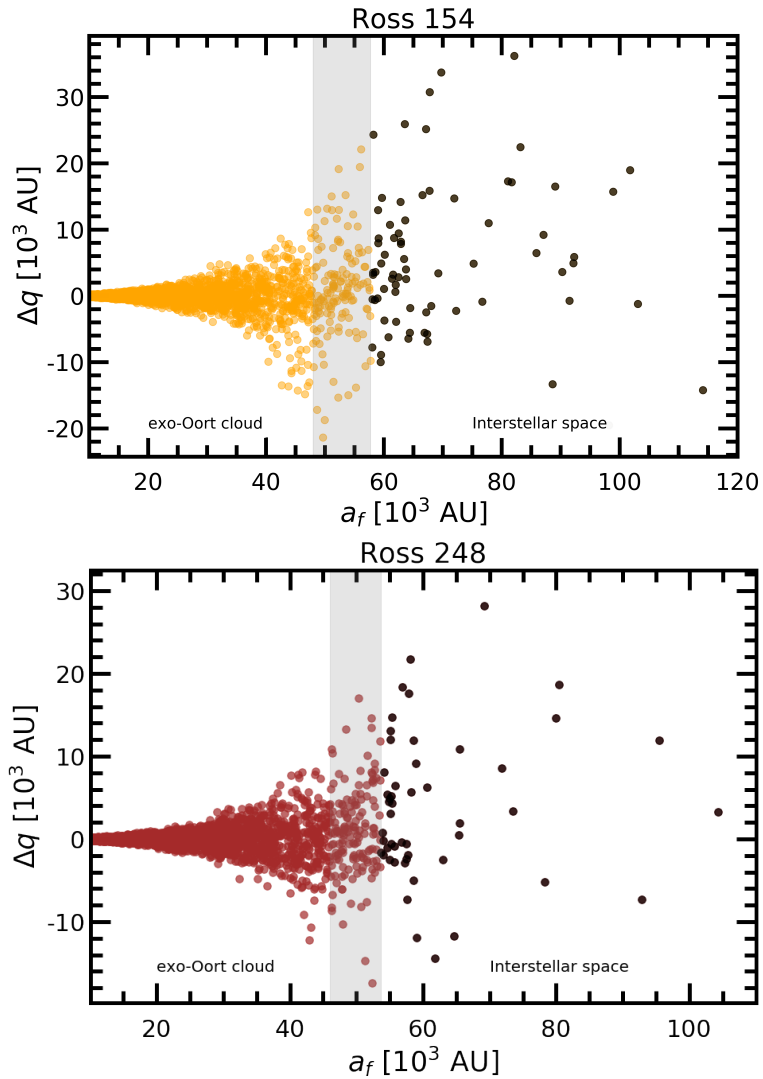


Figure 5.5: Mean periastron changes as a function of the semi-major axis of the particles in the exo-Oort clouds. The grey area corresponds to the region of the initial position of the particles ejected, represented as black dots. The first panel corresponds to Proxima Centauri (red), followed by the systems Barnard's star (blue), Gliese 65 (green), Ross 154 (yellow), and Ross 248 (brown).

5 Dynamics of *exo-Oort clouds in the solar neighbourhood*

solar system entering the Proxima Centauri system. Due to the small perturbations of the *exo-Oort cloud* of Proxima the opposite does not happen. However, our calculations are limited by the incompleteness of our catalogue of stars in the solar neighbourhood. For a complete and accurate sample of star the production of TICs will naturally increase, which also increases the chances of our solar system capturing a comet from Proxima Centauri. Note that Proxima is known to host a planet (Anglada-Escudé et al. 2016) which makes the existence of an *exo-Oort cloud* in this system plausible (see also Schwarz et al. 2018).

Barnard's star With 55 encounters, the encounter history of Barnard's star is the most eventful among the closest stars to the Sun. The cumulative effect of the passing stars and in particular the close encounter at 0.30 pc (near the edge of the *exo-Oort cloud*) raises the semi-major axis and eccentricities of about 0.52% of the total comets in the Oort cloud of Barnard's star becoming TICs. This leads to production rate of TICs during 20 Myr is $\sim 2.6 \times 10^8$ TIC Myr⁻¹. The change in the perihelion of the particles with final semi-major axes between 20 000 and 40 000 au is up to 5 000 au, and for the particles with initial semi-major axes between 47 000 and 53 000 au the change is up to almost 20 000 au (Fig. 5.5). Even though the change in the eccentricity is rather small (Fig. 5.6) future perturbations may lead to the stripping of more particles from the edge of the cloud. The close encounters found in this work are restricted to 3 Myr, a longer window will only increase the perturbations in the system. The possibility of the existence of an *exo-Oort cloud* around Barnard's star is very high if we consider that there are indications of an exoplanet (super-earth) orbiting the star (Ribas et al. 2018) and that the formation and evolution of *exo-comets* are linked to the formation and evolution of planets.

Gliese 65 Among the stars listed in Table 5.1 Gliese 65 is the most perturbed system. The change in the perihelion of the particles is around 15,000 au variation for the region with $52\,000 < a_f < 61\,870$ au. For the inner part of the system ($a_f < 30,000$ au) the change is minimal (Fig. 5.5), and the comets remain in stable orbits. The outer most part of the cloud ($50\,000 < a_f < 61\,870$ au) is heavily perturbed, mainly by the close encounter with a red dwarf with mass of ~ 0.6 at 0.23 pc, a solar-type star with mass of 1 at 0.35 pc, and the Galactic tidal field. The combined effect of the 51 encounters and the tides from the galaxy leads to the ejection

5.3 Dynamical evolution of exo-Oort clouds of the Sun's neighbour stars

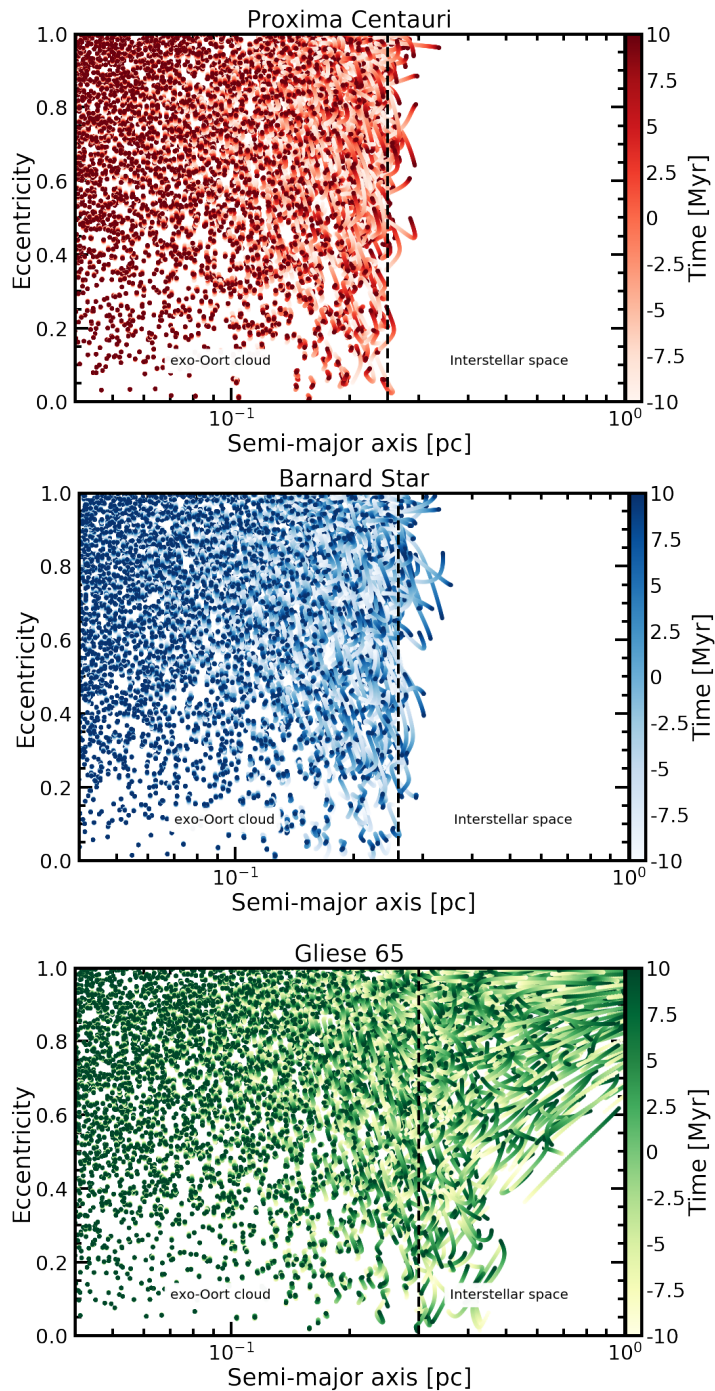


Figure 5.6: Continue...

5 Dynamics of exo-Oort clouds in the solar neighbourhood

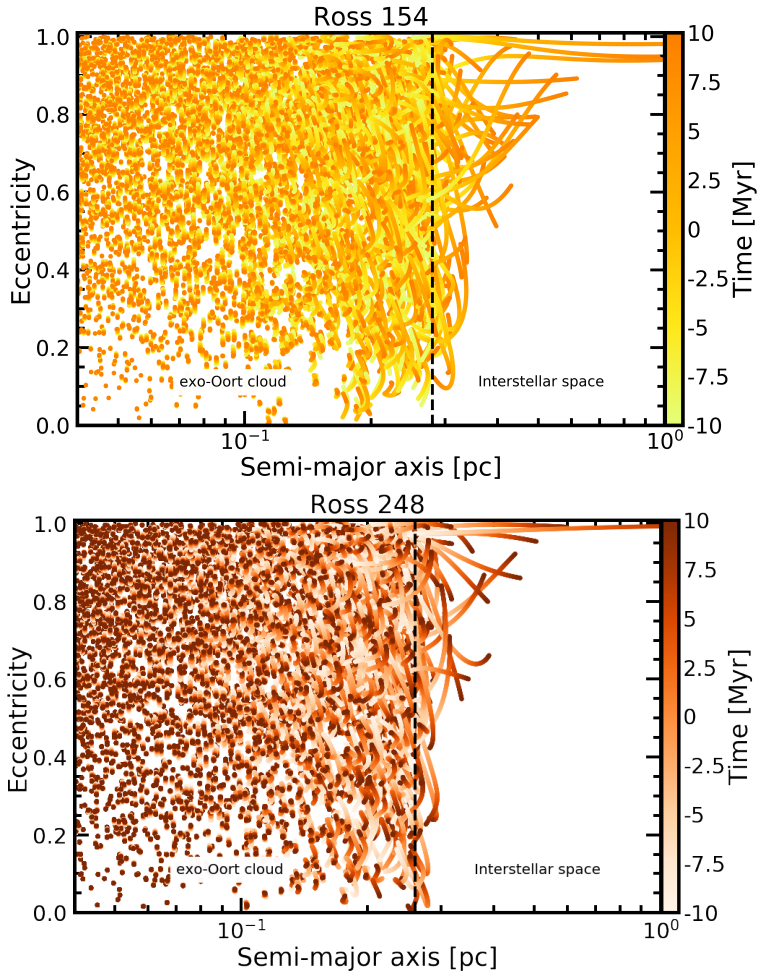


Figure 5.6: Orbital evolution of the particles in the exo-Oort cloud for a period of 20 Myr. First panel corresponds to Proxima Centauri (red), followed by the systems Barnard's star (blue), Gliese 65 (green), Ross 154 (yellow), and Ross 248 (brown).

5.3 Dynamical evolution of exo-Oort clouds of the Sun's neighbour stars

of about 28.78% of the total number of comets in the cloud. Additionally, $\sim 7.98\%$ of the remaining comets become TICs, with semi-major axis between $\sim 6.1 \times 10^4$ to $\sim 2 \times 10^6$ au. This means that TICs or ISOs from Gliese 65 might reach the solar system if we considered that Gliese 65 is 5.5×10^5 au from the Sun. The production rate of TICs and ISOs of Gliese 65 during 20 Myr are $\sim 40 \times 10^8$ TIC Myr $^{-1}$ and 1.4×10^{10} ISO Myr $^{-1}$. The analytic calculation in Sect. 5.2, showed that the effect of passing stars on the comets in the exo-Oort cloud of Gliese 65 is limited. However, when using a detailed N-body calculations and particularly accounting for the cumulative effect of passing stars and the Galactic tidal field shows that the cloud is heavily perturbed. The discrepancy of the results is a clear example of the limitations of using a simple analytic model such as the impulse approximation (Eq. (5.3)). Therefore comparing analytic models with detailed numerical simulations will lead to a more robust conclusion of the results.

Ross 154 This is the second most perturbed system among those listed in Table 5.1, with one close encounter at 0.21 pc (0.41 Myr from today, passing through the exo-Oort cloud) and 45 encounters over 20 Myr. Ross 154 also possesses the second largest exo-Oort cloud among the systems studied in this work, with its edge at 0.28 pc. Particularly the particles with final semi-major axes between 48 000 and 57 750 au are heavily perturbed, with perihelion changes up to $\sim 34 000$ au. Around 0.77% of the comets in this region become TICs, with future encounters further increasing their semi-major axis. Around 7% of the TICs reaches $\sim 400 000$ au, while the rest acquires semi-major axes between 60 000 and 120 000 au. In the inner part of the cloud ($a_f = 2000\text{--}30 000$ au), the particles remain stable with a small variation in their orbital elements (Fig. 5.5 and Fig. 5.6). The TIC production rate of Ross 154 in 20 Myr is $\sim 3.85 \times 10^8$ TIC Myr $^{-1}$. Considering that our simulations are limited to a 20 Myr time interval, if we let the system evolved for more time the production of TICs will increase (due to more stellar encounters and longer action of the Galactic tidal field) and eventually the particles with largest semi-major axis will become interstellar comets.

Ross 248 The encounter history of this system is second in terms of number of encounters, with 53 encounters in 20 Myr and one close encounter at 0.24 pc at the edge of its exo-Oort cloud. The perihelion of

5 Dynamics of exo-Oort clouds in the solar neighbourhood

the particles within $46,000 < a_f < 53,000$ au changes by up to 30,000 au (Fig. 5.5), while the eccentricities in the same region change considerably over time (Fig. 5.6). The production of TICs is comparable with to the case of Barnard's star with 0.52% of the initial comets transformed to TICs and rate of $\sim 2.6 \times 10^8$ TIC Myr⁻¹. However, the TICs from Ross 248 are considerably more perturbed primarily because of its close encounter with an M-dwarf at the edge of the cloud. Around 13% of the TICs acquired semi-major axes larger than 80,000 au, while the rest ranges from 52,000 to 80,000 au. Only 0.01% of the particles in the cloud become hyperbolic. The perturbations due to the Galactic tidal field and the stellar encounters do not change the dynamics of the inner regions of the cloud.

Overall the effect of the stellar flybys and the Galactic tidal field on the Sun's neighbours is relatively large, considering that all the stars studied are M-dwarfs and therefore their exo-Oort cloud is more compact (within 0.2 and 0.3 pc). In this way, the contribution of the Galactic tidal field is rather small and therefore the most dominant perturbation are the close encounters. The most perturbed systems in our simulations are Gliese 65, Ross 154, Ross 248 and Barnard's star primarily due to a very close encounter with a star passing through their exo-Oort cloud regions.

The total effect on these stars, is reflected in the production rate of TICs and ISOs. For Gliese 65 these rates are about 40×10^8 TIC Myr⁻¹ and 1.4×10^{10} ISO Myr⁻¹. Approximately 0.77% of the comets in the Oort cloud of Ross 154 become TICs having a production rate of 3.85×10^{10} TIC Myr⁻¹, which semi-major extends up to 400,000 au. For the systems Ross 248 and Barnard's star, the production rate of TICs is the same ($\sim 2.6 \times 10^8$ TIC Myr⁻¹), but the semi-major of the TICs goes up to 200,000 au for Ross 248 and 80,000 au for Barnard's star. Even though Barnard's star produces the same fraction of TICs as Ross 248, the perturbation of its nearby stars is least strong. This is mainly because the closest encounter with Barnard's star is a brown dwarf, which perturbation is just strong enough to perturb the comets at the edge of its exo-Oort cloud, but is not strong enough to dislodge the comets.

Finally, one of the most interesting systems in our list is the closest star to the Sun, Proxima Centauri. The encounter history of Proxima is the least eventful in our list, however due to encounters with relatively high mass stars, including the Sun, the production rate of TICs is relatively high ($\sim 2.1 \times 10^8$ TIC Myr⁻¹). We speculate that a small fraction of the TICs from our solar system ($\sim 5\%$) will enter the exo-Oort regions of Proxima.

5.3 Dynamical evolution of exo-Oort clouds of the Sun's neighbour stars

The effect of Galactic tidal field on the stars studied here is limited mainly because on average these M-dwarfs possess small exo-Oort clouds that extend only up to 0.25 pc. Therefore the most prominent perturbation that these stars will suffer is due to the passing stars. Because our list of perturbing stars is incomplete the number of stars perturbing these systems is expected to be higher (see Bailer-Jones et al. 2018). This means that the number of TICs as well as interstellar comets will be higher than estimated here.

5.3.1 TICs/ISOs in the solar neighbourhood

Studying the orbits of interstellar comets can help us to understand the dynamical evolution of the planetary system from which the ISO originated. For the nearby stars to the Sun studied in this work (Table 5.1), Gliese 65 is the most perturbed system. After 20 Myrs and two very close encounters, 7.98% of the total comets in the cloud become TICs, while 28.78% are ejected to the interstellar space. Ross 154 is the system which produces the second largest number of TICs, approximately 0.77% of the total number of comets after 20 Myr. Follow by Ross 248 and Barnard's star with 0.52%, and finally Proxima Centauri with 0.40% (Table 5.3). The dynamical evolution of TICs will be dominated by nearby stars and the Galactic tidal field. As time passes, TICs will face more stellar encounters and particularly the effect of the Galactic tidal field will affect their orbit and they will be dialogued from their host systems becoming ISOs.

For the stars studied here, TICs from *Barnard's star* possess the highest relative velocity to the Sun after 10 Myr, with an average of 32.22 km/s (Fig. 5.7). The variation, in their velocity, is small $\sim 32.2-33.2$ km/s. The second system with high relative velocity to the Sun after 10 Myr, is *Gliese 65*, with an average velocity of 24.14 km/s, and with velocities ranging from approximately 24.13-24.14 km/s. The third and last system with high relative velocity is *Ross 248* with an average velocity of 20.63 km/s and a variation going from 20.62-20.64 km/s. The systems *Proxima Centauri* and *Ross 154* have small velocities with respect to the Sun after 10 Myr, ranging from 7.32-7.72 km/s and 3.930-3.942 km/s respectively. The small variation of the TICs relative velocity is expected because the TICs are leaving the system gradually and their velocity is thus dominated by the velocity of the host star.

The small change in velocity is enough to allow the comets to leave the Hill sphere of the host stars and is mainly induced by the cumulative

5 Dynamics of exo-Oort clouds in the solar neighbourhood

Table 5.3: Production of TICs and ISOs from the nearby stars to the Sun. The first column shows the name of the star, followed by the percentage of the total comets in the exo-Oort clouds that becomes TIC or ISO. The last column represents the average of the total relative velocity of the TICs respects to the Sun for each star after 10 Myr of orbital integration.

Star	TIC (%)	ISO (%)	$\langle v_{rel} \rangle$ (km s ⁻¹)
Proxima Centauri	0.40	0	7.22
Barnard's star	0.52	0	32.22
Gliese 65	7.98	28.78	24.14
Ross 154	0.52	0	3.93
Ross 248	0.77	0.01	20.63

effect of the close encounters that each system faced over the 20 Myr of integration. If we compare the relative velocity of the TICs in Table 5.3 with 1I/'Oumuamua (~ 26.3 km/s, Meech et al. 2017) and 2I/Borisov (32.2 km/s, Borisov 2019; Guzik et al. 2019) their velocities match with the TICs from *Gliese 65* and *Barnard's star* respectively. This does not imply that 1I/'Oumuamua and 2I/Borisov came from those stars. However, if we considered that ISOs have small velocity when leaving their systems (Torres et al. 2019b; Hands et al. 2019). The relative velocity of planetary systems can be used to constrain the velocity of the ejected object. For the future detections of ISOs, matching the relative velocity with those stars in the solar neighbourhood and performing backward orbital integration (e.g., Portegies Zwart et al. 2018) will serve as constrain of their possible origin.

Section 5.4

Summary and Conclusions

Following the results and methods of Torres et al. (2019a), in this paper, we explored the dynamical evolution of exo-Oort clouds around the nearest stars to the Sun. We selected the stars within 3 pc from the Sun, which we assumed to possess an Oort cloud-like structure and with accurate astrometric data from Gaia DR2. The selected systems are: Proxima Centauri, Barnard's star, Gliese 65, Ross 154, and Ross 248. In Sect. 5.2, we calculated the number of stellar encounters that each of the systems faced in

5.4 Summary and Conclusions

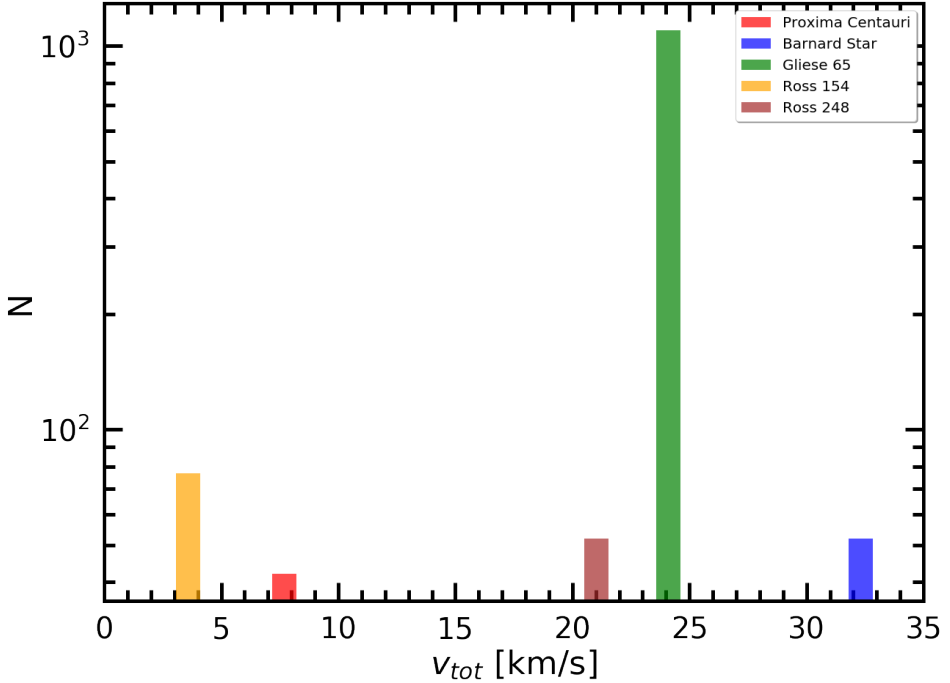


Figure 5.7: Histogram of the relative velocity of the TICs from the stars in Table 5.1 respect to the Sun. Colour bars corresponds to the systems Proxima Centauri (red), followed by the systems Barnard’s star (blue), Gliese 65 (green), Ross 154 (yellow), and Ross 248 (brown).

the past 10 Myr and would encounter in the next 10 Myr. We find that on average, these systems experience around 40-55 encounters in 20 Myr.

Using the impulse approximation (Eq. (5.3)), we calculated the change of the velocity induced by a passing star to a comet in an exo-Oort cloud. We find that the most perturbed systems due to a close encounters are Gliese 65, Ross 154, Ross 248, and Barnard’s star. Their final velocities are below the escape velocity at the edge of their exo-Oort cloud (Table 5.2). For Proxima Centauri the effect of the passing stars do not represent an essential change in the velocity of their comets.

To have a complete study of the effect of passing stars on the Sun’s neighbour stars, in Sect. 5.3 we studied the dynamical evolution of the comets in an exo-Oort cloud. We included the cumulative effect of passing stars within 2.5 pc from each system and the Galactic tidal field. Using the encounter history of the nearby stars to the Sun (Table 5.2), we inte-

5 Dynamics of exo-Oort clouds in the solar neighbourhood

grated the orbits of the comets for 20 Myr (10 Myr in the past, 10 Myr in the future). For the five stars studied in this work (Table 5.1), Gliese 65, is the most perturbed system. Gliese 65 is a binary system of which Oort Cloud extends up to 0.3 pc. It faces 51 encounters in 20 Myr, having two very close encounters at a distance of 0.23 and 0.35 pc. The combined effect of all close encounters (primarily the two closest) and the tides from the Galaxy, leads to a production rate of TICs and ISOs of about 40×10^8 TIC Myr⁻¹ and 1.4×10^{10} ISO Myr⁻¹ over a time interval of 20 Myr. The semi-major axis of the TICs from Gliese 65 ranges from $\sim 6.1 \times 10^4$ to $\sim 2 \times 10^6$ au. This implies that TICs or ISOs from Gliese 65 might reach the solar system's Oort cloud whose is located $\sim 5.5 \times 10^5$ au away.

Ross 154, faced a close encounter with a G-star at 0.21 pc (at the edge of its exo-Oort cloud) and 45 encounters within 2.5 pc. These encounters and the effects from the tides of the Galaxy form approximately 3.8×10^8 TIC Myr⁻¹. The follow most perturbed system are Ross 248, Barnard's star, and Proxima Centauri. The systems Barnard's star and Ross 248 faced similar encounter histories (55, and 53 encounters), which perturbations lead to the formation of $\sim 2.6 \times 10^8$ TIC Myr⁻¹ for both cases over 20 Myr. Nevertheless, the perturbation is larger in Ross 248, due to a close encounter at 0.24 pc (inside of its exo-Oort cloud). This is reflected in the larger semi-major axis of the TICs compared to the ones in Barnard's star (Fig. 5.6). Finally, Proxima Centauri faces 40 encounters during 20 Myr, which together with the tides from the Galaxy leads production rate of $\sim 2.1 \times 10^8$ TIC Myr⁻¹. Due to its proximity to the Sun, the exo-Oort cloud of Proxima Centauri overlaps with $\sim 5\%$ of the TICs originating from the solar system (Fig. 12 in Torres et al. 2019a). Therefore we may speculate that objects coming from the solar system enter Proxima Centauri. Due to the small perturbations of the exo-Oort cloud of Proxima, the opposite does not happen in our calculations.

Overall, the effect of passing stars dominates over the tides from the Galaxy. The impact of the Galactic tidal field is too weak on the short time scale studied here, to affect the orbital elements of the comets in the exo-Oort cloud. Because of the small size of the exo-Oort cloud (approximately half of the Oort cloud of the Sun), and the position of the stars in the Galactic plane. However, it is the combined effect of the Galactic tidal field and stellar encounters which shaped the edge of the exo-Oort clouds studied in this work. It is important to stress that estimates presented in this work are conservative and based on a small sample of known stars. The production rates of TIC scale with the total number of comets in the Oort cloud

5.4 Summary and Conclusions

for all the systems presented in this work is approximately of order 10^8 TIC Myr⁻¹ over a time interval of 20 Myr. A complete sample of nearby stars will naturally increase the number of TICs and ISOs in the local solar neighbourhood. This implies that the nearby systems with an exo-Oort cloud including the solar system might get constantly polluted by interstellar comets. Therefore an interstellar cloud of comets is very plausible.

Acknowledgements ST expresses his gratitude to the Mexican National Council for Science and Technology (CONACYT) for the grant #291004-410 780; to Leiden Observatory for the unconditional support; and to Maxwell Cai and Ylva Götberg, for the discussions and comments on the manuscript. This work has made use of data from the European Space Agency (ESA) mission Gaia (<https://www.cosmos.esa.int/gaia>), processed by the Gaia Data Processing and Analysis Consortium (DPAC, <https://www.cosmos.esa.int/web/gaia/dpac/consortium>). Funding for the DPAC has been provided by national institutions, in particular the institutions participating in the Gaia Multilateral Agreement. This work was carried out on the Dutch national e-infrastructure with the use of *Cartesius* the Dutch national supercomputer and the support of SURF Cooperative.

Bibliography

- Abolfathi, B., Aguado, D. S., Aguilar, G., et al. 2018, *Astrophys. J. Suppl. Ser.*, 235, 42
- Adams, F. C. 2010, *Annu. Rev. Astron. Astrophys.*, 48, 47
- Altwegg, K., Balsiger, H., Bar-Nun, A., et al. 2016, *Sci. Adv.*, 2, e1600285
- Alves, J., Bertout, C., Forveille, T., Guillot, T., & Shore, S. 2015, *Astron. Astrophys.*, 583, 6361
- Anderson, E. & Francis, C. 2012, *Astron. Lett.*, 38, 331
- Andrae, R., Fouesneau, M., Creevey, O., et al. 2018, *Astron. Astrophys.*, 616, A8
- Anglada-Escudé, G., Amado, P. J., Barnes, J., et al. 2016, *Nature*, 536, 437
- Antoja, T., Helmi, A., Dehnen, W., et al. 2014, *Astron. Astrophys.*, 563, A60
- Bacci, P., Maestripieri, M., Tesi, L., et al. 2017, *Minor Planet Electronic Circulars*, 2017-U181
- Bailer-Jones, C. A. L. 2015, *Astron. Astrophys.*, 575, A35
- Bailer-Jones, C. A. L. 2018, *Astron. Astrophys.*, 609, A8
- Bailer-Jones, C. A. L., Rybizki, J., Andrae, R., & Fouesneau, M. 2018, *Astron. Astrophys.*, 616, A37
- Bailey, N. & Fabrycky, D. 2019, *Astron. J.*, 158, 94
- Bannister, M. T., Bhandare, A., Dybczyński, P. A., et al. 2019, *Nat. Astron.*, 3, 594
- Bannister, M. T., Schwamb, M. E., Fraser, W. C., et al. 2017, *ApJ*, 851, L38
- Baxter, E. J., Blake, C. H., & Jain, B. 2018, *Astron. J.*, 156, 243
- Bédorf, J., Gaburov, E., Fujii, M. S., et al. 2014, in *Proceedings of the International Conference for High Performance Computing*, 54–65
- Bédorf, J., Gaburov, E., & Portegies Zwart, S. 2012, *Journal of Computational Physics*, 231, 2825
- Berski, F. & Dybczyński, P. A. 2016, *Astron. Astrophys.*, 15, 4
- Binney, J. & Tremaine, S. 2008, *Galactic Dynamics: Second Edition* (Princeton University Press)
- Bobylev, V. V. & Bajkova, A. T. 2017, *Astron. Lett.*, 43, 559
- Boersma, J. 1961, *Bull. Astron. Inst. Netherlands*, 15, 291
- Bolin, B. T., Weaver, H. A., Fernandez, Y. R., et al. 2018, *ApJ*, 852, L2
- Borisov, G. 2019, *MPEC*, R106
- Bovy, J. 2015, *Astron. J.*, 29
- Bovy, J. 2017, *Mon. Not. R. Astron. Soc.*, 1387, 1360
- Boyajian, T. S., LaCourse, D. M., Rappaport, S. A., et al. 2016, *Mon. Not. R. Astron. Soc.*, 457, 3988

Bibliography

- Brasser, R., Duncan, M. J., & Levison, H. F. 2006, *Icarus*, 184, 59
- Brasser, R., Duncan, M. J., Levison, H. F., Schwamb, M. E., & Brown, M. E. 2012, *Icarus*, 217, 1
- Brasser, R. & Morbidelli, A. 2013, *Icarus*, 225, 40
- Brown, M. E. 2005, *IAU Circ.*, 8636, 1
- Brown, M. E. & Butler, B. J. 2017, *AJ*, 154, 19
- Buder, S., Asplund, M., Duong, L., et al. 2018, *Mon. Not. R. Astron. Soc.*, 478, 4513
- Burgasser, A. J., Logsdon, S. E., Gagné, J., et al. 2015, *ApJS*, 220, 18
- Cai, M. X., Kouwenhoven, M. B., Portegies Zwart, S., & Spurzem, R. 2017, *Mon. Not. R. Astron. Soc.*, 470, 4337
- Cai, M. X., Meiron, Y., Kouwenhoven, M. B., Assmann, P., & Spurzem, R. 2015, *Astrophys. Journal, Suppl. Ser.*, 219
- Cai, M. X., Portegies Zwart, S., & van Elteren, A. 2018, *Mon. Not. R. Astron. Soc.*, 474, 5114
- Caiazzom, I. & Heyl, J. S. 2017, *Mon. Not. R. Astron. Soc.*, 469, 2750
- Capaccioni, F., Coradini, A., Filacchione, G., et al. 2015, *Science (80-.)*, 347
- Chabrier, G. 2003, *PASP*, 115, 763
- Chebotarev, G. A. 1965, *Sov. Astron. AJ*, 8, 787
- Čuk, M. 2018, *ApJ*, 852, L15
- Davison, C. L., White, R. J., Henry, T. J., et al. 2015, *Astron. J.*, 149, 106
- de la Fuente Marcos, C. & de la Fuente Marcos, R. 2017, *Research Notes of the American Astronomical Society*, 1, 5
- de la Fuente Marcos, C. & de la Fuente Marcos, R. 2019, *Mon. Not. R. Astron. Soc.*, 489, 951
- de la Fuente Marcos, C., de la Fuente Marcos, R., & Aarseth, S. J. 2017, *Ap&SS*, 362, 198
- de la Fuente Marcos, C., de la Fuente Marcos, R., & Aarseth, S. J. 2018, *Mon. Not. R. Astron. Soc.*, 476, L1
- de la Fuente Marcos, R. & de la Fuente Marcos, C. 2018, *Res. Notes AAS*, 2, 30
- Dehnen, W. & Binney, J. J. 1998, *Mon. Not. R. Astron. Soc.*, 298, 387
- Delfosse, X., Forveille, T., Ségransan, D., et al. 2000, *Astron. Astrophys.*, 364, 217
- Do, A., Tucker, M. A., & Tonry, J. 2018, *Astrophys. J.*, 855, L10
- Domokos, G., Sipos, A. Á., Szabó, G. M., & Várkonyi, P. L. 2017, *Research Notes of the American Astronomical Society*, 1, 50
- Dones, L., Brasser, R., Kaib, N., & Rickman, H. 2015, *Space Sci. Rev.*, 197, 191
- Dones, L., Weissman, P. R., Levison, H. F., & Duncan, M. J. 2004, *Comets II*, 323, 153
- Duncan, M., Quinn, T., & Tremaine, S. 1987, *Astron. J.*, 94, 1330
- Duncan, M. J. 2008, *Space Sci. Rev.*, 109
- Dybczyński, P. A. 2002, *Earth, Moon Planets*, 90, 483
- Dybczyński, P. A. & Berski, F. 2015, *Mon. Not. R. Astron. Soc.*, 2471, 13
- Dybczyński, P. A. & Królikowska, M. 2018, *A&A*, 610, L11

Bibliography

- Eistrup, C., Walsh, C., & van Dishoeck, E. 2019, *Astron. Astrophys.*, 84, 1
- Engelhardt, T., Jedicke, R., Vereš, P., et al. 2017, *AJ*, 153, 133
- Everhart, E. 1985, *Dyn. Comets Their Orig. Evol. Proc. IAU Colloq.* 83, 115
- Feng, F. & Bailer-Jones, C. A. 2015, *Mon. Not. R. Astron. Soc.*, 454, 3267
- Feng, F. & Jones, H. R. A. 2018, *ApJ*, 852, L27
- Fernández, J. A. & Brunini, A. 2000, *Icarus*, 145, 580
- Fernández, J. A. & Ip, W. H. 1984, *Icarus*, 58, 109
- Ferrin, I. & Zuluaga, J. 2017, *arXiv e-prints*, 4
- Fitzsimmons, A., Snodgrass, C., Rozitis, B., et al. 2018, *Nature Astronomy*, 2, 133
- Fouchard, M., Froeschlé, C., Valsecchi, G., & Rickman, H. 2006, *Celest. Mech. Dyn. Astron.*, 95, 299
- Fouchard, M., Higuchi, A., Ito, T., & Maquet, L. 2018, *Astron. Astrophys.*, 45, 1
- Fouchard, M., Rickman, H., Froeschle, C., & Valsecchi, G. B. 2011, *Astron. Astrophys.*, 535, 86
- Fouchard, M., Rickman, H., Froeschlé, C., & Valsecchi, G. B. 2014, *Icarus*, 231, 99
- Francis, P. J. 2005, *Astrophys. J.*, 635, 1348
- Fraser, W. C., Bannister, M. T., Pike, R. E., et al. 2017, *Nature Astronomy*, 1, 0088
- Fujii, M. S., Bédorf, J., Baba, J., & Portegies Zwart, S. 2018, *Mon. Not. R. Astron. Soc.*, 477, 1451
- Gaia Collaboration, Brown, A. G. A., Vallenari, A., et al. 2018, *Astron. Astrophys.*, 616, A1
- Gaia Collaboration, P., de Bruijne, J. H. J., Brown, A. G. A., et al. 2016, *Astron. Astrophys.*, 595, A1
- Gaia Collaboration, Brown, Vallenari, A., Prusti, T., et al. 2016, *Astron. Astrophys.*, 595, A2
- Gaidos, E., Williams, J., & Kraus, A. 2017, *Research Notes of the American Astronomical Society*, 1, 13
- García-Sánchez, J., Preston, R. A., Jones, D. L., et al. 1999, *Astron. J.*, 117, 1042
- García-Sánchez, J., Weissman, P. R., Preston, R. A., et al. 2001, *Astron. Astrophys.*, 379, 634
- Glassmeier, K.-H., Boehnhardt, H., Koschny, D., Kührt, E., & Richter, I. 2007, *Space Sci. Rev.*, 128, 1
- Gomes, R., Levison, H. F., Tsiganis, K., & Morbidelli, A. 2005, *Nature*, 435, 466
- Gontcharov, G. A. 2006, *Astron. Lett.*, 32, 759
- Guzik, P., Drahus, M., Rusek, K., et al. 2019, *Nat. Astron.* [[arXiv]1909.05851]
- Hamers, A. S. & Portegies Zwart, S. F. 2015, *Mon. Not. R. Astron. Soc.*, 446, 710
- Hands, T. O., Dehnen, W., Gration, A., Stadel, J., & Moore, B. 2019, *Mon. Not. R. Astron. Soc.*
- Hanse, J., Jílková, L., Portegies Zwart, S. F., & Pelupessy, F. I. 2016, *Mon. Not. R. Astron. Soc.*, 473, 5432
- Hansen, B. & Zuckerman, B. 2017, *Research Notes of the American Astronomical Society*, 1, 55

Bibliography

- Heisler, J. & Tremaine, S. 1986, *Icarus*, 65, 13
- Hernquist, L. 1990, *Astron. J.*, 359
- Higuchi, A. & Kokubo, E. 2015, *Astron. J.*, 150, 26
- Higuchi, A. & Kokubo, E. 2019, *Mon. Not. R. Astron. Soc.*, 275, 268
- Hills, J. G. 1981, *Astron. J.*
- Hills, J. G. 1988, *Nature*, 331, 687
- Hoang, T., Loeb, A., Lazarian, A., & Cho, J. 2018, *ApJ*, 860, 42
- Holmberg, J., Nordström, B., & Andersen, J. 2009, *A&A*, 501, 941
- Horneck, G., Klaus, D. M., & Mancinelli, R. L. 2010, *Microbiol. Mol. Biol. Rev.*, 74, 121
- Hughes, A. M., Duchêne, G., & Matthews, B. C. 2018, *Annu. Rev. Astron. Astrophys.*, 56, 541
- Jackson, A. P., Tamayo, D., Hammond, N., Ali-Dib, M., & Rein, H. 2018, *Mon. Not. R. Astron. Soc.*, 478, L49
- Jänes, J., Pelupessy, I., & Portegies Zwart, S. 2014, *A&A*, 570, A20
- Jenkins, J. S., Ramsey, L. W., Jones, H. R. A., et al. 2009, *Astrophys. J.*, 704, 975
- Jewitt, D. 2018, *AJ*, 155, 56
- Jewitt, D. & Luu, J. 2019, *Astrophys. J.*, 886, L29
- Jewitt, D., Luu, J., Rajagopal, J., et al. 2017, *Astrophys. J.*, 850, L36
- Jílková, L., Hamers, A. S., Hammer, M., & Portegies Zwart, S. 2016, *Mon. Not. R. Astron. Soc.*, 457, 4218
- Jílková, L., Portegies Zwart, S., Pijloo, T., & Hammer, M. 2015, *Mon. Not. R. Astron. Soc.*, 453, 3158
- Jiménez-Esteban, F. M., Torres, S., Rebassa-Mansergas, A., et al. 2018, *Mon. Not. R. Astron. Soc.*, 4518, 4505
- Jimenez-Torres, J. J., Pichardo, B., Lake, G., & Throop, H. 2011, *Mon. Not. R. Astron. Soc.*, 418, 1272
- Kaib, N. A. & Quinn, T. 2008, *Icarus*, 197, 221
- Kaib, N. A. & Quinn, T. 2009, *Science*, 325, 1234
- Katz, J. I. 2018, *Mon. Not. R. Astron. Soc.*, 478, L95
- Kiefer, F., des Etangs, A. L., Boissier, J., et al. 2014, *Nature*, 514, 462
- Kipper, R., Tempel, E., & Tenjes, P. 2018, *Mon. Not. R. Astron. Soc.*, 473, 2188
- Kirkpatrick, J. D., Gelino, C. R., Cushing, M. C., et al. 2012, *ApJ*, 753, 156
- Knight, M. M., Protopapa, S., Kelley, M. S. P., et al. 2017, *ApJ*, 851, L31
- Królikowska, M. & Dybczyński, P. A. 2019, *Mon. Not. R. Astron. Soc.*, 484, 3463
- Kroupa, P. 2001, *Mon. Not. R. Astron. Soc.*, 322, 231
- Kuiper, G. P. 1951, *Proceedings of the National Academy of Science*, 37, 1
- Kunder, A., Kordopatis, G., Steinmetz, M., et al. 2017, *Astron. J.*, 153, 75
- Lada, C. J. & Lada, E. A. 2003, *Annu. Rev. Astron. Astrophys.*, 41, 57
- Levison, H. F., Duncan, M. J., Brasser, R., & Kaufmann, D. E. 2010, *Science*, 329, 187

Bibliography

- Levison, H. F., Morbidelli, A., & Dones, L. 2004, *Astron. J.*, 128, 2553
- Lindgren, L., Hernández, J., Bombrun, A., et al. 2018, *Astron. Astrophys.*, 616, A2
- Malhotra, R. 1993, *Nature*, 365, 819
- Mamajek, E. 2017, *Research Notes of the American Astronomical Society*, 1, 21
- Mamajek, E. 2018, *Priv. Commun.*
- Mamajek, E. E., Barenfeld, S. A., Ivanov, V. D., et al. 2015, *Astrophys. J.*, 800, L17
- Mann, A. W., Feiden, G. A., Gaidos, E., Boyajian, T., & Braun, K. V. 2015, *Astrophys. J.*, 804, 64
- Martínez-Barbosa, C. A., Brown, A. G. A., Boekholt, T., et al. 2016, *Mon. Not. R. Astron. Soc.*, 457, 1062
- Martínez-Barbosa, C. A., Brown, A. G. A., & Portegies Zwart, S. 2015, *Mon. Not. R. Astron. Soc.*, 446, 823
- Martínez-Barbosa, C. A., Jílková, L., Portegies Zwart, S., & Brown, A. G. 2017, *Mon. Not. R. Astron. Soc.*, 464, 2290
- Masiero, J. 2017, *arXiv e-prints*, 5
- McGlynn, T. A. & Chapman, R. D. 1989, *ApJ*, 346, L105
- McKay, A. J., Cochran, A. L., Russo, N. D., & DiSanti, M. 2019, 1
- Meech, K., Bacci, P., Mastrapieri, M., et al. 2017a, *Minor Planet Electronic Circulars*, 2017-U183
- Meech, K. J. 2018, *Nature Astronomy*, 2, 112
- Meech, K. J., Kleyna, J., Wells, L., et al. 2017b, *Minor Planet Electronic Circulars*, 2017-W52
- Meech, K. J., Weryk, R., Micheli, M., et al. 2017, *Nature*, 552, 378
- Michalik, D., Lindgren, L., & Hobbs, D. 2015, *Astron. Astrophys.*, 574
- Miyamoto, M. & Nagai, R. 1975, *Astron. Soc. Japan*, 27, 533
- Morbidelli, A. 2005, *eprint arXiv:0512256*, 86
- Morbidelli, A., Levison, H. F., Tsiganis, K., & Gomes, R. 2005, *Nature*, 435, 462
- Morbidelli, A. & Nesvorný, D. 2019, *eprint arXiv:1904.02980*, 67
- Morbidelli, A., Tsiganis, K., Crida, A., Levison, H. F., & Gomes, R. 2007, *Astron. J.*, 134, 1790
- Moro-Martín, A. 2019, *Astron. J.*, 157, 86
- Moro-Martín, A., Turner, E. L., & Loeb, A. 2009, *ApJ*, 704, 733
- Napiwotzki, R. 2009, in *Journal of Physics Conference Series*, Vol. 172, *Journal of Physics Conference Series*, 012004
- Navarro, J. F., Frenk, C. S., & White, S. D. M. 1996, *Astron. J.*, 462, 563
- Nesvorný, D. 2018, *Annu. Rev. Astron. Astrophys.*, 56, 137
- Nesvorný, D. & Morbidelli, A. 2012, *Astron. J.*, 144, 117
- Nesvorný, D., Vokrouhlický, D., Dones, L., et al. 2017, *Astrophys. J.*, 845, 27
- Noll, K. S., Grundy, W. M., Chiang, E. I., Margot, J. L., & Kern, S. D. 2008, *Binaries in the Kuiper Belt*, ed. M. A. Barucci, H. Boehnhardt, D. P. Cruikshank, A. Morbidelli, & R. Dotson, 345

Bibliography

- Nordlander, T., Rickman, H., & Gustafsson, B. 2017, *Astron. Astrophys.*, 603, A112
- Nordström, B., Mayor, M., Andersen, J., et al. 2004, *Astron. Astrophys.*, 418, 989
- Oort, J. H. 1950, *Commun. from Obs. Leiden*, 408
- Pawellek, N., Krivov, A. V., Marshall, J. P., et al. 2014, *Astrophys. J.*, 792, 65
- Pecaut, M. J. & Mamajek, E. 2013, *Astrophys. Journal, Suppl. Ser.*, 208
- Pelupessy, F. I., van Elteren, A., de Vries, N., et al. 2013, *Astron. Astrophys.*, 557, A84
- Perryman, M. 2003, *Astronomical Society of the Pacific Conference Series*, Vol. 298, *The GAIA mission*, ed. U. Munari, 3
- Perryman, M. A. C., Lindegren, L., Kovalevsky, J., et al. 1997, *Astron. Astrophys.*, 323, L49
- Pfalzner, S., Bhandare, A., Vincke, K., & Lacerda, P. 2018, *Astrophys. J.*, 863, 45
- Pfalzner, S., Davies, M. B., Gounelle, M., et al. 2015, *Phys. Scr.*, 90 [[arXiv]1501.03101]
- Pichardo, B., Moreno, E., Allen, C., et al. 2012, *Astron. J.*, 143, 73
- Plummer, H. C. 1911, *Mon. Not. R. Astron. Soc.*, 71, 460
- Portegies Zwart, S. & McMillan, S. 2018, *Astrophysical Recipes: The art of AMUSE* (IOP Publishing)
- Portegies Zwart, S., McMillan, S., Harfst, S., et al. 2009, *New Astron.*, 14, 369
- Portegies Zwart, S., McMillan, S. L. W., van Elteren, E., Pelupessy, I., & de Vries, N. 2013a, *Computer Physics Communications*, 184, 456
- Portegies Zwart, S., Torres, S., Pelupessy, I., Bédorf, J., & Cai, M. X. 2018, *Mon. Not. R. Astron. Soc. Lett.*, 479, L17
- Portegies Zwart, S. F. 2009, *Astrophys. J.*, 696, 2007
- Portegies Zwart, S. F. & Jílková, L. 2015, *Mon. Not. R. Astron. Soc.*, 451, 144
- Portegies Zwart, S. F., McMillan, S. L., van Elteren, A., Pelupessy, F. I., & de Vries, N. 2013b, *Comput. Phys. Commun.*, 184, 456
- Potemine, I. Y. 2010, e-prints arXiv:1004.1557, 3
- Price-Whelan, A. M. 2017, *J. Open Source Softw.*, 2, 388
- Punzo, D., Capuzzo-Dolcetta, R., & Portegies Zwart, S. 2014, *Mon. Not. R. Astron. Soc.*, 444, 2808
- Rafikov, R. R. 2018, *ApJ*, 861, 35
- Raymond, S. N., Armitage, P. J., & Gorelick, N. 2010, *Astrophys. J.*, 711, 772
- Raymond, S. N., Armitage, P. J., & Veras, D. 2018a, *ApJ*, 856, L7
- Raymond, S. N., Armitage, P. J., Veras, D., Quintana, E. V., & Barclay, T. 2018b, *Mon. Not. R. Astron. Soc.*, 476, 3031
- Reid, M. J., Menten, K. M., Brunthaler, A., et al. 2014, *Astrophys. J.*, 783 [[arXiv]1401.5377]
- Rein, H. & Liu, S.-F. 2012, *Astron. Astrophys.*, 537, A128
- Rein, H. & Spiegel, D. S. 2014, *Mon. Not. R. Astron. Soc.*, 446, 1424
- Rettberg, P., Rabbow, E., Panitz, C., Reitz, G., & Horneck, G. 2002, *ESA SP*, 518 [[arXiv]2002ESASP.518..105R]

Bibliography

- Ribas, I., Tuomi, M., Reiners, A., et al. 2018, *Nature*, 563, 365
- Rickman, H. 1976, *Bull. Astron. Institutes Czechoslov.*, 27, 92
- Rickman, H. 2014, *Meteoritics Planetary Science*, 49, 8
- Rickman, H., Fouchard, M., Froeschlé, C., & Valsecchi, G. B. 2008, *Celest. Mech. Dyn. Astron.*, 102, 111
- Rickman, H., Froeschlé, C., Froeschlé, C., & Valsecchi, G. B. 2004, *Astron. Astrophys.*, 428, 673
- Robert A. J. Matthews. 1994, *Q. J. R. astr. Soc.*, 35, I
- Schlichting, H. E., Fuentes, C. I., & Trilling, D. E. 2013, *AJ*, 146, 36
- Schmidt, S. J., West, A. A., Hawley, S. L., & Pineda, J. S. 2010, *AJ*, 139, 1808
- Scholz, R.-D. 2014, *Astron. Astrophys.*, 561, A113
- Schönrich, R., Binney, J., & Dehnen, W. 2010, *Mon. Not. R. Astron. Soc.*, 403, 1829
- Schwamb, M. E. 2014, *Nature*, 507, 435
- Schwarz, R., Bazsó, Georgakarakos, N., et al. 2018, *Mon. Not. R. Astron. Soc.*, 480, 3595
- Shannon, A., Jackson, A. P., Veras, D., & Wyatt, M. 2014, *Mon. Not. R. Astron. Soc.*, 446, 2059
- Shannon, A., Jackson, A. P., & Wyatt, M. C. 2019, *Mon. Not. R. Astron. Soc.*, 485, 5511
- Shepard, M. K., Richardson, J., Taylor, P. A., et al. 2017, *Icarus*, 281, 388
- Sheppard, S. S. & Jewitt, D. 2004, *AJ*, 127, 3023
- Soubiran, C., Jasniewicz, G., Chemin, L., et al. 2018, *A&A*, 616, A7
- Stark, C. C., Kuchner, M. J., Traub, W. A., et al. 2009, *Astrophys. J.*, 703, 1188
- Stern, S. A. 1990, *PASP*, 102, 793
- The Astropy Collaboration, Price-Whelan, A. M., Sipőcz, B. M., et al. 2018, *Astron. J.*, 156, 123
- Thommes, E. W., Duncan, M. J., & Levison, H. F. 1999, *Nature*, 402, 635
- Torres, S., Cai, M. X., Brown, A. G. A., & Portegies Zwart, S. 2019a, *Astron. Astrophys.*, 629, 13
- Torres, S., Cai, M. X., Mukherjee, D., Portegies Zwart, S., & Brown, A. G. A. 2019b, *Astron. Astrophys.*, submitted, 17
- Torres, S., Portegies Zwart, S., & Brown, A. G. A. 2018, *Proc. Int. Astron. Union*, 12, 269
- Torres, S., Zwart, S. P., & Brown, A. G. A. 2020, *Astron. Astrophys.*, Submitted, 10
- Trilling, D. E., Robinson, T., Roegge, A., et al. 2017, *ApJ*, 850, L38
- Tsiganis, K., Gomes, R., Morbidelli, A., & Levison, H. F. 2005, *Nature*, 435, 459
- Valtonen, M. J. & Innanen, K. A. 1982, *Astron. J.*, 307
- Veras, D., Evans, N. W., Wyatt, M. C., & Tout, C. A. 2013, *Mon. Not. R. Astron. Soc.*, 437, 1127
- Veras, D., Shannon, A., & Gänsicke, B. T. 2014, *Mon. Not. R. Astron. Soc.*, 445, 4175

Bibliography

- Veras, D., Wyatt, M. C., Mustill, A. J., Bonsor, A., & Eldridge, J. J. 2011, *Mon. Not. R. Astron. Soc.*, 417, 2104
- Vicente, S. M. & Alves, J. 2005, *Astron. Astrophys.*, 441, 195
- Vokrouhlický, D., Nesvorný, D., & Dones, L. 2019, *Astron. J.*, 157, 181
- Wang, L., Spurzem, R., Aarseth, S., et al. 2015, *Mon. Not. R. Astron. Soc.*, 450, 4070
- Weissman, P. R. 1996, *Earth, Moon Planets*, 72, 25
- Welsh, B. Y. & Montgomery, S. L. 2015, *Adv. Astron.*, 2015, 1
- Wickramasinghe, C. 2011, *Int. J. Astrobiol.*, 10, 25
- Widmark, A. & Monari, G. 2019, *Mon. Not. R. Astron. Soc.*, 482, 262
- Wiegert, P. & Tremaine, S. 1999, *Icarus*, 137, 84
- Williams, G. 2017, *Minor Planet Electron. Circ.*, 2017-U181
- Wright, J. T. 2017, *Research Notes of the American Astronomical Society*, 1, 38
- Ye, Q.-Z., Zhang, Q., Kelley, M. S. P., & Brown, P. G. 2017, *ApJ*, 851, L5
- Yu, J. & Liu, C. 2018, *Mon. Not. R. Astron. Soc.*, 475, 1093
- Zhang, Q. 2018, *ApJ*, 852, L13
- Zhao, G., Zhao, Y. H., Chu, Y. Q., Jing, Y. P., & Deng, L. C. 2012, *Res. Astron. Astrophys.*, 12, 723

Summary

The **goal** of my thesis is to undertake a comprehensive study of the solar system's Oort cloud and the formation and evolution of interstellar comets.

The solar system was formed approximately 4.56 billion years ago. Despite the numerous theories that have been developed over the years, the formation and evolution of the solar system still remains unclear (Pfalzner et al. 2015, and references therein). However, several advances have been made in our knowledge about the solar system. The most accepted theory about its formation and early evolution describes a gravitational collapse of a dense cloud of interstellar gas and dust. The conservation of angular momentum induced a rapid rotation of the collapsing cloud, flattening it until it became a protoplanetary disk. In the central, most dense region of the disk, a star was created — our Sun. In a similar manner, clumpy structures developed in the disk. These eventually grew to form the planets, dwarf planets and moons. The leftovers of this process led to the formation of small bodies, such as asteroids and comets. This is how the five main types of objects in the solar system were formed; the Sun, planets, dwarf planets, moons, and minor bodies (asteroids and comets). A schematic representation of the solar system is shown in Fig. S1.

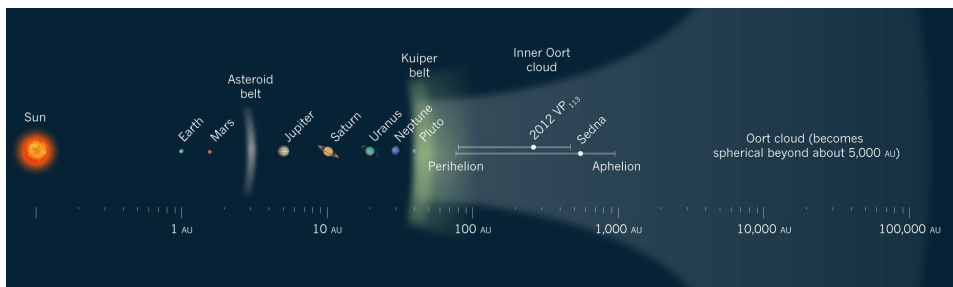


Figure S1: The solar system. Taken from Schwamb (2014).

Summary

To better understand the formation and evolution of the solar system, dynamical models are needed. In particular, the study of comets can reveal critical pieces of information about this process. The orbits of the comets in the inner part of the Oort cloud form a frozen record of the evolution of the solar system. At present, comets in this region are located at such large distances from the center of the solar system that perturbations from planets are negligible. They are rather at risk to be ripped away by passing stars or even the gravitational field of the Milky Way itself. Especially comets in the outermost regions are sensitive to such external influence, already during the early phases of the formation of the solar system (e.g., Torres et al. 2019a,b). These external influences have been shaping the Oort cloud over its history, producing comet showers reaching into the planetary region and stripping comets out into the interstellar space, forming interstellar comets.

Studying the dynamical evolution of comets can help us to constrain and to understand the formation and evolution of the solar system. Both the history of encounters between the solar system and nearby stars and the effect of the tides from the Galaxy are key components. The current distribution of nearby stars and the Galactic potential are reasonably well known. The Gaia mission (Gaia Collaboration et al. 2018, 2016) delivered a magnitude-limited complete sample of nearby stars. These stars dominate the local Galactic potential, and they give rise to occasional close encounters. Therefore, data from Gaia can be used as templates for the initial conditions in detailed simulations at different moments in time. Combining analytical, observational and numerical techniques are the key components to constrain and better understand the formation and dynamical evolution of the solar system.

In this thesis, I explored the formation and dynamical evolution of comets in the Kuiper belt/scattered disk and the Oort cloud, accounting for external perturbations such as passing stars and the galactic tidal field. As a consequence of these perturbations, the formation and evolution of interstellar comets were investigated. This thesis is divided into four chapters. Chapter 2 treats the origin of the interstellar object 1I/2017 U1 ‘Oumuamua by comparing estimates based on observations with simulations (Sect. 2). Chapter 3 focuses on the dynamical evolution of the Oort cloud after the interaction with passing stars and the Galactic tidal field (Sect. 3). In Chapter 4, I studied the formation and evolution of the solar system’s Kuiper belt/scattered disk and Oort cloud in the early stages of their formation, when the Sun was still in its birth cluster (Sect. 4). Finally, Chapter 5 ex-

plores the formation of interstellar comets from the neighbouring stars of the Sun (Sect. 5). Below, I summarize each chapter and the key research questions addressed in this thesis.

1. What is the effect of multiple stellar encounters and the Galactic tidal field on comets in Oort cloud-like structures? (Chapters 3 and 5).
2. Was the formation of the Oort cloud triggered by planet-disk interaction and stellar encounters in the early solar system? (Chapter 4).
3. Where do interstellar comets come from and how do they form? (Chapters 2 and 4).

Chapter 2 Based on: *The origin of interstellar asteroidal objects like 1I/2017 U1 'Oumuamua*, MNRAS 479, L17-L22 201, (Portegies Zwart, Torres et. al., 2018). I studied the origin of the interstellar object 1I/ 'Oumuamua by comparing estimates based on observations with simulations. Using the astrometric data from Gaia-TGAS (Gaia Collaboration, Brown et al. 2016), I integrated the orbit of 'Oumuamua and all the stars within 50 pc from the Sun. I find that about 1.3 Myr ago 'Oumuamua passed nearby the star HIP 17288, and had three other close encounters during its journey towards the Sun. I explored the different scenarios of formation for 'Oumuamua and concluded that objects like 'Oumuamua are formed in the debris disc as a leftover from the star and planet formation process, and subsequently liberated. I find that the mean galactic density of interstellar comets in the solar neighbourhood is $\sim 10^{14}$ per cubic parsec, which means that we expect about 2–12 such visitors per year within 1 au from the Sun.

Chapter 3 Based on: *Galactic tide and local stellar perturbations on the Oort cloud: creation of interstellar comets*, A&A 629, A139, (Torres et. al., 2019). Using the positions, parallaxes and proper motions from the Gaia survey and combining them with radial velocities from RAVE-DR5 (Kunder et al. 2017), GALAH DR2 (Buder et al. 2018), LAMOST DR3 (Zhao et al. 2012), APOGEE DR14 (Abolfathi et al. 2018), and XHIP (Anderson & Francis 2012). I constructed a catalogue of the Sun's neighbour stars. Then, I calculated the closest encounters that the Sun has had with other stars in

Summary

the recent past and will have in the near future (Torres et. al., 2017; Torres et. al., 2019). I find that the star GJ710 will approach the Sun in 1.3 Myr at the distance of 0.06pc instead of 0.3pc as predicted by previous studies (e.g., Dybczyński & Berski 2015, and references therein). Then, using the catalogue of nearby stars, I studied the dynamical evolution of comets in the Oort cloud, accounting for the perturbation of the galactic tidal field and the cumulative effect of nearby passing stars. I find that the comets at the edge of the Oort cloud (80,000-100,000 au) get heavily perturbed and, as a result, the semi-major axis of $\sim 1.1\%$ of the comets have increased to extend into interstellar regions. Since the comets are still bound to the solar system, we consider them *transitional interstellar comets* (TICs). The first TIC candidate is the comet C/2018 V1 (de la Fuente Marcos & de la Fuente Marcos 2019).

Chapter 4 Based on: *Dynamical evolution of the solar system debris disk in its birth cluster*, submitted to A&A recommended for publication (Torres et. al., 2019b). I studied the creation and evolution of the solar system's Oort cloud in the early stages of its formation when the sun was still in its birth cluster (Torres et al. 2019b). I constructed two models for the solar system. In the first model, I assumed a compact debris disk (16-35 au), while the second I assumed an extended debris disk (40-1000 au). For both models, I account for the perturbations of the giant planets and nearby stars in the cluster. I find that the most efficient way to perturb a disk is when the angle of interaction between the solar system and the perturber is between 0-30 degrees independently of the size of the disk. Additionally, I found that the creation of the Oort cloud was triggered by secular encounters, which produce the scattered disk, Sedna, and Oort Cloud like objects, while the giant planets creates Kuiper belt objects. Additionally, approximately 36% of the planetesimals are ejected becoming interstellar comets.

Chapter 5 Based on: *Dynamical evolution of exo-Oort clouds around the Sun's closest neighbours stars due to local stellar perturbations and the Galactic tidal field*, submitted to A&A, (Torres et. al., 2020). Using the catalogue of the closest stars constructed in (Torres et. al., 2017; Torres et. al., 2019), and the methods developed in (Torres et. al., 2019; Torres et. al., 2019b), I calculated the closest encounter for each of the Sun's neighbour stars within 3 pc and with accurate astrometric data from Gaia DR2, i.e., Proxima Centauri, Barnard star, Gliese 65, Ross 154, and Ross 248. I find

Summary

that on average the stars in the solar neighbourhood experience around 40–55 close encounters during 20 Myr, primarily with M-dwarf stars. I then calculated the effect of passing stars and the Galactic tidal field on the comets in exo-Oort clouds around the Sun's neighbour stars. The most perturbed system over a time interval of 20 Myr is Gliese 65 followed by Ross 154, Barnard's star and Ross 248 and finally Proxima Centauri. For Gliese 65 the production rate of transitional interstellar comets and interstellar objects is about 40×10^8 TIC Myr⁻¹ and 1.4×10^{10} ISO Myr⁻¹. For the rest of the systems the rate of TIC production is about 2.1 to 3.8×10^8 TIC Myr⁻¹. This implies that a considerable number of interstellar comets reside in the local neighbourhood. Therefore the Sun and its neighbours are visited by interstellar comets originating from other stars. In this way, it is plausible that an interstellar comet cloud exists.

Resumen

El **objetivo** de mi tesis es realizar un estudio detallado de la nube de Oort del sistema solar y la formación y evolución de cometas interestelares.

El sistema solar se formó hace aproximadamente 4.560 millones de años. A pesar de las teorías que se han desarrollado a lo largo de los años, la formación y evolución del sistema solar aún no está clara (Pfalzner et al. 2015, ver referencias). Sin embargo, se han realizado varios avances en nuestro conocimiento sobre el sistema solar. La teoría más aceptada sobre su formación y evolución temprana describe un colapso gravitacional de una densa nube de gas y polvo interestelar. La conservación del momento angular indujo una rápida rotación de la nube colapsada, comprimiéndola hasta convertirse en un disco protoplanetario. En la región central y más densa del disco, se crea entonces, una estrella: nuestro Sol. De manera similar, se desarrollaron estructuras grumosas en el disco. Estas eventualmente crecieron para formar planetas, planetas enanos y lunas. Los restos de este proceso llevaron a la formación de cuerpos pequeños, como asteroides y cometas. Así es como se formaron los cinco tipos principales de objetos en el sistema solar; Sol, planetas, planetas enanos, lunas y cuerpos menores (asteroides y cometas). Una representación esquemática del sistema solar se muestra en Fig. R1.

Para comprender mejor la formación y evolución del sistema solar, se necesitan modelos dinámicos. En particular, el estudio de los cometas puede revelar información crítica sobre este proceso. Las órbitas de los cometas en la parte interna de la nube de Oort forman un registro de la evolución del sistema solar. En la actualidad, los cometas en esta región están ubicados a distancias tan lejanas del centro del sistema solar que las perturbaciones de los planetas son insignificantes. Estos, corren el riesgo de ser separados por las estrellas que pasan o incluso por el campo gravitacional de la Vía Láctea. Especialmente los cometas en las regiones externas son más sensibles a dicha influencia externa, ya que durante las primeras fases de la formación del sistema solar (e.g., Torres et al. 2019a,b). Estas

Resumen

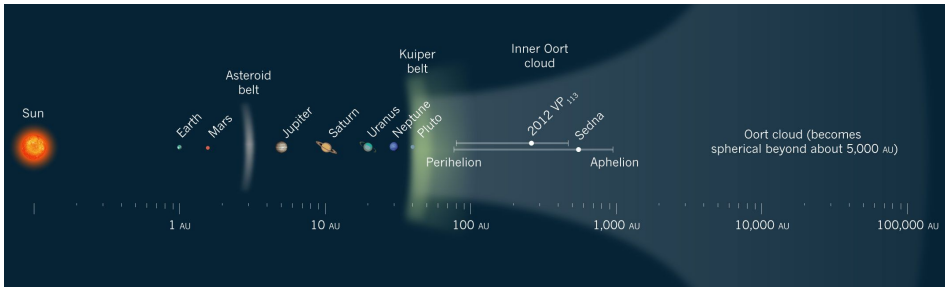


Figure R1: El sistema solar. Tomado de Schwamb (2014).

influencias externas han estado dando forma a la nube de Oort a lo largo de su historia, produciendo lluvias de cometas que llegan a la región planetaria y enviando cometas hacia el espacio interestelar, formando cometas interestelares.

Estudiar la evolución dinámica de los cometas puede ayudarnos a restringir y comprender la formación y evolución del sistema solar. Tanto la historia de los encuentros entre el sistema solar y las estrellas cercanas como el efecto de las mareas de la galaxia son componentes clave. La distribución actual de las estrellas cercanas y el potencial galáctico son bastante conocidos. La misión Gaia (Gaia Collaboration et al. 2018, 2016) produjo una muestra completa de magnitud limitada de estrellas cercanas. Estas estrellas dominan el potencial galáctico local y dan lugar a encuentros cercanos ocasionales. Por lo tanto, los datos de Gaia pueden usarse como plantillas para las condiciones iniciales en simulaciones detalladas en diferentes momentos en el tiempo. La combinación de técnicas analíticas, observacionales y numéricas son los componentes clave para restringir y comprender mejor la formación y la evolución dinámica del sistema solar.

En esta tesis, exploré la formación y la evolución dinámica de los cometas en el cinturón de Kuiper/disco disperso y la nube de Oort, teniendo en cuenta las perturbaciones externas, como las estrellas cercanas al Sol y el campo de marea galáctico. Como consecuencia de estas perturbaciones, se investigó la formación y evolución de los cometas interestelares. Esta tesis se divide en cuatro capítulos. El Capítulo 2 se enfoca en el origen del objeto interestelar 1I/2017 U1 'Oumuamua, usando comparaciones entre estimaciones basadas en observaciones con simulaciones (Sect. 2). El Capítulo 3 se centra en la evolución dinámica de la nube de Oort después

de la interacción con las estrellas que cercanas al Sol y el campo de mareas galáctico (Sect. 3). En el Capítulo 4, estudié la formación y evolución del cinturón de Kuiper/disco disperso del sistema solar y la nube de Oort en las primeras etapas de su formación, cuando el Sol todavía estaba en su grupo de nacimiento (Sect. 4). Finalmente, el Capítulo 5 explora la formación de cometas interestelares en las estrellas vecinas del Sol (Sect. 5). A continuación, resumo cada capítulo y las preguntas clave de investigación abordadas en esta tesis.

1. ¿Cuál es el efecto de múltiples encuentros estelares y el campo de mareas galáctico en los cometas en nubes de Oort y estructuras similares? (Capítulos 3 y 5).
2. ¿Fue la formación de la nube de Oort provocada por la interacción entre los planets, el disco de escombros y encuentros estelares en el sistema solar temprano? (Capítulo 4).
3. ¿De dónde vienen los cometas interestelares y cómo se forman? (Capítulos 2 y 4).

Capítulo 2 Basado en: *El origen de los objetos asteroides interestelares como 1I / 2017 U1 'Oumuamua*, MNRAS 479, L17-L22 201, (Portegies Zwart, Torres et. al., 2018). Estudié el origen del objeto interestelar 1I/ 'Oumuamua comparando estimaciones basadas en observaciones con simulaciones. Utilizando los datos astrométricos de Gaia-TGAS (Gaia Collaboration, Brown et al. 2016), integré la órbita de 'Oumuamua y todas las estrellas dentro de 50 pc del Sol. Encontré que hace aproximadamente 1.3 Myr 'Oumuamua pasó cerca de la estrella HIP 17288, y tuvo otros tres encuentros cercanos durante su viaje hacia el sistema solar. Exploré los diferentes escenarios de formación para 'Oumuamua y concluí que objetos como 'Oumuamua se forman en el disco de escombros como restos del proceso de formación de estrellas y planetas. Descubrí que la densidad galáctica media de los cometas interestelares en el vecindario solar es $\sim 10^{14}$ por parsec cúbico, lo que significa que esperamos de 2 a 12 visitantes por año dentro de 1 au del Sol.

Capítulo 3 Basado en: *Marea galáctica y perturbaciones estelares locales en la nube de Oort: creación de cometas interestelares*, A&A 629,

Resumen

A139, (Torres et. al., 2019). Usando las posiciones, paralaje y movimientos propios de la misión Gaia y combinándolos con velocidades radiales de RAVE-DR5 (Kunder et al. 2017), GALAH DR2 (Buder et al. 2018), LAMOST DR3 (Zhao et al. 2012), APOGEE DR14 (Abolfathi et al. 2018) y XHIP (Anderson & Francis 2012). Construí un catálogo de las estrellas cercanas al Sol. Luego, calculé los encuentros más cercanos que el Sol ha tenido con otras estrellas en el pasado reciente y que tendré en el futuro cercano (Torres et. al., 2017; Torres et. al., 2019). Encontré que la estrella GJ710 se acercará al Sol en 1.3 Myr a una distancia de 0.06 pc, a diferencia de 0.3 pc como lo predijeron estudios previos (por ejemplo, Dybczyński & Berski 2015, y referencias). Luego, utilizando el catálogo de estrellas cercanas, estudié la evolución dinámica de los cometas en la nube de Oort, considerando la perturbación del campo de mareas galáctico y el efecto acumulativo de las estrellas vecinas. Descubrí que los cometas en el borde externo de la nube de Oort (80,000-100,000 au) son altamente perturbados y, como resultado, el semi-eje mayor de aproximadamente 1.1 % de los cometas alcanza distancias hasta las regiones interestelares. Dado que estos cometas aún están unidos al sistema solar, adquiere el nombre *cometas interestelares de transición* (TIC por sus siglas en inglés). El primer candidato es el cometa C/2018 V1 (de la Fuente Marcos & de la Fuente Marcos 2019).

Capítulo 4 Basado en: *Evolución dinámica del disco de escombros del sistema solar en su grupo de nacimiento*, enviado a A&A recomendado para publicación (Torres et. al., 2019b). Estudie la creación y evolución de la nube de Oort del sistema solar en las primeras etapas de su formación cuando el Sol todavía estaba en su cúmulo de nacimiento. Construí dos modelos para el sistema solar. En el primer modelo, asumí un disco de escombros compacto (16-35 au), mientras que en el segundo asumimos un disco de escombros extendido (40-1000 au). Para ambos modelos, considere las perturbaciones de los planetas gigantes y las estrellas cercanas en el cúmulo estelar. Encontré que la forma más eficiente de perturbar un disco es cuando el ángulo de interacción entre el sistema solar y el perturbador está entre 0-30 grados, independientemente del tamaño de este. Además, descubrí que la creación de la nube de Oort fue provocada por encuentros seculares de estrellas en el cúmulos, que indujeron la formación del disco disperso, Sedna y objetos similares a la nube de Oort; mientras que los planetas gigantes crearon objetos del cinturón de Kuiper. Además,

aproximadamente 36 % de los objetos en el disco fueron expulsados convirtiéndose en cometas interestelares.

Capítulo 5 Basado en: *Evolución dinámica de las nubes de Oort alrededor de estrellas vecinas al Sol debido a perturbaciones estelares locales y al campo de mareas galáctica*, enviado a A&A, (Torres et. al., 2020). Utilizando el catálogo de las estrellas cercanas al Sol construido en Torres et al. (2018, 2019a), y los métodos desarrollados en Torres et al. (2019a,b), calculé el encuentro más cercano que cada una de las estrellas vecinas del Sol experimentaron dentro de 3 pc y que poseen datos astrométricos de Gaia DR2, es decir los sistemas Proxima Centauri, estrella de Barnard, Gliese 65, Ross 154 y Ross 248. Encontré que, en promedio, las estrellas en el vecindario solar experimentan alrededor de 40-55 encuentros cercanos durante 20 Myr, principalmente con estrellas enanas. Luego calculé el efecto de las estrellas perturbadoras y el campo de mareas galáctico en los cometas en las nubes exo-Oort en los sistemas seleccionados. El sistema más perturbado en un intervalo de tiempo de 20 Myr es Gliese 65 seguido de Ross 154, la estrella de Barnard, Ross 248 y finalmente Proxima Centauri. Para Gliese 65, la tasa de producción de cometas interestelares de transición y objetos interestelares es de aproximadamente $40 \times 10^8 \text{TIC Myr}^{-1}$ y $1.4 \times 10^{10} \text{ISO Myr}^{-1}$. Para el resto de los sistemas, la tasa de producción de TIC es de aproximadamente 2.1 a $3.8 \times 10^8 \text{TIC Myr}^{-1}$. Esto implica que un número considerable de cometas interestelares residen en el vecindario local. Por lo tanto, el Sol y sus vecinos son visitados por cometas interestelares procedentes de otras estrellas. De esta manera, es plausible que exista una nube de cometa interestelar.

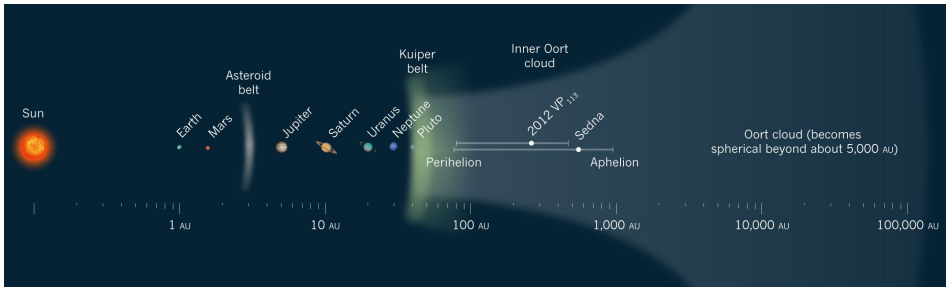
Samenvatting

Het **doel** van mijn thesis is om een uitgebreide studie uit te voeren naar de Oortwolk van het zonnestelsel en de vorming en evolutie van interstellaire kometen.

Het zonnestelsel is bij benadering 4.56 miljard jaar geleden gevormd. Ondanks de vele theoriën die door de jaren heen ontwikkeld zijn blijft het ontstaan en de evolutie van het zonnestelsel onduidelijk (Pfalzner et al. 2015, en referenties daarin). Er zijn echter verscheidene vorderingen gemaakt in onze kennis van het zonnestelsel. De meest geaccepteerde theorie over het ontstaan en de vroege evolutie beschrijft het instorten van een dichte wolk interstellair gas en stof onder zijn eigen zwaartekracht. Het behoud van hoekmoment induceerde een snelle rotatie van de instortende wolk en platte het af tot een protoplanetaire schijf. In het centrale, meest dichte deel van de schijf werd een ster gevormd, onze Zon. Op een soortgelijke manier vormden klonterige structuren in de schijf. Deze groeiden uiteindelijk uit tot planeten, dwergplaneten en manen. Het restant hiervan leidde tot de vorming van kleine lichamen zoals asteroïden en kometen. Dit is hoe de vijf voornaamste type objecten in het zonnestelsel werden gevormd; de Zon, planeten, dwergplaneten, manen en kleinere lichamen (asteroïden en kometen). Een schematische weergave van het zonnestelsel is te zien in Fig. S1.

Om het ontstaan en de evolutie van het zonnestelsel beter te begrijpen zijn dynamische modellen nodig. Met name het bestuderen van kometen kan cruciale informatie geven over dit proces. In de banen van kometen in het binnenste deel van de Oortwolk is de evolutie van het zonnestelsel vastgelegd. Momenteel bevinden kometen in deze regio zich op zulke grote afstanden van het centrum van het zonnestelsel dat verstoringen door planeten verwaarloosbaar zijn. Ze lopen eerder het risico om weggerukt te worden door passerende sterren of het getijdenveld van de Melkweg zelf. Vooral kometen in de buitenste regio's zijn gevoelig voor deze externe invloeden, al vanaf de vroege stadia van het ontstaan van het zonnestelsel (Gaia Collaboration et al. 2018, 2016). Deze externe invloeden hebben de

Samenvatting



Figuur S1: Het zonnestelsel. Meeegenomen van Schwamb (2014).

Oortwolk door zijn geschiedenis heen gevormd, kometenzwermen producerend die tot in de planetaire regio reikten en kometen wegrukkend naar de interstellaire ruimte, waar ze interstellaire kometen werden.

Het bestuderen van de dynamische evolutie van kometen kan ons helpen het ontstaan en de evolutie van het zonnestelsel beter te begrijpen. Zowel de geschiedenis van ontmoetingen tussen het zonnestelsel en naburige sterren en het effect van de getijden van de Melkweg zijn belangrijke onderdelen. De huidige verdeling van naburige sterren en het galactisch potentiaal zijn redelijk bekend. De Gaia missie (Gaia Collaboration et al. 2018, 2016) leverde een magnitude-gelimiteerd volledig monster op van naburige sterren. Deze sterren domineren de plaatselijke galactische potentiaal en komen af en toe dicht bij de Zon. Derhalve kunnen gegevens van Gaia dienen als basis voor de begincondities van gedetailleerde simulaties op verschillende momenten in de tijd. Het combineren van analytische, observationele en numerieke technieken is belangrijk om het ontstaan en de evolutie van het zonnestelsel beter te begrijpen.

In deze thesis heb ik het ontstaan en de evolutie van kometen in de Kuipergordel/verstrooide schijf en de Oortwolk onderzocht, rekening houdend met verstoringen zoals van passerende sterren en het galactisch getijdenveld. Het ontstaan en de evolutie van interstellaire kometen als gevolg van deze verstoringen zijn onderzocht. Deze thesis is verdeeld in vier hoofdstukken. Hoofdstuk 2 behandelt de oorsprong van het interstellaire object I1/2017 U1 'Oumuamua door schattingen gebaseerd op waarnemingen te vergelijken met simulaties (Sect. 2). Hoofdstuk 3 richt zich op de dynamische evolutie van de Oortwolk na interactie met passerende sterren en het galactisch getijdenveld (Sect. 3). In Hoofdstuk 4 bestudeer ik het ontstaan en de evolutie van de Kuipergordel/verstrooide schijf en de Oortwolk van

het zonnestelsel in het vroege stadium van hun ontstaan, toen de Zon zich nog in zijn geboortecuster bevond (Sect. 4). Tenslotte verkent Hoofdstuk 5 de vorming van interstellaire kometen van naburige sterren van de Zon (Sect. 5). Hieronder vat ik elk hoofdstuk en de belangrijkste onderzoeksvragen in deze thesis samen.

1. Wat is het effect van meerdere stellaire ontmoetingen en het galactisch getijdenveld op kometen in Oortwolk-achtige structuren? (Hoofdstukken 3 en 5).
2. Is het ontstaan van de Oortwolk veroorzaakt door planeetschijf interacties en stellaire ontmoetingen in het vroege zonnestelsel? (Hoofdstuk 4).
3. Waar komen interstellaire kometen vandaan en hoe ontstaan ze? (Hoofdstukken 2 en 4).

Hoofdstuk 2 Gebaseerd op: *The origin of interstellar asteroidal objects like 1I/2017 U1 'Oumuamua*, MNRAS 479, L17-L22 201, (Portegies Zwart, Torres et. al., 2018). Ik heb de oorsprong van het interstellaire object 1I/'Oumuamua bestudeerd door schattingen gebaseerd op waarnemingen te vergelijken met simulaties. Gebruikmakend van astrometrische data van Gaia-TGAS (Gaia Collaboration, Brown et al. 2016) heb ik de baan van 'Oumuamua en alle sterren binnen 50 pc van de Zon geïntegreerd. Ik bevond dat ongeveer 1.3 miljoen jaar geleden 'Oumuamua de ster HIP 17288 van dichtbij passeerde, en drie andere ontmoetingen had tijdens haar reis naar de Zon. Ik heb verschillende scenario's voor de vorming van 'Oumuamua onderzocht en geconcludeerd dat objecten zoals 'Oumuamua gevormd worden in de puinschijf als een restant van het ster- en planeetvormingsproces, en vervolgens worden vrijgemaakt van de ster. Ik bevond dat de gemiddelde galactische dichtheid van interstellaire kometen in de buurt van de Zon $\sim 10^{14}$ per kubieke parsec is, wat betekent dat we elk jaar 2–12 van zulke bezoekers kunnen verwachten binnen 1 au van de Zon.

Hoofdstuk 3 Gebaseerd op: *Galactic tide and local stellar perturbations on the Oort cloud: creation of interstellar comets*, A&A 629, A139, (Torres et. al., 2019). Gebruikmakend van de posities, parallaxen en eigenbewegingen in de Gaia data en dat combinerend met radiële snelheids-

Samenvatting

metingen van RAVE-DR5 (Kunder et al. 2017), GALAH DR2 (Buder et al. 2018), LAMOST DR3 (Zhao et al. 2012), APOGEE DR14 (Abolfathi et al. 2018), en XHIP (Anderson & Francis 2012), stelde ik een catalogus samen van de buursterren van de Zon. Toen berekende ik de ontmoetingen die de Zon in het verleden heeft gehad met andere sterren en in de toekomst gaat hebben (Torres et. al., 2017; Torres et. al., 2019). Ik vond dat de ster GJ710 over 1.3 miljoen jaar de Zon gaat naderen tot op een afstand van 0.06pc in plaats van 0.3pc zoals voorspeld door eerdere studies (e.g., Dybczyński & Berski 2015, en referenties daarin). Daarna bestudeerde ik, gebruikmakend van deze catalogus van nabije sterren, de dynamische evolutie van kometen in de Oortwolk, rekening houdend met het galactisch getijdenveld en het cumulatieve effect van dichtbij passerende sterren. Ik vond dat kometen aan de rand van de Oortwolk (80,000-100,00 au) hevig verstoord worden waardoor de halflange assen van $\sim 1.1\%$ van de kometen toenemen tot in de interstellaire regio's. Aangezien kometen nog steeds gebonden zijn aan het zonnestelsel beschouwen we ze als *transitionele interstellaire kometen* (transitional interstellar comets, TICs). De eerste TIC kandidaat is de komeet C/2018 V1 (de la Fuente Marcos & de la Fuente Marcos 2019).

Hoofdstuk 4 Gebaseerd op: *Dynamical evolution of the solar system debris disk in its birth cluster*, ingediend bij A&A, aanbevolen voor publicatie (Torres et. al., 2019b). We hebben het ontstaan en de evolutie van de Oortwolk van het zonnestelsel bestudeerd in de vroege stadia van zijn vorming toen de Zon zich nog in zijn geboortecuster bevond. Ik heb twee modellen voor het zonnestelsel opgezet. In het eerste model namen we een compacte puinschijf aan (16-35 au), en in de tweede een grotere puinschijf (40-1000 au). Voor beide modellen houden we rekening met verstoringen van de reuzenplaneten en van nabije sterren in de cluster. Ik bevond dat de meest efficiënte manier om een schijf te verstoren is wanneer de hoek van de wisselwerking tussen het zonnestelsel en de verstoorder tussen 0-30 graden ligt, onafhankelijk van de grootte van de schijf. Daarnaast bevonden we dat de vorming van de Oortwolk veroorzaakt werd door nabije ontmoetingen met andere sterren, die de verstrooide schijf, Sedna en Oortwolk-achtige objecten produceren, terwijl de reuzenplaneten Kuiper-gordelobjecten maken. Daarnaast wordt ongeveer 36% van de planetesimalen uitgeworpen en wordt interstellaire kometen.

Hoofdstuk 5 Gebaseerd op: *Dynamical evolution of exo-Oort clouds around the Sun's closest neighbours stars due to local stellar perturbations and the Galactic tidal field*, ingediend bij A&A, (Torres et. al., 2020). Gebruikmakend van de catalogus van meest dichtbijge sterren geconstrueerd in (Torres et. al., 2017; Torres et. al., 2019), en van de methodes ontwikkeld in (Torres et. al., 2019; Torres et. al., 2019b), berekende ik de meest dichtbijge ontmoetingen voor elk van de buursterren van de Zon binnen 3 pc en die nauwkeurige astrometrische gegevens van Gaia DR2 hadden, namelijk voor Proxima Centauri, de Ster van Barnard, Gliese 65, Ross 154 en Ross 248. Ik bevond dat de sterren in de buurt van de Zon gemiddeld rond de 40-55 dichtbijge ontmoetingen ervaren gedurende 20 miljoen jaar, voornamelijk met M-dwergsterren. Toen rekende ik het effect van passerende sterren en het galactisch getijdenveld uit op de kometen in de exo-Oortwolken rond de buursterren van de Zon. Het meest verstoorde systeem gedurende een tijdsinterval van 20 miljoen jaar is Gliese 65, gevolgd door Ross 154, de Ster van Barnard en Ross 248 en uiteindelijk Proxima Centauri. Voor Gliese 65 is de productiesnelheid van transitionele interstellaire kometen en interstellaire objecten ongeveer 40×10^8 TIC per miljoen jaar en 1.4×10^{10} ISO per miljoen jaar. Dit impliceert dat er een aanzienlijk aantal interstellaire kometen in de buurt van de Zon is. Derhalve worden de Zon en zijn burens bezocht door interstellaire kometen die van andere sterren komen. Op deze manier is het aannemelijk dat een interstellaire kometenwolk bestaat.

List of publications

Refereed papers

1. *Dynamical evolution of exo-Oort clouds around the Sun's closest neighbour stars due to local stellar perturbations and the Galactic tidal field*, submitted to *Astronomy & Astrophysics*, in review, 2020.
S. Torres, S. Portegies Zwart, and A. G. A. Brown.
2. *Dynamical evolution of the solar system debris disk in its birth cluster*, submitted to *Astronomy & Astrophysics*, recommend for publication, 2019b.
S. Torres, M. X. Cai, D. Mukherjee, S. Portegies Zwart, and A. G. A. Brown.
3. *Galactic tide and Local Stellar Perturbation on the Oort Cloud: Creation of Interstellar Comets*, *Astronomy & Astrophysics* 629 - A139, 2019a.
S. Torres, M. X. Cai, S. Portegies Zwart, and A. G. A. Brown.
4. *The Origin of Interstellar Asteroidal Objects Like 1I/2017 U1 'Oumuamua*, *Monthly Notices of the Royal Astronomical Society (MNRAS)* 479, L17-L22, 2018.
S. Portegies Zwart, **S. Torres**^{*}, I. Pelupessy, J. Bédorf, and M. X. Cai.

Co-author

1. *Once upon a time in the Oort cloud*, submitted to *Science*, 2020.
S. Portegies Zwart, **S. Torres**, A. G. A. Brown, and M. X. Cai.
2. *Evolution of the Outer Planets and Planetesimals due to Gas Drag in Transition Disks*, APS id. C9.006, 2014.
S. Navarro, M. Reyes-Ruiz, H. Aveves, C. Chavez, **S. Torres**.
3. *Effect of a Gaseous Transition Disc on Planetesimal Driven Migration*, DPS #45, id.415.05, 2013.
M. Reyes-Ruiz, H. Aceves, C. Chavez, **S. Torres**.

^{*}Equal contribution as the first author.

4. *The Transneptunian Automated Occultation Survey (TAOS II)*, Asteroids, Comets, Meteors, No. 1667, id.6111, 2012.
M. J. Lehner, S.-Y. Wang, P. Ho, T. Lee, Z.-W. Zhang, W.-L Yen, M. Reyes Ruiz, D. Hiriart, A. P. Granados, **S. Torres**, C. Alcock, A. Szentgyorgyi, J. C. Geary, T. Norton, G. Furesz.

Conference proceedings

1. *Dynamics of the Oort cloud in the Gaia era I: close encounters*, IAU-330 Gaia symposium, 2017.
S. Torres, S. Portegies Zwart, and A. G. A. Brown.
2. *Dynamics and habitability in very low mass stars that belong to stellar clusters*, Astrobiology Science Conference, 2015.
S. Torres & B. Pichardo.
3. *Dynamics of protoplanetary disk in stellar clusters: very low mass stars*, ADELA, 2015.
S. Torres & B. Pichardo.

In preparation

1. *Dynamics of low mass stars in different Galactic environments*, in preparation, 2020.
S. Torres.
2. *Debris disk survivability around very low mass stars*, to be submitted to MNRAS, 2020.
S. Torres & B. Pichardo.
3. *Stellar cluster characterization using artificial intelligent methods to predict Gaia observables*, in preparation, 2020.
J. Albert, **S. Torres**, and S. Portegies Zwart.

Curriculum Vitae

I was born in Mexico city approximately 32 years ago. When I was a child, I was curious about everything, and always asked myself how the things work?. In particular, I was fascinated with one story that my parents used to tell me: *The mystery of the three stars on the sky*, that mysteriously appeared only during Christmas. For so many years, I tried to find the answer to such an event but did not succeed (although I was very close). When finally I entered to the secondary school, I asked my physics teacher, and his answer was: “To disentangle such a mystery you have to become an Astronomer, but in order to do that you have to study first a bachelor degree in Physics, a master degree in Astrophysics and finally a PhD in Astrophysics”, and then the journey who brought me here began.

In 2006 I enrolled in the National Autonomous University of Mexico (UNAM) to study Physics. The first years were tough, but quickly I adapted to the rhythm. In my second year, I went to the Institute of Astronomy to offer my services as a student. The result of that visit completely changed my life. I met Barbara Pichardo, who after a small interview offered me to supervise my bachelor thesis and more important her friendship. With Barbara’s support, I participated in several international projects like APOGEE and TAOS-II. In 2012 I moved to Taipei as part of the scientific team of TAOS-II at the Academia Sinica Institute of Astronomy and Astrophysics (ASIAA). After a successful internship in Taiwan and as a part of the next step in the list to become an Astronomer. At the end of 2012, I won a scholarship from the Spanish government to enrol in the master in Astrophysics at Universidad Autónoma de Madrid - Universidad Complutense de Madrid where I worked closely with Eva Villaver.

Curriculum Vitae

In the fall of 2015, I was notified that I was awarded a fellowship from the Mexican National Council for Science and Technology (CONACYT) for PhD studies abroad. After several meetings with Anthony Brown and a lot of bureaucracy finally, in November 2015, I landed in Schiphol. Full of dreams and enthusiasm I started my PhD in Astrophysics (and the last step in my list) at Leiden Observatory under the supervision of Anthony Brown and Simon Portegies Zwart. During four years, I travelled the world, talked, collaborated and shared with wonderful people and scientists, and I explored the origin and evolution of the outer solar system.

In February 2020, I accepted a postdoctoral fellowship at the University of California, Los Angeles (UCLA) in USA. I will join Smadar Naoz's research group, and I will continue the journey that I started many years ago: discover the universe.

Acknowledgements

About four years ago, I came to the Netherlands to pursue my PhD. I never imagined that my life will completely be changed along these years. I met wonderful people and scientists whose support, advice and friendship helped me to achieve my goal. I will always be grateful to all of you that were with me in one way or another in my PhD journey. Especially, I would like to thank...

To the Mexican National Council for Science and Technology (CONACYT), whose support made my PhD at Leiden Observatory possible. To Leiden Observatory for the unconditional support. In particular, thank you Evelijn, Alexandra, Els, Marjan, Monica, Caroline, Erik Deul, Eric, for always smiling and helping me with all the bureaucracy, computers, and other issues that I faced during my PhD. You made my life at the observatory way more smooth. To Xander for all the support during and especially in the last part of my PhD, you encouraged me to push hard and finish. To all the members of CASTLE, AMUSE, and Gaia groups, for being part of my personal and scientific development, for all the discussions and nice conversions we had in our group meetings. In particular thank you, Lucie, Adrian, Init, Silvia, Fran, Martijn, Jeroen, Max, Eleonora, Tommaso, Stella, Fraser, Steven, Edwin, and Arjen. Thank you, Anthony and Simon, for your patience, advices, scientific discussions, ups and downs, and for pushing me to be a better scientist and finish my PhD.

¡Bárbara!, gracias por compartirme tu pasión por la vida, por los dinosaurios, por la astronomía y por la enseñanza. Me enseñaste a ser una mejor persona, un mejor amigo, un mejor astrónomo. Gracias a ti, a tu confianza y apoyo incondicional concluí mi licenciatura, maestría y ahora doctorado. Fuiste y siempre serás mi amiga, mi colaboradora, mi mentora y mi madre académica. Esta tesis te la dedico a ti.

Acknowledgements

To my friends in the observatory: Eleonora, Igone, Kim, Gaby, Marco, Luis, Tommaso, Clément, Christos, Alex, Andres, Alvaro, Jit, Josh, Valeriya, Mieke, Fran, Max, Tjarda, Noel, Carmen, Jeroen, Thomas Wijnen, Maria Cristina, Gabriela, Anna, Stella, Dilovan, Robin, Aayush, Oscar, Martijn (thank you for helping me with my Dutch summary), Cristina (thank you for all the lunches, I had a lot of fun talking with you about life), among many other nice people I met. My life in the observatory would not have been the same without you. Max, thank you for all the nice discussions about science and life, for being my best collaborator, and for all your help during these years. I enjoyed writing papers with you and I'm sure more will come. Fran, gracias por todo tu apoyo, risas, terapias, group meetings, almuerzos y por ser una office mate de lujo. Luis, compadre extrañare esas largas conversaciones acerca de la vida, que chevere fue compartir el doctorado contigo. Eleonora, tu fuiste la primer persona a la que conocí, gracias por todos los buenos momentos que compartimos, por siempre sonreír y chismear conmigo, pero más importante gracias por tu amistad.

A la mini Latinoamérica en Holanda: Lina, Jorge, Kathy, Karinoa, Arlen, Javiera, Paula, Pedro, Pablo, Nico, Heather, Fran, Liz, Max, Andres, Yanett, Marta Irene, Cristina, Claudio (gracias maestro, por las clases de tenis), gracias a todos por hacerme sentir como en casa. Kathy y Javi, gracias por abrirme las puertas de su casa y por su amistad. Marta, Lina y Jorge, gracias por tantas risas, bailes, platikas, terapias, salidas al Lemmys y por compartir conmigo sus vidas en todos estos años, estoy seguro que nuestros caminos se volverán a cruzar. Noel y Susy no tengo como agradecer todo lo que hicieron por mi desde que llegue a Holanda. Gracias por todas esas cenas y fiestas mexicanas, por su apoyo incondicional, por su amistad, por hacerme sentir como en México, con ustedes siempre me sentí en casa. To my life friends: Alejandro (Mai), Andrea, Silvia, Sophy, Celine, John, Brisa, Paty, Sara, Ofelia, Mathieu, Zavala, Jorge, Iber, Nayeli, Engin, Alejandra, Mabel, Joaquin, Fer, Linn, Maja, Maria, Nikita, Shayen, Ana, Tomas, Thomas van der Toorn, Penny, Amruta, Valentina, Esperanza, Ning, Macla, Kaustubh, Vandana, Smriti, Ciccio, and Ali for all the good times and the ones that are about to come, thank you all! To all my teammates of the very successful and unsuccessful football club that we formed, we certainly had a lot of fun.

Acknowledgements

A mis queridos cascos, Ro, Chero y Sebas, sin ustedes mis últimos años en Leiden no hubieran sido lo mismo. Gracias compadres por todas las fiestas, consejos, macumbas, viajes, desvelos, kebabs, partidos de fut, cervezas, tequilas, pero sobre todo gracias por su amistad, estoy seguro nos volveremos a encontrar y rumbear juntos.

A mis papas, gracias por siempre estar conmigo, por su apoyo incondicional, por siempre confiar en mi y por su cariño. Sin ustedes este logro no hubiera sido posible. Alvaro y Beto gracias por todas esas conversaciones que a pesar de la distancia me hicieron sentir como en casa, gracias por el apoyo que siempre me han dado. Esther y Kichis gracias por siempre recibirme con una sonrisa, por su cariño y apoyo. A mi abuelas Ana y Enriqueta gracias por acompañarme todos estos años en la distancia y siempre darme su cariño. A mi familia Torres y Rodríguez por siempre estar cuando los necesito.

Tack så mycket Lin, Svante, Alice, Theo, Daniel, Arvid, Louise, Jan, för att ni alltid ler mot mig och att ni har välkomnat mig till er underbara familj.

Ylva, tack så mycket för att du är en del av mitt liv, för att du har hjälpt och stöttat mig under alla dessa år, för att vi har skratat, dansat, diskuterat vetenskap, politik, livet tillsammans, för att du alltid finns där och för att du vill upptäcka världen med mig. Mitt liv är nu tusen gånger bättre, och hos dig hittade jag äntligen ett hem. Kom alltid ihåg att du inte bara är min bästa vän, min bästa rådgivare, min förtrogna, men du är också mitt livs kärlek.

With love Santiago.

**–The Universe which, in the supremeness of its
symmetry, is but the most sublime of poems.**

Eureka [extract], Edgar Allan Poe 1848.

